Electrophysiological characterization of neuronal diversity in the substantia nigra pars reticulata in control and parkinsonian mice

Lorena Delgado Zabalza

THÈSE EN COTUTELLE PRÉSENTÉE

POUR OBTENIR LE GRADE DE

DOCTEUR DE L'UNIVERSITÉ DE BORDEAUX ET DE L'UNIVERSITÉ DU PAYS BASQUE (UPV/EHU)

ÉCOLE DOCTORALE des sciences de la vie et de la santé ET (UB)
ÉCOLE DOCTORALE du Pharmacologie et sciences de la vie (UPV/EHU)

Par **Lorena Delgado Zabalza**

- ELECTROPHYSIOLOGICAL CHARACTERIZATION OF NEURONAL DIVERSITY IN THE *SUBSTANTIA NIGRA PARS RETICULATA* IN CONTROL AND PARKINSONIAN MICE -

Sous la direction de Jérôme Baufreton and Cristina Miguelez Palomo

Soutenue le 18/06/2020

Membres du jury :

M. Thomas Boraud	DR. PhD, H.D.R.	CNRS/University of Bordeaux; **Président**
Mme. Corinne Beurrier	CR. PhD, H.D.R.	CNRS/Aix-Marseille University; **Rapporteur**
M. Laurent Venance	DR. PhD, H.D.R.	INSERM/Collège de France (CIRB); **Rapporteur**
Mme. Nagore Puente	Senior Researcher. PhD.	University of the Basque Country; **Examiner**
M. Miguel Valencia	Senior Researcher. PhD.	CIMA/University of Navarra; **Examiner**

Institut des Maladies Neurodégénératives (IMN)

CNRS UMR 5293

Université de Bordeaux

Centre Broca Nouvelle-Aquitaine

3ème étage, 146 rue Léo Saignat

33076 Bordeaux (France)

This Doctoral thesis has been carried out thanks to the economic support of the University of the Basque Country (UPV/EHU). Lorena Delgado Zabalza has held a predoctoral fellowship in Cotutelle with the University of Bordeaux for the period 2017-2020. In addition, Euskampus Fundazioa also contributed economically so that, this thesis could be completed.

Conflict of interest:

The authors declare no conflicts of interest.

INDEX

RÉSUMÉ **1**

ABSTRACT **3**

ACKNOWLEDGEMENTS / REMERCIEMENTS **4**

LIST OF ABBREVIATIONS **8**

LIST OF FIGURES **10**

1. INTRODUCTION **14**

1.1. PARKINSON'S DISEASE 14

1.1.1. Epidemiology and etiology *14*

1.1.2. Neuropathology *15*

1.1.3. Symptomatology *18*

1.1.4. Treatment *20*

1.1.5. L-DOPA induced dyskinesia *24*

1.2. BASAL GANGLIA 29

1.2.1. Anatomy and general functions of basal ganglia *29*

1.2.2. Basal ganglia network *31*

1.2.3. Basal ganglia motor circuit in Parkinson's disease and L-DOPA induced dyskinesia *37*

1.3. SUBSTANTIA NIGRA PARS RETICULATA 42

1.3.1. Neuronal diversity in the SNr *42*

1.3.2. Properties of SNr neurons *44*

1.3.3. Alterations in firing properties of SNr neurons in parkinsonian and dyskinetic animals *50*

1.3.4. Synaptic inputs from the striatum, globus pallidus and subthalamus onto SNr neurons *53*

1.3.5. Synaptic outputs from SNr neurons *58*

1.3.6. Dopaminergic modulation of SNr neurons *60*

1.3.7. GABAergic transmission in the SNr *63*

2. HYPOTHESIS AND OBJECTIVES **67**

3. EXPERIMENTAL PROCEDURES.....70

3.1. ANIMALS AND ETHICAL APPROVAL..... 70
3.2. EXPERIMENTAL DESIGN..... 70
3.3. DRUGS..... 72
3.4. STEREOTAXIC SURGICAL PROCEDURES..... 74
3.5. BEHAVIORAL ASSESSMENT..... 78
3.6. *IN VITRO* ELECTROPHYSIOLOGICAL RECORDINGS..... 80
3.7. IMMUNOHISTOCHEMISTRY..... 88
3.8. STATISTICAL ANALYSIS OF DATA..... 96

4. RESULTS.....98

4.1. STUDY I. INTRINSIC PROPERTIES OF *SUBSTANTIA NIGRA PARS RETICULATA* NEURONS REGARDING THE EXPRESSION OF PARVALBUMIN IN SHAM, PARKINSONIAN AND DYSKINETIC MICE..... 98
4.1.1. Distribution of GABAergic neurons in the SNr.....98
4.1.2. Electrophysiological properties of PV+ and PV- SNr neurons in sham PVcre::Ai9T mice in vitro..... 101
4.1.3. Impact of the 6-OHDA lesion and L-DOPA treatment on electrophysiological properties of PV+ and PV- SNr neurons... 106
4.2. STUDY II. STRIATO-NIGRAL AND PALLIDO-NIGRAL GABAERGIC SYNAPTIC TRANSMISSION IN SHAM AND PARKINSONIAN MICE..... 116
4.2.1. Firing rate of PV+ and PV- SNr neurons without blocking fast synaptic transmission..... 116
4.2.2. Characterization of the striato-nigral pathway..... 118
4.2.3. Characterization of the pallido-nigral pathway..... 126
4.3. STUDY III. GABAERGIC EXTRASYNAPTIC TRANSMISSION IN SNR NEURONS FROM CONTROL AND PARKINSONIAN MICE..... 136
4.3.1. Distribution of extrasynaptic δ and α5-subunits in $GABA_A$Rs of both subtypes of SNr neurons..... 136
4.3.2. Nigral tonic inhibition is mediated by extrasynaptic $GABA_A$ receptors containing δ and α5-subunits..... 140
4.3.3. Impact of dopamine depletion in nigral tonic inhibition..... 146

5. DISCUSSION 152

5.1. STUDY I. INTRINSIC PROPERTIES OF SUBSTANTIA NIGRA PARS RETICULATA NEURONS REGARDING THE EXPRESSION OF PARVALBUMIN IN SHAM, PARKINSONIAN AND DYSKINETIC MICE 152

5.1.1. Molecular evidence for distinct SNr neuron classes 152

5.1.2. PV+ and PV- SNr neurons have different intrinsic electrophysiological properties 153

5.1.3. Divergent effect of dopamine loss and L-DOPA treatment on the excitability of PV+ and PV- SNr neurons 157

5.2. STUDY II. STRIATO-NIGRAL AND PALLIDO-NIGRAL GABAERGIC SYNAPTIC TRANSMISSION IN SHAM AND PARKINSONIAN MICE 161

5.2.1. Striatal and pallidal inputs to the SNr innervate PV+ and PV- neurons 161

5.2.2. Striato-nigral synaptic changes after dopamine depletion 162

5.2.3. Pallido-nigral synaptic changes after dopamine depletion 163

5.3. STUDY III. GABAERGIC EXTRASYNAPTIC TRANSMISSION IN SNR NEURONS FROM CONTROL AND PARKINSONIAN MICE 167

5.3.1. Extrasynaptic $\alpha 5$ and δ subunits expressed in the SNr 167

5.3.2. Extrasynaptic $GABA_A$ receptors mediate tonic inhibition mainly in PV- SNr cells 168

5.3.3. Tonic inhibition remains unaltered after the 6-OHDA lesion in SNr neurons 171

6. CONCLUSIONS AND PERSPECTIVES 172

7. BIBLIOGRAPHY 178

RÉSUMÉ

Caractérisation électrophysiologique de la diversité neuronale dans la *substantia nigra pars reticulata* chez les souris contrôle et parkinsonienne

La substance noire réticulée (SNr) est la principale structure de sortie des ganglions de la base (BG), un réseau sous-cortical contrôlant l'élaboration des programmes moteurs ainsi que des fonctions d'apprentissage cognitives et associatives. L'identification de types de cellules distincts dans le BG a joué un rôle clé pour comprendre les propriétés et les fonctions de ce circuit. Des études récentes suggèrent que la SNr est composé de plusieurs types de cellules mais jusqu'à présent cette diversité neuronale n'a jamais été prise en compte concernant le fonctionnement normal et pathologique de ce noyau, notamment dans la maladie de Parkinson (MP). En combinant des approches immunohistochimiques et électrophysiologiques chez la lignée de souris PVCre::Ai9T, nous avons démontré que les neurones de la SNr exprimant la protéine parvalbumine (PV+) ont des propriétés anatomiques et électrophysiologiques différentes de celles des neurones ne l'exprimant pas (PV-). Notre analyse anatomique montre que les neurones PV+ et PV- sont présents à proportion égale dans la SNr, mais avec une distribution distincte, les neurones PV+ étant enrichis dans la partie latérale de la SNr alors que les neurones PV- sont présents dans la partie médiale de ce noyau. Nos enregistrements électrophysiologiques *in vitro* ont révélé que les neurones PV+ ont une activité électrique plus élevée que les cellules PV-. De plus, nos données indiquent que la perte de dopamine (DA) et le traitement à la L-DOPA induisent une réduction profonde de l'excitabilité des neurones PV+ de la SNr dans un modèle murin de MP (la souris 6-OHDA) sans modifier l'activité des neurones PV-.

Il est bien connu que l'activité des neurones de la SNr est contrôlée par les afférences GABAergiques des neurones striataux (STR-SNr) de la voie directe (dSPN) et du globus pallidus (GP-SNr). Nous avons effectué une manipulation optogénétique de ces deux voies inhibitrices et montré que ces deux populations neuronales sont innervées de manière équivalente par le STR et le GP. Nos résultats ont également révélé que l'inhibition striatale était plus efficace que l'inhibition pallidale pour réduire l'activité des deux sous-types de neurones SNr. De plus, nous avons observé que les

synapses STR-SNr et GP-SNr affichent la même plasticité à court terme sur les neurones PV+ et PV- de la SNr. Enfin, nous avons montré que la transmission GABAergique est affectée de manière différentielle sur les cellules PV+ et PV- suite à une déplétion DAergique. D'une part, les neurones PV+ sont plus sensibles à l'inhibition striatale que les cellules PV- après une déplétion en DA. D'autre part, l'inhibition pallidale est réduite sur les neurones PV+ et augmentée sur les PV- après la perte de DA, suggérant un déséquilibre de l'inhibition pallidale entre ces deux populations SNr.

Il est aussi connu que les niveaux extracellulaires de GABA sont élevés dans la SNr chez les modèles rongeurs de MP, ce qui suggère que les neurones de la SNr pourraient être inhibés de manière permanente par une inhibition dite tonique. Ainsi, Nous avons caractérisé la transmission extrasynaptique GABAergique dans la SNr des souris témoins et 6-OHDA. Nos enregistrements de patch-clamp ont révélés que les neurones PV- présentent une inhibition tonique plus importante que les cellules PV+ chez les souris témoins. La présence et l'implication des sous-unités δ et $\alpha5$ dans les récepteurs GABAA extrasynaptiques ont également été étudiées, révélant une présence et un effet majeurs des sous-unités $\alpha5$ sur les neurones PV. Cependant, contrairement à ce qui était attendu, la déplétion chronique en DA ne provoque aucun changement de l'inhibition tonique ni dans les cellules PV+ ni dans les neurones PV- de la SNr.

Nos résultats mettent en évidence l'importance de différencier les populations cellulaires de la SNr pour une meilleure connaissance du fonctionnement des BG en situation physiologique et physiopathologique tel que dans la MP.

Mots clés: Excitabilité neuronale; Transmission synaptique; GABA; Maladie de Parkinson; Dyskinésies L-DOPA-induites; Electrophysiologie.

ABSTRACT

Electrophysiological characterization of neuronal diversity in the *substantia nigra pars reticulata* in control and parkinsonian mice

The substantia nigra pars reticulate (SNr) is the main output structure of the basal ganglia (BG), a subcortical network controlling the elaboration of motor programs as well as cognitive and associative learning functions. The identification of distinct cell-types within the BG has played a key role for understanding the properties and functions of this circuit. Recent studies suggest that the SNr is composed of several cell types but until now this neuronal diversity has never been taken into consideration regarding normal and pathological functioning of this nucleus, particularly in Parkinson's disease (PD). By combining immunohistochemical and electrophysiological approaches in the PVCre::Ai9T mouse line, we have demonstrated that SNr neurons expressing the protein parvalbumin (PV+) exhibit different anatomical and electrophysiological properties than non PV-expressing (PV-) neurons. Our anatomical analysis reveal that PV+ and PV- neurons are present in equal proportion in the SNr, but with a distinct distribution, PV+ being enriched in the lateral part of the SNr, while PV- are found in the medial portion of the nucleus. *In vitro* electrophysiological recordings from identified PV+ and PV- neurons in the SNr also revealed that PV+ neurons fired at relatively higher rates than PV- cells. Additionally, our data revealed that DA loss and subsequent L-DOPA treatment induce a profound reduction of the excitability of PV+ SNr neurons in a 6-OHDA mouse model of PD while the activity of PV- remains unchanged by these treatments.

It is well known that the activity of SNr neurons is controlled by GABAergic inputs from striatal dSPN and the GP. We performed optogenetic manipulation of STR-SNr and GP-SNr inputs in order to determine whether PV+ and PV- SNr neurons received equivalent inputs from these two nuclei. We tested the impact of STR-SNr or GP-SNr activation on the activity of SNr neurons in cell-attached configuration and then switched to whole-cell voltage-clamp to characterize short-term plasticity of these synapses. Our results show that both PV+ and PV- SNr neurons are innervated by the STR and the GP. They also revealed that inhibition from dSPN was more powerful to silence activity of both subtypes of SNr neurons. Indeed, we observed that both STR-SNr and GP-SNr synapses displayed short-term depression in PV+ and PV- SNr neurons. DA loss affected GABA transmission in a different manner in PV+ and PV-

SNr cells. On one hand, PV+ neurons were more sensible to striatal synaptic inhibition than PV- cells after DA depletion. On the other hand, PV-GP inputs were reduced on PV+ neurons and increased in PV- cells after DA loss suggesting a disequilibrium in pallidal inhibition between these two SNr populations.

Furthermore, considering that rodent models of PD have shown elevated extracellular levels of GABA in the SNr which can exert a tonic extrasynaptic inhibition on SNr neurons, we decided to characterize GABAergic extrasynaptic transmission in the SNr of control and 6-OHDA lesioned mice. We studied $GABA_A$ mediated tonic inhibition by performing whole-cell patch-clamp recordings of PV+ and PV- SNr neurons in acute slices. We observed that PV- SNr neurons displayed larger $GABA_A$ receptor-mediated tonic currents than PV+ cells in the SNr of control mice. The presence and involvement of δ and/or $\alpha5$ extrasynaptic subunits in $GABA_A$ receptors mediating this type of transmission was also studied, revealing a major presence and effect of $\alpha5$-subunits on PV- neurons probably mediating the tonic currents observed in these neurons. However, contrary to expected, chronic DA-depletion did not trigger any increase in tonic inhibition neither in PV+ cells nor in PV- SNr neurons.

All these findings highlight the importance of differentiating cell populations in the SNr to a better knowledge of the BG circuit in normal and pathological states such as in PD.

Keywords: Neuronal excitability; Synaptic transmission; GABA; Parkinson's disease; L-DOPA induced dyskinesia; Patch Clamp.

ACKNOWLEDGEMENTS / REMERCIEMENTS

What a journey! This PhD in cotutelle started in Bilbao with Cristina Miguelez trusting me from the beginning. Then quite soon I moved to Bordeaux, new country, new language, new colleagues, new supervisor, briefly, new life for almost 1 year and

a half. I will never forget the first day I met Jerome Baufreton in the IMN when he introduced me everyone and I started listening by first time in my life, the famous “Salut, ça va?” I was in France and I did not speak any word in French, I was a bit scared but he, as always, with a smile in his mouth, open to explain me things once and again, to come to the set-up to fix something or just to share ideas or findings… He helped me quite a lot in this adventure. Thank you for your patience and for introducing me into the *in vitro* electrophysiology’s world. Thank you also Cristina Miguelez for everything you taught me, the support, guidance and good vibes. You both made me a better scientist and person. Definitively, I have had the best supervisors I could ever imagine, but also the best fans of my watercolors. To end, I would like to specially mention the support you both provided me with my father’s illness, my sincerest thanks to you.

Besides my PhD advisors, I would like to thank to all the members of thesis committee: Corinne Beurrier, Laurent Venance, Thomas Boraud, Nagore Puente and Miguel Valencia for kindly offering their time to evaluate my work. I am deeply honored that you accepted to be present during my PhD defense, in case the COVID-19 situation allows us.

I am also very grateful to all the members of the Baufreton’s laboratory: Morgane Le Bon-Jego, Anne Taupignon, François George, Christelle Glangetas and Jeremy Cousineau. Je tiens à vous remercier pour vous encouragements, pour votre sympathie, pour votre intérêt envers les expériences, mes aquarelles ainsi que pour ma vie personnelle. Sans vous rien n’aurait été possible et mon français ne serait pas aussi bon. Merci Maurice Garret pour tous les conseils sur l’immunofluorescence et les belles images que tu as apporté à ce projet. Je remercie très sincèrement Guillaume Dabée pour ta bonne humeur quotidienne, ta gentillesse et générosité. Merci pour t’occuper de mes animaux, une solidarité qui a grandement permit à rendre ce projet possible.

J’adresse également mes remerciements à Delphine Charles et Renaud Borderie pour me donner l’opportunité de participer au concours “Ma thèse en 180 seconds“. Merci pour votre confiance, vos encouragements et vos conseils. Je garderai de très bons souvenirs de cette incroyable expérience même si la prononciation m’a joué des tours…

Grazie mille anche alla mafia italiana formata da Massimo Barressi e Giulia Fois per il vostro supporto, sorriso ogni giorno e per avermi aiutato a migliorare un po'il mio italiano. De la mafia vasca en Bordeaux, eskerrik asko Asier Aristieta por tantísimo

dentro y fuera del laboratorio, tu positividad, tranquilidad y consejos de científico loco me han ayudado muchísimo.

Gracias a todos los compañeros del laboratorio de la UPV entre los que quiero destacar a Luisa Ugedo, Teresa Morera, Sergio Vegas, Mario Antonazzo y Lise Guilmesang. Especialmente gracias Elena Paredes por esos coffes, charlas trascendentales de todo y de nada y por lucir con tanta class la camiseta de Madame Ananas. Gracias también a las Meanas por sus buenas energías y charletas durante los "breaks" que han hecho más amena la escritura de la tesis. No puedo olvidarme de Tere, que además de dejar impoluto el laboratorio era como una amatxu para todos, gracias por esa labor de psicóloga en esa fase final de la tesis.

Enfin, je voudrais spécialement remercier Marco parce que plus qu'un coloc il est devenu ma famille à Bordeaux (avec Couscous bien sûr). Merci pour tous ces moments de complicité qui n'appartiennent qu'à nous, pour ton soutien, ta tranquillité et simplicité, dans le bon sens. Ces moments privilégiés passés avec toi font partie des meilleurs souvenirs de cette thèse.

Gracias ama y Jose por enseñarme a no rendirme nunca, por no soltarme la mano cuando más os he necesitado y por los valores que me habéis transmitido. Aunque esto sea lo que más me cueste escribir…Gracias aita, por quererme tal y como soy, por tu apoyo incondicional, porque contigo puedo ser yo misma, y porque si ya tenía claro que eras imprescindible en mi vida, después de recibir aquella llamada de urgencias en la que te batías entre la vida y la muerte…tengo más claro que nunca que esta aventura no hubiera sido posible si tu no le hubieras vencido la batalla a esa disección de la aorta. Más fuerte que nadie, eres mi ejemplo.

Gracias Ane, Enara, Mery, Miriam y Alba por toda vuestra paciencia, por aguantar mi monotema tesis y por seguir siempre ahí al pie del cañón pese a no verme el pelo en meses. Porque eso es una kuadrilla y lo demás son tonterías. Gracias a mis ZaBurdeas, Virgi y Martis, por vuestras visitas, momentazos y paciencia que también forman parte de estos 3 años.

Gracias al hípster de Neich, porque desde el primer día que el destino nos unió en Burdeos, tuvimos un feeling especial and you know it! Gracias por tus masajitos, tus cocinitas, tus bailes, por cuidarme, por cuidarnos y por ser la mejor compañía posible para un confinamiento. Finalment gràcies Laraland per la teva paciència, per aparèixer

quan menys ho esperava, per ser tu mateixa i estar sempre aqui, encara que sigui desde la distància.

LIST OF ABBREVIATIONS

6-OHDA	6-Hydroxydopamine
AADC	Aromatic amino acid decarboxylase
AAV	Adeno-associated virus
ACSF	Artificial cerebrospinal fluid
AIMs	Abnormal involuntary movements
AHP	After hyperpolarization
AMPA	α-amino-3-hydroxy-5-methyl-4-isoxazolepropionic acid
ANOVA	Analysis of the variance
AP	Action potential
BG	Basal ganglia
ChR2	Channelrhodopsin 2
CNS	Central nervous system
COMT	Catechol-O-methyltransferase
DA	Dopamine
DAT	Dopamine transporters
DBS	Deep brain stimulation
DR	Dorsal *raphe*
DS	Dorsal *striatum*
EPN	Entopeduncular nucleus
EYFP	Enhanced yellow fluorescent protein
FSIs	Fast-spiking inhibitory interneurons
GABA	Gamma-aminobutyric acid
GAD	Glutamic acid decarboxylase
GPe	*Globus pallidus*, external segment
GPi	*Globus pallidus*, internal segment
HCN	Hyperpolarization-activated cyclic nucleotide-gated
hSyn	Human synapsin
Hypoth	*Hypothalamus*
I.C.	Intracranial
I_h	Hyperpolarization-activated current

I.P.	Intraperitoneal
IPSC	Inhibitory post-synaptic current
ISI	Interval interspike
JP	Junction potential
L-DOPA	3,4-Dihydroxy-L-phenylalanine methyl ester
LC	*Locus coeruleus*
LID	L-DOPA induces dyskinesia
MAOB	Monoamine oxidase type B
MAPK	Mitogen-activated protein kinases
MFB	Medial forebrain bundle
MPTP	1-Methyl-4-phenyl-1,2,3,6 tetrahydropyridine
NAc	*Nucleus accumbens*
NALCN	Sodium leak channel
NeuN	Neuronal nuclear antigen
NMDA	N-methyl-D-aspartate
PD	Parkinson's disease
PPN	Pedunculopontine nucleus
PV	Parvalbumin
S.C.	*Subcutaneous*
S.E.M.	Standard error of the mean
SNc	*Substantia nigra pars compacta*
SNr	*Substantia nigra pars reticulata*
SPN	Spiny projection neurons
STN	*Subthalamic nucleus*
STR	*Striatum*
TH	Tyrosine hydroxylase
TRPC3	Transient receptor potential Type 3
TTX	Tetrodotoxin

LIST OF FIGURES

Figure 1.1. Braak's theory progression of α‑synuclein aggregation in PD.

Figure 1.2. Symptomatology associated to development of Parkinson disease.

Figure 1.3. Pharmacological targets in PD.

Figure 1.4. Schematic representation of presynaptic and postsynaptic molecular mechanisms related to LID.

Figure 1.5. BG circuitry in rodents.

Figure 1.6. Molecular markers and projection targets of prototypic neurons and arkypallidal neurons.

Figure 1.7. Schematic representation of the BG motor circuit in normal, parkinsonian and dyskinetic states.

Figure 1.8. The SN is a BG structure located in the midbrain.

Figure 1.9. Topographical distribution of GABAergic and dopaminergic neurons.

Figure 1.10. GABAergic and dopaminergic neurons in the SNr depict different electrophysiological properties.

Figure 1.11. Burst firing pattern of SNr neurons after blockade of DA receptors.

Figure 1.12. Diagram of inputs to SNr neurons.

Figure 1.13. Inputs to SNr neurons in a $Gad2^{cre}$ and $Pvalb^{Cre}$ mice.

Figure 1.14. The SNr output pathways.

Figure 1.15. Schema depicting the effects of stimulating STR-SNr activity under control or parkinsonian conditions.

Figure 1.16. Schematic drawing of $GABA_A$ receptors activation.

Figure 3.1. Chronology of the experimental procedure followed in the three studies for electrophysiology.

Figure 3.2. Mouse preparation for craniotomy.

Figure 3.3. Mechanism of Cre-Lox system.

Figure 3.4. L-DOPA induced dyskinesia in mice with unilateral 6-OHDA lesion of the MFB.

Figure 3.5. Schematic illustration of the patch clamp set-up.

Figure 3.6. The AP analysis.

Figure 3.7. Methods of measuring tonic GABA current shifts.

Figure 3.8. Immunohistochemical validation of the DA depletion.

Figure 3.9. The normalized excitation/emission spectra for the fluorophores used.

Figure 3.10. Optogenetic validation of the transfection and the registered neurons in the SNr.

Figure 4.1. Immunohistochemical identification of SNr neurons in PVcre::Ai9T transgenic mouse line.

Figure 4.2. Distribution of tdTomato and PV immunoreactivity in SNr neurons.

Figure 4.3. Difference in the autonomous pacemaking of PV+ and PV- SNr neurons in sham PVcre::Ai9T mice.

Figure 4.4. Electrophysiological properties of PV+ and PV- SNr neurons, in whole cell configuration depicting differences between both populations of SNr neurons sham PVcre::Ai9T mice.

Figure 4.5. Excitability of PV+ and PV- SNr neurons.

Figure 4.6. Firing properties of PV+ SNr neurons in sham, 6-OHDA lesioned and dyskinetic mice.

Figure 4.7. Electrophysiological properties of PV+ SNr neurons in sham, 6-OHDA lesioned and dyskinetic mice.

Figure 4.8. Excitability of PV+ SNr neurons in sham, lesioned and dyskinetic mice.

Figure 4.9. Firing rate properties of PV-SNr neurons in sham, 6-OHDA lesioned and dyskinetic mice.

Figure 4.10. Electrophysiological properties of PV- SNr neurons in sham, 6-OHDA lesioned and dyskinetic mice.

Figure 4.11. Excitability of PV- SNr neurons in sham, 6-OHDA lesioned and dyskinetic mice.

Figure 4.12. Chronic DA loss affects the firing of both PV+ and PV- SNr neurons without blocking GABAergic transmission.

Figure 4.13. Response of striatal SPNs to optogenetic stimulation.

Figure 4.14. Impact of STR-SNr synapses on the activity of PV+ SNr neurons.

Figure 4.15. Characterization of STR-SNr IPSC short-term plasticity for PV+ neurons in sham and 6-OHDA mice.

Figure 4.16. Impact of STR-SNr synapses on the activity of PV- SNr neurons.

Figure 4.17. Characterization of STR-SNr IPSC short-term plasticity for PV- neurons in sham and 6-OHDA mice.

Figure 4.18. Response of PV-expressing GP neurons to light stimulation.

Figure 4.19. Impact of GP-SNr synapses on the activity of PV+ SNr neurons.

Figure 4.20. Characterization of GP-SNr IPSC short-term plasticity for PV+ neurons in sham, 6-OHDA and dyskinetic mice.

Figure 4.21. Impact of GP-SNr synapses on the activity of PV- SNr neurons.

Figure 4.22. Characterization of GP-SNr IPSC short-term plasticity for PV- neurons in sham and 6-OHDA mice.

Figure 4.23. STR-SNr transmission onto PV+ and GP-SNr transmission onto PV- SNr neurons altered in PD.

Figure 4.24. $GABA_A$ receptor δ-subunit is expressed in the SNr.

Figure 4.25. Expression profile of $GABA_AR$ δ subunit in SNr neurons from PVcre::Ai9T mice

Figure 4.26. Expression profile of $GABA_AR$ $\alpha5$ subunit in SNr neurons from PVcre::Ai9T mice.

Figure 4.27. $GABA_A$-mediated neurotransmission in SNr neurons from PVcre::Ai9T mice.

Figure 4.28. Nigral tonic inhibition is mediated by δ–containing extrasynaptic $GABA_A$.

Figure 4.29. Extrasynaptic $GABA_A$ receptors of PV+ and PV- SNr neurons contain δ-subunits in DA-intact mice.

Figure 4.30. Nigral tonic inhibition is mediated by $\alpha5$-containing extrasynaptic $GABA_A$ receptors in PV- SNr neurons.

Figure 4.31. Impact of 6-OHDA lesion on $GABA_A$-mediated extrasynaptic transmission in SNr neurons from PVcre::Ai9T mice

Figure 4.32. Extrasynaptic $GABA_A$ receptors of PV+ and PV- SNr neurons express δ-subunits in DA depleted mice.

Figure 4.33. Presence of $\alpha5$-subunit in $GABA_A$ receptors of PV+ and PV- SNr neurons in DA-depleted mice.

1. INTRODUCTION

1.1. PARKINSON'S DISEASE

Parkinson's disease (PD) is a common movement disorder seen in neurological practice, but the diagnosis and management is challenging. The diagnosis is clinical and sometimes difficult, considering the large number of motor and non-motor symptoms suffered by these patients. This neurodegenerative disorder is characterized by early prominent death of dopaminergic neurons in the *substantia nigra pars compacta* (SNc) and wide spread presence of Lewy aggregates – called Lewy bodies - containing alpha synuclein (α-syn), an intracellular protein. The medical management of PD patients is also difficult, as pharmacological treatments are limited. So far, L-DOPA (levodopa or 3,4-dihydroxyphenylalanine) is the mainstay of the therapy; however, the long-term treatment leads to highly disabling side effects, which are commonly seen in PD patients few years after the beginning of the treatment.

1.1.1. Epidemiology and etiology

Nowadays PD is considered the second most common neurodegenerative disorder affecting approximately 0.3% of the world population. The estimated incidence for the population older than 60 years is 1% and likewise increases sharply with age to >3% in those older than 80 years (Poewe et al., 2017). It affects men slightly more frequently than women, likely due to the protective effect of female sex hormones (de Lau and Breteler, 2006) and the higher exposure to environmental risk factors. The prevalence also seems to vary depending on race, ethnicity, genotype or environment (Baldereschi et al., 2000; Poewe et al., 2017).

James Parkinson, in his essay ‘‘An Essay on the Shaking Palsy’’ from 1817, described for the first time the disease as a recognized medical condition carefully outlining the major motor signs that are still considered the hallmarks of PD; bradykinesia, rigidity and tremor. The term was coined by William Rutherford Sanders in 1865 and later entered general usage through the influence of Jean-Martin Charcot who first used the term “maladie de Parkinson” or PD in 1875 (Goedert and Compston, 2018).

Over the last few years, the interest of the scientific community in PD has grown noticeably, triggered by the discovery of several causative monogenetic mutations. However, these mutations (α-synuclein, parkin, PINK-1, UCHL-1, LRRK-2, and DJ-1) among others, only account for about 5-15% of all PD patients while the majority of total cases belong to idiopathic or sporadic PD whose causes are largely unknown (de Lau and Breteler, 2006). Exposure to the toxin 1-methyl 4-phenyl 1,2,3,6-tetrahydropyridine (MPTP), the herbicide paraquat or the pesticide rotenone might also be related to increase the risk of PD (Langston et al., 1983; Betarbet et al., 2000).

1.1.2. Neuropathology

Characteristic features of PD include neuronal loss in specific areas of the *substantia nigra* (SN) and widespread intracellular protein (α-syn) accumulation. However, neither the loss of pigmented dopaminergic neurons in the SNc nor the deposition of α-syn in neurons are specific criteria for a conclusive diagnosis of idiopathic PD (Dickson et al., 2009; Halliday et al., 2011). Although the exact cause of the cell death is unknown in PD, the following pathogenic mechanisms have been proposed to explain the cause of this cell loss.

I. Inclusions of α-synuclein

Intraneuronal protein aggregates that are mostly composed of α-syn fibril forms are found in all patients with PD. The existence of specific mutations of SNCA (gene encoding α-syn) cause heritable forms of PD. The α-syn acquires neurotoxic properties during a pathogenic process in which soluble α-syn monomers initially form oligomers, and then progressively combine to form small protofibrils and eventually large, insoluble α-syn fibrils. Intracellular homeostasis of α-syn is maintained by the ubiquitin–proteasome and the lysosomal autophagy system, which are responsible for the protein degradation. Several lines of evidence suggest that impairment of these degradation systems could contribute to α-syn accumulation (Xilouri et al., 2009, 2013). Furthermore, a relationship between increasing age, the most risk factor for PD, and the reduction of lysosomal autophagy system and ubiquitin–proteasome system functions have been proved (Kaushik and Cuervo, 2015).

Indeed, cell culture studies have demonstrated that the impairment of the lysosomal autophagy system leads to increased secretion of α-syn into the extracellular space through exosomes and that endocytosis is a crucial mechanism for up taking extracellular α-syn. Thus, initial α-syn misfolding in a small number of cells could progressively lead to the spread of α-syn aggregates to multiple brain regions, which is consistent with the idea that α-syn pathology gradually engages more brain regions as the disease progresses, as suggested by Braak and colleagues (**Fig. 1.1**). In addition, this model supports the idea that the first sites of α-syn aggregation might be the gut enteric nerves and the olfactory bulb, underlying the presymptomatic or prodromal phase of PD (Stages I and II). The symptomatic phase occurs during stages III and VI once the SN becomes involved (George et al., 2013; Berg et al., 2015; Mahlknecht et al., 2015).

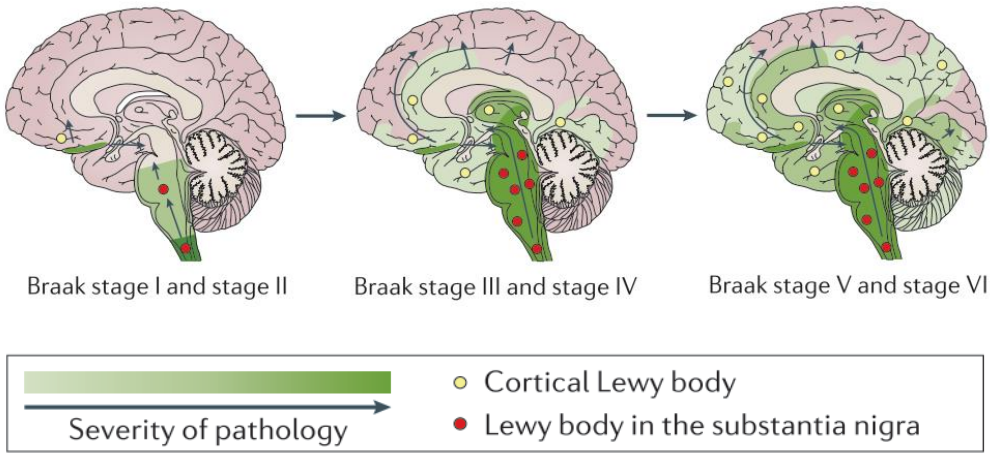

Figure 1.1. Braak's theory progression of α‑synuclein aggregation in PD. The first α-syn aggregates in the central nervous system appear in the anterior olfactory structures and the dorsal motor nucleus of the vague nerve, following by lower raphe system and the *locus coeruleus* in stage II. The SNc is affected together with the amygdala, tegmental pedunculopontine nucleus, and the higher raphe nuclei, among others in stage III. During the stage IV, α-syn spreads to the hippocampal formation and specific cortical areas. Finally, in the last two stages (V and VI), almost the whole cortex is damaged. Image taken and modified from Poewe et al., 2017.

II. Mitochondrial function

Some lines of evidence have reported mitochondrial dysfunction as a key element in the pathogenesis of PD. In several isolated tissues from PD patients, the activity of mitochondrial complex I is reduced (Schapira, 2007; Bose and Beal, 2016).

Indeed, a recent meta-analysis of mitochondrial complex I and IV enzyme activity in patients with PD has shown a strong reduction of these complexes in blood, muscle, and brain (Holper et al., 2019). For example, inhibition of complex I has been reported in platelets (Yoshino et al., 1992) and skeletal muscles (Blin et al., 1994). In the same way, activity of complex IV is also reduced in the frontal cortex (Mizuno et al., 1990) and the SN (Gu et al., 1998) when compared to the controls. Complex II and III activity is also reduced in platelets from PD patients (Haas et al., 1995). Recent publications have revealed the key importance of the correct functioning of molecular pathways governed by proteins and encoded by genes for avoiding the disease development. For example, proteins encoded by PARK2 and PINK1, which are autosomal recessive PD genes, cooperate in the clearance of damaged mitochondria through mitophagy (Pickrell and Youle, 2015).

III. Oxidative stress

An imbalance between the levels of reactive oxygen species produced and the ability of a biological system to detoxify the reactive intermediates, provokes a dangerous state which contributes to cellular damage known as oxidative stress (Dias et al., 2013).

Selective degeneration of the dopamine (DA) neurons of the SNc suggests that DA itself may be a source of oxidative stress (Segura-Aguilar et al., 2014). DA is synthesized from tyrosine by tyrosine hydroxylase (TH) and aromatic amino acid decarboxylase (AADC) which degradation produces hydrogen peroxide (Adams et al., 1972). Importantly, this hydrogen peroxide is also converted by several reactions to produce the highly toxic hydroxyl radical in the presence of the high levels of iron, normally found in the *sustantia nigra pars reticulata* (SNr); (Jenner, 2003). Also, the auto-oxidation of DA produces electron-deficient DA quinones or DA semiquinones (Sulzer and Zecca, 1999). Some studies have proved a regulatory role for quinone

formation in DA neurons in the L-DOPA-treated PD model induced by neurotoxins and in methamphetamine neurotoxicity (Asanuma et al., 2003). DA quinones can modify a number of PD-related proteins and have been shown to cause inactivation of the DA transporter (DAT) and the TH enzyme (Kuhn et al., 1999; Whitehead et al., 2001).

IV. Neuroinflammation

In the past 15 years, a wide range of publications have suggested that inflammation-derived oxidative stress and cytokine-dependent toxicity could contribute to nigrostriatal pathway degeneration and hurry progression of disease in humans with idiopathic PD. The existence of ongoing inflammatory processes contributing to progression of PD is supported by evidence that a transient initiation factor such as toxins, bacterial, or viral infections can affect the cycle of chronic neuroinflammation helping to further promote clustering of activated microglia around DA neurons (McGeer et al., 1988; Hirsch and Hunot, 2009). This phenomenon could contribute to irreversible neuronal dysfunction and cell death.

Furthermore, some authors through subchronic micro infusion of prostaglandin J2 into the SN have been able to mimic pathological features similar to the ones observed in PD, including DA loss in the SNc, microglia and astrocyte activation and behavioral changes (Pierre et al., 2009). However, it remains uncertain whether immune-associated mechanisms are the main cause of the progressive loss of dopaminergic neurons (Hirsch and Hunot, 2009).

1.1.3. Symptomatology

While PD has traditionally been considered a motor system disorder, it is now recognized to be a complex condition with diverse clinical features that include neuropsychiatric and other non-motor manifestations as well as motor symptomatology.

I. Motor symptoms

The cardinal features of PD are mainly motor symptoms and include resting tremor (initially unilateral), bradykinesia (slowness in spontaneous and voluntary movements), and rigidity (muscle stiffness, shuffling gait and postural instability). Tremor and rigidity are considered as "positive" phenomena, while bradykinesia together with postural reflex abolition and the freezing are considered as "negative" phenomena. These latter ones are considered the most disabling problems for PD patients. Tremor is the most common and easily recognized symptom. It is unilateral and occurs at a frequency between 4 and 6 Hz. Rigidity is an increase in passive tone, in flexor and extensor muscle groups that extends through the range of movement. Bradykinesia refers to slowness of movements and is the most characteristic clinical feature of PD. Postural instability is sometimes judged as a cardinal feature, but is non-specific and usually absent early in the disease. This latter feature refers to the gradual development of poor balance, leading to an increased risk of falls (Postuma et al., 2015).

II. Non-motor symptoms

Neuronal dysfunction in PD may start long before the motor features arise, indeed, non-motor symptoms seem to antedate the onset of classic motor symptoms in individuals with PD (**Fig. 1.2**). Non-motor symptoms are common, frequently underappreciated and can be as disabling as the motor symptoms (Sullivan et al., 2007). These non motor fluctuations can be classified in three categories: dysautonomic, mental (cognitive/psychiatric), and sensory/pain.

The most common autonomic dysfunction fluctuations are drenching sweats (64%), facial flushing (44%), oral dryness (44%), dyspnea, dysphagia, and constipation (40%). Mental fluctuations are divided into cognitive fluctuations being slowness of thinking in a 58% the most common indication, while for the psychiatric fluctuations, anxiety (66%), fatigue (56%), irritability (52%), and hallucinations (49%) establish the most frequent signs found in PD patients. The most recurrent sensory fluctuations reported by the patients are akathisia characterized by inner restlessness (54%), contraction (42%), and tingling sensations (38%). Diffuse and neuralgic pain is also reported in 36% and 18% of PD patients, respectively. Most of these symptoms are associated with the "off" state; however, the facial flushing, fatigue, irritability,

hallucinations, akathisia and contraction take place always during the “on” or pre- “on” state (Witjas et al., 2002).

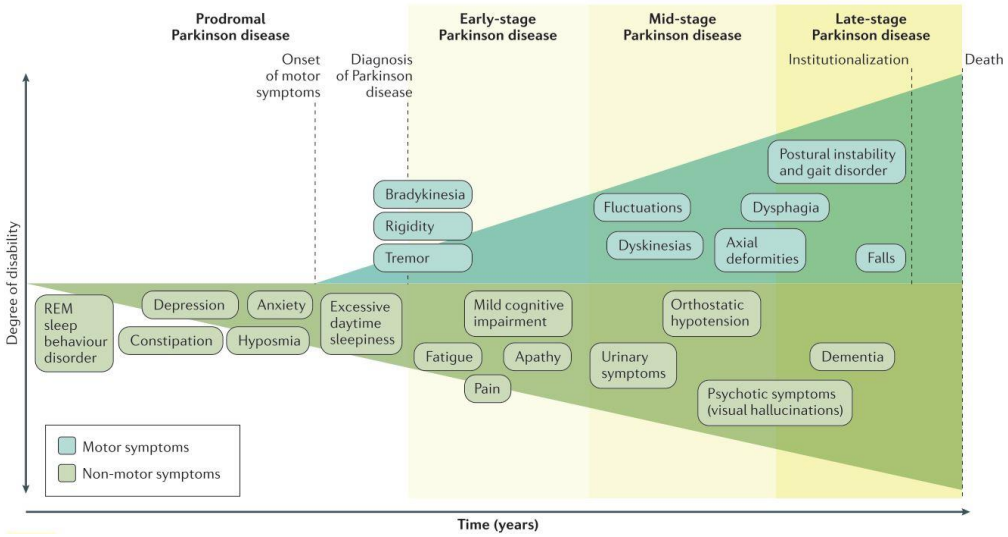

Figure 1.2. Symptomatology associated to the development of Parkinson’s disease. Scheme depicting the presence of non-motor symptoms from the beginning of the illness (prodromal PD) while the diagnosis of the disease does not occur until the early-stage. This stage overlaps with the appearance of motor symptoms. Both, motor and non-motor symptoms became increasingly relevant over the course of the illness. At mid-stage after L-DOPA treatment, motor complications can fluctuate. Image taken from (Poewe et al., 2017).

1.1.4. Treatment

There are no established disease-modifying or neuroprotective therapies for PD (AlDakheel et al., 2014). However, after Parkinson's Essay some therapies have emerged such as the use of solanaceous alkaloids (Ordenstein et al., 1867) or the antimuscarinic drugs (Fahn, 2015) as well as stereotactic neurosurgery helping to restore the muscular functions of thousands victims of PD (Das et al., 1998). Nowadays, after demonstration by Cotzias and colleagues of the remarkable benefit from L-DOPA therapy (Cotzias et al., 1969), the pharmacological treatment is the first election resource for PD patients in the early stages. Generally, the surgery is reserved for patients who do not tolerate the medication, present strong side effects or have small therapeutic benefit/profit.

1.1.4.1. Pharmacological treatment

The replacement therapy with L-DOPA is considered the main therapeutic tool to treat motor complications of PD, which can be used in the majority of patients at any moment of the disease. L-DOPA is the precursor of DA and crosses the blood-brain barrier through a large amino acid transporter. Once in the brain the AADC, transforms L-DOPA into DA (Fahn, 2008). In order to avoid the peripheral transformation of L-DOPA in DA, L-DOPA is often coadministered with inhibitors of the AADC, such as carbidopa or benserazide. Another strategy to enhance the bioavailability and the half-life of L-DOPA is to inhibit its ortho-methylation using catechol-O-methyltransferase (COMT) blockers, as entacapone or opicapone, among others (**Fig. 1.3**). The use of COMT inhibitors is of particular benefit in patients who have developed motor fluctuations (Müller, 2015). L-DOPA induces the improvement of dopaminergic transmission, producing a rapid amelioration of the signs and symptoms of PD. However, its chronic use can induce motor complications known as dyskinesia (see above, section **1.2**).

Inhibitors of the glial enzyme monoamine oxidase type B (MAOI-B), such as selegiline, rasagiline or safinamide (recently approved), are often used alone or in combination with L-DOPA with the proposal to inhibit DA degradation (Rascol et al., 2005). MAOI enhances the availability of DA both endogenous and exogenous to be uptaken by DAT into dopaminergic terminals. Other adjuncts therapies are the DA agonists, such as bromocriptine, pramipexole or ropirinole that mainly act on the postsynaptic D2 receptor family. The use of one of these dopaminergic agonists at the beginning of the treatment could be useful to delay the beginning of the L-DOPA therapy, and the subsequently motor side effects. Currently, amantadine an N-methyl-D-aspartate (NMDA) receptor antagonist is the only pharmacological treatment available for effectively ameliorate L-DOPA-induced dyskinesia (LID) in the clinic. Indeed, an extended-release formulation of amantadine has successfully completed phase III (Fox et al., 2011).

Anticholinergics were the first drugs available for the symptomatic treatment of PD but nowadays, their use is anecdotal. These drugs been used especially in young patients with tremor but they are often poorly tolerated by old patients. The exact mechanism of action of anticholinergic drugs remains undetermined, although they may regulate the striatal DA/acetylcholine imbalance originated by the DA depletion.

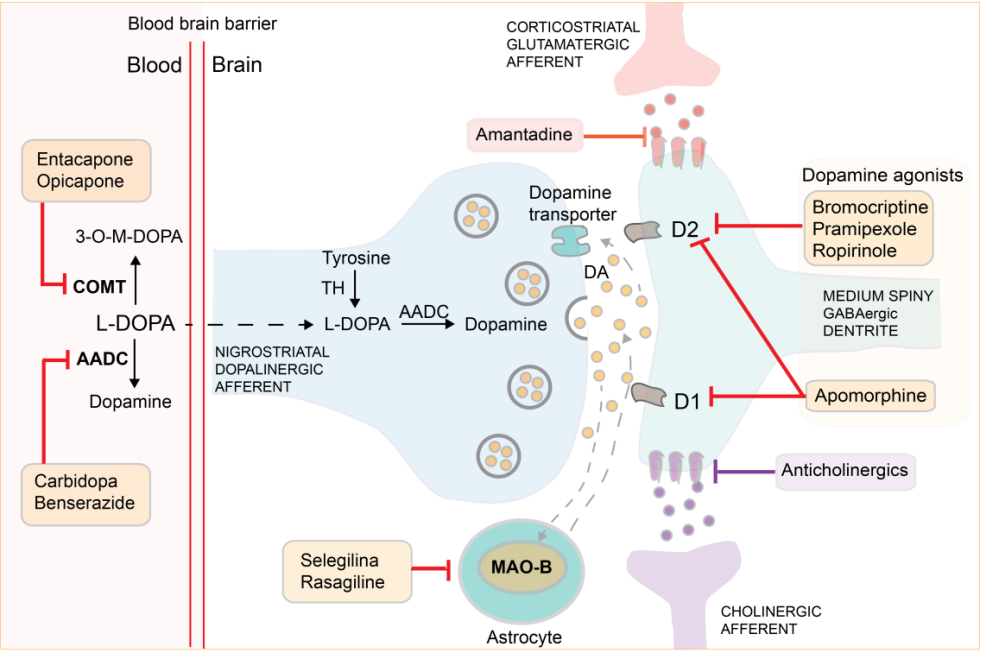

Figure 1.3. Pharmacological targets in PD. Presynaptic targets include L-DOPA replacement combined with peripherally active inhibitors of aromatic amino acid decarboxylase (AADC) or catechol-O- methyltransferase (COMT). At synaptic level, monoamine oxidase type B (MAOB) inhibitors avoid DA degradation. Postsynaptically, DA agonists targets D1 and D2 receptors. Moreover, anticholinergic drugs and amantadine act on postsynaptic receptors for other neurotransmitters in the STR. Adapted from Poewe et al., 2017.

More recently, other non-dopaminergic neurotransmission systems have been studied to develop new drugs for the treatment of PD. The glutamatergic receptor antagonists, adenosine A_{2A} receptors antagonists, opioid receptors antagonists, cannabinoids and nicotinic receptors agonists have all shown interesting results to improve the symptoms of the disease or to induce neuroprotection (Pinna et al., 2005; Freitas and Fox, 2016).

New therapeutic agents that selectively inhibit extra-synaptic α5-containing gamma-aminobutyric acid ($GABA_A$) receptors seem to be a new promising treatment for neurodegenerative disorders. These drugs can improve cognitive function (Atack, 2011) and recovery post-stroke (Clarkson et al., 2010). The extrasynaptic α5-containing $GABA_A$ receptor regulates neuronal excitability through tonic inhibition in the mammalian brain, which is essential for many brain functions such as plasticity and learning (see section **1.4.6**).

1.1.4.2. Other treatments

I. Surgical treatment

The surgical treatment is an alternative option for PD, especially when the pharmacological therapy is not able to improve the symptoms or the prolonged use of L-DOPA causes complications. The surgical procedures include the ablation or lesion and the neurostimulation (deep brain stimulation, DBS) of the *subthalamic nucleus* (STN) or the *internal globus pallidus* (GPi, also called the entopeduncular nucleus in rodents, EPN). Nowadays the stimulation is the preferred surgical procedure, due to, the reversibility of its effects, the low morbid-mortality, the possibility to remove it in case of adverse effects or the discover of better treatments, and the possibility to adjust the parameters in each patient (Starr PA, Vitek JL, 1999; Nilsson et al., 2005). It also has some limitations as fragility of the electrode system, elevated economic cost, difficulty to control or the requirement of batteries for the proper functioning (Doshi, 2011; Falowski et al., 2015).

Although there are no studies demonstrating the clinical advantages of the STN over the GPi (Cury et al., 2015), this nucleus is often the elected nucleus for DBS in patients with advanced disease (Krack et al., 1997; Krause et al., 2001). Both lesions and DBS of these targets can be very effective in improving a number of motor symptoms. Surgery is however less effective at treating other symptoms including gait disturbances, freezing, balance, speech, and cognition (Collomb-Clerc and Welter, 2015). For this reason, currently in addition to the GPi and STN, there has been interest in exploring other targets to improve these other symptoms, such as the pedunculopontine nucleus (PPN) for gait improvement (Stefani et al., 2007) and nucleus basalis of Meynert for cognition (Gratwicke et al., 2018).

I. Cell transplant

In 1987 the first fetal tissue of the ventral midbrain was implanted in PD patients, showing cell survival and DA neuron functionality even 20 years after implantation in some cases (Barker et al., 2013). However, some problems have rendered the cell transplant unsuccessful, such as ethical questions, the way to prepare the fetal tissue or the surgical procedure as well as the difficulty to scale the results (Barker et al., 2017).

Two studies have proposed that cell transplant does not produce any significant improvement of the symptoms in PD patients and that these patients develop dyskinesia. Both studies have also demonstrated that the *striatum* (STR) is re-innervated by the transplanted cells (Olanow et al., 2003; Freed et al., 2010).

Other types of transplants of DA releasing cells have been proposed, such as autotransplantation of human caroid cell aggregates (Arjona et al., 2003) or transplantation of embryonic porcine mesencephalic tissue in PD patients (Schumacher et al., 2000). However, the cell types that have gained importance in recent years are the human pluripotent stem cells, which are derived from early pre-implantation embryos or reprogrammed adult somatic cells, and they can differentiate into reliable midbrain dopaminergic neurons (Kriks et al., 2011; Kirkeby et al., 2012).

II. Genetic treatment

The advance in the knowledge of the genes implicated in the development of the PD is very important information to discover the proteins related to the pathogenesis of this neurodegenerative disease, and to find new targets for the treatment. In 2018, at least 5 major autosomal dominant genes, have been identified (Ferreira and Massano, 2017). The most notable of these are mutations are polymorphisms of Leucine-rich repeat kinase 2 (Milosevic et al., 2009) and the glucocerebrocidase gene which encodes a lysosomal enzyme involved in sphingolipid degradation in the context of idiopathic PD (O'Regan et al., 2017).

1.1.5. L-DOPA induced dyskinesia

As mentioned before, dopaminergic replacement therapy has been the gold standard treatment for PD patients since its introduction in the late 60s (Cotzias, 1967). Once in the brain, L-DOPA can be converted to DA in the dopaminergic neurons, but also within serotonergic fibers in the STR and SNr (Yamada et al., 2007a) and to noradrenaline in noradrenergic neurons (Mercuri and Bernardi, 2005). The standard oral L-DOPA therapy is well established in the clinic and provides general satisfactory symptomatic relief. However, long-term L-DOPA treatment produces motor fluctuations and shortens the duration of the antiparkinsonian ("wearing off" phenomenon). Initially,

these fluctuations are predictable but they can become unpredictable with sudden switches between mobility and immobility ("on-off" phenomenon); (Nutt J.G, 2001). Motor complications occur in about 50% of patients with PD who received L-DOPA for more than 5 years, and in as many as 100% of patients with young-onset disease (Golbe, 1991; Aquino and Fox, 2015).

LID has a variety of clinical forms, including dystonic and choreic movements. The most common type of dyskinesia is named "peak-dose" dyskinesia and appears when plasma and brain concentrations of L-DOPA and DA are high. This type of dyskinesia is often choreiform in nature, although they can also manifest as dystonia and other movement disorders. The less common form of dyskinesia, so-called "biphasic dyskinesia", can appear at or just before the onset of the on response, disappear during the on period, and re-emerge as the off period begins. Biphasic dyskinesia is typically comprised of abnormal dystonic postures mainly affecting the legs (Olanow et al., 2006). With disease progression, delivery of a dose of L-DOPA that provides both a satisfactory antiparkinsonian effect and avoids dyskinesia becomes increasingly difficult. Although the cause of these side effect are not completely understood, the development of LIDs has been associated with several factors such as earlier age at onset of L-DOPA treatment, L-DOPA total exposure, sex and possible genetic factors (Zappia et al., 2005).

The repeated pulsatile treatment with dopaminergic drugs, mainly oral L-DOPA therapy, and the degeneration of the nigrostriatal dopaminergic system (Olanow et al., 2009) are condition *sin equanon* for developing LID. The nigrostriatal degeneration induces an upregulation of the dopaminergic receptors in the STR and L-DOPA therapy acts on supersensitive dopaminergic receptors, in particular D1 and likely on D3 receptors (Bézard et al., 2003; Aubert et al., 2005). At the level of the basal ganglia (BG), a principal abnormality responsible for the expression of "peak-dose" dyskinesia is the overactivity of the direct striatal output pathway from the STR to the EPN and SNr (Bezard et al., 2001). Some authors have proposed that LIDs are related to a reduced neuronal activity of the BG output nuclei (Crossman, 1987; Obeso et al., 2008) and the STN in MPTP-treated monkeys (Papa et al., 1999) and PD patients (Merello et al., 1999). Interestingly, the GPi lesion reduces LID, although according to the classic theory, it should facilitate LID by reducing the efferent activity from the GPi to the motor *thalamus*; (Marsden and Obeso, 1994; Jankovic et al., 1999). Another recent studies have shown that optogenetic activation of the STR, can induce dyskinesias in the 6-

hydroxydopamine (6-OHDA) rat model of PD (Hernández et al., 2017; Keifman et al., 2019).

Apart from the dopaminergic, non-dopaminergic systems also contribute to the expression of LID, among others, glutamatergic, endocannabiniod, adrenergic and serotonergic systems (Brotchie, 2005; Calabresi et al., 2008; Fox et al., 2009). A study looking at the metabolic activity (gene expression of cytochrome oxidase subunit I, COX I) of several BG nuclei in rats revealed that the 6-OHDA lesion increases COX I metabolic activity in the GP, STN, SNr and EPN (Salin et al., 2002). In contrast, the L-DOPA chronic treatment reduced this increased activity to control values in the GP, STN and SNr (Lacombe et al., 2009). Nevertheless, the lesion of the EPN does not reverse the shortening in the duration of the L-DOPA-induced rotational response nor the metabolic activity of the GP, SNr and STN, but reduces the expression of the preproenkephalin in the STR that is increased in LID (Périer et al., 2003).

1.1.5.1. Molecular mechanisms underlying L-DOPA-induced dyskinesia

The DA depleted state and the chronic L-DOPA treatment produce several molecular modifications. Promising advances in experimental research focusing on LID have recently emerged, including identification of the differential role of presynaptic versus postsynaptic mechanisms, the distinct role of DA receptors subtypes, and the role of ionotropic and metabotropic glutamate receptors and non-dopaminergic neurotransmitter systems.

A presynaptic mechanism related to the development of LID is explained as consequence of an abnormal DA metabolism. Nigral neuronal projections to the STR which is responsible for the synthesis and the storage of the DA are reduced with the progression of the PD. Thus, the loss of these neurons produces a dysregulation of the DA metabolism in the STR which is innervated by serotonergic fibers. These serotonergic fibers can transform the L-DOPA to DA that normally is re-uptaken by nigral dopaminergic fibers projecting to the STR. However, in PD, due to the loss of nigral projections to the STR, DA cannot be re-uptaken, producing an increase of the striatal DA concentration (Abercrombie et al., 1990; Carta et al., 2007; Navailles et al., 2010). These large fluctuations in extracellular DA concentrations can then produce aberrant postsynaptic responses. Besides, endocannabinoid CB1 receptors and

metabotropic glutamate receptors expressed in striatal glutamatergic terminals take part in the presynaptic mechanisms (Calabresi et al., 2010); (**Fig. 1.4**).

At the postsynaptic level, several molecular mechanisms seem to be involved including the downstream cascades initiated by NMDA receptor activation, DA D1 receptors, and metabotropic glutamate receptors. Briefly, the activation of NMDA and metabotropic glutamate receptors triggers an increase of intracellular calcium concentrations which consecutively modulate the RAS/RAF/MEK/ERK pathway whose activation results in a number of different physiological outcomes (Crittenden et al., 2009). The blockade of NMDA receptors by amantadine (weak NMDA receptor antagonist) has a long-term antidyskinetic efficacy (Wolf et al., 2010). It is also worth to mention that L-DOPA through the activation of D1 receptors, triggers profound alterations in the activity of three molecular markers for LID, known as ΔFosB, DARPP-32, and ERK1 and ERK2 (Santini et al., 2007; Westin et al., 2007; Nicholas et al., 2008; Berton et al., 2009). To sum up, D1 receptor inactivation blocked the development of dyskinesia; this genetic manipulation also reduced the associated molecular changes in the lesioned STR, such as the increased expression of FosB and dynorphin, the phosphorylation of ERK, and H3 phosphoacetylation. Conversely, inactivation of the D2 receptor had no major effect on the behavioural or molecular response to long-term treatment with L-DOPA (Picconi et al., 2003).

Data from a recent experimental study showed that none of the parameters studied (such as genetic variations, delay of treatment onset after lesion, or time of day of the drug treatment) directly affected LID, proposing a complex combination of individual factors interacting to regulate the onset and development of abnormal movements in some patients, but not in others (Monville et al., 2009).

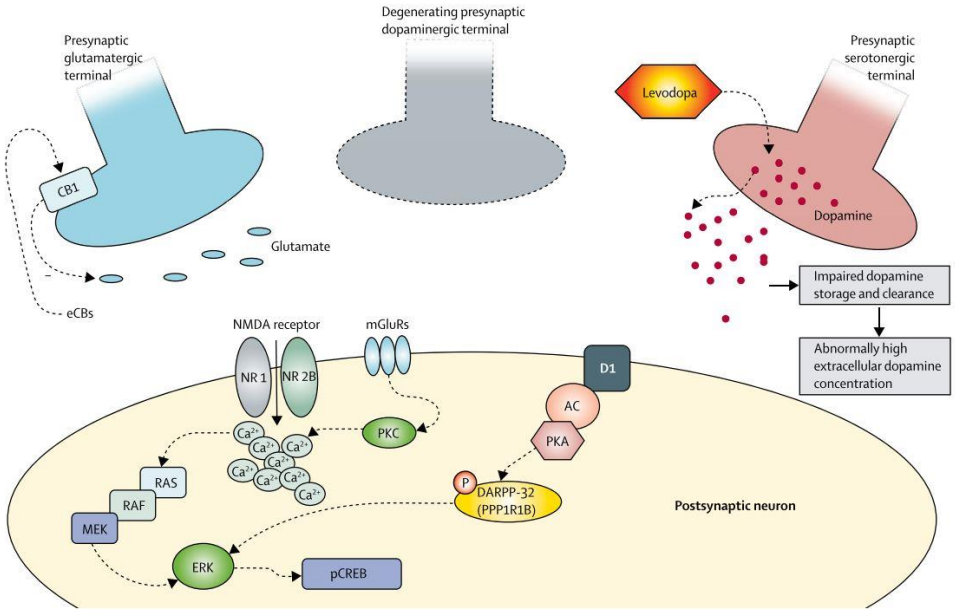

Figure 1.4. Schematic representation of presynaptic and postsynaptic molecular mechanisms related to LID. After dopaminergic terminals denervation, L-DOPA administration produces large fluctuations in extracellular DA levels, due to alterations in the metabolism of DA. In this situation, the increased DA levels observed after L-DOPA administration induce the postsynaptic molecular modifications involved in the development of LID. List of abbreviations: AC:adenylyl cyclase; Ca2+:calcium ion; CB1:endocannabinoid receptor 1; pCREB:cAMP response element-binding protein; D1:DA receptor; PPP1R1B:protein phosphatase 1 regulatory (inhibitor) subunit 1B; eCB:endogenous cannabinoid; ERK:extracellular signal-regulated kinase; Glu:glutamate; mGluR:metabotropic glutamate receptor; PKA:protein kinase A; PKC:protein kinase C. Image taken from Calabresi et al., 2010.

1.2. BASAL GANGLIA

1.2.1. Anatomy and general functions of basal ganglia

The BG are a collection of organized subcortical nuclei which connect to the motor cortex, specific areas of premotor and prefrontal cortex through the *thalamus* (Albin et al., 1989). The BG circuit is involved not only in planning and execution of movements but also in associative (cognitive) and limbic (emotional) loops (Middleton and Strick, 2000).

The principal structures within the BG, in rodents, are the *globus pallidus* (GP), STR, EPN, STN, SNc, and SNr. In humans and primates, the GP is divided into two parts: the GPe and the GPi. In rodents, the EPN and the GP are homologous structures for the GPi and GPe, respectively (Nambu, 2007). The STR and the STN constitute the input areas of the BG and receive projections from cortical and subcortical areas, while the EPN and the SNr are the main output structures of the BG. According to the classic model (Albin et al., 1989), three different pathways have been described in the BG: (1) the hyperdirect pathway, which connects the cortex with the BG output nuclei (EPN/SNr) through the STN; (2) the direct pathway, which directly connects the STR to the BG output nuclei, and (3) the indirect pathway, which connects the STR and the BG output nuclei through the GPe and the STN (Bolam et al., 2000; Nambu et al., 2002; Wichmann and Dostrovsky, 2011). In addition to these three pathways, new connections between BG nuclei have been described, such as GP-SNr inputs (Smith and Bolam, 1991) the reciprocally-connected GP-STN loop (Bevan et al., 2002b), the GP-STR pathway (Mallet et al., 2012, 2016) and bridging collaterals from direct-pathway spiny projection neurons (dSPN) to the GP (Kawaguchi et al., 1990; Cazorla et al., 2014).

A distinctive feature of BG organization is that all efferent projections (except for those originating in the STN and SNc) mainly use the inhibitory neurotransmitter, GABA. Glutamate, however, is vital to regulate information processing in the BG, being the neurotransmitter used by both cortico-striatal and thalamo-cortical projections, and by efferent projections originating in the STN (Eid and Parent, 2016). Indeed, the DA innervation plays a key role in the control of BG functions through modulation of cellular and synaptic properties at each stage of the BG network (Mallet et al., 2019; **Fig 1.5**).

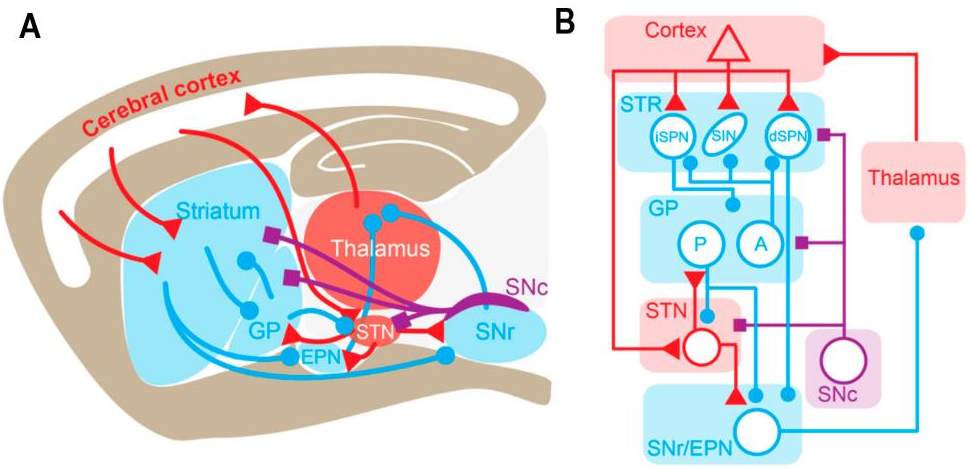

Figure 1.5. BG circuitry in rodents. A: Sagittal section of the rodent brain representing the main connections of the BG network. **B:** Corresponding anatomical-functional scheme adapted from the Albin model of the BG (Albin et al., 1989). Dopaminergic, GABAergic, and glutamatergic projections and nuclei are depicted in blue, purple and red, respectively. SNc: *substantia nigra pars compacta*; dSPN: direct-pathway spiny projection neuron; SIN: Striatal interneurons; iSPN: indirect-pathway spiny projection neuron; GP: *globus pallidus*; A: arkypallidal neuron; P: prototypic neuron; STN: *subthalamic nucleus*. SNr: *Substantia nigra pars reticulata*; EPN: *entopeduncular nucleus*. From Mallet et al., 2019.

To summarize, thanks to intrinsic and extrinsic regulations, the neurons of the SNc release DA in a tonic or phasic manner and ensure the proper functioning of the BG network. In normal state, activation of cortico-striatal projections leads to the inhibition of the EPN/SNr *via* the direct pathway. This produces a reduction of the GABAergic inhibitory input from the BG output nuclei to the *thalamus* increasing the excitatory activity over the motor cortex, in turn facilitating the movement. In contrast, activation of cortico-striatal projections leads to the reduction of GP activity. The GP induces a lower inhibitory effect over the STN. Thus, the STN increases the excitatory glutamatergic activity over the BG output nuclei. These EPN/SNr nuclei increase the inhibition over the *thalamus*, inhibiting the thalamo-cortical connections and movement execution. This effect is mediated *via* the indirect pathway. Both pathways activity may be necessary for the development of a normal movement pattern (**Fig. 1.7A**). Therefore, it is known that the slightest dysfunction in DA transmission lead to network disturbances and is the origin of multiple pathologies such as PD when there is a lack of DA in BG, or Huntington's disease in case of excess of DA. LID has consistently been related to excessive DA release.

1.2.2. Basal ganglia network

I. Striatum

The STR is the major entry nucleus of the BG and the principal recipient of cortical inputs. In this GABAergic nucleus, the majority (~95% of total striatal neurons) are spiny projection neurons (SPNs). Despite their morphological similarities, SPNs can be divided into two subpopulations based on their neurochemical content and axonal projection sites. The first type expresses D1 receptors (D1Rs) and contains the neuropeptides substance P and dynorphin DYN, besides; they are activated by DA and innervate BG output neurons of the SNr and EPN in a monosynaptic manner (Gagnon et al., 2017). These neurons represent the direct pathway (dSPNs) of the BG (Gerfen et al., 1990; Smith et al., 1998). DA favors striato-nigral (STR-SNr) activation which pauses SNr neuron tonic firing, disinhibiting the *thalamus*, brainstem, and superior colliculus (SC); (Deniau et al., 2007) and facilitates the movement (Gerfen and Surmeier, 2011; Freeze et al., 2013). The second type of SPN expresses D2 receptors (D2Rs), contains enkephalin and instead is inhibited by DA. They are part of the indirect pathway (iSPNs) and project to BG output nuclei via a polysynaptic route involving the GP and STN. The net effect of activating the indirect pathway is to increase the activity of EPN/SNr neurons and consequently inhibit the *thalamus* which in turn disinhibits motor areas. However, this dual opposing physiological effect is under revision because there is growing experimental evidence indicating that both pathways are co-activated before movement initiation (Cui et al., 2013).

The iSPNs display higher excitability than dSPNs at rest (Gertler et al., 2008). The membrane potential of SPNs displays shifts between a very negative resting state (down state) and depolarizing *plateaus* (up states), which are due to excitatory cortical inputs. Because striatal SPNs fire action potentials (AP) only during the up state, these plateau depolarizations have been perceived as “enabling events” that allow information processing through cortex-BG circuits (Cepeda et al., 2008). SPNs neurons exhibit in their membranes a subtype of potassium channels (the inward rectifiers, Kir) which in acute *in vitro* preparations, where active synaptic input is greatly reduced, holds the membrane potential of SPNs hyperpolarized (Wilson, 1993).

The STR also counts with a diverse array of interneurons representing only the 5% of all neurons, but being essential for striatal function (Gittis and Kreitzer, 2012). These interneurons are divided into cholinergic and three subtypes of GABAergic

interneurons that differ in electrophysiological properties and neurochemical content (Kawaguchi, 1993; Tepper, 2010). Cholinergic interneurons (1-3%), also known as tonically active interneurons, extend their axonal arbors throughout the whole STR playing a key role in the control of striatal function (Zhou et al., 2002; Bonsi et al., 2011) and LID (Bordia et al., 2016). GABAergic interneurons are immunoreactive for Parvalbumin (PV+) and contrary to SPNs, they issue 5-8 aspiny, often varicose, dendrites (Tepper, 2010). Indeed, the fact that PV+ interneurons receive substantial monosynaptic input from the cortex, contrary to spiny cells which receive only one or two synapses, accounts for the greater responsiveness of PV+ interneurons to cortical stimulation compared to SPNs (Mallet et al., 2005). Electrophysiological properties of PV+ interneurons have been well described showing their fast-spiking capability, hyperpolarized resting membrane potential and narrow AP with rapid and large amplitude (Koós and Tepper, 1999; Taverna et al., 2007). These fast-spiking interneurons are important for mediating feed forward inhibition of spiny neurons (Cowan et al., 1990; Tepper, 2010). Besides, DA depletion seems to affect their firing properties *in vitro* (Salin et al., 2009; Gittis et al., 2011) and L-DOPA treatment failed to normalize their fast-spiking activity (Hernandez et al., 2013).

II. Globus pallidus

The GP has been long considered a simple relay nucleus in the indirect pathway receiving inputs from the STR (Parent and Hazrati, 1995; Kita et al., 1999). However, recent investigations have revealed the molecular and functional complexity of the GP identifying different subpopulations with distinct physiological properties and anatomical projections (Parent and Hazrati, 1995; Mallet et al., 2012; Mastro et al., 2014; Saunders et al., 2015; Oh et al., 2017).

At least two cell types have been identified in the GP. On one hand, prototypic neurons represent more than 70% of the total GP neurons, express the transcription factor Nkx2.1 and show a regular fast-spiking discharge *in vitro.* Besides, a large proportion of prototypic neurons (3/4 approximately) are also PV+ in addition to Nkx2.1. On the other hand, arkypallidal neurons (Mallet et al., 2012) represent between 15 to 28% of GP neurons in mice and rats, respectively (Abdi et al., 2015; Dodson et al., 2015). Arkypallidal neurons express FoxP2 and display a low and irregular firing discharge. All arkypallidal neurons co-express the NPas-1, but a small proportion of

prototypic neurons also express it (Dodson et al., 2015; Hernández et al., 2015); (**Fig.1.6**).

Prototypical and arkypallidal subpopulations also differ as for their anatomical projections. While prototypic neurons project to downstream nuclei (the STN, SNr and EPN) and the STR (Abdi et al., 2015; Saunders et al., 2016), arkypallidal neurons are characterized by their exclusive and massive axonal striatal innervation (Mallet et al., 2012; Hegeman et al., 2016). These results revealed that not only the arkypallidal neurons but nearly all of the prototypic neurons project to the STR with numerous axon varicosities (Fujiyama et al., 2016). A recent study has also confirmed that GP-PV+ neurons, which represent ~40 - 50% of the GP neurons, provide the major axonal arborization to the STN and the SNr/SNc (Saunders et al., 2016). This result along with the finding of Mastro and colleagues demonstrating that movement, in DA depleted mice, can be persistently rescued by manipulations of PV-GPe neurons highlights the functional importance of this cell-type, and potentially of the GP-SNr pathway (Mastro et al., 2017).

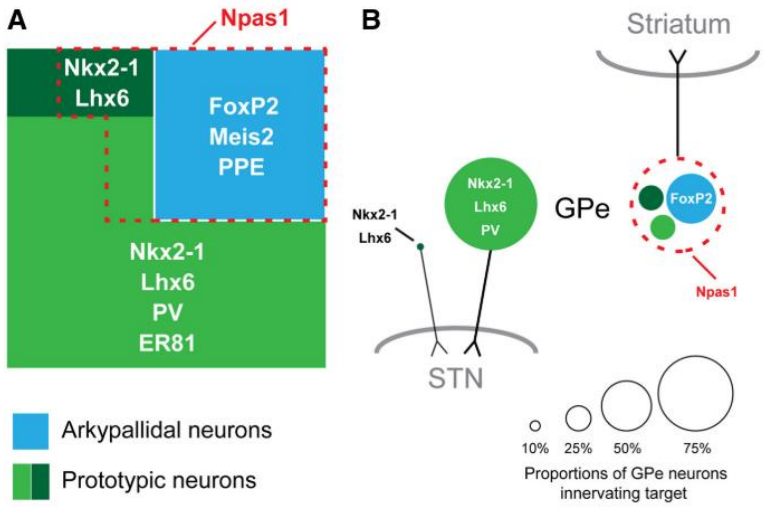

Figure 1.6. Molecular markers and projection targets of prototypic and arkypallidal neurons. A: Summary of the two major GABAergic cell types in the rat GP. Arkypallidal neurons (blue) and prototypic neurons (light and dark greens) represented respect to all GABAergic GP neurons. The molecular markers seen in both subtypes are also indicated. **B:** Diagram of the major GP cell types innervating the STN (left) or dorsal *striatum* (right). Whereas the majority prototypic neurons innervate the STN, arkypallidal neurons seem to innervate the STR. Image taken from Abdi et al., 2015.

III. Subthalamic nucleus

The STN is the only glutamatergic nucleus of the BG and is considered to be one of the main regulators of motor function. It plays a fundamental role within BG circuitry (Parent and Hazrati, 1995). The different functional circuits we mentioned before, such as the motor, associative and limbic territories of the BG are also found in the STN. The primate STN is subdivided into several areas, one related directly to motor tasks and others to emotional and cognitive functions (Haynes and Haber, 2013).

Briefly, the principal afferent connections to the STN arise from the cortex and GP. Although the most important cortico-STN projections originated from the primary motor cortex, the STN also receives projections from the supplementary motor area and the dorsal and ventral premotor cortex (Nambu et al., 2002). The GABAergic projections from GP are one of the most important afferents to the STN as they may innervate all STN neurons (Bevan et al., 2002a). Additionally, the STN receives glutamatergic projections from the *thalamus*, dopaminergic projections from the SNc, cholinergic projections from the PPN and serotonergic projections from the dorsal raphe nucleus (DR), for review see (Hamani et al., 2004). On the other hand, STN neurons principally project to the GP, EPN and SNr, although some axons also reach the SNc (Benarroch, 2008). This STN-SNc connection seems important for controlling DA release in the SNc (Smith et al., 1990b). The STN also sends projections and controls the activity of the STR, PPN and the ventral tegmental area (VTA) (Smith et al., 1990a; Parent and Hazrati, 1995).

Activation of STN neurons, induces excitatory postsynaptic currents or potentials in SNr GABA neurons (Shen and Johnson, 2006; Ding et al., 2013). Thus, STN neuron excitation can drive SNr GABA neurons into burst firing, which indeed seems to be an emerging sign in rat PD models (Murer et al., 1997; Tseng et al., 2001; Ding et al., 2013). In contrast, STN lesion and functional inhibition is able to reduce oscillatory firing and normalize the firing pattern in the SNr (Murer et al., 1997; Tseng et al., 2001). Indeed, STN-DBS can also induce dyskinesias in both rodent PD models (Boulet et al., 2006; Oueslati et al., 2007) and patients (Benabid et al., 2009).

IV. Entopeduncular Nucleus

The EPN, as well as the SNr, is one of the output nuclei of the BG. The EPN is subdivided in rostral and caudal sections composed of somatostatin-positive, PV+ neurons (Rajakumar et al., 1994; Hontanilla et al., 1997) and a third neuronal population, negative for both SOM and PV (Miyamoto and Fukuda, 2015; Wallace et al., 2017). Whereas SOM+ EPN neurons project to the lateral habenula participating in the evaluation of the motor outcome, PV+ EPN neurons innervate the motor *thalamus* and control motor program selection (Stephenson-Jones et al., 2016).

Like the SNr, the EPN receives convergent inputs from the striatal direct-pathway, the GP, and the STN (Bevan et al., 1997). Pallido-entopeduncular (GP-EPN) and striato-entopeduncular (STR-EPN) synapses display the same properties as STR-SNr and GP-SNr synapses (Lavian and Korngreen, 2016); (see section **1.4.4**). The impact of DA loss on these synapses has not been further studied, but it is thought that DA depletion facilitates GP-EPN synapses and depresses the STR-EPN ones, generating an imbalance between direct and indirect pathway GABAergic inputs in the EPN (Mallet N et al., 2019).

V. Substantia nigra pars compacta

Located at the level of the midbrain, the SN is divided into two parts anatomically and functionally distinct. The SNc, located at the dorsal level, is a dense area containing dopaminergic neurons, which regulates the activity of the whole BG network. The SNr has a much lower neuronal density and contains mainly GABAergic projection neurons.

The SNc, along with the VTA, is the main source of DA in the BG. Axons from these DA neurons provide rich innervation of the distant striatal complex (Matsuda et al., 2009). Within the BG, the functional balance between the direct and indirect pathways is controlled by DA, which is principally released by the terminals of SNc neurons. However an important challenge for the ‘‘classical’’ model of the BG circuitry, has been the discovery that the STR is not the only nucleus receiving connections from the SNc, as the STN and GP are also innervated (Hassani et al., 1996; Cossette et al., 1999). Specifically, two types of nigrostriatal dopaminergic fibers have been described,

ones that travel directly to the STR with poorly emitting collaterals and the others arborized profusely in various extra striatal structures, including the GP, the EPN and STN, and branched only sparsely in the STR (Gauthier et al., 1999).

Regarding afferences, the SNc is the target of GABAergic projections from the STR and GP (Smith and Bolam, 1989; Gerfen, 1985). It also receives glutamatergic afferents from the STN and PPN (Kita and Kitai, 1987). Especially in rats, the SNc is the structure of the BG receiving the strongest cholinergic inputs from the PPN (Mena-Segovia et al., 2008). It is important to mention that collaterals of the GABAergic SNr neurons have also been reported to affect the activity of the dopaminergic SNc neurons (Tepper et al., 1995), which constitutes an ultra-short inhibitory pathway.

In the SNr, DA cells constitute nearly the 20% of the total population (González-Hernández and Rodríguez, 2000). These DA neurons are electrophysiologically different from SNr GABAergic cells. During intracellular and patch-clamp recordings, the AP of DA-nigral cells, is followed by an after-hyper polarization, mainly due to calcium-activated potassium conductance (Shepard and Bunney, 1991). Some additional distinct characteristics of dopaminergic neurons is their regular spontaneous firing activity (1–3 Hz) when recorded in slices (Grace and Onn, 1989) and the noticeable sag potential that they exhibit after hyperpolarization (AHP) as a result of a prominent time and voltage dependent conductance (Mercuri et al., 1995).

In general, the firing rate of DA neurons is negatively modulated by GABAergic inputs coming from the STR, GP, collaterals from the SNr and SNc interneurons. On the contrary, excitatory inputs, derives from the glutamatergic projections of the medial prefrontal cortex, STN, PPN and the lateral hypothalamic area. Recently, a glutamatergic neuronal population has also been described within the VTA (Yamaguchi et al., 2015) that may provide a local glutamatergic input to dopaminergic neurons. The dopaminergic cells also receive serotonergic projections from the medial and dorsal raphe nuclei and noradrenergic inputs from the *locus coeruleus* (for review, see Blandini et al., 2000). All these neurotransmitters control firing activity and subsequent local and distal DA release. The spontaneous firing rate of SNc DA neurons, leading to stable striatal DA concentration and continuous activation of striatal DA receptors are essential for normal BG functions (Bottcher, 1975).

1.2.3. Basal ganglia motor circuit in Parkinson's disease and L-DOPA induced dyskinesia

In PD there is a degeneration of neuromelanin-containing neurons of the SNc which results in a loss of DA in the STR. This produces a reduction of the activity of dSPN, and in consequence, a reduction of the inhibition of these striatal neurons over the EPN/SNr. On the other hand, iSPN become hyperactive leading to inhibition of GP neurons, hyperactivity of the STN, and in consequence, excessive release of glutamate in the EPN/SNr. The hyperactivity of the output nuclei produces hypoactivity of the thalamic-cortical projections causing bradykinesia in PD patients (Albin et al., 1989; Galvan and Wichmann, 2008; Wichmann and Dostrovsky, 2011); (**Fig. 1.7B**).

External administration of L-DOPA and LID expression induce the opposite changes in the BG circuits. It is commonly assumed that L-DOPA induces dyskinesia by excessive inhibition of iSPN with the subsequent disinhibition of the GP. This disinhibition leads, in turn, to overinhibition of the STN, reduced STN excitatory drive and hypoactivity of EPN/SNr output neurons. Moreover, enhanced sensitivity of D1 DA receptors has been described in dyskinetic rodents (Feyder et al., 2011; Murer and Moratalla, 2011) which leads to an overinhibition of BG output nuclei. The net effect of these imbalances would be a hyperactivity of the thalamic-cortical projections, which is associated with chorea and dystonia also seen in conditions as Huntington's disease (Crossman, 1987; Bezard et al., 2001); (**Fig. 1.7C**).

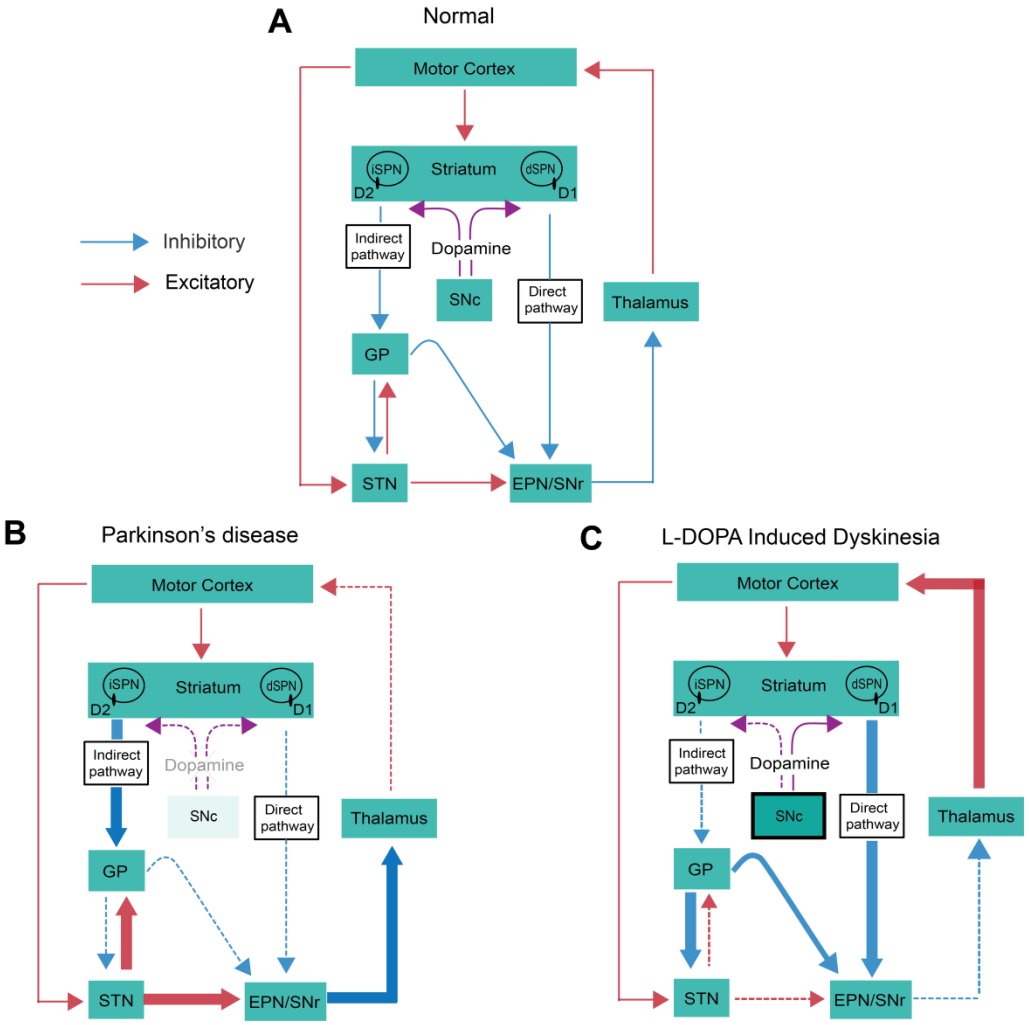

Figure 1.7. Schematic representation of the BG motor circuit in normal, parkinsonian and dyskinetic states. Dopaminergic, GABAergic (inhibitory), and glutamatergic (excitatory) projections are depicted in purple, blue, and red, respectively. The thickness of the arrows corresponds to their presumed activity. Abbreviations: SNc, *substantia nigra pars compacta*; dSPN, direct spiny projection neurons; iSPN, indirect spiny projection neurons; D1 and D2, DA receptor subtypes; GP, *globus pallidus*; STN, subthalamic nucleus; EPN: entopeduncular nucleus; SNr, *substantia nigra pars reticulata*.

Although the classical theory of Albin and colleagues explains some of the changes observed in the BG from PD and LID, it has also several limitations. Remarkably, it does not provide an adequate explanation for the two cardinal features of PD, rigidity and tremor. Despite proposing hypoactivity of GP cells, experimental data from animal models and patients demonstrated that GP activity is not changed or increased in PD (Vila et al., 2000; Breit et al., 2007). According to the model, it is expected that lesion or DBS of the GPi produced dystonia in PD patients, however this phenomenon is not observed in these patients (Lanciego et al., 2012). In fact, these two procedures are effective for ameliorating LID (Laitinen et al., 1992; Volkmann et al., 1998). Apart from these discordances some changes in neuronal activity within the BG often fits the model (Lanciego et al., 2012).

I. Changes in neuronal activity in the basal ganglia in Parkinson's disease

Chronic loss of DA results in significant changes in the firing rates of extra striatal BG nuclei. The classical model predicts that parkinsonian motor features are related to increased neuronal firing frequency of BG output neurons, whereas LID is associated with decreased firing of these neurons.

In PD, the model suggests that DA depletion leads to increased neuronal firing activity of STN neurons and reduced firing of dSPN. These changes combine to result in excessive firing of GPi/EPN and SNr neurons, with consequent overinhibition of the *thalamus*, reduced activation of cortical motor regions, and resultant parkinsonian motor features. This is supported by neurophysiologic studies in patients with PD and MPTP monkeys showing increased neuronal firing rates in the GPi/SNr and STN (Albin et al., 1989; DeLong, 1990; Bergman et al., 1994; Obeso et al., 2002). The loss of DA, decreases activation of striatal D1-receptors which leads to a decrease in STR-SNr transmission and at the same time, promotes activation of D2-receptors increasing GP-SNr and STN-SNr transmissions (Ibáñez-Sandoval et al., 2007; Aceves et al., 2011b).

Also in PD, levels of GABA in the SNr have been reported to be either increased (Windels et al., 2005) or unchanged (Bianchi et al., 2003; Ochi et al., 2004). Changes in GABAergic transmission have been evaluated with measurements of mRNA or protein levels for the GABA-synthesizing enzyme glutamate acid decarboxylase (GAD).

A selective increase in GAD mRNA in DA-depleted animals has been observed in iSPN, GPi and SNr neurons (Kincaid et al., 1992; Laprade and Soghomonian, 1999; Salin et al., 2002). Finally, changes in GABAergic transmission can also be assessed by measuring the binding or density of GABA receptors which have revealed an increase in $GABA_A$ and $GABA_B$ receptor binding or mRNA expression for these receptors in GPi/SNr, in animal models and parkinsonian patients (Pan et al., 1985; Chadha et al., 2000; Katz et al., 2005).

II. Changes in neuronal activity in the basal ganglia in L-DOPA induced dyskinesia

The classic model hypothesizes that the effects of DA replacement result in a reduced activity STN-GPi pathway (Crossman et al., 1988) and decreased firing in GPi output neurons (Olanow et al., 2009). The same results have been observed after recording field potentials from the SNr in 6-OHDA lesioned rats with LID (Meissner et al., 2006; Lacombe et al., 2009; Aristieta et al., 2016). However, the notion that GPi hypoactivity is the primary mechanism responsible for the development of dyskinesias contrasts with a well-established finding in monkeys and human patients, which demonstrated that pallidotomy abolishes dyskinesia (Baron et al., 1996). The antidyskinetic effect of pallidotomy has led to the revision of the pathophysiology of dyskinesia which is not only the result of GPi hypoactivity but is also due to abnormal firing patterns in BG output neurons (Obeso et al., 2000).

Evidences also support the role of the striatal D1R in the development of dyskinesias. It has been shown that L-DOPA does not induce dyskinesia in DA-denervated D1 knockout mice, while knocking out D2R does not influence LID expression in 6-OHDA lesioned mice (Darmopil et al., 2009; Murer and Moratalla, 2011; Halje et al., 2012). The fact that D1R knockout animals do not show abnormal involuntary movements (AIMs) with prolonged L-DOPA treatment suggests that D1R stimulation is essential for the development of LID. In line with this, optogenetic activation of STR-SNr terminals in the SNr is able to generate a full dyskinetic state in DA-depleted wild-type mice (Keifman et al., 2019). These results suggest that the STR-SNr synapse could be an attractive therapeutic target for future strategies to reduce LID. On the other hand, the contribution of iSPN to LID seems to be controversial. However, there is a publication showing that optogenetic co-stimulation of dSPNs and

iSPNs induces dyskinesia in PD rats (Alcacer et al., 2017), suggesting a possible participation of iSPNs in LID.

Similarly, it has become evident that striatal interneurons are major determinants of network activity and behavior in PD and LID (Zhai et al., 2019). In accordance with this, a recently optogenetic study has revealed the critical role played by striatal cholinergic interneurons in tuning the intensity of dyskinesia. The authors have shown that short pulse stimulation of cholinergic interneurons enhanced dyskinesia while longer pulse stimulation of cholinergic interneurons reduced them (Bordia et al., 2016).

1.3. SUBSTANTIA NIGRA PARS RETICULATA

The SNr was first described in 1910 by Torata Sano who introduced the terms "*substantia nigra zona reticulata*" and "*substantia nigra zona compacta*" (Sano, 1910). In these years Ramon y Cajal distinguished also two zones regarding nigral neurons, a cell-rich superior region (the SNc) and a cell-sparse inferior zone identified as the SNr (**Fig.1.8**). In the last decade, anatomy, physiology or functions of the SNr have been further clarified.

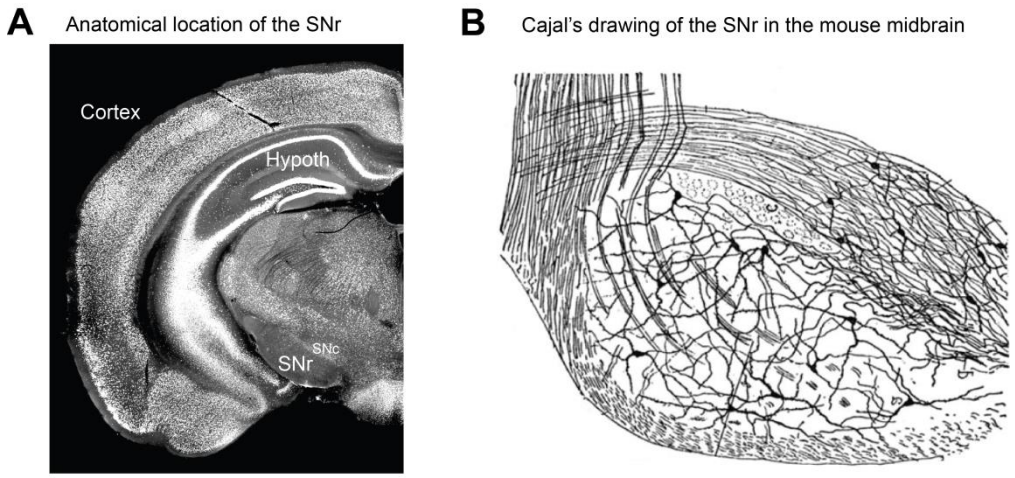

Figure 1.8. The SN is a BG structure located in the midbrain. A: Coronal section from a mouse depicting the anatomical position of the SN and the subdivision into SNr and SNc. **B:** Cajal's drawing of Golgi-stained *substantia nigra* in a sagittal section of mouse brain. Image taken from Ramon y Cajal, 1909.

1.3.1. Neuronal diversity in the *SNr*

The SNr is a distinct and relatively large ventral midbrain structure with a critical role in the cortico-BG-thalamo-cortical loop. Although important findings have been made in recent years regarding the SNr, the study of the neuron subtypes within the nucleus has received less attention. The understanding of the neuronal diversity of the STR or the GPe has been helpful to comprehend the functional organization of these nuclei; conversely while neurochemical, morphological, and functional properties of SNr neurons have started to be investigated, a clear cellular diversity has not been yet established (Zhou and Lee., 2011) and globally the SNr is still considered as a homogeneous nucleus.

According to the synthesis and release of neurotransmitter, nigral neurons have been classified into GABAergic and dopaminergic neurons (Grace and Onn, 1989; González-Hernández and Rodríguez, 2000) which represent a population of 30,000 and 7,000 neurons respectively, per hemisphere in the rat (Oorschot, 1996). Topographically, GABAergic cells are more numerous at rostral and lateral levels and are preferentially arranged in dorsoventrally elongated clusters. In contrast, bodies of DA-containing neurons are arranged in two groups within the SNr, one rostrodorsal that corresponds to the SNc dorsal and another caudoventral that corresponds to the SNc ventral (González-Hernández and Rodríguez, 2000); (**Fig. 1.9**).

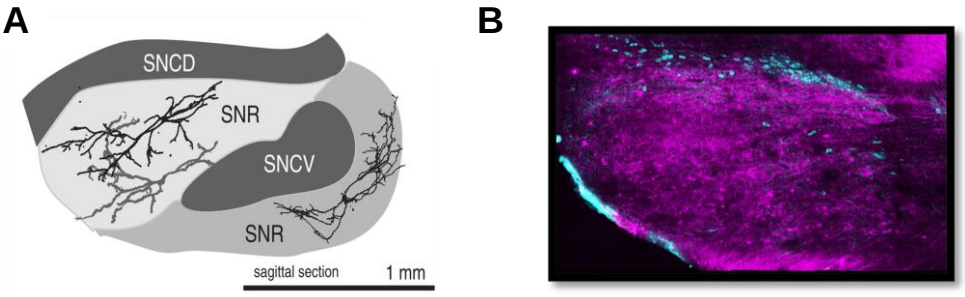

Figure 1.9. Topographical distribution of GABAergic and dopaminergic neurons. A: Diagram of a sagittal section of the substantia nigra depicting the double organization of dopaminergic neurons of SNc at dorsal (SNCD) and ventral levels (SNCV). Image taken from Dudman and Gerfen, 2015. **B:** Confocal image from a mouse brain reflecting the mentioned characteristic distribution of GABAergic (magenta) and dopaminergic neurons (cyan).

Considering their neurochemical content, immunohistochemical studies of the SNr have revealed controversial results. Previous findings suggested that the majority of SNr GABAergic neurons express GAD, and most of them (~80%) contain PV (Reiner and Anderson, 1993; Rajakumar et al., 1994; González-Hernández and Rodríguez, 2000). The SNr also contains a small subset of cells expressing calretinin (Liang et al., 1996; McRitchie et al., 1996), nitric oxide synthase or acetylcholine transferase (Martínez-Murillo et al., 1989; González-Hernández and Rodríguez, 2000). Among GABA neurons there is a substantial variation in morphological characteristics. In relation to topographical distribution of these neurons, it has been described that in the rostrolateral SNr, GABAergic cells are large and contain PV and nitric oxide synthase. In caudomedial positions, most of them are small and express only PV, and in rostromedial portions, they are predominantly small and contain either calretinin, nitric oxide synthase or PV (González-Hernández and Rodríguez, 2000).

However, recent publications have shown by single-cell gene-expression analysis that PV (encoded by Pvalb) and glutamic acid decarboxylase 2 (GAD2, encoded by Gad2) are preferentially expressed in distinct SNr GABAergic populations (Liu et al., 2020). These authors also looked at spatial distribution of these neurons into the SNr depicting differences. Whereas PV neurons were predominantly located in the lateral SNr, GAD2 neurons were more present into the medial SNr (Liu et al., 2020). Indeed this distribution fits with previous studies performed by Rajakumar and colleagues, in which they demonstrated not only that the density of PV containing varicosities decreased towards the medial part of the nucleus but also related separate regions of the SNr with differentiated striatal inputs to distinct functions (Rajakumar et al., 1994). Also Rizzi and colleagues divided the SNr into two subpopulations of neurons, containing either vesicular transporter for GABA (VGAT) or PV (Rizzi and Tan, 2019). Interestingly, by using optogenetic manipulation of these two sub-types and employing a series of motor tests, these authors have revealed that VGAT and PV cells in the SNr govern different aspects of motor behavior.

Other authors have demonstrated that, apart from GABA cells, some SNr neurons also express the vesicular glutamate transporter vGluT2 and release glutamate in the *thalamus* (Kha et al., 2001; Yamaguchi et al., 2013; Antal et al., 2014). These vGluT2-positive neurons have been further investigated by Antal and colleagues elucidating an excitatory connection between the SNr and the *thalamus*. They also observed many vGluT2-positive neurons expressing TH, meaning they are also dopaminergic (Antal et al., 2014). It is worth to mention an interesting publication from Saunders and colleagues where they screened markers of global clusters for expression in the SNr. In the first cluster they found neurons sharing selective markers such as *Sema3*, *Adarb2*, *Pax5* and *Pou6f2*. The second cluster expressed *Slc17a6* which likely corresponded to the glutamatergic projection neurons to *thalamus* (Antal et al., 2014). The last subcluster was $Gad2^{+}$/$Pvalb^{-}$ and expressed *Zfpm2* (Saunders et al., 2018).

1.3.2. Properties of SNr neurons

As we have already mentioned, neurochemical analysis of SNr neurons, clearly distinguishes three different classes, but electrophysiological characterization of GABAergic cells and correlation with the neurochemical profile has yet to be fully

developed. PV+ cells have been associated with high firing frequency (Rodríguez and González-Hernández, 1999), but this characteristic does not seem to be cell-specific. Indeed, calretinin-containing cells show similar projection targets, local arborization, morphological, and electrophysiological characteristics to PV-positive cells (Lee and Tepper, 2007). More recent studies describe four subtypes of GABAergic cells in the SNr, whose electrophysiological profile is complex and varies according to the posture and movement of the animal (Barter et al., 2014, 2015).

In general, a large part of studies have addressed the neurophysiological characteristics of GABAergic neurons with respect to dopaminergic neurons in the SNr in awake/anesthetized animals or in brain slice preparations (Atherton and Bevan, 2005; Connelly et al., 2010; Zhou and Lee, 2011; Zhou, 2016). A remarkable neurophysiological feature of the SNr GABA neurons is their sustained high firing frequency. In awake animals, SNr GABA neurons fire spikes of short duration (~ 1 ms) spontaneously at very high frequencies, 25–30 Hz in awake rodents and around 65 Hz in awake primates (DeLong et al., 1983; Gulley et al., 1999, 2004; Maurice et al., 2003; Nevet et al., 2004; Wichmann and Kliem, 2004; Windels and Kiyatkin, 2006a, 2006b; Walters et al., 2007). In contrast, nigral DA neurons fire spikes of long duration (about 2.5 ms) at low frequency around 1–4 Hz (Lacey et al., 1989; Hyland et al., 2002; Guzman et al., 2009). Electrophysiological recordings *in vitro* show lower firing frequencies, as 10-20 Hz for GABA cells and 2 Hz for DA neurons (Lacey et al., 1989; Zhou et al., 2006; Tepper and Lee, 2007b; Connelly et al., 2010; Seutin and Engel, 2010; Ding et al., 2011b, 2011a) which is mostly due to low recording temperatures (~30°C). The GABAergic neurons differ from the dopaminergic ones showing higher firing rate, shorter duration AP, short latency and small amplitude afterhyperpolarization, and a much less pronounced voltage sag in response to hyperpolarizing current pulses. These criteria were the primary factors allowing the electrophysiological signature of nigral GABAergic neurons from dopaminergic neurons (**Fig. 1.10**).

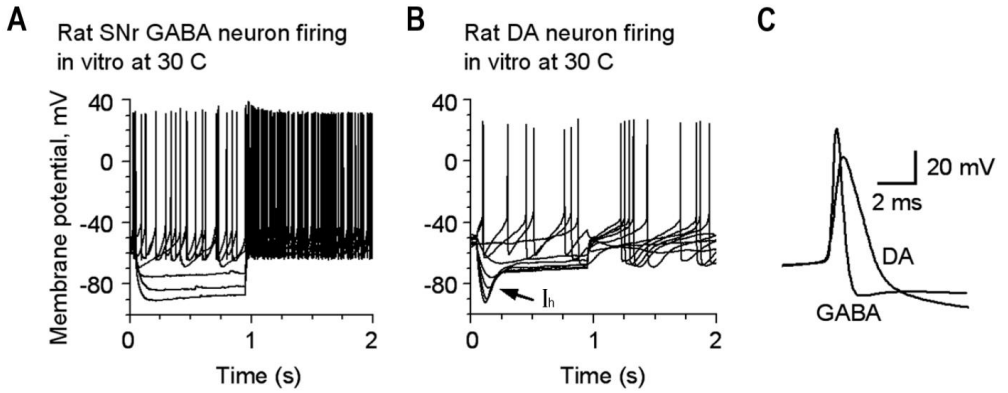

Figure 1.10. GABAergic and dopaminergic neurons in the SNr depict different electrophysiological properties. A: SNr GABA neurons are capable of sustained spontaneous high firing frequency and minimal I_h-mediated depolarizing sag in response to hyperpolarizing current injection. **B:** Nigral-DA neuron depicting spontaneous low spiking frequency and prominent I_h-mediated depolarizing sag (arrow) in response to hyperpolarizing current injection. **C:** Overlay of a GABA neuron spike and a DA neuron spike showing that those from SNr GABA neurons are larger in amplitude and shorter in duration than nigral DA neurons. Source from Ding et al., 2011b.

It is worth to mention that SNr neurons are known to both increase and decrease their firing rates in relation to movement (Gulley et al., 1999; Basso and Wurtz, 2002; Fan et al., 2012; Freeze et al., 2013; Barter et al., 2015). To explain these opponent answers, it has been discussed that the BG output disinhibits some actions while inhibiting competing actions (Mink, 1996; Cui et al., 2013).

1.3.2.1. Ionic conductances underlying pacemaking in SNr neurons

Several recent studies indicate that multiple ion channels are critical not only for maintaining SNr neurons depolarized such as the type 3 transient receptor potential (TRPC3), sodium leak (NALCN) or voltage-gated persistent sodium current (I_{NaP}), but also others contributing to spiking *per se* among which, voltage-activated sodium channels (Nav), potassium (Kv), calcium (CaV) and calcium-activated potassium (KCa) channels have been described (Atherton and Bevan, 2005; Zhou et al., 2008; Seutin and Engel, 2010; Ding et al., 2011a).

Type 3 transient receptor potential channels

Based on experiments using the Na_V channel blocker tetrodotoxin (TTX) and sodium replacement, Atherton and Bevan, (2005) detected a Na-dependent, TTX-insensitive background cation responsible for depolarization to AP threshold in SNr GABA neurons, but the nature of this background conductance was not identified. Recent studies have provided evidence that the transient receptor potential channels type 3 (TRPC3) contributes to depolarization of SNr GABA neurons and suggested that TRPC3 channels are relatively highly expressed in these neurons (Zhou et al., 2008). Moreover, the inhibition of these channels by infusion of a TRPC3 antibody into SNr GABA neurons, decreased the firing frequency and increased firing irregularity of these neurons (Albert et al., 2006; Amaral and Pozzo-Miller, 2007; Zhou et al., 2008). However, another study showed that spontaneous firing of SNr neurons is unaffected after genetic deletion of these channels, questioning the participation of these channels in the pacemaking of SNr neurons (Lutas et al., 2014). This discrepancy can be explained by the lack of a specific blocker of non-specific cationic channels used by Zhou and colleagues to show the involvement of TRPC3 channels in the depolarized potential of SNr neurons.

Briefly, constitutively active TRPC3 channels can depolarize SNr GABA neurons at very negative membrane potentials but since Zhou and colleagues shown that the TRPC3 current reversal potential is around −35 mV it is expected that the current becomes smaller as the neuron gets close to the AP threshold, a situation that is not ideal for reliable spike generation. So other cation channels might contribute to depolarize the membrane potential of SNr neurons.

Sodium leak channel

SNr neurons have a leak current (a sodium-dependent tonic current) that maintains their membrane potential sufficiently depolarized to allow spontaneous triggering of APs in the absence of synaptic input (Atherton and Bevan, 2005; Zhou and Lee, 2011).

In addition, a more recent study has discovered that SNr neurons express the sodium leak channel (NALCN); (Lu et al., 2007), and that genetic deletion impairs spontaneous firing in these neurons (Lutas et al., 2016). Because the activity of NALCN is strongly dependent upon glycolysis, alterations in this metabolic pathway can

significantly impair autonomous pacemaking in SNr neurons and contribute to pathological activity of this nucleus (Lutas et al., 2014, 2016).

Voltage-activated sodium channels

It is known that Na_V channels are the most important ion channels for the generation of AP (Bean, 2007), but some studies have also shown that a voltage-gated persistent sodium current (I_{NaP}) appears when the membrane potential reaches -65 to -60 mV, depolarizing the membrane potential of SNr GABA neurons up to threshold (Atherton and Bevan, 2005; Seutin and Engel, 2010; Ding et al., 2011b). I_{NaP} is generated when a small fraction of Na_V channels remain open for long periods of time (Alzheimer et al., 1993; Bant and Raman, 2010) which could explain the fact that multiple cation channels contribute to depolarize the membrane potential of SNr GABA neurons. At −50 mV or slightly below this potential, the large transient voltage-activated sodium current (I_{NaT}) starts to activate and eventually triggers the rapid rising phase of the AP. SNr GABA neurons have a high density of I_{NaT}, contributing to the fast rise and large amplitude of their APs (Seutin and Engel, 2010; Ding et al., 2011b). Moreover, it has been exposed the high capacity of I_{NaT} to recover from inactivation enabling the sustained high firing frequency in SNr GABA neurons (Do and Bean, 2003; Mercer et al., 2007).

Atherton and colleagues also performed *in vitro* electrophysiological recordings from rat brain slices to study the contribution of I_{NaP} to spontaneous spike firing in SNr GABA neurons, as blocking fast GABAergic and glutamatergic synaptic transmission did not affect SNr neuron pacemaking (Atherton and Bevan, 2005). Immunohistochemical (Notomi and Shigemoto, 2004) and *in situ* hybridization (Monteggia et al., 2000; Santoro et al., 2000) studies have indicated that all known hyperpolarization-activated cyclic nucleotide-gated (HCN) channel subunits, are expressed within the SNr, especially the HCN2. However HCN do not seem to contribute to the depolarization toward AP threshold as their blockade by ZD7288 or CsCl does not alter the autonomous firing of SNr neurons (Atherton and Bevan, 2005) suggesting that I_h contribute little to pacemaking under normal conditions.

Voltage-activated potassium currents

Kv currents are the main force to repolarize the neuron after the AP has reached its peak or even before the peak (Bean, 2007). Indeed, a combined molecular and electrophysiological study has indicated that SNr GABA neurons express a strong Kv3-like fast delayed rectifier ($I_{DR\text{-}fast}$) current with fast activation and slow inactivation kinetics, ideally suited for the sustained high frequency firing capability in these neurons (Ding et al., 2011a).

Immunohistochemical studies have shown that Kv3.1, Kv3.2, and Kv3.3 subunits are expressed in the SNr region while Kv4.3 mRNA is expressed in the SNc region (Weiser et al., 1995; Ozaita et al., 2002; Chang et al., 2008). Using qRT-PCR analysis, Ding et al., (2011a) have shown that SNr fast-spiking GABA neurons express Kv3.1 and Kv3.4 mRNA. The association of these two subunits can form the fast delayed rectifier type K channels ($I_{DR\text{-}fast}$) which are sensitive to 1 mM tetraethylammonium (Coetzee et al., 1999; Rudy and McBain, 2001). In contrast, nigral DA neurons express Kv4.2 and Kv4.3 mRNAs that form transient I_A type channels which are relatively insensitive to tetraethylammonium. It is important to mention that even if SNr GABA neurons express a weak I_A, this allows these neurons to fire at high frequencies (Koyama and Appel, 2006; Ding et al., 2011a). These pharmacological and kinetic properties of this $I_{DR\text{-}fast}$ current indicate that Kv3-like channels are conducting this K current, just like in other GABAergic fast-spiking neurons from other brain regions (Martina and Jonas, 1997; Baranauskas et al., 2003).

Voltage-gated calcium channels and calcium-activated potassium channels in SNr GABA neurons

Ca_V channels also contribute actively to the excitability of SNr GABA neurons. Ca_V channels have been shown to be involved not only during spontaneous activity of these neurons but also in the genesis of more complex behaviors such as burst firing (Atherton and Bevan, 2005; Ibáñez-Sandoval et al., 2007; Tepper and Lee, 2007a). Activation of Ca_V channels can lead to either increases or decreases in SNr neuron excitability. Calcium entry through N-type calcium channels ($Ca_V2.2$) causes activation of K_{Ca} channels that decreases the firing rate and increases the regularity of firing in SNr GABA neurons.

SNr GABA neurons express K_{Ca} channels that play a role in regulating the spontaneous firing rate and regularity of these neurons. They are active during spontaneous activity *in vitro,* their blockade reduces the amplitude of the spike afterhyperpolarization (AHP) and increases the firing rate of SNr GABA neurons (Atherton and Bevan, 2005; Yanovsky et al., 2005). K_{Ca} channel activity is also responsible for firing regularity, which increases when these channels are blocked (Atherton and Bevan, 2005). When K_{Ca} channels are pharmacologically activated SNr neuron firing rate decreases but regularity increases (Yanovsky et al., 2006). In the literature calcium-activated potassium SK channels are associated to entry of Ca2+ ions into SNr neurons through Cav2.2 channels which in turn causes activation ok K_{Ca} channels (Atherton and Bevan, 2005). For this reason SK channels seem to play an important role in the maintenance of the frequency and precision of single-spike firing not only in SNr GABA neurons but also in GP and STN neurons (Wilson et al., 2004; Ramanathan et al., 2008; Deister et al., 2009).

The majority of SNr GABA neurons exhibit a depolarizing *plateau* potential following depolarization from a hyperpolarized membrane potential (Nakanishi et al., 1987; Lee and Tepper, 2007c). The *plateau* potential is dependent on calcium, but the conductance underlying the *plateau* uses sodium as a charge carrier. Although the exact type of channel underlying the *plateau* potential is unknown it is likely mediated by both, Ca_V and TRP channels (Nakanishi et al., 1987; Lee and Tepper, 2007).

Together, these intrinsic ion channels provide SNr GABA neurons with the capabilities to fire autonomous, sustained high frequency spikes. Additionally, SNr GABA neuron activity is also regulated by excitatory, inhibitory and modulatory inputs that sculpt the default tonic high frequency firing into a significant control signal.

1.3.3. Alterations in firing properties of SNr neurons in parkinsonian and dyskinetic animals

In DA-depleted animals, extracellular single cell recordings have revealed changes in firing rate and pattern in SNr neurons. The presence of burst firing pattern is frequently described in the literature. These bursts have been detected in anesthetized rats (Murer et al., 1997; Rohlfs et al., 1997; Lee et al., 2001; Wang et al., 2010; Seeger-Armbruster and Von Ameln-Mayerhofer, 2013; Aristieta et al., 2016), awake and anesthetized mice (Lobb and Jaeger, 2015; Willard et al., 2019), monkeys

(Wichmann et al., 1999; Wichmann and Soares, 2006) or in slices after application of dopaminergic antagonists (Ibáñez-Sandoval et al., 2007; Aceves et al., 2011b). Likewise, similar findings have been shown in PD patients (Hutchison et al., 1997); (**Fig. 1.11**).

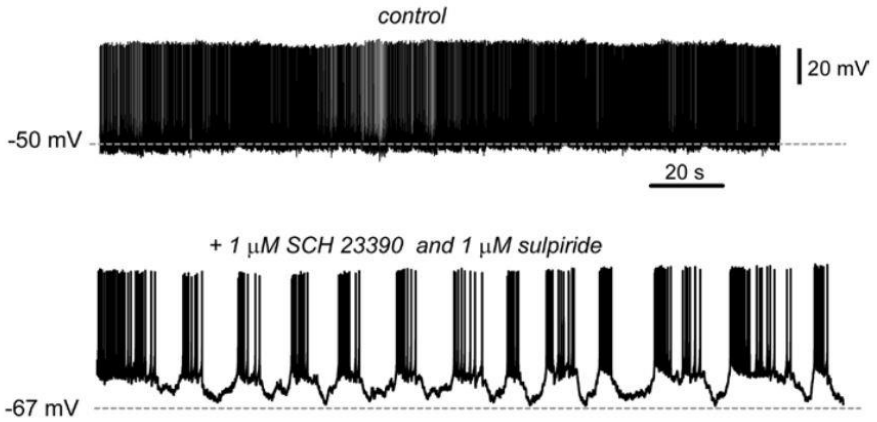

Figure 1.11. Burst firing pattern of SNr neurons after blockade of DA receptors. *In vitro* electrophysiological recordings in the SNr from control rat brains, depicted spontaneous tonic firing (top). During acute blockade of D1 (SCH 23390) and D2 (sulpiride) receptors, SNr neurons shifted from tonic to a bursting patter. Image taken from Aceves et al., 2011a.

Even if this bursting phenomenon has been widely observed in anesthetized and awake animals, changes of the spontaneous firing rate on SNr neurons are much more controversial in the literature. This seems to be attributed to many factors such as varying recording sites within the SNr (Wang et al., 2010), recording different GABA SNr cell subpopulations, using different protocols for inducing parkinsonism or varying post lesion recording times (Rodríguez Díaz et al., 2003). Some authors observed decreased (MacLeod et al., 1990; Murer et al., 1997; Rohlfs et al., 1997; Delaville et al., 2012) increased (Burbaud et al., 1995; Meissner et al., 2006; Breit et al., 2008; Lacombe et al., 2009) or no firing differences in SNr cells from 6-OHDA-lesioned rats 2-7 weeks after the lesion (Tai et al., 2003; Wang et al., 2010; Aristieta et al., 2016). In the contralateral SNr, an increased rate was described in comparison to naïve or sham-lesioned rats (Rohlfs et al., 1997; Rodríguez Díaz et al., 2003; Breit et al., 2008). In long-term lesioned animals (6 month post lesion) the SNr firing rate of 6-OHDA-lesioned rats regained the values of control groups (MacLeod et al., 1990).

Those authors supporting the idea that neuronal activity is elevated in the SNr of DA-depleted rats, suggest that this fact is not only due to a reduction of inhibitory striatal innervation caused by DA loss but also to the increased excitatory glutamatergic input from the STN. Indeed, hyperactivity of the STN in PD patients and experimental models of PD have been shown by many authors (Bergman et al., 1994; Hassani et al., 1996; Vila et al., 2000; Magill et al., 2001; Breit et al., 2007; Aristieta et al., 2012). Interestingly, the STN lesion and functional inhibition is able to normalize the firing pattern in SNr GABA neurons (Murer et al., 1997; Tseng et al., 2001). These BG functional alterations induced by PD, are also affected by L-DOPA treatment (Obeso et al., 2008), as we mentioned previously in the BG motor circuit section (see **1.2.3**).

Concerning changes on spontaneous firing rate after chronic L-DOPA treatment, SNr neurons from dyskinetic rats showed an enhanced firing rate (Meissner et al., 2006; Aristieta et al., 2016). However, 20-120 minutes after an acute challenge of L-DOPA resulted in reduction of the firing rate and the number of bursting neurons in the SNr (Aristieta et al., 2016). In addition, a recent publication has described a decreased in firing rate of SNr neurons in L-DOPA + Zonisamide–treated PD model mice when they clearly showed LID but no differences in just L-DOPA treated mice (Sano and Nambu, 2019). However, the clear cellular mechanisms underlying the changes in rate and pattern of SNr cells under DD or LIDs, have not been yet explored *in vitro* and this will take part of this PhD work.

It should be noted the classical triphasic response of SNr neurons evoked by *in vivo* electrical stimulation in the motor cortex consisting of early excitation, inhibition, and late excitation in the control state, which represents the sequential activation of hyper-direct, direct and indirect-pathways (Sano et al., 2013). This typical response pattern seems to be affected in parkinsonian mice reflecting a large duration and amplitude of the early excitation together with longer duration but smaller amplitude of the late excitation (Sano and Nambu, 2019). The same authors described decreased firing rate in SNr neurons in L-DOPA treated mice (Sano and Nambu, 2019).

1.3.4. Synaptic inputs from the *striatum*, *globus pallidus* and *subthalamus* onto SNr neurons

SNr GABA neurons receive converging synaptic inputs mainly from the STR, GP and STN that carry critical information for motor control, cognition, habit formation, learning, and memory and reward (Simpson et al., 2010; Friend and Kravitz, 2014; Graybiel and Smith, 2014; Hikosaka et al., 2014). These inputs can affect the firing intensity and pattern of SNr GABA neurons and hence, their output. Pallido-nigral (GP-SNr) terminals form large baskets around the somatic domain and proximal dendrites of SNr cells, whereas STR-SNr synapses are formed on fine distal dendrites (Smith and Bolam, 1991; von Krosigk et al., 1992; Smith et al., 1998). In addition to their subcellular locations, these two GABAergic synapses have also distinct properties that we will explain in more detail (**Fig. 1.12**).

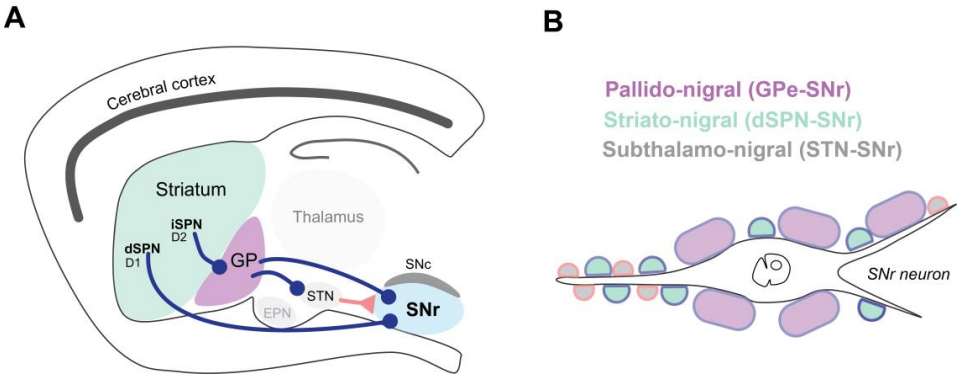

Figure 1.12. Diagram of inputs to SNr neurons. A: The direct and indirect striatal projection pathways from two subsets of striatal spiny projection neurons. Indirect projecting neurons expressing D2 receptors (iSPN) are indirectly connected to the SNr through connections that involve the GP and the STN. Direct striatal projection neurons express D2 receptors (dSPN) and project directly to the SNr. Besides, SNr GABA projection neurons also receive GABA input from GP neurons. **B:** Schema illustrating the synaptic location of glutamatergic-excitatory (red) and GABAergic-inhibitory (blue) inputs to GABAergic neurons of the SNr.

Modifications to this simple schema of SNr inputs have been recently proposed by Liu and colleagues, who differentiated two sub-populations of SNr neurons (Liu et al., 2020). The authors observed that while PV neurons, localized in the lateral of the SNr, receive inputs mainly from the BG nuclei such as the dorsal STR, GP and STN, GAD2 neurons, situated in the medial SNr, receive inputs from more dispersed brain areas such as the *hypothalamus* and midbrain regions apart from the BG nuclei. As a result, while PV neurons serve mainly as a BG output to motor-control regions, GAD2 neurons integrate a much wider range of inputs and project broadly to brain-state as well as motor-control regions (Liu et al., 2020); (**Fig 1.13**).

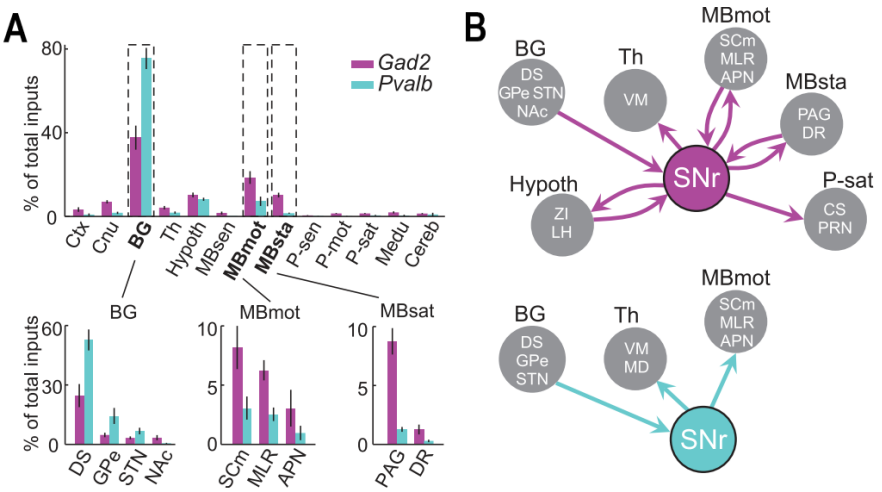

Figure 1.13. Inputs to SNr neurons in a Gad2^{cre} and Pvalb^{Cre} mice. A: Input distribution for GAD2 (magenta) and PV (cyan) neurons in the SNr. **B:** Diagram summarizing major inputs and outputs for SNr GAD2 and PV neurons. Abbreviations defined here; Hypoth: *Hypothalamus*; ZI: Zona incerta; LH: Lateral hypothalamic area; BG: BG; DS: Dorsal *striatum*; GPe: *Globus pallidus*; STN: Subthalamic nucleus; NAc: *Nucleus accumbens*; Th: *Thalamus*; VM: Ventral medial nucleus; MD: Mediodorsal nucleus; MBmot: Midbrain motor related; SCm: Superior colliculus, motor related; MLR: Mesencephalic locomotor region; APN: Anterior pretectal area; MBsta: Midbrain behavioral state related; PAG: Periaqueductal gray; DR: Dorsal nucleus raphe; P-sat: Pons, behavioral state related; CS: Superior central nucleus raphe: PRN: *Pontine reticular nucleus*. Image taken from (Liu et al., 2020).

I. Striato-nigral GABAergic inputs

Identification of the STR-SNr projections and their topography has been well described in the 1970s-1990s by tracing techniques (Gerfen, 1985; Deniau et al., 1996;

Mailly et al., 2001, 2003). In rats where the three-dimensional organization of the SNr is best known at cellular and circuit levels, SNr neurons and their striatal afferents were ordered along longitudinal and curved laminae arranged in an onion-like manner. Thus, in the lateral half of the SNr innervated by striatal sub-territories, neurons were associated to sensory and motor cortical functions, while the medial part of SNr was related to prefrontal and limbic cortical areas (Deniau and Chevalier, 1992; Rajakumar et al., 1994; Deniau et al., 1996; Mailly et al., 2003). This spatial distribution of nigral neurons is consistent with the recent publication of Liu and colleagues in which the activation of SNr GAD2 neurons (in the medial SNr) but not PV neurons promoted sleep generation (Liu et al., 2020).

In the 1990s, combined histochemical and molecular studies established that dSPNs expressing D1 receptors but not iSPNs, project strongly to the SNr (Gerfen et al., 1990). While electrophysiological recordings in intact animals suggested that the STR-SNr input inhibits SNr GABA neurons (Hikosaka et al., 2000), recordings in freely moving rats showed that SNr GABA neurons are under the influence of tonic GABA inhibition. These findings were achieved by local application of the $GABA_A$ receptor blocker bicuculline in awake and unrestrained animals but also under chloral hydrate anesthesia (Windels and Kiyatkin, 2004, 2006a). Indeed, in recent studies using optogenetic techniques which enable selective activation of specific groups of neurons by introducing light-sensitive ion channels (channelrhodopsin-2, ChR2) into either dSPNs or iSPNs, evidenced that activation of dSPNs inhibits the spontaneous firing of SNr GABA projection neurons, whereas activation of iSPNs has the opposite effect (Kravitz et al., 2010; Friend and Kravitz, 2014). These new results confirm the classical BG model that dSPNs inhibit and iSPNs excite GPi (EPN) and SNr GABA neurons, respectively (Albin et al., 1989; DeLong, 1990). Although this model is supported by a number of studies, other observations seem to be incompatible with the disinhibition hypothesis. For example, neurons in the SNr are known to both increase and decrease their firing rates in relation to movement (Gulley et al., 1999; Basso and Wurtz, 2002; Fan et al., 2012; Freeze et al., 2013).

The detailed cellular and synaptic aspects of the inhibitory effect of the STR-SNr projection to SNr GABA neurons have also been studied in sagittal brain slices from C57BL/6 mice (Connelly et al., 2010). Consistent with the anatomical description SNr neurons receive inputs from multiple striatal subregions, and robust inhibitory post-

synaptic currents (IPSCs) can be evoked in SNr neurons by stimulation delivered in dorsal, middle, and ventral striatal subregions (Ding et al., 2015a, 2015b). These results point out not only that dSPNs in the dorsal, middle, and ventral striatal subregions provide converging GABAergic inputs to inhibit SNr GABA neurons but also that this major BG output nucleus is a hub which receives and integrates information from the ventral STR, that serves reward and limbic functions (Haber and Knutson, 2010). These findings support the emerging view that the SNr besides being important for motor control is also markedly involved in multiple aspects of other physiological functions associated with the cortico-BG-thalamo-cortical loop. Further studies will be needed to determine if dSPNs, from different striatal subregions, converge onto the same SNr GABA population of neurons (Saunders et al., 2018; Rizzi and Tan, 2019; Liu et al., 2020).

II. Pallido-nigral GABAergic inputs

In the 1970's anatomical studies using axon tracing and ultrastructural techniques characterized the inhibitory synaptic connection from GPe neurons to the BG output neurons, the GPi/EPN and the SNr, respectively (Carter and Fibiger, 1978; Kita and Kitai, 1991; Smith and Bolam, 1991; Bevan et al., 1996). Although this pathway has been confirmed by many laboratories, it did not appear in the influential model of PD pathophysiology (Albin et al., 1989) nor even in the subsequent findings concerning this model (Obeso et al., 2002; Freeze et al., 2013). Until very recent studies it was not thought that GP-SNr pathway played an important role in functional models of the BG (Hikosaka et al., 2019). This might be due to the difficulty of separately activate STR-SNr and GP-SNr axons, and the general belief that the main route by which iSPN and the GPe exerted control on BG output was through the STN (usually known as indirect pathway).

On the one hand, electrical stimulation in a sagittal brain slice preparation have demonstrated that activation of even a single GPe neuron evokes large IPSCs in SNr neurons (Connelly et al., 2010; Ding et al., 2015b). Besides, these authors found that during paired or repetitive activation, the STR-SNr synapse show short-term facilitation, whereas the GP-SNr synapse is governed by short-term depression. A recent study calls for a re-evaluation of the functional importance of the GP-SNr pathway, by showing

that elevating the activity of PV-GPe neurons restores movement in DA-depleted mice and attenuates pathological activity of SNr neurons (Mastro et al., 2017).

While GP-SNr GABA release is augmented by D1Rs, GP-SNr synaptic transmission is reduced by D4R activation. Activation of these D4Rs, localized on the GABAergic projections that GP neurons send to the reticular nucleus of the *thalamus*, the SNr and the STN, also induced a decrease in locomotor activity (Aceves et al., 2011a; Erlij et al., 2012).

It is already known that STR-SNr and GP-SNr pathways have different amount of synaptic convergence and differ in synaptic locations on the SNr neuron. The projection of the indirect pathway to a single SNr neuron consists of a very small number of presynaptic pallidal neurons, making individually strong synaptic inhibitory connections. Due to the depressing nature of the GP-SNr synapse and the high frequency spontaneous firing of GPe neurons, this synapse may be more effective in inhibiting SNr GABA neurons. Because of the powerful GPe-SNr projection, activation of iSPNs can increase SNr neuron activity by inhibiting GPe neurons (Kravitz et al., 2010; Chuhma et al., 2011).

By contrast, approximately 50 dSPN project to each SNr neuron (Oorschot, 1996). However, the direct pathway synapses are individually weaker than those from the GPe (Connelly et al. 2010), possibly because of their location on the dendrites, which extend for long distances in the nucleus (Smith and Bolam, 1991). Indeed, when the usually silent dSPNs are activate by strong glutamate inputs from cortical and thalamic areas (Smith et al., 2014), dSPNs may produce a robust barrage of IPSPs and effectively inhibit or pause SNr neurons. All these results along with the demonstration that electrical signals passing from the dendrites to the soma of SNr cells shown a substantial attenuation (Tiroshi and Goldberg, 2019) suggest that the direct and indirect pathways, function in a complementary manner. Indeed, it has been proposed that the direct pathway is involved in controlling the rate of SNr cell firing and the indirect pathway influences spike timing (Simmons et al., 2020).

III. Subthalamo-nigral glutamatergic inputs

It is well known that the STN is the main source of excitatory inputs to the SNr (Smith and Parent, 1988; Ammari et al., 2010; Dupuis et al., 2013). Neurophysiological studies have demonstrated that STN neuron activation, induces excitatory postsynaptic currents or potentials in SNr GABA neurons (Ibañez-Sandoval et al., 2006; Dupuis et al., 2013). However, the same type of stimulation delivered in the STN gives rise to complex EPSCs which might be due to activation of STN local axon collaterals (Shen and Johnson, 2006; Ammari et al., 2010). Both D1Rs and D2Rs have been described on STN-SNr synaptic terminals, and their activation triggers opposite effect on this transmission. The activation of D1Rs enhances STN-SNr EPSC amplitude, whereas the activation of D2Rs decreases the amplitude of EPSC (Ibañez-Sandoval et al., 2006).

STN neuron excitation may drive burst-firing in SNr neurons (Murer et al., 1997; Tseng et al., 2001; Ding et al., 2013) which has pathophysiological implications. Electrophysiological recordings in animal models of PD indicate excessive oscillatory burst firing in STN neurons (Bevan et al., 2006; Walters et al., 2007). Indeed, some studies have shown that STN lesion and functional inhibition is able to reduce oscillatory firing and normalize the firing pattern in SNr neurons in a rat PD model, further demonstrating the important influence of STN on SNr neuron activity (Murer et al., 1997; Tseng et al., 2001). In particular, high frequency stimulation of the STN is able to induce dyskinesias in both rodent PD models (Boulet et al., 2006; Oueslati et al., 2007) and patients (Benabid et al., 2009), however, these can be suppressed by reducing stimulation intensity.

1.3.5. Synaptic outputs from SNr neurons

Taking in account a large number of studies supporting that SNr GABA neurons are projection neurons, cellular differences have been based more on topographical innervation patterns than on neuronal diversity until now. Overall, neurons in the SNr are considered medium to large sized and have mostly ovoid or fusiform soma that emits 2–6 primary dendrites which often branch (Grofova et al., 1982; Cebrián et al., 2007; Tepper and Lee, 2007a). A single main axon typically arises from the soma or a primary dendrite and courses through the SN issuing one or more local axon collaterals before leaving the nucleus (Grofova et al., 1982; Mailly et al., 2003).

Although it is well known that the main target of SNr is the *thalamus* (Kha et al. et al., 2001), up to four neuron types have been identified based on the axonal projection targets. Type I cells project specifically to the *thalamus*, type II neurons target the *thalamus*, SC and PPN nucleus, type III cells project to the periaqueductal gray matter and *thalamus*, and type IV neurons send projections to the deep mesencephalic nucleus and the SC (Cebrián et al., 2005; Hikosaka, 2007). Indeed, some SNr neurons have been shown to send also local projections locally to the compacta region (Tepper and Lee, 2007b). However, this classification should be reviewed after the emerging findings considering the SNr neuronal diversity (Rizzi and Tan, 2019; Liu et al., 2020); (**Fig. 1.14).**

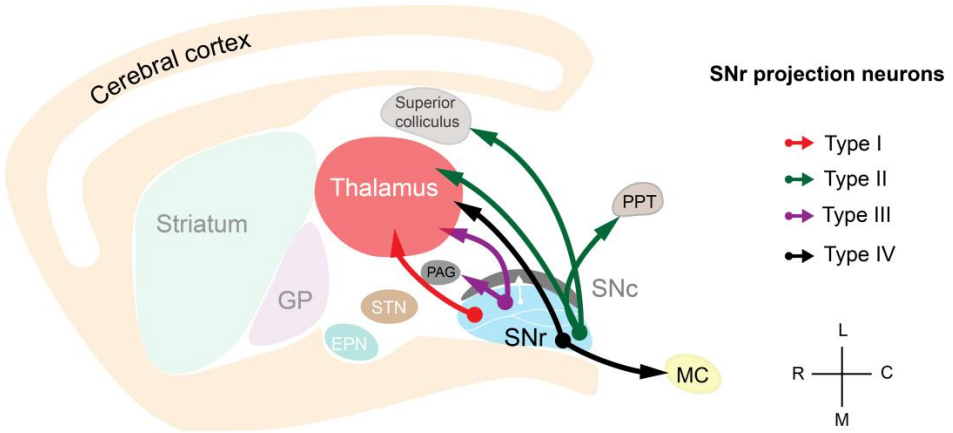

Figure 1.14. The SNr output pathways. The outputs from the SNr are directed to the *thalamus*, superior colliculus, pedunculopontine nucleus (PPN), periaqueductal gray matter (PAG) and mesencephalic nucleus (MC). Looking at their axonal projections, SNr neurons can be divided into Type I (red) projecting to the *thalamus* exclusively, Type II (green) projecting to the *thalamus* and sending collaterals to the superior colliculus and PPN, Type III (purple) also projecting to the *thalamus* but collaterals arise the PAG and type IV (black) sending projections to the MC and the superior colliculus.

Considering their projections, SNr neurons will be involved in the control of different functions. In rats, some SNr neurons project to the ventro-median and parafascicular thalamic nuclei, which are motor-related nuclei, and therefore provide

anatomical basis for motor coordination (Deniau and Chevalier, 1992; Deniau et al., 1996; Tsumori et al., 2003; Cebrián et al., 2005). Even if the relationship between nigro-thalamic neuron activity and behavior is complex due to the nature of the thalamo-cortical circuit (DeLong et al., 1983; Tanibuchi et al., 2009), it has been proved that the inhibition of nigral neurons can induce movements in multiple body parts (Sakamoto and Hikosaka, 1989; Trevitt et al., 2002; Inchul et al., 2005) or even dyskinesia or dystonia (Dybdal et al., 2013).

In contrast, SNr neurons projecting to the SC and to regions of the PPN are implicated in tasks like orienting behavior, postural tone and locomotion, respectively (Appell and Behan, 1990; Redgrave et al., 1992; Takakusaki et al., 2004). The stimulation of the PPN nucleus is sufficient to produce changes in muscular tension (perhaps related to elements of postural control or orienting responses), and this effect can be attenuated by activation of SNr neurons (Takakusaki et al., 2004).

As happens in other BG nuclei, axon collaterals of SNr neurons can extend for several millimeters and give rise to multiple collaterals that innervate multiple distinct target regions (Kha et al. et al., 2001; Cebrián et al., 2005). This singularity of SNr neurons could explain also the results obtained by Liu and colleagues in which after discriminating between PV- and GAD2-expressing SNr neurons, they observed that each SNr GAD2 neuron sends axon collaterals to multiple brain regions (**Fig 1.13**). Interestingly, these authors found that optogenetic activation of SNr GAD2 neurons suppressed movement and enhanced sleep (Liu et al., 2020). The involvement of some SNr neurons in sleep regulation is consistent with previous lesion studies in rats (Gerashchenko et al., 2006; Qiu et al., 2010).

In general, all these afferent inputs in combination with efferent connections provide the anatomical bases for SNr GABA neurons to affect multiple aspects of movement control (but not exclusively) under physiological and pathological conditions.

1.3.6. Dopaminergic modulation of *SNr* neurons

Dopaminergic modulation of the SNr is achieved through an unconventional release of DA by the dendrites of SNc neurons which constitutes an ultra-short dopaminergic pathway (Rice and Patel, 2015). In situ hybridization and

immunohistochemistry studies have shown that several dopaminergic receptors are expressed in the SNr. The most intensely labeled receptors are D1Rs, especially in STR-SNr terminals. D4Rs and D5Rs are present in the SNr but mainly on perikarya (Mrzljak et al., 1996; Ciliax, 2000; Kliem et al., 2010) and D1/D5Rs have been found both on SNr neurons and astrocytes (Nagatomo et al., 2017). D1-like agonists excite SNr neurons, and this modulation is mediated by a PKA-dependent enhancement of constitutively active TRPC3 channels, which depolarizes SNr neurons (Zhou et al., 2009). Interestingly these authors were able to mimic this effect artificially elevating DA levels which supports its physiological and functional relevance. In addition, acute blockade of D1-like and D2-like receptors induces hyperpolarization of SNr neurons and triggers the switch from tonic regular firing to irregular or burst firing (Cáceres-Chávez et al., 2018). This pharmacological manipulation induces an increase in the activity of SNr neurons very similar to the one recorded *in vivo* in anesthetized (Wichmann and Soares, 2006; Wang et al., 2010; Seeger-Armbruster and Von Ameln-Mayerhofer, 2013; Lobb and Jaeger, 2015), and in awake (Willard et al., 2019) DA depleted rodents.

As early as in 1998, Radnikow and Misgeld reported that the D1-like agonist, SKF38393 substantially increased the amplitude of evoked $GABA_A$ receptor-mediated IPSCs in SNr GABA neurons by increasing the vesicular GABA release (Radnikow and Misgeld, 1998). This phenomenon has also been confirmed later by another laboratory which demonstrated that D1-like ligand stimulation increased IPSC amplitude when these axon terminals were selectively photo-stimulated locally in the SNr (Chuhma et al., 2011). Another study confirmed the presynaptic enhancement of STR-SNr IPSCs by D1R activation and in turn extended those findings by demonstrating a concentration-dependent shift from D1R-mediated IPSC enhancement to non specific inhibition (Aceves et al., 2011a). Indeed, the presynaptic D1R facilitation is a common mechanism for the STR-SNr input originating in dorsal, middle, and ventral striatal subregions (Ding et al., 2015b). It has been observed that repetitive activation of these terminals evokes IPSCs which exhibit short-term facilitation (Connelly et al., 2010). Therefore, under normal conditions, DA acting on D1R strengthens direct-pathway inhibition of SNr neurons by increasing dSPN excitability and GABA release probability at STR-SNr terminals to inhibit SNr neuron firing. The behavioral advantage of this arrangement can be appreciated in motor control as some authors have shown that a robust STR-SNr GABA input facilitates movement (Hikosaka et al., 2000; Friend and Kravitz, 2014).

The idea that DA denervation elicits sensitization to L-DOPA in part *via* stimulation of the STR-SNr pathway is supported by observations in which DA

denervated animals exhibit increased D1R-mediated release of GABA within the SNr (Rangel-Barajas et al., 2008; Mango et al., 2014). In addition, homeostatic changes driven by the loss of DA lead to increased excitability of D1-SPNs, which is not normalized by L-DOPA (Warre et al., 2011; Fieblinger et al., 2014) indicating that adaptive responses extend beyond activation of D1Rs. In a recent study conducted by the group of Dr Sulzer in which they employed DA-lesioned mice and used optogenetic approaches, reported that DA-depletion induces a strong increase in STR-SNr IPSC amplitude and besides, they showed that dysfunctional $GABA_B$ receptors and loss of presynaptic reduction of GABA release probability was responsible for this augmented transmission (Borgkvist et al., 2015); (**Fig. 1.15**).

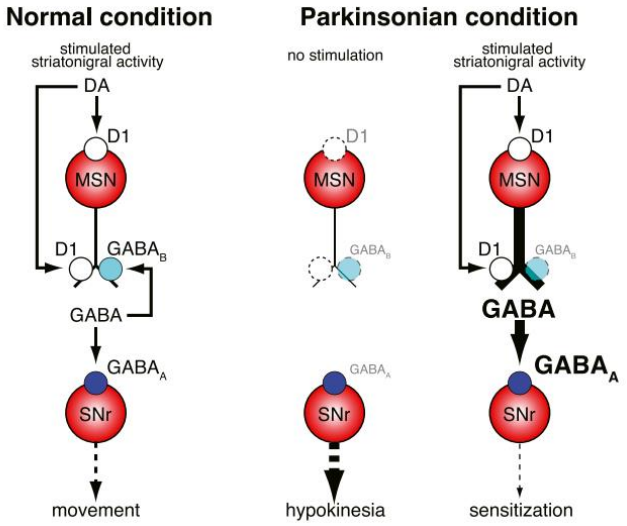

Figure 1.15. Schema depicting the effects of stimulating STR-SNr activity under control or parkinsonian conditions. Left, in control conditions, stimulation of the striato-nigral SPNs in the presence of D1R agonists including DA, provides normal GABA release in the SNr, which activates postsynaptic $GABA_A$ receptors thereby inhibiting SNr firing and facilitating the initiation of movement. Right, the loss of DA in PD led to a deregulation of STR-SNr activity. Image taken from (Borgkvist et al., 2015).

In relation with the findings mentioned before, direct injection of L-DOPA or a D1 agonist into the SNr stimulated motor activity, which was blocked by a D1 antagonist (Robertson and Robertson, 1989; Trevitt et al., 2002). Additionally, since presynaptic D1Rs also facilitate the STR-SNr projection from the ventral STR, D1R agonist in the SNr can enhance limbic functions and reward-related signals originating in the ventral STR. As we explained previously, the ethiopathogenesis and mechanisms underlying

LID are not very well understood, for this reason an important finding recently published by (Hernández et al., 2017) could help to clarify this phenomenon. In this study, they observed, using optogenetic techniques, that the selective activation of the dorsolateral STR in the 6-OHDA rat model triggered dyskinesia. This effect was associated with a preferential activation of the direct STR-SNr pathway. In the same way Keifman and colleagues showed that D1R are essential to induce dyskinesias (Keifman et al., 2019). These results support the emerging importance of the SNr as a node within the BG not only regarding PD but also could open new avenues in the understanding of the mechanisms involved in LID.

In conclusion, DA maintains equilibrium between somatic and dendritic inhibitory inputs received by SNr neurons, whose precise function remains to be elucidated. The impact of DA depletion on GP-SNr synaptic transmission has not been described so far, but a recent publication has revealed an increase in IPSC amplitude after DA depletion in rats (Faynveitz et al., 2019).

1.3.7. GABAergic transmission in the SNr

In the central nervous system (CNS), the IPSCs events occur when postsynaptic $GABA_A$ receptors are activated following brief exposure to a high concentration of GABA, which is released from presynaptic vesicles. The resultant increase in membrane conductance underlies what is known as 'phasic' inhibition. In recent years, it has been manifested that GABA receptor activation can also take place in a less spatially and temporally controlled manner. GABA escaping from the synaptic cleft can activate receptors on presynaptic terminals or at neighboring synapses on the same or nearby neurons (a phenomenon called 'spillover'). In addition, low GABA concentrations in the extracellular space can result in the persistent or 'tonic' activation of $GABA_A$ receptors. These two forms of GABAergic inhibition coexist to control the excitability of neuronal networks (Farrant and Nusser, 2005). While fast, phasic synaptic transmission, specifically regulates AP generation and synchronize activity among neurons (Cobb et al., 1995; Baufreton et al., 2005; Baufreton et al., 2009), the persistent tonic inhibition, sets the level of excitability of neurons (Semyanov et al., 2004).

Both phasic and tonic inhibition transmission are under the control of GABA transporters (GATs) present on GABAergic terminals or/and on astrocytes and whose

main functions are to rapidly remove GABA from the synaptic cleft to prevent GABA spillover to neighboring synapses (Overstreet and Westbrook, 2003) and limit excessive activation of synaptic and extrasynaptic GABA receptors (Brickley and Mody, 2012). Not much is known about the role played by GATs in the SNr, but in the GP, our laboratory has revealed that DA-depletion induces a reduction of the expression of GAT-3 in GP astrocytes, leading to reduced uptake and elevation of ambient extracellular GABA levels promoting the activation of extrasynaptic $GABA_AR$-mediated tonic inhibition (Chazalon et al., 2018). As basal levels of GABA are elevated in SNr in hemiparkinsonian rats (Windels et al., 2005), it is likely that at least GABAergic tonic transmission could suffer major modifications in parkinsonian animals.

I. Phasic GABAergic transmission

As we have explained, STR-SNr and GP-SNr fibers converge onto SNr neurons and these GABAergic inhibitory inputs are mediated by the ionotropic $GABA_A$ and the metabotropic $GABA_B$ receptors producing an increase in chloride conductance that underlies fast IPSC. Both, $GABA_A$ and $GABA_B$ receptors have been found on the membrane of SNr neurons (Bowery et al., 1987; Nicholson et al., 1992; Charara et al., 1999; Boyes and Bolam, 2003), nevertheless stimulation of striatal or pallidal afferents, triggered inhibition and IPSC mediated, predominantly or exclusively by postsynaptic $GABA_A$ receptors (Tepper et al., 1995; Paladini and Tepper, 1999). $GABA_A$ receptors are pentameric assemblies usually made up from at least three different proteins selected from 19 different subunits. These include α_{1-6}, β_{1-3}, γ_{1-3}, δ, ε, θ, π, and ρ1-3 (Olsen et al., 2009). The $GABA_B$ receptor is a metabotropic receptor (Bowery et al., 1997; Bowery, 2007) and is known to consist of at least two heteromeric subunits, namely, the $GABA_BR1$ and $GABA_BR2$ subunits (Jones et al., 1998; Kaupmann et al., 1998; White et al., 1998)

In the SNr, GABAergic synaptic transmission is mediated by $GABA_ARs$ containing α1, β2/3 and/or γ2 subunits at synapses (**Fig. 1.16**). Immunolabelling for these subunits of the $GABA_A$ receptor within the SNr has been widely described (Nicholson et al., 1992; Pirker et al., 2000; Schwarzer et al., 2001; Fujiyama et al., 2002). Indeed, the quantitive analyses performed by Fujiyama et al., 2002 allowed to reveal the subunit composition of the axon terminals from the STR and GP. These authors demonstrated that axon terminals derived from the STR formed synapses that express

α1, β2/3 and/or γ2 subunits. The same subunits were found for GP and/or local collaterals of SNr neurons. Besides, some studies in the SNr have shown that in particular the α1 subunit (mRNA) expression is age and gender related. In postnatal 30 days rats, α1 levels were higher than in 15 days rats (Moshé et al., 1994), as well as in female rats compared to male rats (Veliskova et al. et al., 1998; Ravizza et al., 2003). It is worth to mention that some authors who discerned among PV+ and PV- neurons in the SNr, showed that PV+ SNr neurons display $GABA_A$ receptors containing α1 subunits and at least one subtype ($GABA_BR2$) of the $GABA_B$ receptor (Ng and Yung, 2000, 2001).

II. Tonic GABAergic transmission

Immunocytochemical and electron microscopic studies investigating the subunits composition of extrasynaptic $GABA_A$ receptors mediating tonic inhibition contain δ, α4, α5 or α6 subunits (Nusser et al., 1998; Pirker et al., 2000; Farrant and Nusser, 2005; Luo et al., 2013). However, the majority of tonic current is generated by extrasynaptic $GABA_A$ receptors that contain either δ or α5 subunits (Stell et al., 2003; Caraiscos et al., 2004b; Glykys et al., 2008; Bright et al., 2011); (**Fig. 1.16**).

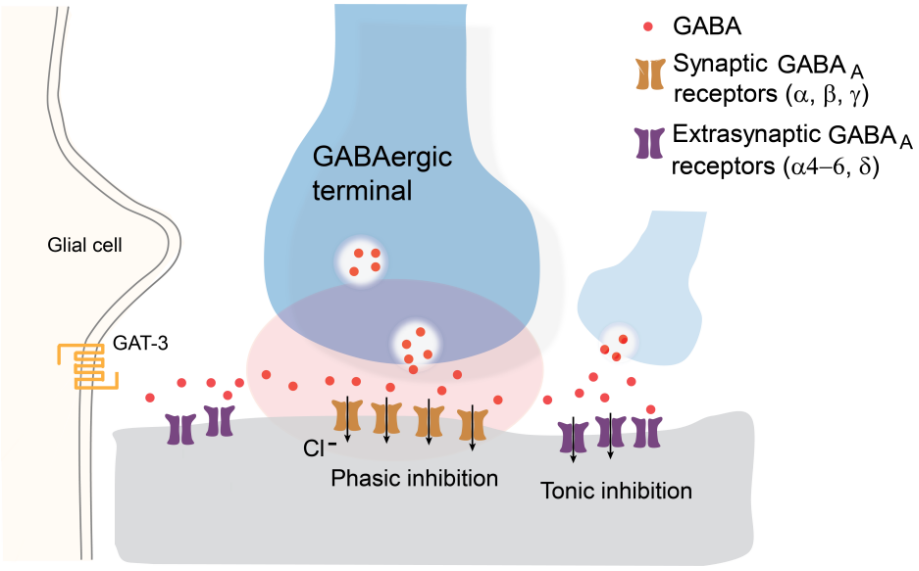

Figure 1.16. Schematic drawing of $GABA_A$ receptors activation. A vesicle can liberate several thousand GABA molecules into the synaptic cleft activating GABA synaptic receptors normally

conformed of α, β, and γ subunits. Low concentration of ambient GABA, which persists despite the activity of the neuronal and glial GABA transporters GAT-3, tonically activates high-affinity extrasynaptic receptors. These receptors contain normally α5 or δ subunits and mediate tonic inhibition.

Most studies of tonic inhibition have been conducted *in vitro* in acute brain slice preparations and these have allowed the identification of tonic $GABA_A$ receptor-mediated conductances in all major brain areas including cortex, hippocampus, *thalamus*, *hypothalamus* or brain stem (Farrant and Nusser, 2005; Brickley and Mody, 2012). Recordings of tonic inhibition have been made in many different labs under a variety of different experimental conditions, many of which are likely to influence the magnitude of the tonic conductance. The subunits responsible for tonic conductance are fairly well established in other brain regions (Glykys et al., 2008), but those subunits that mediate tonic conductance in the SNr remain almost elusive.

Regarding δ–$GABA_A$ receptors, it is important to mention some remarkable properties that discriminate them as an important receptor subtype in the CNS. First, they generate a persistent, "tonic" current that profoundly affects neuronal excitability (Maguire et al., 2009; Bonin et al., 2011). Indeed it has been assumed not only to regulate a variety of behaviors such as memory, anxiety and nociception (Whissell et al., 2013; Cushman et al., 2014; Lee and Maguire, 2014) also it has been considered a therapeutic target in the treatment of neurological and neuropsychiatric disorders (Maguire and Mody, 2008; Olmos-Serrano et al., 2011). The δ–$GABA_A$ receptors exhibit a remarkable capacity for dynamic changes in expression levels under different physiological and pathological conditions. For example, the level of expression of the $GABA_A$ δ subunit is age- and sex- dependent in the SNr (Chudomel et al., 2015). Interestingly, up-regulation of δ-subunit seems to be associated with negative side effects on memory and motor function (Diaz et al., 2014). The increased expression of this subunit is also thought to contribute to memory impairment following injury (Wiltgen et al., 2005; Moore et al., 2010) and/or disrupt post-stroke recovery of motor function (Clarkson et al., 2010).

Focusing on $GABA_A$Rs incorporating the α5 subunit, some studies have shown its expression in hippocampus, cortex and ventral STR of humans (Mendez et al., 2013). In rodents, this receptor has been found in cortex, amygdala, olfactory bulb and spinal cord, and particularly densely expressed in the hippocampus (Rudolph and Möhler,

2014). Specific blockers of tonic inhibition mediated by α5-containing $GABA_A$Rs and knockout mice for α5 exhibited learning and cognition improvement (Martin et al., 2009; Atack, 2011; Rudolph and Möhler, 2014). Besides, mice with a partial or full deficit of α5-$GABA_A$Rs show improved performance in associative learning and memory tasks (Collinson et al., 2002; Crestani et al., 2002; Yee et al., 2004). Pharmacologically, the use of negative allosteric modulators specific for α5-$GABA_A$Rs, such as α5IA, L-655,708, or RO-493851, enhance learning and cognitive performance in rodents (Navarro et al., 2002; Chambers et al., 2004; Dawson et al., 2006; Ballard et al., 2009; Etherington et al., 2017).

To sum up, the ongoing development and refinement of negative allosteric modulators specific for α5-$GABA_A$Rs and other drugs that modulate tonic inhibition mediated by δ-$GABA_A$Rs, hold promise as novel treatments for PD, Alzheimer's disease, or other neurological and psychiatric disorders characterized by deficits in learning, memory, or cognition.

2. HYPOTHESIS AND OBJECTIVES

The SNr is a key output nucleus of the BG mainly composed of GABAergic neurons that participate in movement, cognition or emotional–motivational processes, among others. SNr neurons exhibit a tonic firing rate regulated by inputs from other nuclei of the BG such as the STR, GP and STN. In PD, the absence of DA triggers not only an increase of GABA levels in the SNr, but also alters the pattern of activity of SNr neurons producing an over-activation of this nucleus. In addition, the long-term administration of L-DOPA induces potentially disabling abnormal movements known as LID attributed to increased synaptic plasticity in the SNr. Although the SNr has been classically considered a homogeneous nucleus, different types of GABAergic neurons can be found, as PV+ and PV- neurons. As already known for other BG nuclei, further investigating this neuronal diversity is essential for understanding SNr functioning in control and pathological states.

Taking these findings into account, we hypothesized that dopaminergic lesion and subsequent L-DOPA treatment, could induce differential modifications in the excitability of SNr neuron subpopulations that could be responsible, at least in part, for the altered firing rate and pattern of activity described in animal models of PD and LID. We also hypothesized that dopaminergic degeneration could lead to important modifications of GABAergic tonic and phasic transmission in SNr neuron subpopulations.

The global aim of this study was to determine the modifications induced by the DA depletion on the excitability of SNr neurons and GABAergic transmission taking into account the cellular diversity of this nucleus.

To this end, the specific objectives of the present study were:

I. **To study the distribution and proportion of PV+ and PV- neurons in the SNr, the electrophysiological properties of these two cell-types *in vitro* and the changes in their excitability induced by DA depletion and L-DOPA chronic treatment.**

   For this purpose, we performed immunohistochemical identification of SNr neurons followed by cell-attached and whole cell recordings from sham, DA depleted and L-DOPA treated mice.

II. **To electrophysiologically characterize *in vitro* the striatal and pallidal inputs to PV+ and PV- SNr neurons in control and DA depleted conditions.**

For this purpose, we employed optogenetic approaches to compare the short-term plasticity evoked by STR-SNr and GP-SNr stimulation on PV+ and PV- SNr neurons from sham and 6-OHDA lesioned mice.

III. **To characterize tonic GABAergic inhibition in PV+ and PV- SNr neurons, analyzing the subunit composition of extrasynaptic $GABA_A$ receptors and the alteration of this tonic inhibition in DA depleted conditions.**

For this purpose, we performed whole-cell recordings in brain slices from control and DA depleted mice and studied tonic GABAergic transmission by applying the specific $GABA_A$ antagonist, GABAzine. To identify specific components of the tonic current, we used subunit-selective drugs of $GABA_A$ extrasynaptic receptors as the α5 inverse agonist, L-655,708 or the δ-agonist, THIP.

3. EXPERIMENTAL PROCEDURES

3.1. Animals and ethical approval

Experiments were performed in PVcre::Ai9T (PV-IRES-Cre, JAX #008069; Ai9T, JAX #007909) and B6.129-Gabrd^{tm1Geh}/J (δ knock out, δ−/− and wild-type δ+/+; JAX 003725) mice. In the PVcre::Ai9T transgenic mouse line, the Cre recombinase is transcribed under regulatory control of the endogenous PV locus (PVcre) and Cre expression is visualized with a fluorescent reporter (Rosa26$^{lsl\text{-}tdTomato}$; Ai9T). Animals were housed under a 12:12 light-dark cycle with food and water provided *ad libitum*. All efforts were made to minimize animal suffering and to reduce the number of animals used. Experimental procedures comply with the ARRIVE guidelines and were performed in accordance with the EU Directive 2010/63/EU. Experimental protocols were approved by the local ethical committees (CEEA/M20-2015-024 for the UPV/EHU) and by the French Ministry of Research A5012075 and APAFIS#14255.

3.2. Experimental design

In all the studies the number of mice was expressed as m= value and the number of neurons as n= value. **Figure 3.1** shows a schematic representation of the experimental design and chronology of the procedures carried out in the three studies for electrophysiological recordings. TH immunostaining was performed in mice brain slices after *in vitro* experiments (see section **3.7.1**).

STUDY I

We first studied the distribution of SNr neurons in transgenic PVcre::Ai9T mice (sham, m=2), then we analyzed the percentage of co-localization between tdTomato and PV using the same mouse line but in this case we used sham (m=2) and 6-OHDA (m=2) mice. For the *in vitro* electrophysiological properties of SNr neurons we first characterized the two subpopulations in sham (m= 3) animals. In addition, we studied the impact of the 6-OHDA lesion (m=2) and chronic L-DOPA treatment (m=2) in the intrinsic properties of PV+ and PV- SNr neurons *in vitro*. All the recordings were performed at least 2-3 weeks after 6-OHDA/vehicle lesion and 2 additional weeks for L-

DOPA treated mice. Before electrophysiological recordings all animals were subjected to the cylinder test.

STUDY II

We characterized the impact that optostimulation of STR-SNr pathway triggered on PV+ and PV- SNr neurons in sham (m=5) and 6-OHDA (m=6) PVcre::Ai9T mice. We performed *in vitro* electrophysiological recordings of PV+ or PV- SNr in cell-attached and whole cell configuration 4-5 weeks after the virus injection. For the characterization of the GP-SNr pathway and the impact of its optostimulation on PV+ and PV- SNr neurons, we performed cell-attached and whole cell recordings from sham (m=3) and 6-OHDA (m=4) animals 4-5 weeks after the virus injection. The validation of the optogenetic approach for opsin expression in the STR or GP was performed in two sham mice from each group. All animals were subjected to the cylinder test before electrophysiological experiments.

STUDY III

To study tonic inhibition in SNr neurons, *in vitro* electrophysiological recordings of PV+ and PV- SNr cells were obtained from control (m=9) and 6-OHDA lesioned (m=6) PVcre::Ai9T mice. The control group was not subjected to surgery. The recordings from the lesioned group were obtained 2-3 weeks after the stereotaxic injection.

To study the $GABA_AR$ containing δ-subunit contribution to tonic inhibition, we first performed immunohistochemical analysis in wild-type (m=2) and knock-out (m=2) mice for δ-subunit. Whole-cell voltage-clamp recordings were performed in these mice from brain slices of wild-type (m=2) and knock-out (m=2) animals.

In addition, we studied the expression of δ and $\alpha 5$ subunits in the SNr of control (m=2) PVcre::Ai9T mice, for which we processed 3 nigral serial sections for the Immunolabelling of each subunit. Then we performed *in vitro* electrophysiological recordings to study the contribution of the activation of δ-subunits in PV+ and PV- SNr neurons in control (m=3) mice and the impact of 6-OHDA lesion (m=1) on δ-subunit expression. The same *in vitro* electrophysiological recordings were performed to study the contribution of $GABA_A$ α5 subunits in nigral tonic inhibition in control (m=8) and 6-OHDA lesioned (m=7) mice.

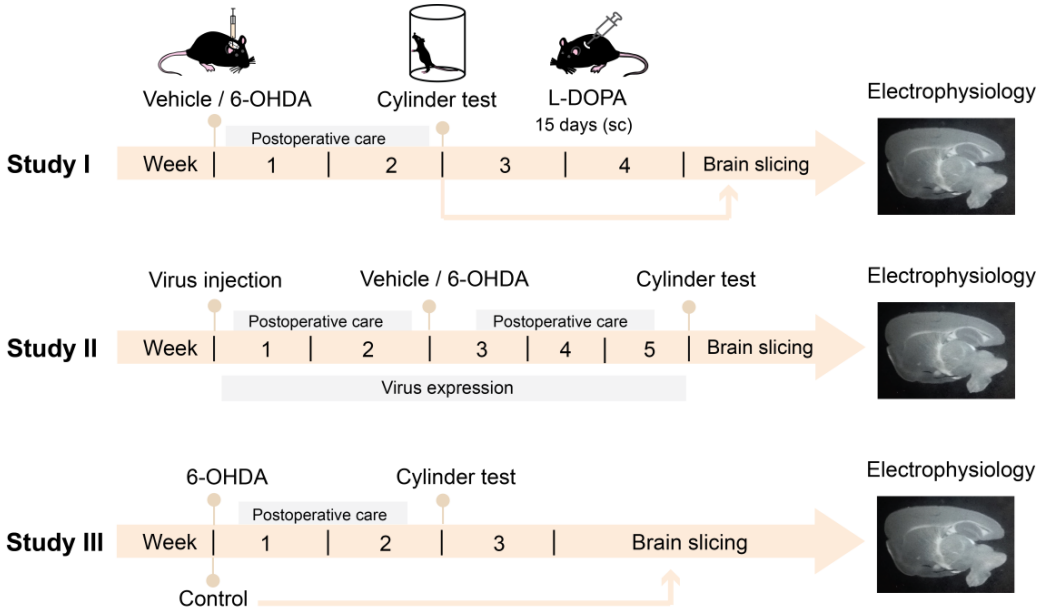

Figure 3.1. Chronology of the experimental procedure followed in the three studies for electrophysiology.

3.3. Drugs

For the lesion/injection, all drugs (Table **3.1**) were prepared on the day of the surgery. Benserazide, desipramine, L-DOPA, were prepared in physiological saline (0.9% NaCl) and 6-OHDA in 0.02% ascorbic acid and NaCl 0.9%. For the *in vitro* recordings, drugs stock was prepared in deionized water as concentrated stock solutions and stored at -20°C. On the day of the experiment, drugs were diluted in artificial cerebrospinal fluid (ACSF) and applied through the bath perfusion system.

TABLE 3.1. | List of drugs.

Chemicals	Action	Distributor	Concentration	References
6-OHDA (6-Hydroxydopamine hydrobromide)	Catecholaminergic neurotoxin	Tocris Bioscience	4 mg/ml (i.c.)	(Lundblad et al., 2004)
Desipramine hydrocholoride	Prevent damage of NAergic neurons	Sigma-Aldrich	25 mg/Kg (i.p.)	(Cenci and Lundblad, 2007)
Benserazide hydrochloride	Inhibitor of AADC	Sequoia research	6 mg/Kg (i.p.)	(Cenci and Lundblad, 2007)
L-DOPA (3,4- Dihydroxi-L-phenylalanine)	Precursor of dopamine	Sequoia research	12 mg/Kg (i.p.)	(Cenci and Lundblad, 2007)
D-AP5	NMDA antagonist	Tocris Bioscience	50 µM	(Baufreton et al., 2005)
DNQX disodium salt	AMPA/Kainate receptor antagonist	Tocris Bioscience	20 µM	(Baufreton et al., 2005)
Picrotoxin	$GABA_A$ receptor antagonist	Tocris Bioscience	50-100 µM	Avshalumov et al., 2000
SR-95531 (Gabazine)	$GABA_A$ receptor antagonist	Tocris Bioscience	10 µM	(Baufreton et al., 2005)
QX 314 chloride	Intracellular Na+ channel blocker	Abcam	5 mM	(Brown et al., 2014)
THIP hydrochloride	Agonist of $GABA_A$ receptor δ subunits	Tocris Bioscience	1 µM	(Meera et al., 2011)
L-655,708	Inverse agonist $GABA_A$ receptors α5 subunit	Tocris Bioscience	1 µM	(Quirk et al., 1996)
Biocytin	Intracellular dye	Sigma-Aldrich	4-5.4 mM	(Abdi et al., 2015)
Rimadyl	Anti-inflammatory	Virbac	50 mg/ml (s.c.)	(Seeger-Armbruster and Von Ameln-Mayerhofer, 2013)

3.4. Stereotaxic surgical procedures

3.4.1 Unilateral 6-OHDA injections

Mice were pretreated, approximately 25 min before the injection of 6-OHDA, with desipramine (25 mg/kg, i.p; Sigma) in order to prevent the damage of noradrenergic neurons. Male and female mice (postnatal 6-12 weeks) were anesthetized with 5% vaporized isofluorane (Tem-Sega Inc. Pessac) and placed in a stereotaxic frame with a mouse-adaptor (David Kopf Instruments with Digital Display Console). The level of anesthesia was checked by the lack of withdrawal reflex to pinching of the hind limbs and maintained with isofluorane (1.5-2% v/v in O_2). Analgesia was achieved by subcutaneous (s.c.) injection of 0.05 ml/10 g body weight, of Rimadyl (Carprofen, 250 mg/kg). A heating-pad was positioned underneath the animal to keep the body temperature at 37°C and eye dehydration was prevented by topical application of ophthalmic gel. After disinfection of the skin with betadine we made a small craniotomy and proceed to inject the neurotoxin 6- OHDA which was dissolved in 0.9% w/v NaCl solution containing 0.02% w/v ascorbate to a final concentration of 4 mg/ml. We injected 1 μL of 6-OHDA unilaterally into the medial forebrain bundle (MFB) at the following coordinates (in mm relative to bregma, sagittal suture and dural surface, cf. Paxinos and Franklin, 2001): AP: −1.3 mm, ML: -1.2 mm, DV: −4.75 mm. After each injection, the needle was left in place for an additional 2–4 min to allow the toxin to diffuse into the structure before being slowly retracted. Sham lesion was carried out by 1 μl injection of 0.02% ascorbic acid-saline at the same coordinates. To minimize unspecific tissue damage, the injections were performed at a rate of 0.5 μl/min using a glass micropipette connected to a Picospritzer (Parker Hannifin) to ensure that volumes dispensed are linear with time and pressure. After injections, animals were kept warm and allowed to recover from anesthesia (**Fig. 3.2**).

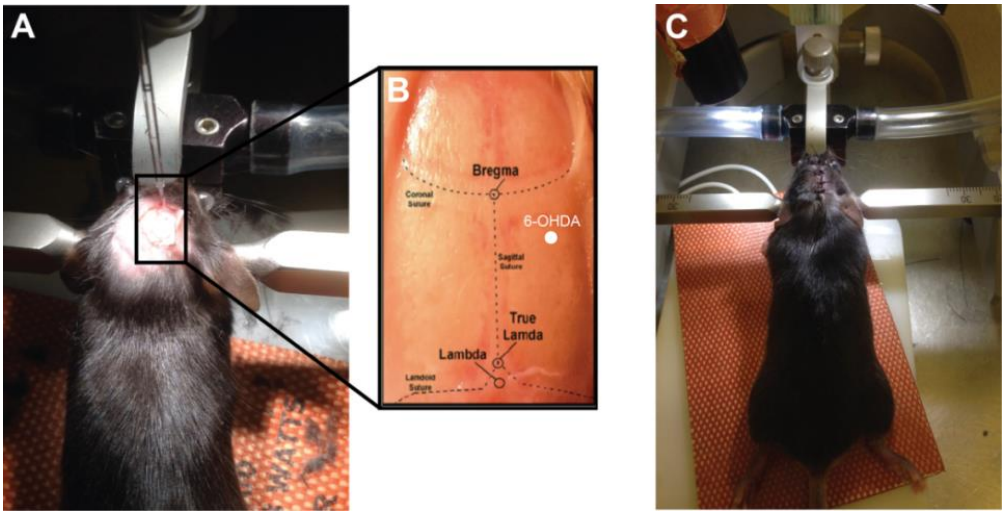

Figure 3.2. Mouse preparation for craniotomy. A: Mouse placed in the stereotaxic frame and centered by symmetrical adjustment of the ear bars and mouth clamped to ensure the perfusion of isoflurane (1.5-2%). The calibrated glass micropipette guaranteed the injection of 1 μL. **B:** Cranial sutures from the mouse head. Bregma and lambda are defined as the points of intersections of the sagittal suture. The white point reflects the coordinates used for the injection. **C:** Mouse placed on the heating pad (37°) after removing the pipette and sutured the incision using surgical needle.

The first 2 post-operative weeks after MFB lesions caused less than 10% mortality thanks to the improved nursing protocol that is described below. To prevent dehydration mice received sterile glucose–saline 20% (0.1 ml/10 g body weight, s.c.) immediately after surgery and once a day during the first post-operative week. In addition, during the first 4-5 days or until they stop losing weight, we injected Rimadyl (0.05 ml/10 g body weight, s.c.) in the morning. Then we replaced this nonsteroidal anti-inflammatory drug (Rimadyl) by saline injections (0.9% NaCl, 0.5 ml/20 g body weight, s.c) during the following days. Mice that showed difficulties for eating due to severe postural asymmetry were hand-fed (i.e. they were presented with the food while being held by the hands of the investigator). In order to avoid competition for the food, weaker mice were placed in separate cages.

3.4.2. Striatal and pallidal viral vector transfection

The surgical procedure used for viral vector transfections was similar to the one used for 6-OHDA lesion. Two viral strategies were followed. On the one hand, for the striatal transfection, we used an adeno-associated virus (AAV) vector expressing the H134R variant of the cation ChR2 (ChR2(H134R)) and fused with enhanced yellow fluorescent protein (EYFP). Under human synapsin (hSyn) promoter we guaranteed the expression of our virus (AAV5-hSyn-ChR2(H134R)-EYFP) into the STR of male and female PVcre::Ai9T mice.

On the other hand, for the GP transfection, we used a Cre-Lox expression strategy to selectively express ChR2 in PV-GP neurons of male and female PVcre::AI9T mice. We administered the AAV vector (AAV5-DIO-hChR2(H134R)-EYFP) into the GP. As it has been described in the literature, only prototypic GP neurons project to downstream nuclei (e.g. STN, EPN and SNr) of the BG and most of them express PV (Abdi et al., 2015; Dodson et al., 2015). The Cre-LoxP system is a widely used powerful technology for gene editing. It consists of a Cre recombinase, which was discovered as a 38-kDa DNA recombinase produced from cre (**c**yclization **re**combinase) gene of bacteriophage P1 and which thereby recognizes the specific DNA fragment sequences called *loxP* (**l**ocus **o**f **x**-over, **P**1) site and mediates site-specific deletion of DNA sequences between two loxP sites (Sauer, 1998). Regarding the mechanism of Cre-loxP system, a single Cre recombinase recognizes two directly repeated *loxP* sites, then the Cre excises the *loxP* flanked (floxed) DNA, thus creating two types of DNA with circular, excised and inactivated gene Y. In our case, we used DIO constructs (double-floxed inverted open reading frame) to express ChR2–YFP fusions in Cre-expressing neurons carrying the EF-1α promoter and the WPRE to enhance expression. Then the opsin is flipped around into the right position (**Fig. 3.3**).

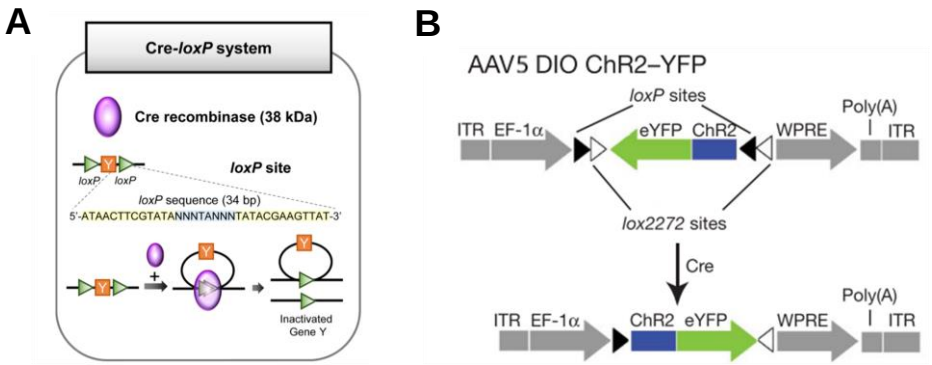

Figure 3.3. Mechanism of Cre-Lox system. A: An overview of Cre-loxP system. 38 kDa Cre recombinase recognizes the *loxP* sites of specific 34 bp DNA sequences. **B:** Diagram of the double-floxed inverted open Cre-dependent AAV5 vector expressing ChR2–YFP under control of the EF-1α promoter. DIO, double-floxed inverted open reading frame; eYFP, enhanced YFP; ITR, inverted terminal repeat; WPRE, woodchuck hepatitis virus post-transcriptional regulatory element. Image **A** from (Kim et al., 2018), image **B** from (Kravitz et al., 2010).

For striatal transfection, one injection of 500 nl was performed in the right STR −2.7 mm and AP: +0.8 mm, ML: −2.0 mm, (relative to bregma). For the transfection into the GP, two injections of 200 nl were made in the right GP at different depths (relative to bregma): AP: -0.5 mm, ML: −2.0 mm, DV: -3.8 and 4.1 mm. After each injection the needle was left in place for an additional 2-4 min and then slowly retracted. After injections, animals were kept warm and allowed to recover from anesthesia, and then they were in observation for postoperative care until 6-OHDA/vehicle injections. Viral vectors were provided by the University of North Carolina (UNC) vector facility.

3.5. Behavioral assessment

3.5.1 Cylinder test

The cylinder test was used to assess the degree of motor impairment produced by DA depletion and the screening of the lesion was evaluated 2 weeks after surgery when the DA depletion is considered stabilized (Cenci and Lundblad, 2007). Briefly, mice were placed individually in a 15 cm diameter glass cylinder, which was located in front of a vertical mirror in order to observe the mice from all angles, and allowed to move freely for 1 min. Mice were immediately video recorded for 3 min. These recordings have been used as a qualitative assessment of the degree of DA depletion and have not yet been examined to count the exact number of supporting wall contacts. However, DA depletion was confirmed *post-hoc* by TH immunohistochemistry and only mice with striatal TH loss > to 80% were included in the study (**see section 3.7.1**).

3.5.2. Abnormal involuntary movements

Sixteen days after the 6-OHDA lesion the cylinder test was used to evaluate the degree of motor impairment and at that moment chronic L-DOPA treatment was initiated. L-DOPA methyl ester (6 mg/kg i.p., Sequoia Research) plus benserazide (12 mg/kg i.p., Sequoia Research) were given intraperitoneally (Mela et al., 2007). This dose of benserazide is within the range required to ensure a sufficient duration (>2 h) of the biochemical and motor effects of single L-DOPA doses in rodents (Da Prada et al., 1987). Every day, immediately after L-DOPA administration, the mice were placed in separated cages during at least 2 hours, and AIMs were rated as previously described (Cenci and Lundblad, 2007).

The mice were evaluated a total of three times during the chronic L-DOPA treatment period on days 1, 7 and 15, respectively. Each mouse was observed individually for 1 min every 20 min for 3 h, starting 20 min after L- DOPA/benserazide administration. Only hyperkinetic and dystonic movements that could be clearly distinguished from naturally occurring behaviors (i.e. grooming, sniffing, rearing and gnawing) were considered in the ratings. The AIMs were classified into three different subtypes based on their topographic distribution: (i) axial AIMs, i.e. Lateral flexion of the neck or torsional movements of the upper trunk towards the side contralateral to the lesion; (ii) forelimb AIMs, i.e. hyperkinetic, jerky stepping movements of the forelimb

contralateral to the lesion, or small circular movements of the forelimb to and from the snout; (iii) orolingual AIMs, i.e. It is recognizable as bursts of empty masticatory movements, accompanied to a variable degree by jaw opening. Each AIM subtype was scored on a severity scale from 0 to 4: 0, absent; 1, present during less than half of the observation time; 2, present during more than half of the observation time; 3, present all the time but suppressible by external stimuli; 4, continuous, severe and not suppressible. Examples of the three subtypes of dyskinetic behavior and scheme depicting the experimental procedure are shown in the **Figure 3.4**. The last day of L-DOPA treatment (day 15), brains were removed 20–120 minutes after the L-DOPA injection (the time period of intense dyskinetic behaviour).

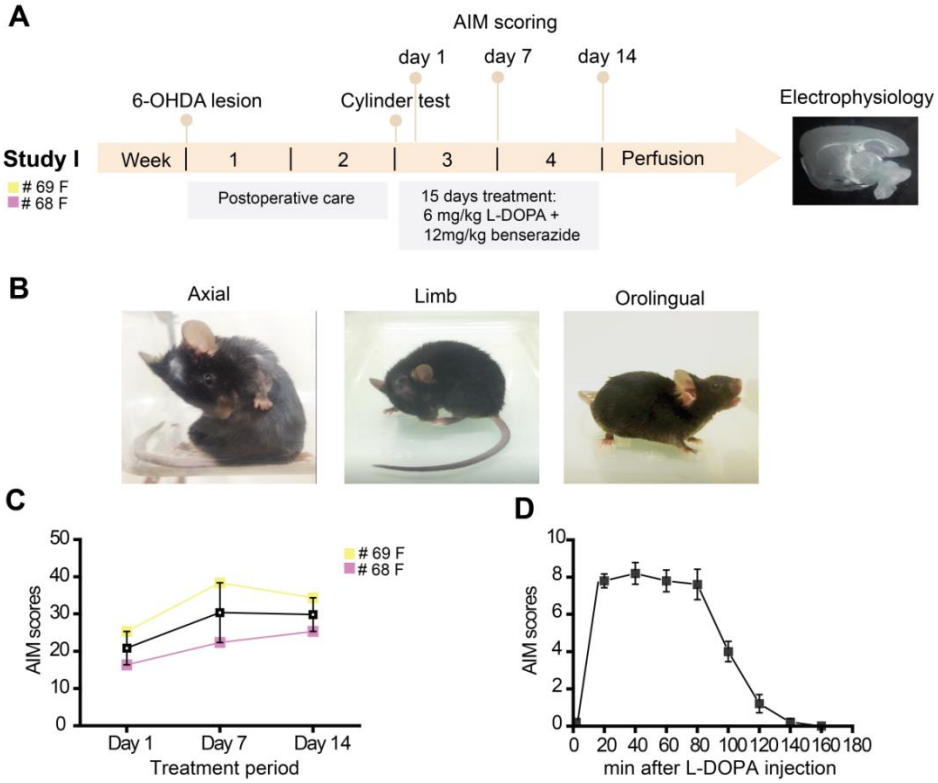

Figure 3.4. L-DOPA induced dyskinesia in mice with unilateral 6-OHDA lesion of the MFB. **A:** Chronology of the experimental procedure followed for the Study I**. B:** Images of different L-DOPA-induced dyskinesia subtypes. **C:** The sum of axial, limb and orolingual abnormal involuntary movements (AIM) scores per session during chronic L-DOPA treatment (the L-DOPA dose was 6/mg/kg/day combined with 12 mg/kg/day of benserazide). **D:** Just 20 min after L-DOPA injection AIMs could be observed, concluding at 140 min with plateau of about 60 min (data of session day 15 is displayed for 2 mice included in the Study I).

3.6. *In vitro* electrophysiological recordings

3.6.1. *In vitro* Slice Preparation

Animals were anesthetized with a mixture of ketamine and xylazine (75 mg/kg and 10 mg/kg, respectively, i.p.) and transcardially perfused with ice-cold modified ACSF, equilibrated with 95% O_2 and 5% CO_2, and containing (in mM): 230 sucrose, 26 $NaHCO_3$, 2.5 KCl, 1.25 NaH_2PO_4, 0.5 $CaCl_2$, 10 $MgSO_4$ and 10 glucose. The brain was then quickly removed from the skull, blocked in the parasagittal plane, glued to the stage of a vibratome (VT1200S; Leica Microsystems, Germany) and sectioned into 300 µm-thick parasagittal slices. Slices containing the SNr were then left to equilibrate for ~1 h (at ~35°C) in ACSF of the following composition (in mM): 126 NaCl, 26 $NaHCO_3$, 2.5 KCl, 1.25 NaH_2PO_4, 2 $CaCl_2$, 2 $MgSO_4$, 10 glucose, 1 sodium pyruvate and 4.9 L-gluthathione reduced (gassed with 95% O2–5% CO_2). Then, slices were kept at room temperature (22-26°C) in oxygenated ACSF until transfer to the recording chamber.

3.6.2. Electrophysiological recordings

Single slices were transferred to a recording chamber, perfused continuously with oxygenated ACSF at 32-34°C, and visualized using infrared gradient contrast video microscopy (E600FN, Eclipse workstation, Nikon, Japan) and a water-immersion objective (Nikon Fluor 60 X/1.0 NA). The microscope was also equipped with epifluorescence (Nikon Intensilight C-HGFI) that allowed us to perform selective patch-clamp targeting of PV-expressing or PV non-expressing SNr neurons in real time. Recordings were obtained using a Multiclamp 700B amplifier and Digidata 1320A/1550B digitizers controlled by Clampex 10.3 (Molecular Devices, Sunnyvale, CA, USA).

For the optogenetic experiments we used a high power optogenetics-LED module (Prizmatix, Israel) connected to an optic fiber (∅=500µm, NA: 0.63) placed above the brain slice. The set-up employed for all electrophysiological experiments is described in the **Figure 3.5**.

Recordings from individual neurons were made using pipettes (impedance, 3–6MΩ) prepared from borosilicate glass capillaries (G150–4; Warner Instruments,

Hamden, CT, USA) with a micropipette puller (P- 97; Sutter Instruments, Novato, CA, USA). In whole cell voltage-clamp recordings, cells were hold at −60 mV and series resistance was monitored by a step of –5 mV. Data were discarded if series resistance exceeded 25 MΩ or when the series resistance changed ± 20%. Signals were low-pass filtered at 2 kHz and sampled at 10 kHz for voltage clamp mode, and at 4 kHz and sampled at 20 kHz for current clamp mode. After electrophysiological recordings, slices were fixed overnight in a solution of paraformaldehyde at 4% and maintained in PBS-azide at 0.2% at 4°C until immunohistochemical processing for *post-hoc* verification of cell identity (**see section 3.5.4**).

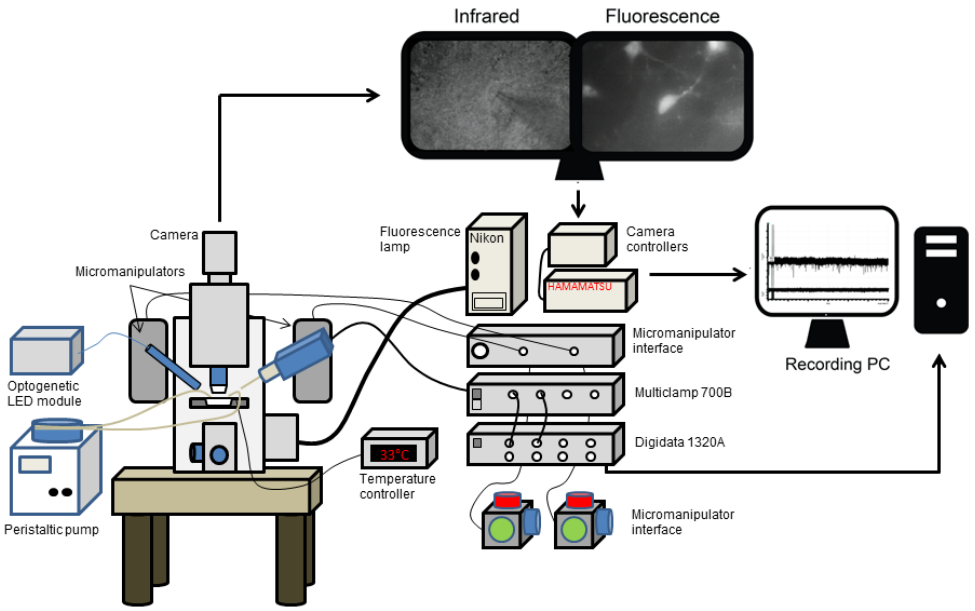

Figure 3.5. Schematic illustration of the patch clamp set-up. Data from the recordings was acquired using a Multiclamp 700B amplifier, digitized with a digidata and stored on-line using the pClamp 10 software. To visualize the cells, the image from the microscope was enhanced with a camera to a camera controller and displayed on a TV monitor.

I. Intrinsic properties of SNr neurons

In experiments designed to define the autonomous and driven firing of the SNr, neurons were first recorded in cell-attached mode and then in whole-cell current-clamp

mode. The patch pipette solution contained (in mM): 120 Kgluconate, 10 KCl, 10 NaCl, 11 Na_4-EGTA, 10 HEPES, 1 $CaCl_2$, 0.4 Na_3GTP, 2 $Mg_{1.5}ATP$ and 4 biocytin. The pH and osmolarity of the pipette solution were adjusted at 7.2 and 290 mOsm l^{-1}, respectively. In cell-attached configuration SNr neurons were recorded for 2–4 min at a holding potential of 0 mV after the stable establishment of the gigaseal. Once completed, the holding potential was set at -60 mV to switch in whole-cell configuration and the spontaneous firing of SNr neurons was recorded in current-clamp mode. Negative and positive steps of currents were injected through the patch-pipette to collect membrane properties and driven activity of SNr neurons. All recordings were achieved in the presence of NMDA and AMPA glutamatergic receptor antagonists (50 µM D-AP5, 20 µM DNQX, respectively) and GABAergic synaptic transmission (50 µM picrotoxin). The junction potential (JP) with our KGluconate-based internal was calculated as +13 mV and was not corrected unless otherwise mentioned (JPCalc, Clampex 10).

II. Electrophysiological verification of viral transfection in GP and STR cells

For the optogenetic approach, we used the same set-up previously presented but in this case we used an optic fiber connected to a blue laser with a wavelength of 460 nm with a maximum output of 440 mW. An optical fiber was positioned above an area with good striatal and pallidal transfection, as observed under a fluorescence microscope. Continuous pulse (100 ms) of blue light was flashed onto the transfected area first to validate the optogenetic approach for opsin expression in the STR and/or GP.

In order to verify that striatal SPN or PV-GP neurons were transfected with ChR2 cell attached recordings were performed in the STR or the GP depending on the type of transfection. All recordings were made in the presence of potent and selective blockers of glutamatergic synaptic transmission (50 µM D-AP5, 20 µM DNQX). The patch pipette solution contained (in mM): 120 Kgluconate, 5 QX-314, 10 KCl, 10 NaCl, 11 Na_4-EGTA, 10 HEPES, 1 $CaCl_2$, 0.4 Na3GTP, 2 $Mg_{1.5}ATP$ 4 biocytin. The pH and osmolarity of the pipette solution were adjusted at 7.2 and 290 mOsm l^{-1}, respectively.

A continuous 100-ms long flash of blue light was delivered over the transfected area (STR/GP). Firing rates of SPN or PV-GP neurons before, during and after the flash were compared. We tested that the viral expression of ChR2 was sufficient to excite

striatal SPNs or PV-GP neurons, respectively. We identified SPN neurons because they are silent and do not express the PV and in the same way we identified PV-GP neurons for expressing the PV and fire spontaneously. We only included in the study the recordings in which direct activation of ChR2 in recorded neurons increased the firing activity of neurons at least in a 40-50% of the total current.

III. Characterization of STR-SNr and GP-SNr GABAergic synaptic transmission.

For studying STR-SNr or GP-SNr synaptic transmission, cell-attached and whole-cell voltage-clamp recordings were performed using the same perfused and pipette solutions than for viral verification.

In this case, the optical fiber was placed more close to the SNr with the purpose of stimulating axon terminals projecting to the SNr and studying the impact of STR-SNr and GP-SNr synaptic transmission on the activity of SNr neurons. First, SNr neurons were recorded in cell-attached mode and a train of 10 optical stimulations of 1 ms duration at 10 Hz were delivered with a light power of 90 mW in order to successfully trigger an AP in presynaptic terminals (Xu-Friedman and Regehr, 2005) and promote GABA release for both striatal and pallidal transfections. Inhibition-driven changes in firing rate of SNr neurons were then quantified and those cells, in which the optoactivation of STR-SNr or GP-SNr synapses did not trigger IPSCs, were excluded from the study.

The properties of STR-SNr and GP-SNr synapses were examined in whole-cell voltage-clamp mode at a holding potential of -25 mV, and the JP was not corrected (i.e. -38 mV after JP correction). Single pulse or train (10 pulses) of optical stimulation at various frequencies (5-60Hz) were used to characterize the amplitude of single IPSC and the short-term plasticity of STR-SNr and GP-SNr synapses in control and 6-OHDA lesioned mice.

IV. Characterization of tonic GABAergic inhibition in SNr neurons

To study spontaneous GABAergic transmission and tonic inhibition a CsCl-based internal solution containing (in mM): 135 CsCl, 3.6 NaCl, 1 MgCl2.6H2O, 10 HEPES, 5 QX-314, 0.1 Na4EGTA, 0.4 Na3GTP, 2 Mg1.5ATP and 5.4 biocytin (pH of 7.2 and osmolarity of 290mOsml-1) was used. Spontaneous IPSCs $GABA_A$ receptor-mediated inhibitory postsynaptic currents were recorded at a holding potential of −60 mV (i.e. -64 mV, JP not corrected= 4mV). All recordings were performed in the presence of NMDA and AMPA receptor antagonists (50 µM D-AP5, 20 µM DNQX, respectively). Tonic inhibition was measured as a shift in holding current induced by bath application of 20µM of GABAzine; (**Fig. 3.7**). Once GABAzine was applied, the slice was not further used.

3.6.3. Electrophysiological data analysis

Analyses were carried out off-line using Clampfit application of pClamp 10.3 software and OriginPro 8.0 (Microcal Software). Figures were generated using Illustrator CS5. Data are presented as the median and interquartile range unless otherwise stated. Box plots (central line: median; box: 25%–75%; whiskers: 10%–90%) are used to illustrate sample distributions with individual values represented by circles, diamonds or triangles depending on the specific condition (sham, 6-OHDA or L-DOPA).

I. Intrinsic properties of SNr neurons

Mean firing rate was calculated from the total number of spikes per data epoch (30 s) both in cell-attached and whole-cell current-clamp recordings. Spikes were detected and interval interspike (ISI) calculated using Clampfit. The mean firing rate was then calculated as the inverse of the mean ISI (1/ISI) and express in Hz. The coefficient of variation (CV) which reflects the regularity of the pacemaking of SNr neurons was calculated as $SD_{ISI}/mean_{ISI}$ and expressed in percentage.

AP characteristics were calculated using Origin 8.0. The AHP peak value is obtained in Origin 8 by detecting the most negative membrane potential value peaks occurring after each AP (**Fig. 3.6A**). The AP threshold (APth) was calculated using a custom algorithm (Baufreton et al., 2005) that detected the first point of sustained

positive “acceleration” of membrane voltage [(dV/dt)/dt] that was >2 SDs of baseline voltage potential few ms before AP threshold. The AHP magnitude (AHPmag) was calculated by subtracting the APth from the AHP peak. These parameters can be visualized on the phase-plot representation of the AP (**Fig. 3.6B**).

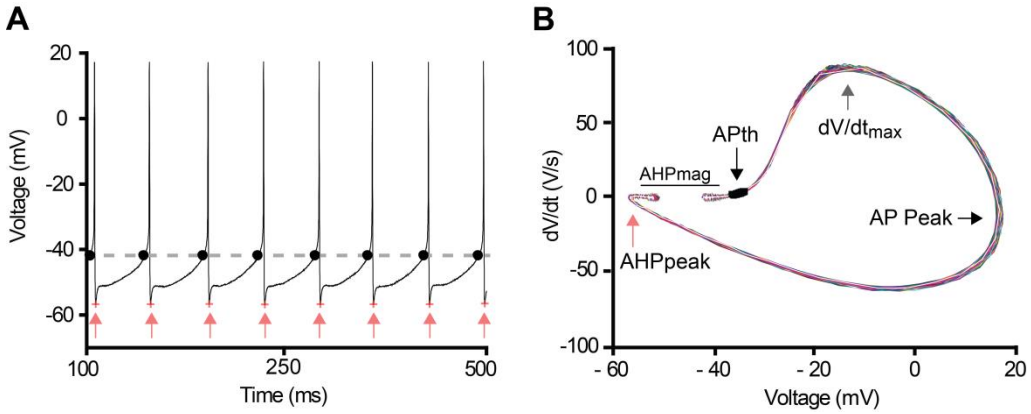

Figure 3.6. The AP analysis. A: The after hyperpolarization peak (AHP) value is the result of the average from the detection of the most negative peak occurring after AP (red arrows). The AP_{th} is the result of averaging the most positive peaks (back dots). **B:** Plot depicting the rate of change of membrane potential (dV/dt) plotted against the membrane potential (phase plot). The inflection denoting APth is indicated for each AP as a black square. The maximum rate of rise of the AP (dV/dt_{max}, grey arrow), the peak of the AP (dV/dt=0, black arrow), and the most hyperpolarized point of the AHP (dV/dt=0, red arrows) can also be extracted from the phase plot. The AHP magnitude (AHPmag) is calculated by subtracting the APth from the AHP peak (AHPmag=APth-AHPpeak) and is also represented on this diagram. Several AP are superimposed.

The sag recovery is obtained by dividing the sag peak by the peak when neurons were hyperpolarized to -150 pA of current for 1s duration (shown in results). Frequency-current (F-I) response curves were obtained by injecting incremental current pulses from -150 pA to 325 pA (1 s duration; 25 pA steps). The frequency gain (FRgain) was a result of dividing the maximal frequency (at 325 pA) by the spontaneous frequency. An index of firing rate adaptation was calculated as the ratio between the instantaneous firing frequencies of the first two spikes and last two spikes fired in response to a current pulse of 100 pA.

II. Optogenetic experiments

The effect of optogenetic manipulations on the excitability of transfected SPNs/PV-GP neurons or on the firing rate of SNr neurons was addressed in cell-attached recordings. For characterization of striatal or pallidal transfection we studied the change in firing rate with a continuous optical stimulation of 100 ms at a laser power of 4 mW at the tip of the optic fiber. Raster plot graphs were generated for each trial and mean firing rate was calculated for each neuron on bin size of 50 ms in order to generate representative population plots. Mean firing rate was calculated from OFF/ON epochs of laser stimulation. The same analysis was applied for the calculation of SNr firing rate during STR-SNr and GP-SNr optical stimulation with pulse trains at 10Hz (10 pulses, 1ms duration; laser power: 90mW).

Optically-evoked IPSC amplitude was measured as the peak of outward current relative to the baseline holding current preceding each light pulse. For trains of stimulation, normalized IPSC amplitude was calculated by dividing the amplitude of each IPSC of the train by the amplitude of the first IPSC ($IPSC_n/IPSC_1$).

III. Tonic inhibition analysis

Spontaneous IPSC were detected using an in-house software (DetectionMini 8.0; M. Goillandeau) and detection was checked by manually by the experimenter for validation. From the detection, IPSC amplitude, frequency and kinetic parameters were determined. For the calculation of tonic inhibition, all-points histograms were generated on 30 s of recordings under basal condition and in presence of GABAzine with Origin.

Each distribution was fitted by a Gaussian distribution to define the holding current value (**Fig. 3.7).**

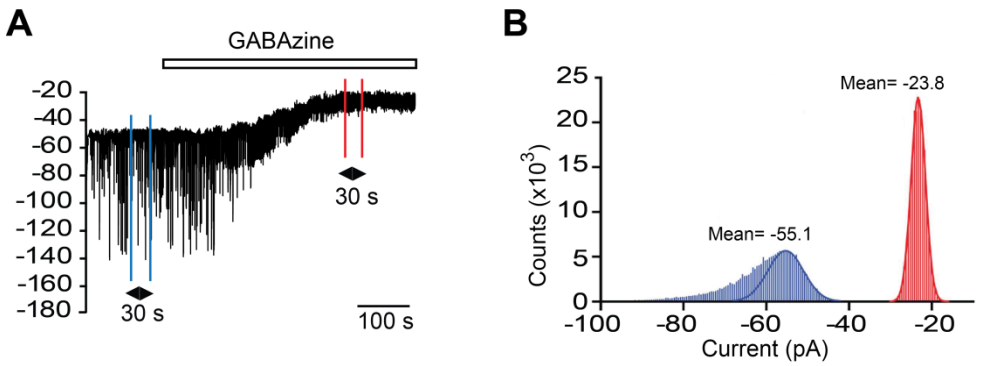

Figure 3.7. Methods for measuring tonic GABA current shifts. A: Example current trace recorded from a SNr neuron illustrating the block of a tonic GABA current, revealed by the outward shift in the holding current. **B:** The tonic current is defined by generating all-points histograms for the control and GABAzine epochs and then fitting Gaussian curves to the positive side of these histograms. The mean values from the Gaussian fits are used to define the currents and calculate the holding current by resting 55.1-23.8 = 31.3 pA.

3.7. Immunohistochemistry

All the antibodies used within the three studies are shown in the **Table 3.2** at the end of this section.

3.7.1. Histological processing after in vitro experiments

I. TH immunostaining

Sagittal brain slices (300 μm-thick), used for *in vitro* electrophysiology, from 6-OHDA lesioned and L-DOPA treated mice, were processed for TH immunoreactivity to quantitatively confirm the decreased of dopaminergic fibers expected after the 6-OHDA lesion into the MFB. Slices conserved in PBS-azide (at 0.2%, 4°C) were first rinsed (2 washes for 5 min) in PBS and then we proceed to inactivate the endogenous peroxidases (3% H_2O_2 in PBS for 20 min). We repeated again 2 washes for 5 min in PBS and then sections were incubated for 60 min in 1% bovine serum albumin (BSA) in PBS containing 0.3% Triton X-100. Next, slices were incubated in primary antibody anti-TH (1:1000) overnight in gently agitation at room temperature.

The day after, we rinsed the slices (6x5 min) and then, the sections were treated with the secondary antibody (1:1000 biotinylated donkey anti-rabbit IgG; Vector Laboratories) for 90 min at room temperature. Both immunoreagents were diluted in PBS containing 1% BSA and 0.3% Triton X-100. Finally, sections were incubated in avidin-biotin peroxidase complex (1:500; Vector Laboratories) for 60 min and immunoreactivity was revealed using DAB Peroxidase Substrate Kit (Vector Laboratories). For that, we prepared and mixed a working solution from this kit containing for 5 ml of distilled water; 2 drops of Buffer pH 7.5, 4 drops of DAB and 2 drops of Peroxide (H_2O_2). We incubated the slices with the substrate working solution at room temperature for 1-5 minutes; the time was determined by the investigator who stopped the reaction when considered colored-enough. Then slices were transferred to a 0.1 M Tris-HCl (pH 7.4) solution to stop the reaction. At last, sections were rinsed (6x5 min) and dehydrated following the next sequence in seconds; 90% ethanol (30 s); 90% ethanol (30 s); 100% ethanol (30 s); 100% ethanol (30 s); xylene (30-60 s). Finally, we proceed to mount on gelatin-coated slides, and coverslipped in EUKITT mounting medium (contains 45% acrylic resin and 55% xylenes, from Sigma). The entire procedure was performed at room temperature under gentle agitation.

Optical density was used to measure the percentage of DA depletion. At least two sections from each hemisphere containing the STR were scanned (Microscope Slide Scanner, Leica Biosystems) and further processed (ViewScan). Mean optical density was measured on the STR from the contralateral and ipsilateral slices to the lesion and analyzed using the tool “Set Measurements” from ImageJ software. Values were corrected for background staining (measured in the cortex above the STR). TH optical density levels were expressed as the mean percentage of the values from the ipsilateral side respect to the contralateral non-lesioned side. Animals with unilateral 6-OHDA infusions included in the study showed >80 % reduction in TH-fiber density in the STR on the ipsilateral side to the lesion (**Fig. 3.8**).

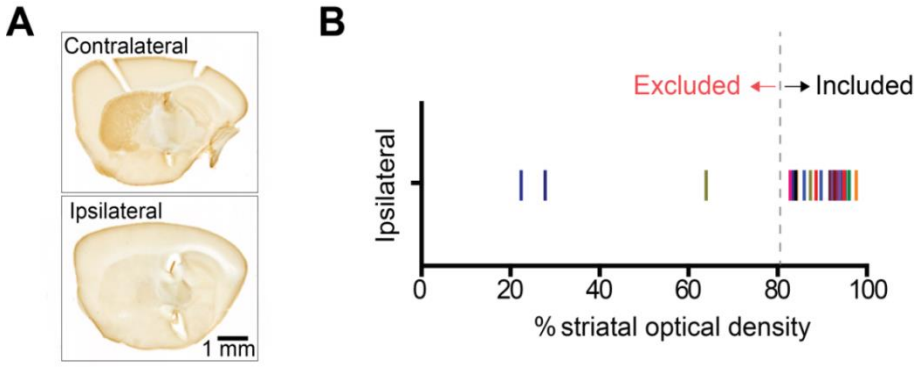

Figure 3.8. Immunohistochemical validation of the DA depletion. A: TH-immunostaining in the STR of 300-µm thick sagittal sections of a DA depleted mouse. Note the total absence of staining in the ipsilateral site to the 6-OHDA injection. **B:** Population graph showing the mean percentage value of striatal TH-fiber density in the ipsilateral site to the lesion (n=30). Note that mice with unilateral 6-OHDA lesion included in the three studies showed >80 % reduction in TH-fiber density in the STR.

II. Verification of viral vector transfection and cell recording

All sagittal brain slices (300 µm-thick), used for *in vitro* electrophysiology in the Study II and containing the STR, GP and SNr were processed for immunohistochemistry to qualitatively confirm the success of the virus transfection into the STR or GP, and to verify if recorded neurons (biocytin-filled) were localized in STR-SNr or GP-SNr input-recipient area of the SNr. Slices were immersed overnight in 4% w/v PFA in PBS at 4°C. The day after the PFA was removed and replaced by PBS-azide 0.2% until the

immunohistochemistry was performed. At this time, slices were rinsed (5 x 6 min) in PBS and then incubated for 1 h at room temperature in a blocking solution of PBS containing 1% bovine serum albumin (BSA-Sigma) and 0.3% Triton X-100 (Sigma). Next, slices were incubated overnight at room temperature in the same solution containing the secondary antibody Streptavidin 647 (1:500, Life technologies). The day after, excess protein was removed by washing sections (6 x 5 min) in PBS then, mounted on non-gelatin slides, and coverslipped in Vectashield (Vector Laboratories) to preserve the fluorescent signal. In this case we did not use primary antibodies because the immunoreactivity was assured the PVcre::Ai9t mouse line with tdTomato, the channel rhodopsin EYFP (ChR2-EYFP) and biocytin-staining thanks to Streptavidin-Alexa 647 which is useful for detecting biotinylated antibodies. Slices were imaged 24 h after the procedure.

Brain hemisphere sections from the transfected mice into the GP or STR were imaged on an epifluorescence microscope (Carl Zeiss, AxioImager.M2) running Axiovision software (Carl Zeiss). Appropriate sets of filter cubes were used to image the fluorescence channels: EYFP (excitation 450–490 nm, beam splitter 522 nm, emission 500–550 nm); tdTomato (excitation 450–600 nm, beam splitter 568 nm, emission 550–650 nm); and AlexaFluor-647 (excitation 625–655 nm, beam splitter 660 nm, emission 665–715 nm); (**Fig. 3.9**). Images of each of the channels were taken sequentially and separately to avoid possible crosstalk of signal across channels.

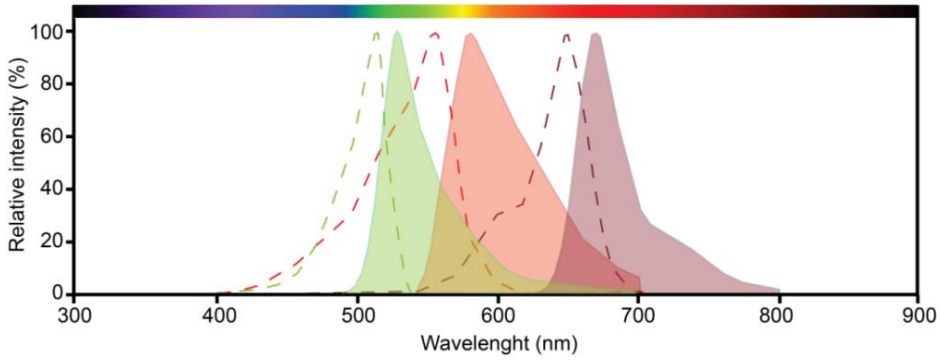

Figure 3.9. The normalized excitation/emission spectra for the fluorophores used. The spectrum profile for EYFP (green), tdTomato (red) and AlexaFluor-647 (dark-red) is represented with a dotted-line waveform for the excitation and filled waveform for the emission range for each fluorophore. EYFP has an excitation/emission maximum at 512/530 nm; tdTomato at 554/582 nm, and Alexa Fluor at 650/670 nm, respectively.

Injection sites into the STR and/or GP were verified for each mouse through EYFP staining. If the viral injection was not in the dorsomedial STR or GP the animal was excluded from the study. Also biocytin-filled neurons localized far from the transfected zone in the nigra were excluded from the Study II. Slides were imaged first using a 5 X 0.16 NA objective lens for observing the whole section and then the SNr was zoomed at 20 X 0.16 NA for doing the identification of every recorded neuron. This analysis was performed very carefully for each recorded slice, and we served from our previous mapping (noted in the lab book) of registered neurons during the day of experiment to confirm whether the recorded-neurons expressed the protein tdTomato or not. This way, we could consolidate our subdivision between PV+ and PV- SNr neurons (**Fig. 3.10**).

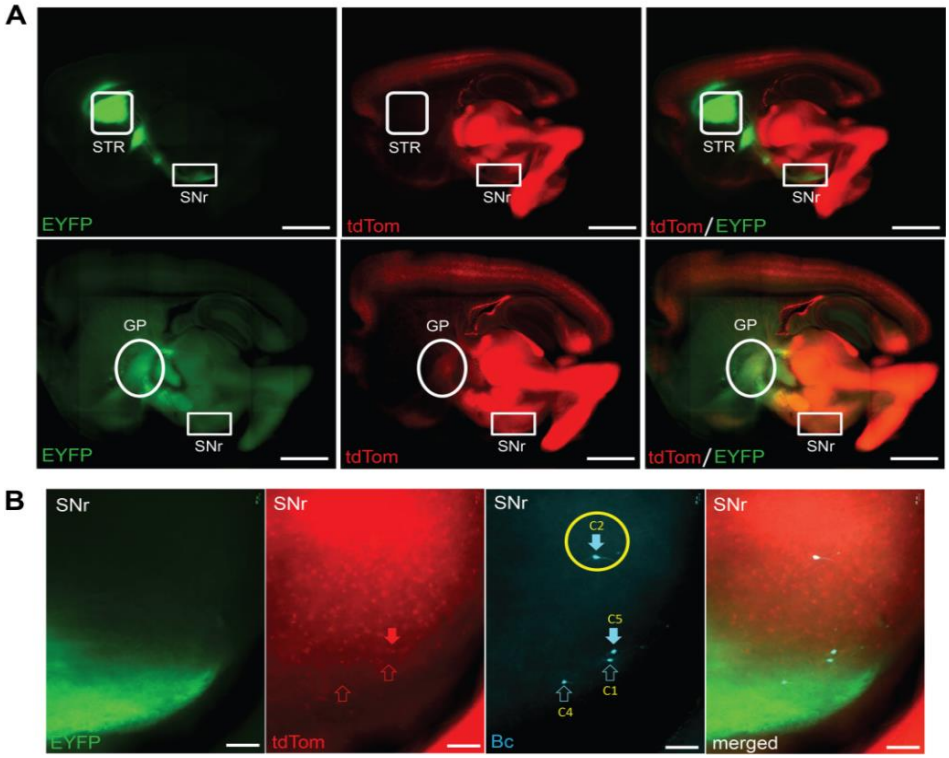

Figure 3.10. Optogenetic validation of the transfection and the registered neurons in the SNr. A: Low-magnification images from sagittal brain slices to prove the success of the striatal/pallidal transfection. Note axon terminals projecting to the SNr in both cases. **B:** Higher-magnification images of the SNr used to confirm not only if the registered neurons expressed the PV (filled arrows) or not expressed the PV (empty arrows) but also to confirm if biocytin-filled neurons (arrowheads) where in the transfected zone. Neurons such us the one shown in the circle were excluded from the study. Scale bars: A, 1 mm; B, 100 μm.

3.7.1. Molecular characterization of SNr neurons

Adult mice (X-12 weeks-old, 25-30g) were deeply anesthetized with a mixture of ketamine and xylazine (75 mg/kg and 10 mg/kg, respectively, i.p.), killed and perfused transcardially with ice-cold modified ACSF, equilibrated with 95% O_2 and 5% CO_2, and containing (in mM): 230 sucrose, 26 $NaHCO_3$, 2.5 KCl, 1.25 NaH_2PO_4, 0.5 $CaCl_2$, 10 $MgSO_4$ and 10 glucose. Brains were post-fixed overnight in a solution of 4% w/v PFA in 0.1 M phosphate buffered saline, pH 7.4 (PBS) at 4°C. The day after PFA was removed and brains were stored in PBS-azide 0.2% before being cut into 50 μm coronal sections on a vibratome (VT1000S; Leica Microsystems).

I. Quantification of molecular marker expression in populations of SNr neurons

Free-floating tissue sections (50 μm-thick) were collected in series, washed in PBS, and those containing "rostral," "central," and "caudal" SNr were selected (see results section, **Figure 4.1**). In adults, these sections, respectively, correspond to approximate distances of 2.8, 3.0, and 3.2 mm posterior to Bregma); (Paxinos and Franklin, 2001) and processed for indirect immunofluorescence to reveal molecular markers. Briefly, sections were washed six times for 5 min in PBS then incubated for 1 h at room temperature in a blocking solution of PBS containing 1% bovine serum albumin (BSA-Sigma) and 0.3% Triton X-100 (Sigma). Slices were incubated overnight in the same solution containing primary antibody anti-RFP (1:1000), anti-neuronal nuclear marker (NeuN, 1:2000) and anti-TH (1:1000). The next morning, sections were washed six times for 5 min in PBS then incubated for 90 min at room temperature in blocking solution containing a cocktail of secondary antibodies conjugated to fluorescent probes (Alexa-488, -568, and 647-conjugated donkey anti-rat, -guinea pig, -rabbit (1:500, Jackson Immunoresearch). Sections were then rinsed in PBS, mounted on gelatin-coated slides, and coverslipped in Vectashield (Vector Laboratories). The entire procedure was performed at room temperature under gentle agitation.

Epifluorescent acquisitions (Carl Zeiss, AxioImager.M2) of each channel were taken using a 5 X 0.16 NA objective lens first to perform coronal mosaic images.

Subsequently, 20 X 0.16 NA objective in the three channels was used to capture our interest region, the SNr. The medial and lateral borders of the SNr were readily delineated according to TH staining (see results section, **Figure 4.1A**). For the purposes of this study, we carried out the counting over the entire SNr in both hemispheres, as sectioned at the designated rostral, central, and caudal levels. To minimize confounds and ensure a more exact cell counts, we used confocal images from a BX51 Olympus Fluoview 500 microscope using an oil-immersion 20 X objective 0.8 numerical aperture. Laser light sources were an Argon laser, a Helium-Neon (green) laser, and Helium-Neon (red) laser. We used the "cell-counter" tool from ImageJ defining the Type 1 for all neurons in the SNr expressing NeuN. The type 2 was used for all NeuN cells expressing also TH^+ and the type 3 was employed for NeuN cells expressing also $tdTomato^+$. Data from rostral, central, and caudal SNr of both hemispheres were pooled for further analyses. In the bar graphs shown in figures, black bars represent averages from all mice tested. Immunoreactivity was scored (either positive or undetectable) by two independent investigators.

II. Validation of the reliability of PVcre::Ai9T mice as reporter mice for PV

Briefly, coronal sections (50 μm-thick) were washed 3 times for 10 min in PBS then incubated in a 1x PBS blocking solution containing 4% normal donkey serum and 0.3% Triton X-100 for 1 hour at room temperature. Slices were then incubated overnight at 4°C in the same solution containing anti-PV (1:1000) and anti-mCherry (1:1000) primary antibodies. The next morning, sections were washed 3 times for 10 minutes in 1x PBS and then incubated for 1 hour at room temperature in the blocking solution containing Alexa-488, -568 conjugated donkey anti-goat and rat antibody (1:500, Jackson Immunoresearch). Slices were then washed and coverslipped with glycerol (75%) fluorescence mount with strong antifading agent 1,4-phenylenediamide (0.1%) in 25% PBS. Confocal images were acquired with a BX51 Olympus Fluoview 500 slide scanning microscope system using an oil-immersion 20 X and 60 X objective and 0.8 and 1.4 numerical aperture. An Argon Laser was used for scanning confocal images. For quantification of $tdTomato^+$ and PV+ immunoreactivity in the SNr of two sham and two lesioned PVcre::Ai9T mice we used at least three sections containing the SNr from each mouse, co-localization was quantified on these images and the percentage of double-positive (tdTomato+, PV+) neurons in the SNr was determined.

Immunoreactivity was scored (either positive or undetectable) by two independent investigators and the results were pooled (see results section, **Figure 4.2**).

III. Delta expression in δ-KO and WT

Concisely, sections (50 μm-thick) were washed 3 times for 10 min in PBS then incubated in a 1x PBS blocking solution containing 4% normal donkey serum and 0.3% Triton X-100 for 1 hour at room temperature. Slices were then incubated overnight at 4°C in the same blocking solution containing anti-PV (1:4000) and anti-δ (1:1000) as primary antibodies. The next morning, sections were washed 3 times for 10 minutes in 1x PBS and then incubated for 1 hour at room temperature in the blocking solution containing Alexa-568, -647 conjugated donkey anti-goat and rabbit antibody (1:500, Jackson Immunoresearch). Slices were rinsed and coverslipped with the same antifading strong mounting medium of 75% glycerol, 0.1% p-phenylenediamine and 25% PBS. Confocal images from a BX51 Olympus Fluoview 500 microscope using an oil-immersion 20 X objective and 0.8 numerical aperture. Laser light sources were an Argon laser with the Helium-Neon laser for red and far-red light. We selected the *thalamus* as control nucleus, which is known to have the highest level of δ–subunit expression in the brain in which we found a strong labeling in the two wild-type ($\delta^{+/+}$) however the two knock-out ($\delta^{-/-}$) mice did not express this subunit. When we took images from the SNr of these two mice, we observed a weaker labeling compare to the *thalamus* but it was clearly delineating the membrane of both PV+ and PV- SNr neurons. All these conclusions are based on overlap images but we did not perform a quantitative analysis from these acquisitions (see results section, **Figure 4.24**).

IV. Delta and Alpha5 in PVcre::Ai9T

Sections (50 μm-thick) were washed 3 times for 10 min in PBS then incubated in a 1x PBS blocking solution containing 4% normal donkey serum and 0.3% Triton X-100 for 1 hour at room temperature. Slices were then incubated overnight at 4°C in two different solutions. For delta labeling, we used the same blocking solution containing

but containing anti-PV (1:1000), anti-mCherry (1:1000) and anti-δ (1:2000) as primary antibodies. For α-5 labelling we incubated the slices with the blocking solution containing the same anti-PV and anti-mCherry antibodies at the same concentration but in this case we included anti-α5 (1:1000) as primary antibodies instead of Delta. The next morning, sections were washed 3 times for 10 minutes in 1x PBS and then incubated for 1 hour at room temperature in the blocking solution containing the same seconday antibodies Alexa-488, -568, -647 conjugated donkey anti-goat, -rabbit, -rat antibody (1:500, Jackson Immunoresearch). Slices were rinsed and coverslipped with the same antifading strong mounting medium of 75% glycerol, 0.1% p-phenylenediamine and 25% PBS.

For quantification of δ and α5 subunits in PV+ and PV- cells in the SNr, PV and tdTomato were labeled with visible-wavelength emission (Alexa Fluor 488 and 568) and the subunits with far-red-emitting dye invisible to the naked eye (Alexa Fluor 647). For each animal, 3 nigral serial sections (one of every 10 sections) were taken for labeling and analysis of each subunit. Observation and acquisition were performed with a BX51 Olympus Fluoview 500 confocal microscope using an oil-immersion 60 X objective and 0.8 numerical aperture equipped with an Argon laser. PV cells were identified by eye and imaged. The tdTomato labeling was used to draw the outline of the cell and define the region of interest. Overlap images were useful to quantify using the "Cell Counter" tool from ImageJ software. Quantification was performed in two different ways. Labeling of δ or α5 was used to estimate the total of our labelled neurons in the SNr. Taking this value and the value of the total of PV+/PV- cells, we could then determine the percentage of δ or α5 subunits in both subtypes of SNr neurons. The percentage of PV+ cells expressing each subunit is also shown in these sections. It has been calculated as a result of considering PV expression as the total of stained neurons. As we explain in the results we can estimate the proportion of PV- neurons these subunits but NeuN immunostaining would be necessary to determine the exact percentage (see results section, **Figure 4.25 and 4.26**).

TABLE 3.2. | List of primary and secondary antibodies used for immunohistochemistry.

Target	Source	Catalog #	Dilution	Host species	Reference
Primary Antibodies					
$GABA_AR$ δ	Millipore	AB_ 9752	1:1000 1:2000	Rabbit	(Sarkar et al., 2011)

$GABA_AR$ α5	Synaptic Systems	224 503	1:1000	Rabbit	(Brady and Jacob, 2015)
NeuN	Synaptic Systems	266 004	1:500	Guinea pig	(Kang et al., 2012)
Parvalbumin	Frontier Institute Synaptic Systems	AF_460 195 004	1:1000 1:4000	Goat Guinea pig	(Reichel et al., 2015)
mCherry/ tdTomato	ChromoTeck	5f8	1:1000	Rat	(Rottach et al., 2008)
Tyroxine Hydoxylase	Novus	NB_ 300109	1:1000	Rabbit	(Hidalgo-Figueroa et al., 2012)
	Secondary antibodies				
Anti-Rat 488	Jackson Immuno Research	AB_ 2340686	1:500	Donkey	(Du et al., 2017)
Anti-Guinea Pig 568	Jackson Immuno Research	AB_ 2340468	1:500	Donkey	(Du et al., 2017)
Anti-Rabbit 647	Jackson Immuno Research	AB_ 2340437	1:500	Donkey	(Du et al., 2017)
Streptavidin-AF647	Life Technologies	405237	1:500	-	(Shade et al., 2015)

3.8. Statistical analysis of data

Experimental data were analysed using Clampfit 11.0.3 (Molecular Devices), Origin version 7.0 and OriginPro 8.0 (Molecular Devices), Detection Mini 8.0 (In house software: Goillandeau M) and ImageJ. The statistical analysis was carried out with the computer programme GraphPad Prism (v. 6.01, GraphPad Software, Inc). Box plots, generated in Origin (central line: median; box: 25%–75%; whiskers: 10%–90%), were

used to illustrate sample distributions with individual values. Data in the text are presented as mean value ± standard error of the mean (S.E.M.). The nonparametric Mann-Whitney U (MW-U) test was used for unpaired statistical comparisons. For multiple group comparisons, we used the Friedman and Kruskal-Wallis ANOVA (K-W) test followed by Dunn's multiple comparison post-hoc tests for paired and unpaired comparisons. For comparison of groups or F-I response curves, statistical analysis was performed using two-way ANOVA, followed by Sidak's multiple comparison *post hoc* test. Data were considered significant for $p<0.05$.

4. RESULTS

4.1. STUDY I. Intrinsic properties of *substantia nigra pars reticulata* neurons regarding the expression of Parvalbumin in sham, parkinsonian and dyskinetic mice.

4.1.1. Distribution of GABAergic neurons in the SNr

The aim of the present study was to provide a comprehensive description of the different nigral cell populations, integrating neurochemical and electrophysiological criteria. Using coronal slices from PVcre::Ai9T mouse brains (m=2), we performed immunohistochemical triple-labeling to characterize SNr neuron population. The NeuN, tdTomato red fluorescent protein and TH were used as cell markers (**Fig. 4.1A**). NeuN was used to identify all neurons in the SNr. Among those cells 46 ± 1.7 % also expressed tdTomato while 49 ± 1.6 % were only positive for NeuN. In agreement with the literature (González-Hernández and Rodríguez, 2000), we found that dopaminergic neurons represent a small proportion (4 ± 2.8 %) of SNr neurons. These dopaminergic neurons in the SNr were identified by tdTomato-/TH+ staining (**Fig. 4.1B**). We also performed analyses of immunofluorescence signals in rostral, central and caudal sections to further describe the distribution of tdTomato+, tdTomato- and TH+ neurons across the SNr (**Fig. 4.1C**). We noticed that tdTomato+ neurons have a dorsolateral distribution preference which is in accordance with previous studies in mice, rats, cats, and monkeys (Nagai et al., 1983; Ottersen and Storm-Mathisen, 1984; Smith et al., 1987; Ficalora and Mize, 1989; von Krosigk et al., 1992; Liu et al., 2020), reporting that most PV+ cells are mainly localized in the lateral region of the SNr. Furthermore, we quantified the number of NeuN+ and tdTomato+ somata within the SNr at the three levels, the rostral, central and caudal thirds of the SNr. We did the same for NeuN+ and tdTomato-, and for NeuN+ and TH+. We observed that the proportion of the three SNr neuron subtypes was relatively constant across the rostral, central and caudal levels of the SNr (**Fig. 4.1D**).

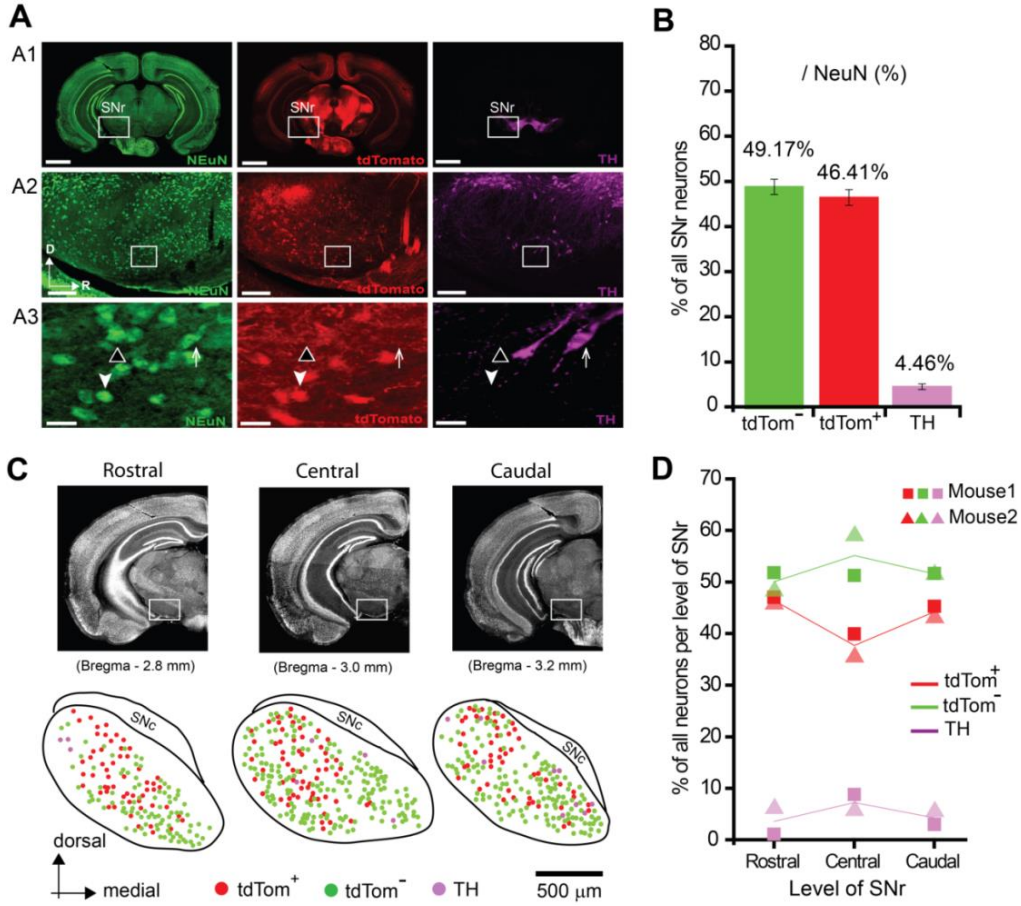

Figure 4.1. Immunohistochemical identification of SNr neurons in PVcre::Ai9T transgenic mouse line. A1: Low-magnification images showing triple immunofluorescence labeling for the Neuronal Nuclear protein (NeuN, green), tdTomato (red) and Tyrosine Hydroxylase (TH, magenta) in coronal slices (50 µm). **A2:** High-magnification images of the SNr. Note the dorsolateral distribution preference for tdTomato+ neurons. **A3:** NeuN was used as neuronal marker for the labeling of all SNr neurons which allows identifying tdTomato+/TH- (arrowheads), tdTomato-/TH- (black triangles) and tdTomato-/TH+ (arrows) neurons. A1-A3: Illustrations coming from epifluorescent acquisitions (Carl Zeiss, AxioImager.M2). **B:** Proportion of tdTomato-, tdTomato+ and TH+ SNr neurons expressed as a percentage of NeuN. Confocal images were used for the analysis. Data were collected from 2 mice, 10 slices, both hemispheres. **C:** Coronal sections illustrating rostral, central, and caudal levels of the SNr where neuron molecular expression was quantified (approximate distance from Bregma). At the bottom, maps showing distribution of tdTomato+, tdTomato-, and TH+ neurons across the SNr. **D:** Percentage of tdTomato+, tdTomato-, and TH neurons at rostral, central and caudal levels of the SNr (n=2 mice). Average proportions of cell types in mice 1-2 are indicated with colored lines. Data were collected from both hemispheres, 3 slices per mouse. Scale bars: A1, 1mm; A2, 200 µm; A3, 30 µm.

With the objective of identifying the cells in the SNr expressing PV we tested whether PVcre::Ai9T mice faithfully express Cre in PV+ SNr neurons. For that, we fixed coronal sections of these transgenic mice and revealed tdTomato+ neurons within the SNr (**Fig. 4.2A**). After we performed PV immunohistochemistry (**Fig. 4.2B**) using slices from reporter mice and determined the co-localization between tdTomato+ and PV+ SNr neurons (**Fig. 4.2C**). This analysis was performed on two sham-injected and two 6-OHDA-lesioned mice. In sham PVcre::Ai9T mice 76.7 ± 0.2 % (**Fig 4.2D**) were double-positive (tdTomato+, PV+), while 17 ± 3 % expressed only tdTomato (tdTomato+, PV-) and 6 ± 2.8 % were only immunostained for PV (tdTomato-,PV+). In 6-OHDA-lesioned mice (**Fig. 4.2E**) the percentages were quite similar representing almost 79 ± 2 % double-positive (tdTomato+, PV+) neurons, 10.16 ± 0.6 % of tdTomato+/PV- and 10.9 ± 1.4 % of tdTomato-/PV+ neurons. Thus while Cre is expressed primarily in PV+ neurons, these Cre+ neurons make up approximately 80% of the total PV+ SNr population. The same degree of recombination has also been reported in the GPe (Saunders et al., 2016).

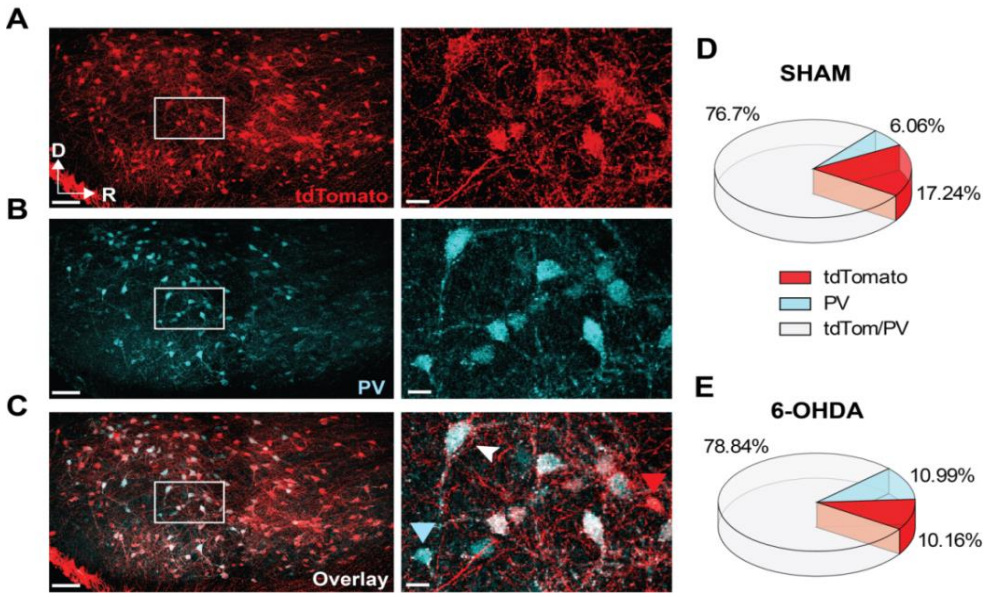

Figure 4.2. Distribution of tdTomato and PV immunoreactivity in SNr neurons. A-C: Left, coronal brain section of the SNr from a PVcre::Ai9T mouse where Cre expression is reported by tdTomato (A, red), PV immunolabeling in cyan (B) and the co-localization between the two markers (C). Right, high magnification of boxed areas containing PV- (red arrow) and PV+ (cyan arrow) neurons and their co-localization (white arrow). **D:** Quantification of co-localization between tdTomato and PV in the SNr using confocal microscopy for sham-mice. **E:** Percentage of co-localization in DA depleted mice (unilateral 6-OHDA lesion). Data was obtained from 2 sham and 2 DA-depleted mice (6 sections per mouse). Scale bars: Left, 200µm; Right, 30µm.

4.1.2. Electrophysiological properties of PV+ and PV- SNr neurons in sham PVcre::Ai9T mice *in vitro*

To test whether PV expression defined functionally distinct SNr neuron sub-populations, we prepared sagittal brains slices from PVcre::Ai9T mice and performed *in vitro* cell-attached recordings of neighboring tdTomato+ and tdTomato- neurons (**Fig. 4.3A**). To limit the effects of synaptic transmission, we included blockers of $GABA_A$ (picrotoxin, 50 µM), AMPA (DNQX, 20 µM) and NMDA (D-AP5, 50 µM) receptors. The internal solution of our pipette contained Kgluconate. Under these conditions, we depicted differences in spontaneous firing rates between PV+ and PV- SNr neurons (**Fig. 4.3B**). While PV+ neurons fired AP at fast rate on average ($mean_{FR}$=22.7 ± 2.8 Hz, n=11/m=3), PV- neurons autonomous pacemaking is significantly slower ($mean_{FR}$=10.7 ± 0.8 Hz; n=9/m=3; P<0.0001, Mann-Whitney test). The CV was similar for both subtypes (PV+, $mean_{CV}$=8.7 ± 0.7 %; PV-, $mean_{CV}$=10 ± 1.2 %; P>0.05, Mann-Whitney test); (**Fig. 4.3C**).

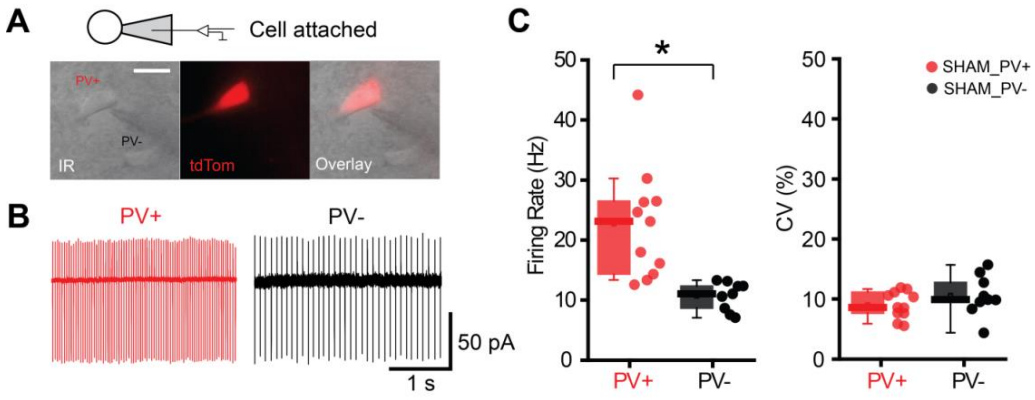

Figure 4.3. Difference in the autonomous pacemaking of PV+ and PV- SNr neurons in sham PVcre::Ai9T mice. A: DIC image (gray) overlaid with tdTomato fluorescence (red) showing a recorded slice containing one PV+ cell, one PV- cell and a patch-clamp recording electrode. **B:** Examples of cell-attached recordings of PV+ and PV- SNr neurons. **C:** Population data showing that PV+ neurons (n=11) fire at higher rates than PV- (n=9) SNr neurons (*P<0.001; MW-U test) but with a similar regularity. Scale bar: 20 µm.

Whole-cell configuration recordings were used not only to confirm data obtained in cell-attached configuration but also to analyze more electrophysiological parameters between the two subtypes of SNr neurons. Internal and external solutions were the same. The autonomous firing frequency between PV+ and PV- SNr neurons was also different (**Fig. 4.4A-B**) when neurons were recorded without current injection (0 pA) in whole-cell configuration. While PV+ neurons carried on firing faster ($mean_{FR}$ = 21.2 ± 2.5 Hz; n=13), PV- neurons were firing slower ($mean_{FR}$ = 11.2 ± 2.3 Hz; n=9; P=0.011, Mann-Whitney test). The CV was similarly unaffected in whole-cell configuration (PV+, $mean_{CV}$ = 9.7 ± 6.7 %; PV-, $mean_{CV}$ = 10.3 ± 11.2 %; P>0.05 Mann-Whitney U test).

We then investigated the properties of the APs for PV+ and PV- SNr neurons. First, our data revealed that APth was significantly more depolarized in PV+ compared to PV- SNr neurons (PV+, $mean_{APth}$= 35.4 ± 1.4 mV; n=13; PV-, $mean_{APth}$= 43.7 ± 2.2 mV; n=9; P=0.009; Mann-Whitney test). Furthermore, the AHP was consistently more depolarized in PV+ neurons compared to PV- SNr neurons (PV+, $mean_{AHP}$= 54.9 ± 0.9 mV, PV-, $mean_{AHP}$= 63.5 ± 1.8 mV; P=0.0008; Mann-Whitney test). However, we did not depict differences in AHP magnitude between both populations of SNr neurons (PV+, $mean_{AHPmag}$= 19.4 ± 1.0 mV, PV-, $mean_{AHPmag}$= 19.7 ± 1.6 mV; P>0.05; Mann-Whitney U test Mann-Whitney test); (**Fig. 4.4C**).

These striking differences in spike waveform and pattern indicate qualitative and/or quantitative differences in intrinsic ion channels in SNr PV+ and PV- neurons. The fact that the AP threshold tends to be some mV more negative in PV- SNr GABA neurons as well as the AHP peak, could be due to modifications affecting sodium channels like I_{NaP}, I_{NaT}, TRCP3, NALCN or SK channels (Atherton and Bevan, 2005; Zhou et al., 2008; Lutas et al., 2016).

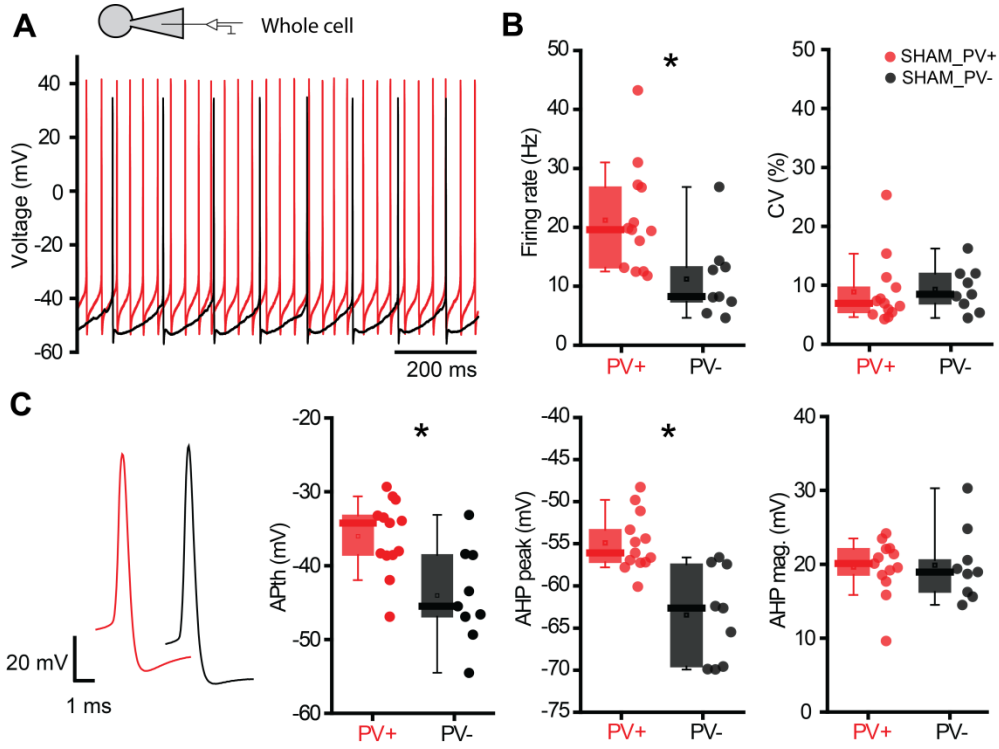

Figure 4.4. Electrophysiological properties of PV+ and PV- SNr neurons, in whole cell configuration depicting differences between both populations in sham PVcre::Ai9T mice. **A:** Representative whole cell autonomous firing (0 pA current injection) for PV+ (red) and PV- (black) SNr cells. **B:** Box plots depicting the firing rate of PV+ and PV- SNr neurons (PV+, n=13; PV-, n=9; P= 0.0111 MW-U test). **C:** AP properties such as AP threshold (APth; P<0.01; MW-U test), after hyperpolarization peaks (AHP; P<0.001; MW-U test) and AHP magnitude (APth-AHP) depicting significant differences between both subtypes of SNr neurons.

Intrinsic membrane channels influence the excitability of the SNr neurons and part of this project has consisted also in the characterization of the excitability of PV+ and PV- SNr neurons. We have observed that both PV+ and PV- neurons exhibit a *plateau* potential that manifests a prolonged membrane depolarization following a depolarizing current pulse. Indeed, somatic injections of depolarizing current pulses (200 pA for 1 second) revealed that the "driven" firing of PV+ was as vigorous as that of PV- neurons (**Fig. 4.5A**). L-type calcium channels are normally responsible of *plateau* potential generation in SNr GABA neurons (Tepper and Lee, 2007b). Upon somatic injections of hyperpolarizing current pulses (-150 pA for 1 second), both PV+ and PV- neurons exhibited a brief hyperpolarization-activated current (I_h)-induced "sag" (**Fig.**

4.5B). When PV+ and PV- SNr neurons were hyperpolarized to equivalent peak voltage deflections their sag amplitudes were similar (PV+, $mean_{sag}$= 16.5 ± 2.1 mV, PV-, $mean_{sag}$= 19.4 ± 4.0 mV; P>0.05, Mann-Whitney test). These data suggest that the subunit composition, density, and/or distribution of HCN channels along the membranes of the two cell types are similar, although voltage-clamp recordings would be needed to confirm it (Atherton and Bevan, 2005; Biel et al., 2009). In line with this, the firing rate-injected current (F-I) response curves of these cell types, did not reveal marked differences between PV+ and PV- neurons meaning that they both response in the same manner to injected current. However, we observed that the firing was affected in both subtypes by current injection ($F_{(19,4)}$= 176; P<0.0001, Two-way ANOVA; **Fig. 4.5C**).

We also looked at the capacity of SNr neurons to fire APs at high frequency, depicting that PV- cells support a better capacity to fire high frequency spikes and provide rapid repolarization of the membrane potential following AP depolarization (PV+, $mean_{FRgain}$= 6.9 ± 0.9, PV-, $mean_{FRgain}$= 15.2 ± 1.7; P=0.0004; Mann-Whitney test); (**Fig 4.5D**).

Considering that spike accommodation prevents generation of high frequency firing (Wigmore and Lacey, 2000), we also measured the driven firing adaptation index (2s current pulse of 100 pA) of PV+ and PV- SNr neurons not depicting statistical differences between both subtypes (PV+, $mean_{index}$= 0.67 ± 0.03, PV-, $mean_{index}$= 0.62 ± 0.03; P>0.05; Mann-Whitney U test; **Fig. 4.5E**).

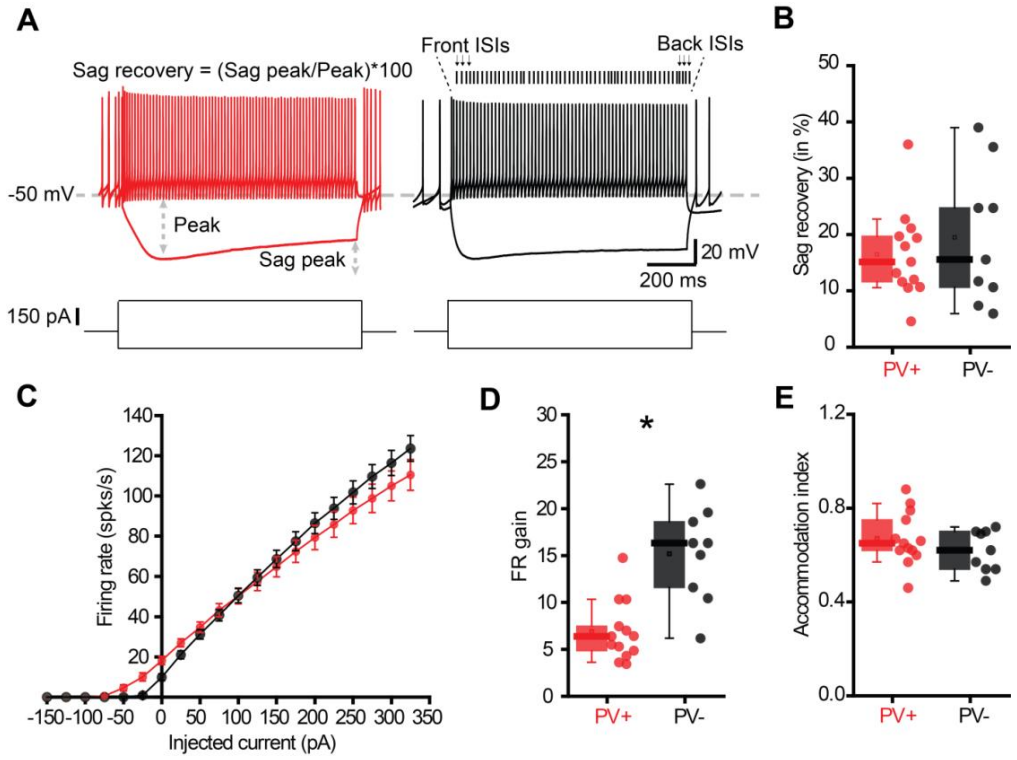

Figure 4.5. Excitability of PV+ and PV- SNr neurons. **A:** Typical activity of a PV+ (red) and PV- (black) SNr neuron recorded in a whole cell configuration in a brain slice from a sham mouse. Superposition of the driven firing (200 pA injection for 1s) and response to hyperpolarizing current pulse (-150 pA for 1 s) eliciting peak voltage deflections of ~100 mV and a subsequent "sag peak". **B:** Sag recovery graph obtained according to the formula described in panel A, not showing differences between both subtypes of SNr neurons. **C:** Relationship between mean firing rate and injected current. No significant differences in terms of excitability between both subtypes of SNr neurons were seen. **D:** Graph depicting the ratio (frequency gain; FR gain) between the maximal evoked frequency and the spontaneous firing rate supporting a better capacity of PV- SNr neurons to fire APs at high frequency. P<0.001; MW-U test. **E:** Accommodation index calculated by dividing front 2 ISIs by back 2 ISIs.

Taking into account all these differences in the studied parameters, we could consider that PV expression conferred SNr neurons distinct electrophysiological features. Besides, we suggest that probably both subtypes of SNr cells express distinct ion channels further supporting the observed differences in their firing rate. Specific experiments will be needed to address this question.

4.1.3. Impact of the 6-OHDA lesion and L-DOPA treatment on electrophysiological properties of PV+ and PV- SNr neurons

The cellular mechanisms underlying the changes in firing rate and pattern of SNr neurons under DA-depletion have not been yet explored *in vitro*. For that, we decided to investigate how the excitability of SNr neurons is directly impacted, not only by the loss of DA but also by the chronic L-DOPA treatment. The present study was undertaken in PVcre::Ai9T mice with 6-OHDA unilateral lesions of the MFB 15 days after the lesion. Another group of 6-OHDA lesioned mice was further treated with chronic L-DOPA subcutaneous injections for 15 additional days and AIMs were rated as we previously described in the methods (**Figure 3.4**; Cenci & Lundblad, 2007). For electrophysiological experiments we prepared sagittal brain slices and performed *in vitro* cell-attached recordings differentiating between PV+ and PV- SNr neurons. As for the previous characterization of SNr neurons, fast-synaptic GABAergic and glutamatergic transmission were blocked.

First, we focused on PV+ SNr neurons and the impact of DA-depletion and subsequent chronic L-DOPA treatment on firing rate and pattern in cell-attached configuration (**Fig. 4.6A**). Statistical differences were reported for the firing frequency among the groups (P= 0.0006, Kruskal-Wallis ANOVA). We found a decrease in firing rate after 6-OHDA lesion in comparison with data from sham mice (6-OHDA, n= 10/m= 2; $mean_{FR}$=8.2 ± 1.1 Hz; P=0.0006, Dunn's multiple comparison test). Furthermore, this reduction in firing rate was not modified by L-DOPA chronic treatment (n= 10/m= 2; $mean_{FR}$=11.7 ± 2.1 Hz; P=0.0288, Dunn's multiple comparison test; **Fig. 4.6B**). The CV was not modified by the 6-OHDA procedure or L-DOPA treatment (P>0.05; Kruskal-Wallis ANOVA; **Fig. 4.6C**).

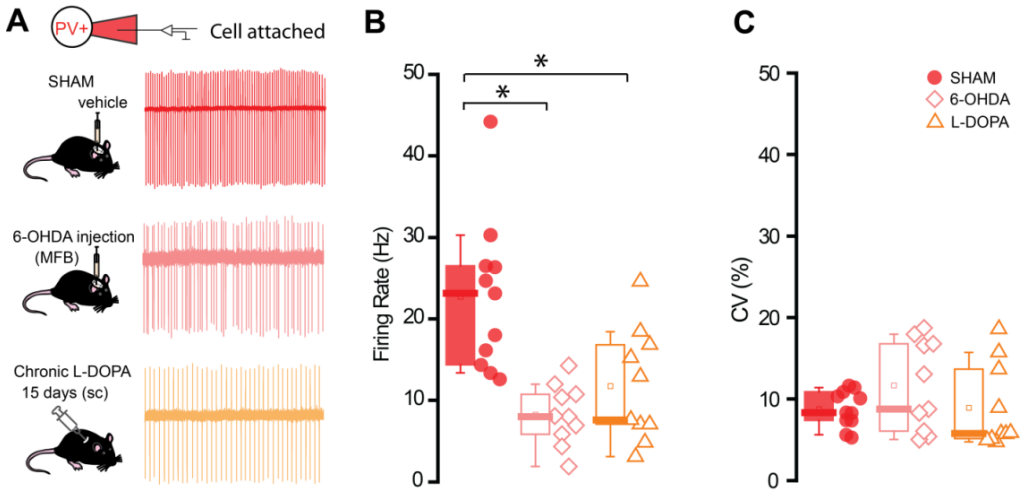

Figure 4.6. Firing properties of PV+ SNr neurons in sham, 6-OHDA lesioned and dyskinetic mice. A: Left, scheme depicting the experimental procedures performed before *in vitro* electrophysiology experiments. Sham and 6-OHDA lesioned mice received unilateral injections of vehicle and 6-OHDA directly in the MFB. Fifteen days after surgery, L-DOPA treatment started and dyskinesia rating was evaluated during the following two weeks. Right, cell-attached recordings of PV+ SNr neurons from PVCre::Ai9T mouse brain in sham, lesioned and dyskinetic conditions. **B:** Population data showing the change on firing rate for PV+ neurons in sham (n=11), 6-OHDA (n=10) and dyskinetic (n=10) mice. Note a reduction in firing rates after DA depletion and after L-DOPA treatment (*P<0.05, Kruskal-Wallis ANOVA, followed by Dunn's test) in presence of picrotoxin, D-AP5 and DNQX to block fast synaptic transmission. **C:** Box plots depicting the CV of the firing rate of PV+ SNr neurons.

As previously done to characterize the two subtypes of SNr neurons, whole-cell configuration recordings were performed and the firing rate and CV of PV+ SNr neurons for the three groups were compared. The autonomous firing of PV+ neurons was again statistical different after the 6-OHDA and L-DOPA treatment in whole-cell configuration without current injection (0 pA); (P= 0.0007, Kruskal-Wallis; **Fig. 4.7A and B**). For the sham group firing frequency was high and in the same range as in cell-attached configuration ($mean_{FR}$= 21.2 ± 2.5 Hz) while the 6-OHDA group the firing rate was reduced (n=7; $mean_{FR}$= 9.0 Hz ± 1.4; P= 0.0052, Dunn's multiple comparison test). In the L-DOPA treated group PV+ SNr neurons also showed a reduction in firing rate compared to the sham group (n= 5; $mean_{FR}$= 9.0 ± 1.3 Hz; P= 0.007, Dunn's multiple comparison test). The CV was similarly unaffected in whole-cell configuration (P>0.05; Kruskal-Wallis ANOVA; **Fig. 4.7B**).

We also observed marked differences in AHP peak among the groups (P= 0.0133 Kruskal-Wallis ANOVA; **Fig. 4.7C**). We observed a significant decrease after L-DOPA treatment (sham, n=13, $mean_{FR}$= 54.9 ± 0.9 mV; 6-OHDA, n=7, $mean_{FR}$= 58.1 ± 1.4 mV; L-DOPA, n=5, $mean_{FR}$= 64.2± 2.7 mV; P=0.012, Dunn's multiple comparison test). APth and AHPmag were not modified after 6-OHDA lesion nor after L-DOPA treatment (P>0.05; Kruskal-Wallis ANOVA).

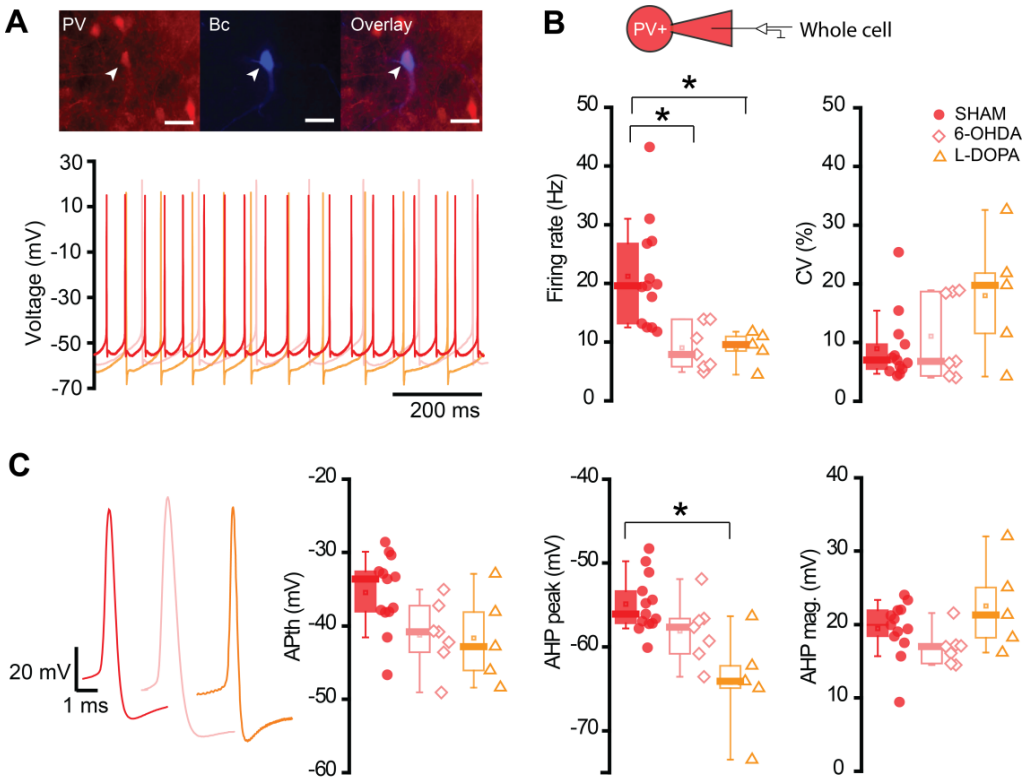

Figure 4.7. **Electrophysiological properties of PV+ SNr neurons in sham, 6-OHDA lesioned and dyskinetic mice. A:** Top, epifluorescent images of an identified neuron filled with biocytin (Bc) and expressing PV (arrowheads). Bottom, autonomous firing (0 pA current injection) of PV+ SNr cells from sham (red) 6-OHDA lesioned (pink) and L-DOPA treated (orange) groups. **B:** Box plots of the firing rate and CV of the autonomous pacemaking of PV+ SNr cells. Note that firing frequency was significantly decreased in DA-depleted conditions and after L-DOPA treatment (sham, n= 13; 6-OHDA, n= 7, L-DOPA, n=5). *P<0.05 Kruskal-Wallis ANOVA, followed by Dunn's test. **C:** AP properties such as threshold (AP_{th}), afterhyperpolarization peaks (AHP) and magnitude (AHP_{mag}) did not change in the 6-OHDA group. Note that AHP peak in L-DOPA group was significantly more negative compared to the sham group (*P<0.05, Kruskal-Wallis ANOVA, followed by Dunn's test). Scale bar: 10 μm.

Upon somatic injections of hyperpolarizing current pulses in current-clamp mode, all PV+ SNr neurons in the three conditions exhibited membrane potential "sag" (**Fig. 4.8A**). Once PV+ SNr neurons were hyperpolarized to equivalent amount of current (-150 pA for 1 second) their sag recovery was significantly different after L-DOPA treatment (P= 0.009, Kruskal-Wallis ANOVA, **Fig. 4.8B**). While the sag recovery was not different between the sham and the 6-OHDA groups (sham, n=13; $mean_{sag}$= 16.5 ± 2.1 %; 6-OHDA, n= 7; $mean_{sag}$=20.0 ± 2 %; P>0.05; Kruskal-Wallis ANOVA), this parameter become significantly higher in the L-DOPA treated group (n= 5; $mean_{sag}$= 33.7± 1.9 %; P=0.006, Dunn's multiple comparison test). These data suggest that the subunit composition, density or distribution of HCN channels along the membranes of PV+ SNr neurons is possibly altered after L-DOPA chronic treatment.

In line with this, to further elucidate whether changes in firing were induced by DA depletion, we performed a F-I curves by injecting several current steps in the three conditions depicting differences after 6-OHDA lesion of SNr neurons (**Fig. 4.8C**). More specifically, the driven firing rates after 6-OHDA lesion were significantly lower across a range of current pulses compared with sham group neurons ($F_{(2,22)}$= 5.68; P=0.0103, Two-way ANOVA; **Fig. 4.8C**), suggesting that the excitability of PV+ cells after 6-OHDA lesion was reduced when all synaptic transmission to the SNr was blocked. These difference were found for all current injections ranging from 75 pA to 325 pA (* P<0.05, Sidak's multiple comparison test). Interestingly, F-I curves between the 6-OHDA and the L-DOPA group just reported a significant difference at depolarized pulse of 300 pA (#P<0.05, Sidak's multiple comparison test) suggesting a partial rescue of the driven activity.

Furthermore, we observed statistical differences in the capacity of SNr neurons to fire APs at high frequency (P=0.0005 Kruskal-Wallis ANOVA; **Fig. 4.8D**). After 6-OHDA lesion, PV+ SNr supported a better capacity to fire APs at higher frequency (sham, $mean_{FRgain}$= 6.9 ± 0.9; 6-OHDA, $mean_{FRgain}$= 15.4 ± 1.1; L-DOPA, $mean_{FRgain}$= 13.7 ± 2.3; P=0.0006, Dunn's multiple comparison test; **Fig. 4.8D**). Many factors can explain this phenomenon such as changes in membrane resistance, capacitance or other voltage-gated channels alterations, etc. The accommodation index remained unchanged upon the three conditions (P>0.005; Kruskal-Wallis ANOVA; **Fig. 4.8E**).

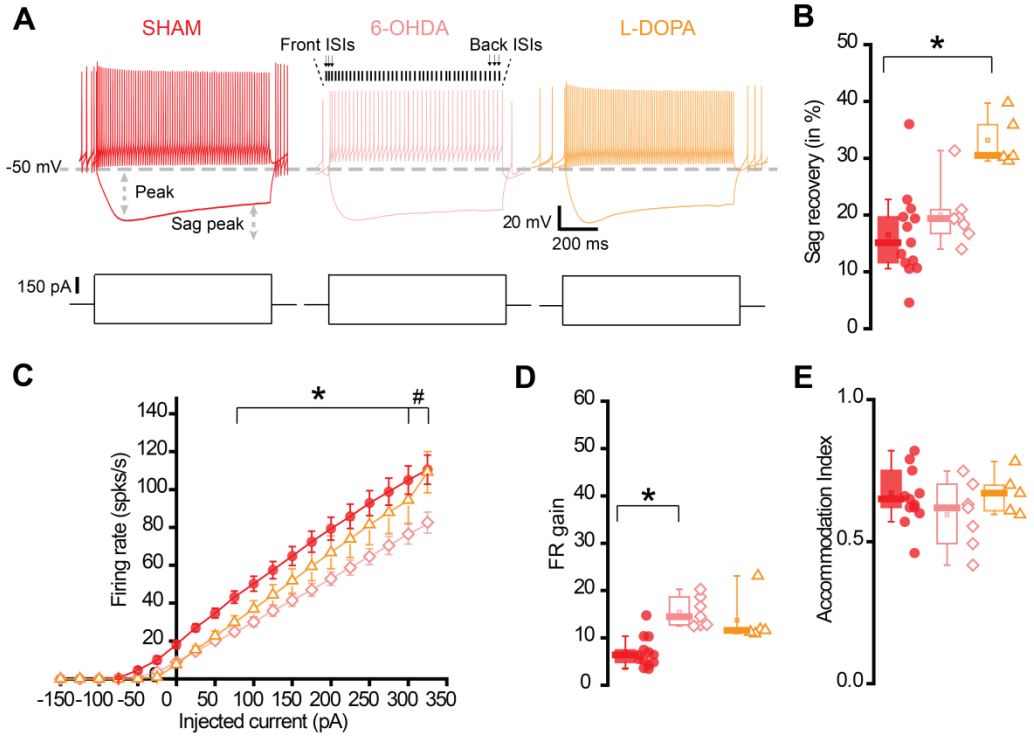

Figure 4.8. Excitability of PV+ SNr neurons in sham, lesioned and dyskinetic mice. A: Representative response in whole cell configuration of SNr PV+ cells in sham, 6-OHDA and dyskinetic mice to depolarizing (200 pA injection for 1s) and hyperpolarizing (-150 pA for 1s) current steps eliciting peak voltage deflections to ~100 mV and a subsequent "sag peak". **B:** Sag recovery was calculated with the formula described previously depicting a big significant recovery for L-DOPA compared to sham (*P<0.009 Kruskal-Wallis ANOVA, followed by Dunn's test). **C:** Relationship between mean firing rate and injected current. For depolarizing pulses, PV+ cells from 6-OHDA were characterized by a significantly slower rate of growth compared with sham animals. *P<0.05 Two way-ANOVA, followed by Sidak's test for all current injections ranging from 75 pA to 325 pA. In the L-DOPA group, differences with the 6-OHDA group were only significant at depolarized pulse of 300 pA. #P<0.05 two way-ANOVA, followed by Sidak's test. **D:** Graph depicting the ratio between the maximal evoked frequency and the spontaneous firing rate supporting a better capacity after 6-OHDA lesion to fire APs at high frequency (*P<0.001 Kruskal-Wallis ANOVA, followed by Dunn's test). **E:** Accommodation index calculated by dividing front 2 ISIs by back 2 ISIs not showing differences after DA depletion or L-DOPA chronic treatment.

In the second part of the study, we focused on PV- SNr neurons and the impact of DA loss and chronic L-DOPA treatment on firing rate and pattern in cell-attached configuration (**Fig. 4.9A**). Contrary to what was observed previously for PV+ SNr neurons and following the same experimental procedures, the firing rate was unaltered by 6-OHDA lesion or L-DOPA treatment (sham, n= 10/m= 2; $mean_{FR}$=10.7 ± 0.8 Hz; 6-OHDA, n= 6/m= 2; $mean_{FR}$=6.2 ± 2.4 Hz; L-DOPA, n= 10/m= 2; $mean_{FR}$=12.5 ± 3.4 Hz; P>0.05, Kruskal-Wallis ANOVA, followed by Dunn's test; **Fig. 4.9B**). In the same way, the CV was similar in all groups (P>0.05; Kruskal-Wallis ANOVA; **Fig. 4.9C**).

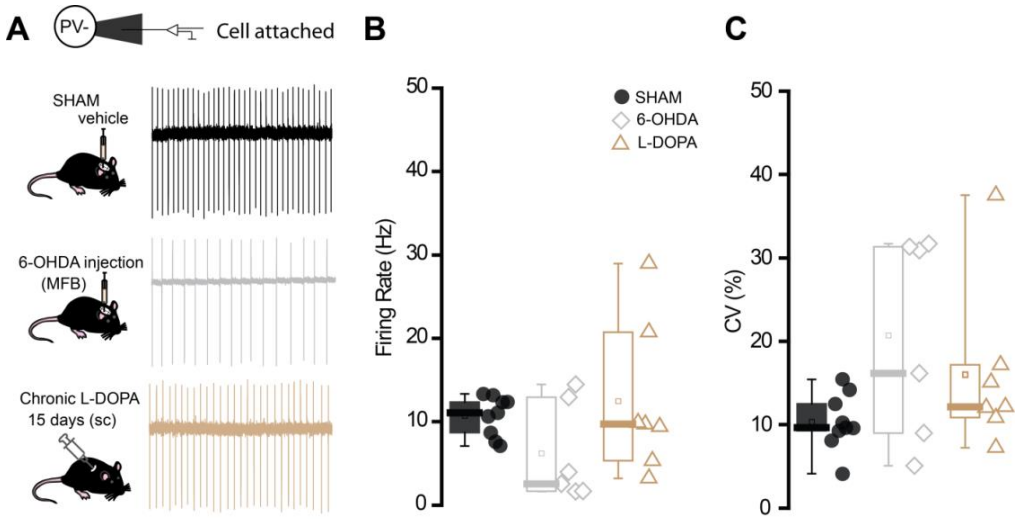

Figure 4.9. Firing rate properties of PV- SNr neurons in sham, 6-OHDA lesioned and dyskinetic mice. A: Same scheme of the experimental procedures than for the study of PV+ neurons was used for *in vitro* electrophysiology experiments in which PV- SNr neurons were recorded in sham (*black*), lesioned (*gray*) and dyskinetic (*brown*) conditions. **B-C:** Box plots of the firing rate and CV for PV- neurons in sham (n=9), 6-OHDA (n=6) and dyskinetic (n=7) mice not showing differences among the groups. For all experiments GABA and glutamate transmission were blocked by picrotoxin (50µM), D-AP5 (50µM) and DNQX (20µM), respectively.

As we did for PV+ SNr neurons, whole-cell configuration recordings were performed and the firing rate and CV of PV- SNr neurons for the three conditions were compared (**Fig. 4.10A**). The autonomous firing of PV- neurons was not different after the 6-OHDA and L-DOPA treatment in whole-cell configuration without current injection (0 pA); (sham, n= 9; $mean_{FR}$=11.2 ± 2.3 Hz; 6-OHDA, n= 6; $mean_{FR}$=3.7 ± 2.2 Hz; L-DOPA, n= 4; $mean_{FR}$=12.0 ± 3.1 Hz; P>0.05, Kruskal-Wallis ANOVA, followed by

Dunn's test; **Fig 4.10B**). The CV was similarly unaffected in whole-cell configuration (P>0.05; Kruskal-Wallis ANOVA; **Fig 4.10C**).

We also evidenced that AP waveforms of PV- SNr GABA neurons after 6-OHDA lesion or L-DOPA treatment were unaffected (P>0.05; Kruskal-Wallis ANOVA; **Fig. 4.10C**). None of the measured parameters, such as the APth, AHPpeak or AHPmag, suffered alterations after the lesion or after L-DOPA treatment.

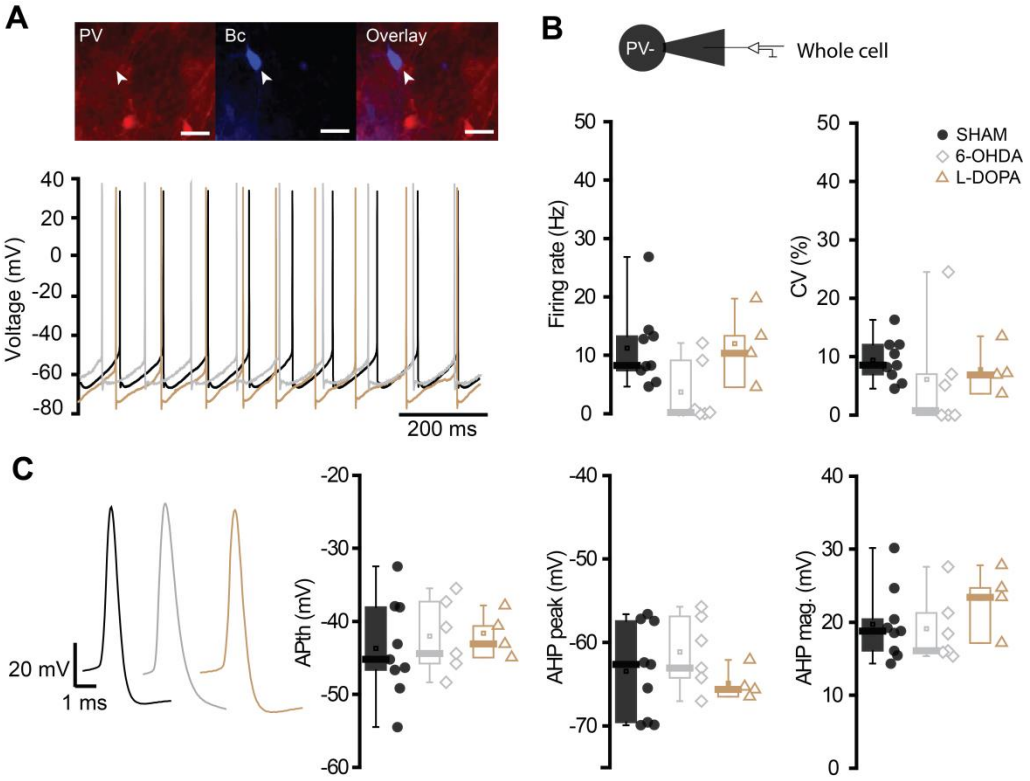

Figure 4.10. Electrophysiological properties of PV- SNr neurons in sham, 6-OHDA lesioned and dyskinetic mice. A: Top, example of a neuron filled with biocytin and not expressing PV (arrowheads). Bottom, autonomous firing (0 pA current injection) for sham (black), 6-OHDA (gray) and L-DOPA (brown) PV- SNr cells. **B:** Box plots representing the mean firing rate and coefficient of variation. No significant differences in firing rates were shown in whole cell recordings (sham, n= 9; 6-OHDA, n= 6; L-DOPA, n= 4) which agrees with the results obtained in cell attached. **C:** AP properties, such as APth, AHPpeak and AHP_{mag} were analyzed. Scale bar: 10 μm.

When studying the excitability of PV- SNr neurons in sham, 6-OHDA lesion or L-DOPA chronic treatment mice, we observed that all PV- SNr neurons in the three conditions exhibited a *plateau* potential after a depolarizing current pulse (200 pA for 1 second) and that the "driven" firing of PV- was fast in the three states (**Fig. 4.11A**). After somatic injections of hyperpolarizing current pulses (-150 pA for 1 second) cells from all groups showed weak membrane potential "sag" ($P>0.05$; Kruskal-Wallis ANOVA; **Fig. 4.11B**). No changes in the expression, distribution or kinetics of HCN channels are therefore expected.

However, the F-I response curve of PV- neurons in the three conditions was significantly different ($F_{(2,16)}= 4.79$; $P=0.0234$, Two-way ANOVA; **Fig. 4.11C**). More specifically, the significances comparing sham and 6-OHDA were found for all current injections ranging from 150 pA to 325 pA (*$P<0.05$, Sidak's multiple comparison test), suggesting that after 6-OHDA lesion, PV- neurons were comparatively less responsive to excitation. The same result was observed previously for PV+ SNr neurons (**Fig. 4.8C**). Furthermore, we observed significant differences regarding 6-OHDA and L-DOPA groups for all current injections ranging from 75 pA to 325 pA (#$P<0.05$, Sidak's multiple comparison test) meaning that L-DOPA chronic treatment recovers the ability to response to excitation in PV- SNr neurons.

We also evidenced that the capability of PV- SNr GABA neurons to fire sustained high frequency APs was unaffected after 6-OHDA lesion or L-DOPA treatment ($P>0.05$; Kruskal-Wallis ANOVA; **Fig. 4.11D**). In the same way, no changes in the accommodation index were detected upon the three conditions ($P>0.05$; Kruskal-Wallis ANOVAs; **Fig. 4.11E**).

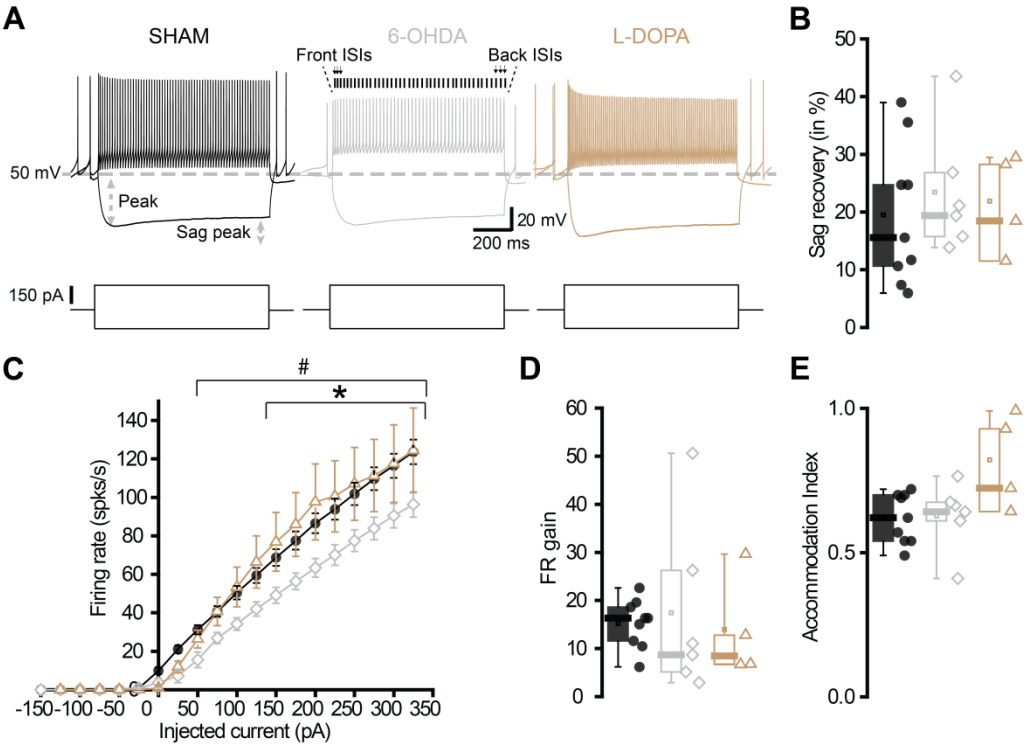

Figure 4.11. Excitability of PV- SNr neurons in sham, 6-OHDA lesioned and dyskinetic mice. **A:** Typical activity of a SNr neuron from sham (black), 6-OHDA (gray), L-DOPA (light brown) animals recorded in whole cell configuration. Superposition of the driven firing (200 pA injection for 1s) and response to a hyperpolarizing current pulse (-150 pA for 1 s; eliciting peak voltage). **B:** No significant differences in terms of sag recovery were observed. **C:** Relationship between mean firing rate and injected current. For depolarizing pulses, PV- cells from 6-OHDA were characterized by showing significantly slower rate of growth compared with sham animals. *P<0.05 Two way-ANOVA, followed by Sidak's test for all current injections ranging from 150 pA to 325 pA. In the L-DOPA group, differences with the 6-OHDA group were significant from 75 pA to 325 pA. #P<0.05 two way-ANOVA, followed by Sidak's test. **D:** Graph depicting the ratio between the maximal evoked frequency and the spontaneous firing rate not showing changes between the different conditions for PV- neurons to fire APs at high frequency. **E:** accommodation index calculated by dividing front 2 ISIs by back 2 ISIs not showing differences.

With the purpose of summarizing all the intrinsic parameters recorded in PV+ and PV- SNr neurons, as well as their alterations after DA-depletion and/or subsequent L-DOPA treatment, we provide the following **Table 4.1.**

Table 4.1. Intrinsic properties of SNr neurons and changes after DA-depletion or LID.

	Cell-attached		Whole cell							
PV+	FR	CV	AP threshold	AHP peak	AHP mag	FR	CV	Sag Rec.	FR gain	F-I
SHAM	~20Hz	~9%	-35 mV	-55 mV	~19mV	~20Hz	~10%	16%	7	
6-OHDA	↘	=	=	=	=	↘	=	=	↗	↘
L-DOPA	↘	=	=	↘	=	↘	=	↗	=	= ↗
PV-										
SHAM	~10Hz	~10%	-43mV	-63 mV	~19mV	~10Hz	~10%	19 %	15	
6-OHDA	=	=	=	=	=	=	=	=	=	↘
L-DOPA	=	=	=	=	=	=	=	=	=	↗

*All the symbols refers to respective control states

4.2. STUDY II. Striato-nigral and pallido-nigral GABAergic synaptic transmission in sham and parkinsonian mice

4.2.1. Firing rate of PV+ and PV- SNr neurons without blocking fast synaptic transmission

The aim of this second study was to characterize the inputs that SNr neurons receive from the STR and the GP. For this reason, we did not block $GABA_A$ receptors, but glutamate receptors were blocked by AMPA (DNQX, 10 µM) and NMDA (D-AP5, 50 µM). To set these experiments, we prepared sagittal brain slices from sham and 6-OHDA lesioned PVcre::Ai9T mice. Then we assessed *in vitro* cell-attached recordings of identified PV+ and PV- neurons in the SNr (**Fig. 4.12A and C**). We investigated the spontaneous firing of these subtypes of SNr neurons and tested whether the blockade of GABAergic transmission was masking some change on the firing rate of SNr neurons. Under these conditions, statistical differences were reported for the firing frequency of both PV+ and PV- SNr neurons in comparison of sham (m=8) and 6-OHDA lesioned (m=10) mice.

Regarding PV+ cells, DA loss evoked a noticeable reduction in firing rate (sham, $mean_{FR}$= 17.8 ± 1.2 Hz, n=32; 6-OHDA, $mean_{FR}$=9.4 ± 0.7 Hz, n=29; P<0.0001, Mann-Whitney test). The CV was not affected by the 6-OHDA procedure on PV+ neurons (sham, $mean_{CV}$=11.6 ± 1.1 %; 6-OHDA, $mean_{CV}$=15.6 ± 1.7 %; P>0.05, Mann-Whitney test); (**Fig. 4.12B**). Similarly, PV- neurons from sham mice fired AP at fast rate on average ($mean_{FR}$=13.7 ± 0.9 Hz, n=29), while after DA loss, the autonomous pacemaking was significantly slower ($mean_{FR}$=7.7 ± 0.6 Hz; n=30; P<0.0001, Mann-Whitney test). The CV of these neurons remained unaltered (sham, $mean_{CV}$=13.8 ± 1.2 %; 6-OHDA, $mean_{CV}$=16.7 ± 2.0 %; P>0.05, Mann-Whitney test); (**Fig. 4.12D**).

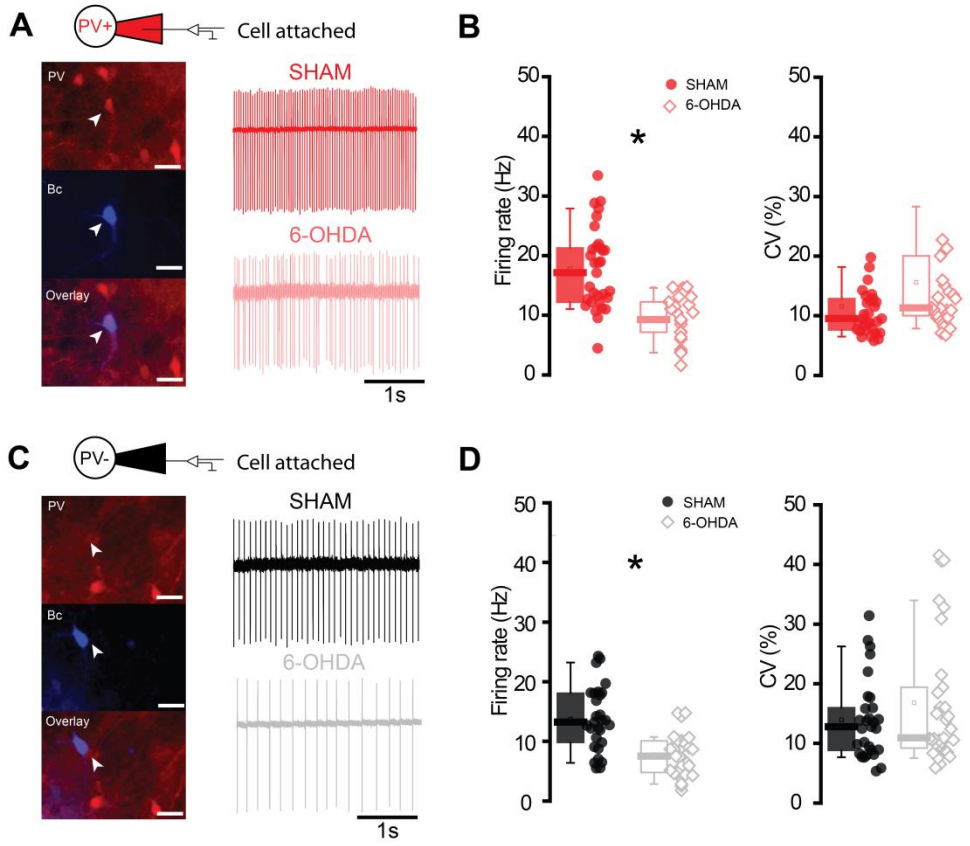

Figure 4.12. Chronic DA loss affects the firing of both PV+ and PV- SNr neurons without blocking GABAergic transmission. A: Left, epifluorescent image of an identified neuron filled with biocytin (Bc) and expressing PV (arrowheads). Right, cell-attached recordings from PV+ neurons in brain slices of sham (red) and unilateral 6-OHDA lesioned mice (pink) using the PVcre::Ai9T mouse line. **B:** Frequency and coefficient of variation of PV+ SNr neurons from sham (n=32) and 6-OHDA (n=29) mice recorded in cell-attached mode. Note a significant reduction in firing rates after the lesion (*P<0.001; MW-U test) but a similar regularity. **C:** Left, example of a neuron filled with biocytin and not expressing PV (arrowheads). Right, cell-attached recordings of PV- SNr neurons from sham (black) and 6-OHDA lesioned mice (grey). **D:** Population data showing the change on firing rate for PV- neurons in sham (n=29) and 6-OHDA (n=30) mice depicting significant differences in their excitability after DA depletion (*P<0.001; MW-U test) but not changes in their coefficient of variation. Scale bars A-C: 30 mm

4.2.2. Characterization of the striato-nigral pathway

Validation of the optogenetic approach for opsin expression in the SNr

At the time of these experiments, we did not have the possibility to selectively express ChR2 in dSPN and simultaneously monitor PV expression. Therefore, we decided to inject the pan-neuronal adeno-associated viral vector (AAV5-hSyn-hChR2(H134R)-EYFP) in the dorsal STR of PVcre::Ai9T mice (**Fig. 4.13A-C**). Once viral injection was done, we waited 2-3 weeks for the expression of the virus and then injected saline or 6-OHDA; 2 weeks later optogenetic experiments were performed.

First of all, we verified that the viral expression of ChR2 was sufficient to excite striatal SPNs. For that, we performed cell-attached recordings from SPNs neurons, identified as silent cells with no PV expression (tdTomato-); (**Fig. 4.13D-E**). We observed that 100 ms low-power blue light (473 nm; 4 mW) illumination elicited a time-locked increase in firing rate in all recorded striatal cells (**Fig. 4.13F**). The light-driven firing rate reaches 80.3 ± 23.13 Hz (n=3/m=2) with a very similar time-course display for all recorded SPN neurons (**Fig. 4.13G**).

Once our optogenetic approach was validated (see experimental procedures, **Figure 3.10**) and after demonstrating in the previous study that the expression of PV confers different electrophysiological properties, we further studied if the STR-SNr input differentially innervated PV+ or PV- neurons, and if this connection was modified in DA depletion conditions.

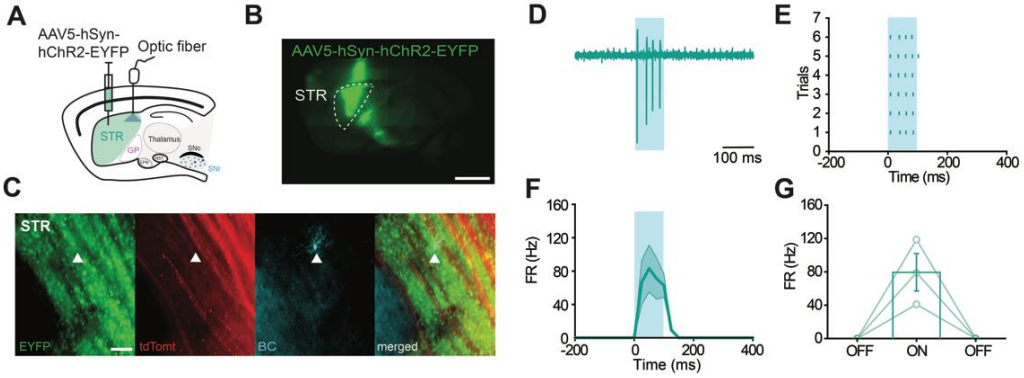

Figure 4.13. Response of striatal SPNs to optogenetic stimulation. A: Scheme showing adeno-associated viral vector (AAV5-hSyn-hChR2(H134R)-EYFP) injection in PVCre::Ai9Tmice and placement of the optic fiber optic. **B:** Fluorescence images of a sagittal section showing ChR2-EYFP transfection (green) 6 weeks after AAV injection. **C:** High-magnification fluorescence images from the STR showing ChR2-EYFP transfection (green), tdTomato (red), biocytin-filled neurons (cyan) and the overlay of the 3 labeling. SPN which do not express PV (arrowheads) are identified by biocytin labeling. **D:** Typical example from a SPN neuron depicting the increase of firing activity in response to blue light stimulation (single pulse of 100 ms duration) in cell-attached configuration. **E:** Raster diagrams of responses to light stimulation for 6 trials. **F**: Graph showing the average increase in firing rate of SPN neurons (n=3) induced by light stimulation (Bin=100 ms). **G:** Population graph showing the change of firing rate (FR) induced by light stimulation of SPN (n=3). Scale bars: B, 1mm; C, 30 µm.

4.2.2.1. Impact of STR-SNr synapses on PV+ SNr neurons

For studying the impact of STR-SNr synapses on the activity of PV+ SNr neurons from sham and 6-OHDA lesioned mice (**Fig. 4.14A**), the optical fiber was placed dorsal to the SNr to stimulate dSPN axon terminals projecting to the SNr (**Fig. 4.14B**). Cell-attached voltage clamp recordings from sagittal brain slices were used to record PV+ neurons in the SNr. We used biocytin, KGluconate and QX-314 as patch pipette solution and perfused DNQX (20 µM) and D-AP5 (50 µM) to block glutamatergic AMPAR and NMDAR, respectively. As expected from the strong convergence of the direct pathway on SNr neurons (Smith et al., 1998), we found that direct pathway activation was sufficient to produce robust inhibition of PV+ SNr neurons. As seen in **Figure 4.14C and D,** optogenetic stimulation by pulsed train illumination (10 pulses of 1 ms duration during 1s at 10 Hz), at an intensity of 90 mW, markedly inhibited the firing of PV+ SNr neurons in sham and 6-OHDA conditions (sham, n=12/m=5, 6-OHDA, n=14/m=6); ($P<0.05$, Friedman ANOVA). In DA-intact mice, stimulation of STR-SNr

inputs produced a reduction of firing frequency of 67 ± 7% (light OFF $mean_{FR}$=14.1 ± 1.7 Hz; Light ON $mean_{FR}$=4.4 ± 1.1 Hz, n=12/m=5; P=0.0001, Dunn's multiple comparison test; **Fig. 4.14C and E**). In 6-OHDA mice, the reduction of the firing rate was 69 ± 5 % (light OFF $mean_{FR}$=9.6 ± 0.9 Hz; Light ON $mean_{FR}$=3.1 ± 0.7 Hz, n=14/m=6; P< 0.0001, Dunn's multiple comparison test; **Fig. 4.14D and E.** As seen in **Fig. 4.14E** the percentage of reduction in firing rate was similar in sham and 6-OHDA condition (P> 0.05 Mann Whitney test).

Thus, stimulation of STR-SNr inputs caused GABA release that inhibited SNr tonic firing via activation of $GABA_A$ receptors. This demonstration is not shown in the following figures but was verified by perfusion of GABAzine (10 µM), confirming their identity as $GABA_A$-mediated IPCS.

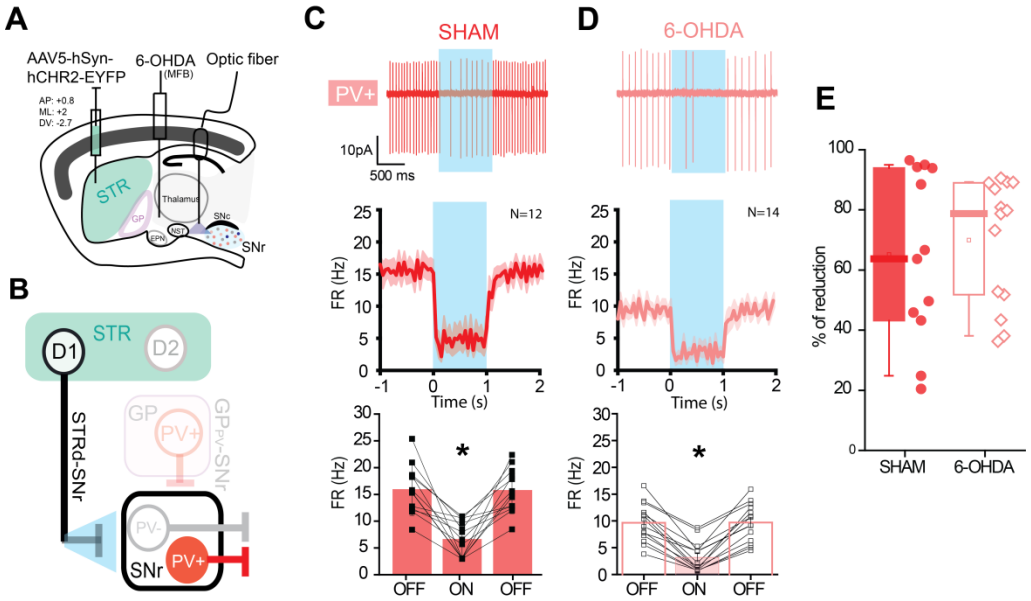

Figure 4.14. Impact of STR-SNr synapses on the activity of PV+ SNr neurons. A: Scheme showing adeno-associated viral (AAV) vector injection into the STR and the optic fiber placement activating the axon terminals of PVCre::Ai9Tmice. First, the virus injection was performed and 15 days later, 6-OHDA injection into the medial forebrain bundle (MFB) was implemented. **B:** Schematic diagram of the optogenetic approach showing the activation of dSPN. **C:** Top, representative cell-attached recording from a PV+ SNr neuron during light stimulation (10Hz, 1s) of sham mice. Middle, graph showing the average decrease in firing rate of PV+ cells induced by light stimulation (Bin=1000 ms). Bottom, population graphs showing the efficiency of the light stimulus reducing the cell firing rate (67 ±7%). **D:** Same as C for 6-OHDA PV+ cells. Percentage of firing frequency reduction was similar to sham mice (69 ±5.5%). *P<0.05; Friedman ANOVA, followed by Dunn's test. **E:** Percentage of inhibition for sham (n=12) and 6-OHDA (n=14) PV+ SNr neurons.

Because cell-attached recordings provide a limited readout of the properties of STR-SNr synapses, we undertook whole-cell voltage-clamp recordings to determine if DA depletion altered the STR-SNr synaptic transmission in PV+ SNr neurons. Whole-cell recordings were performed at a holding potential of -38 mv (after JP correction of 13mV in our recording conditions) in order to trigger outward light-evoked IPSC (**Fig. 4.15A**). We first compared the amplitude of STR-SNr IPSC and did not reveal a significant difference between sham and 6-OHDA mice ($P<0.05$ Mann Whitney test; **Fig. 4.15B**). We then compared the short-term plasticity dynamics of STR-SNr synapses using trains of optostimulation (10 pulses, 1ms duration) at various frequencies (5-60 Hz). Representative examples of responses elicited at 10 and 40Hz are presented in **Fig. 4.15C-D**. Although IPSC amplitude was similar in both conditions, paired-pulse ratio (normalized IPSC) revealed a frequency-dependent increase in short-term depression in 6-OHDA mice (**Fig. 4.15C-E**); (sham, $mean_{N.AMPLITUDE}=0.5 \pm 0.05$; 6-OHDA, $mean_{N.AMPLITUDE}=0.34 \pm 0.07$, $P=0.0011$, Mann Whitney U test). This data suggest that STR-SNr inputs in sham mice are more resistant to trigger synaptic depression in PV+ neurons than in 6-OHDA mice (**Fig. 4.15D, right**). Furthermore, when we compared the plasticity of PV+ SNr neurons in sham and 6-OHDA mice at different frequencies, we observed that 6-OHDA neurons were more sensible to synaptic depression ($F_{(1,17)}= 15.57$; $P=0.0010$, Two-way ANOVA; **Fig. 4.15E**). Specifically, this difference in short-term depression was observed for frequencies similar or higher than 20 Hz frequency ($P<0.05$, Sidak's multiple comparison test).

The IPSCs recorded in SNr neurons are presumably due to a combination of $GABA_A$ currents elicited by STR-SNr, GP-SNr, and local SNr inputs (Grofova et al., 1982; M et al., 1992).

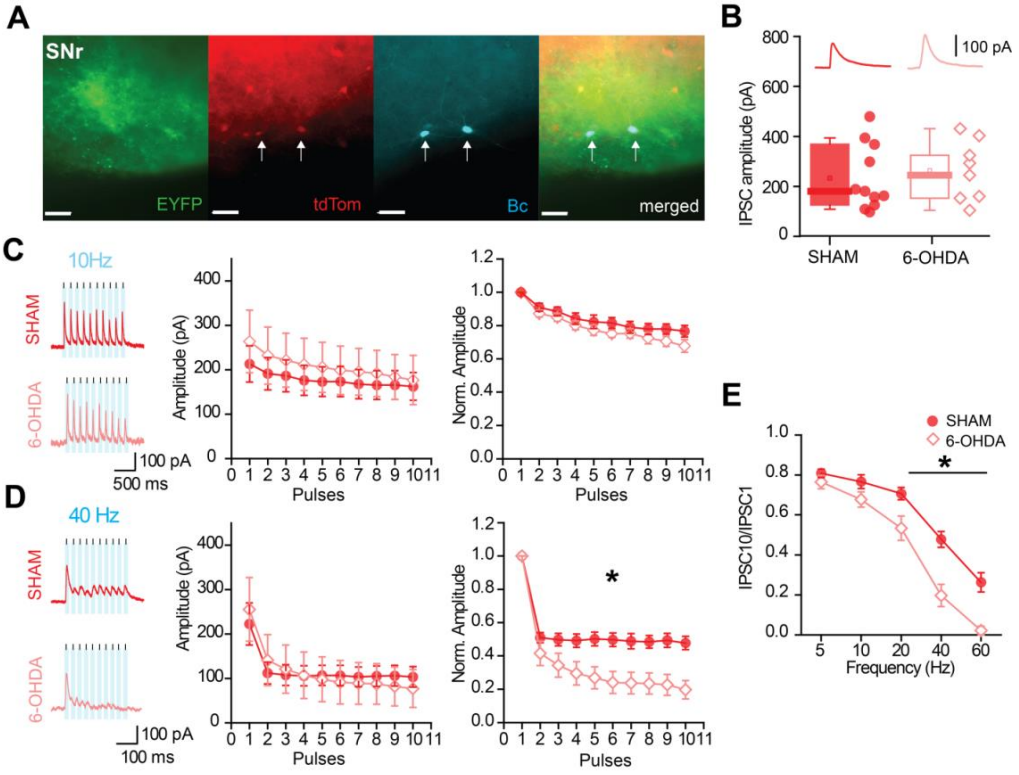

Figure 4.15. Characterization of STR-SNr IPSC short-term plasticity for PV+ neurons in sham and 6-OHDA mice. A: Striatal viral expression and recorded cell types in the SNr of a PVcre::Ai9T mouse where virus expression is reported by EYFP (green), Cre expression by tdTomato (red) and biocytin-recorded neurons (cyan). Immunofluorescence images display many neurons in the SNr that are tdTomato+, including the recorded neurons (arrows). Right, overlay shows the biocytin-filled neurons expressing PV and the fact that all of them are in the transfected zone. **B:** Population graph showing the amplitude of single STR-SNr IPSC at 10 Hz frequency. **C:** Examples of STR-SNr IPSCs recorded in sham (red) and 6-OHDA (pink) mice stimulated by light (10 pulse, 1 ms). Amplitude and normalized amplitude is represented at 10 Hz of frequency with a protocol of 10 pulses. Data from sham (n=11) and 6-OHDA (n=8). **D:** Examples and graphs depicting the amplitude and normalized amplitude at 40 Hz of frequency. Note a significant difference in plasticity after 6-OHDA lesion for PV+ neurons ($P<0.05$; MW-U test). **E:** Plasticity is represented by dividing the last IPSC by the first. *Significantly different plasticity with all frequencies ranging from 20 Hz to 60 Hz regarding sham and 6-OHDA ($P<0.05$; two-way ANOVA, followed by Sidak's test). Scale bars: 50 μm.

4.2.2.2. Impact of STR-SNr synapses on PV- SNr neurons

For the study of the impact of STR-SNr synapses on the activity of PV- SNr neurons from sham and DA depleted mice, we followed the same experimental procedure than for PV+ neurons (**Fig. 4.16A**). Conversely, this time we focused on PV- SNr neurons (**Fig. 4.16B**). Cell-attached voltage clamp recordings from sagittal brain slices were used to record PV- neurons in the SNr. **Figure 4.16C and D**, show example responses and average data for PV- SNr cell in sham and 6-OHDA lesioned mice. Thus in total, we observed a significant change in firing rate ($P< 0.05$, Friedman ANOVA) in response to laser stimulation, suggesting that our stimulation conditions strongly modulated SNr output in sham and 6-OHDA conditions (sham, n=12/m=5, 6-OHDA, n=10/m=5). In sham mice, stimulation of STR-SNr inputs induced a significant reduction of firing frequency of 74 ± 6.68 % (Light OFF $mean_{FR}$=12.8 ± 0.7 Hz; Light ON $mean_{FR}$=3.3 ± 0.9 Hz; P=0.0001, Dunn's multiple comparison test), similar to what was observed for 6-OHDA PV- neurons (Mean reduction=87 ± 4.3%; light OFF $mean_{FR}$=7.9 ± 0.6 Hz; Light ON $mean_{FR}$=0.9 ± 0.1 Hz; P= 0.0001, Dunn's multiple comparison test).

As we shown for PV+ SNr neurons, cell-attached recordings from PV- SNr neurons also revealed no differences in the percentage of reduction of autonomous pacemaking after DA denervation ($P<0.05$ Mann Whitney test; **Fig. 4.16E**). In contrast, when we compared the impact of STR-SNr synapses on the activity of PV+ and PV- together, we observed that this input affects in a stronger way to PV- SNr neurons after DA denervation (P=0.02; Mann-Whitney U test). This difference of effect of STR-SNr inputs between PV+ and PV- SNr could be explained in part by the lower firing rate of the former cell type.

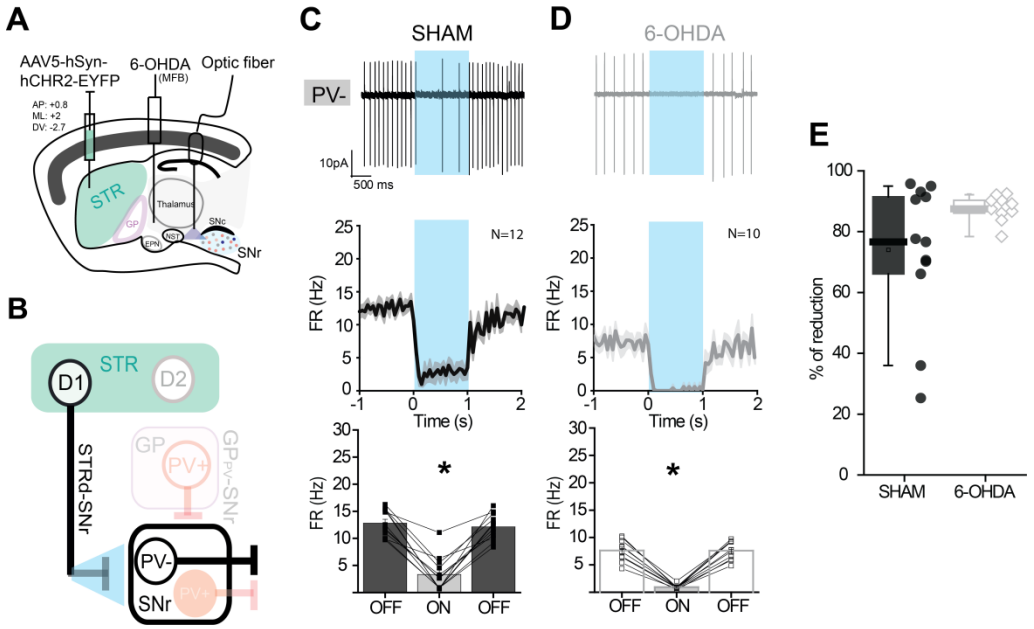

Figure 4.16. Impact of STR-SNr synapses on the activity of PV- SNr neurons. A: Scheme showing the same experimental procedure than for the study of PV+ SNr neurons. **B:** Diagram of the optogenetic approach showing the activation of dSPN and the impact on PV- neurons in the SNr. **C:** Top, representative cell-attached recording from a PV- SNr neuron during light stimulation (10Hz, 1s) in a sham (black) and 6-OHDA (grey) mouse. Middle, graph showing the average decrease in firing rate of PV- cells induced by light stimulation (Bin=1000 ms). **D:** Representative cell-attached of a 6-OHDA PV- SNr neuron during light stimulation. As for the sham, normalized PSTH and population data showing the reduction in firing rate. *P<0.05; Friedman ANOVA, followed by Dunn's test. **E:** Percentage of reduction in firing frequency for sham 74 ± 6.68% (n=12) and 6-OHDA 87 ± 4.3% (n=10) PV- SNr neurons.

As for PV+, we undertook whole-cell voltage-clamp recordings to investigate the impact of DA-depletion on the properties of STR-SNr synapses in PV- SNr neurons. These cells were filled with biocytin in order to perform *post-hoc* immunohistochemistry and confirm that these neurons were indeed tdTomato$^-$ and located in an area of the SNr receiving STR-SNr inputs (**Fig. 4.17A**). Light-evoked outward $GABA_A$-mediated IPSCs were recorded at a holding potential of -38mV. As for PV+ SNr neurons, the amplitude of single IPSCs was not markedly different in DA-depleted mice compared to sham mice (P>0.05 Mann Whitney test; **Fig. 4.17B**).

To examine differences in short-term plasticity of STR-SNr inputs received by PV- SNr neurons, we also compared the short-term dynamics of STR-SNr synapses using train of stimulation (10 pulses, 1 ms duration) at various frequencies (5-60Hz). Typical responses are depicted at frequencies of 10 Hz (**Fig. 4.17C**) and 40 Hz (**Fig. 4.17D**) in sham and 6-OHDA lesioned mice. The amplitude and paired-pulse ratio (normalized amplitude) of IPSCs was studied for these two frequencies not showing significant differences. No differences were found across the whole range of frequencies tested (P>0.05 Two-way ANOVA, followed by Sidak's test; **Fig. 4.17E**). These data suggest that STR-SNr synapses received by PV- SNr neurons are not impacted by DA-depletion. However, this absence of alterations represents a marked difference with the change of short-term plasticity observed in PV+ neurons.

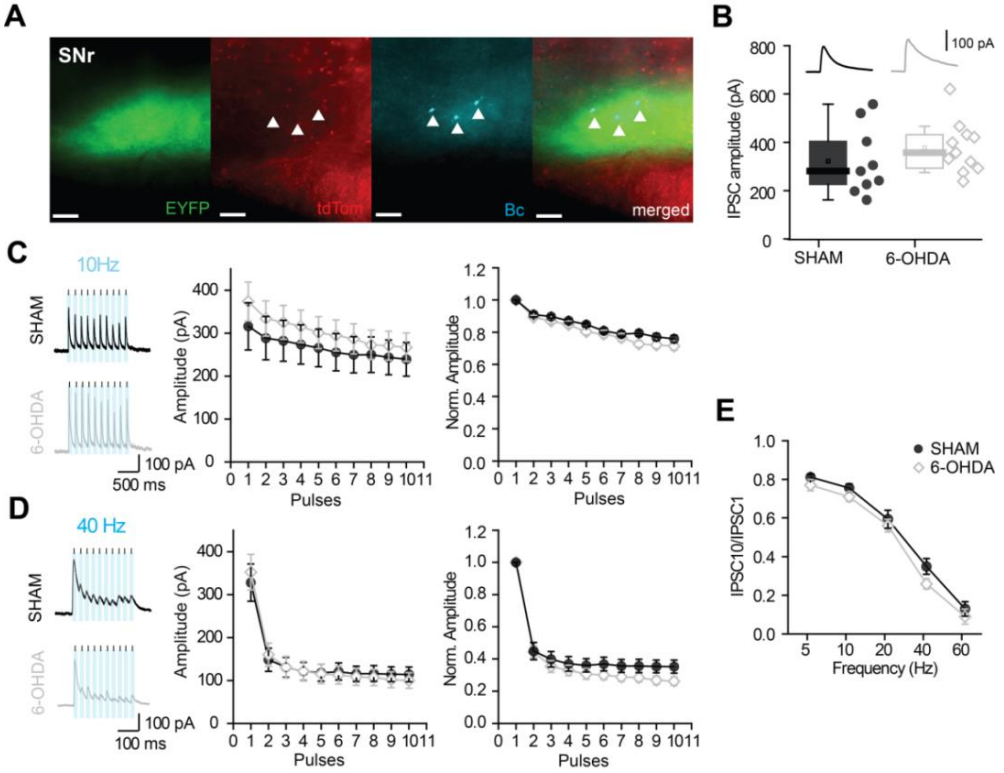

Figure 4.17. Characterization of STR-SNr IPSC short-term plasticity for PV- neurons in sham and 6-OHDA mice. A: Striatal viral expression in the SNr of a PVcre::Ai9T mouse where viral expression is reported by EYFP (green), Cre expression by tdTomato (red) followed by immunolabeling for neurons stained by biocytin (cyan) and overlay. **B:** Population graphs depicting the amplitude of the first STR-SNr IPSCs at 10 Hz. **C:** Examples of STR-SNr IPSCs recorded in sham (black) and 6-OHDA (gray) mice stimulated by light (10 pulses, 1 ms). Amplitude and normalized amplitude is represented at 10 Hz of frequency with a protocol of 10 pulses. Data from sham (n=9) and 6-OHDA (n=11). **D:** Examples and graphs depicting the amplitude and normalized amplitude at 40 Hz of frequency. **E:** Plasticity is represented by dividing the last IPSC by the first not showing differences between groups. Scale bars: 50 μm.

4.2.3. Characterization of the pallido-nigral pathway

Validation of the optogenetic approach for opsin expression in the GP

A recent study has shown that optogenetic manipulation of PV-expressing GPe neurons can rescue Parkinson-like motor symptoms Mastro et al., 2017 in Nature Neuroscience), which highlights the key role of this nucleus in the BG circuitry operations and the importance of differentiating cell-types within the BG. In order to study the GP-SNr pathway we decided to restrict ChR2 expression to PV-expressing GPe neurons which are known to project to downstream nuclei (STN, SNr) of the BG (**Fig. 4.18A**). For that, we administered the AAV vector (AAV5-DIO-hChR2(H134R)-EYFP) into the GP of PVcre::Ai9T mice unilaterally and then, we waited for 4-5 weeks to ensure the expression of the virus (**Fig. 4.18B-C**). Cre-dependent expression of ChR2 (ChR2- H134R variant) was achieved by using a double-floxed inverted open reading frame (DIO) driven by an ubiquitous EF1α promoter (see experimental procedures, **Figure 3.3**).

First of all, we wanted to verify that our Cre-Lox strategy used for a selective expression of ChR2 in PV-expressing GP was successful and efficient enough to drive activity in this GP subpopulation. With that purpose, we performed cell-attached recordings from PV-GP neurons, identified by the observation of tdTomato fluorescence. These neurons are also known for their high autonomous firing rate *ex vivo* (Chan et al., 2004; Abdi et al., 2015). In agreement with the known properties of PV-GP neurons, the basal firing rate of the PV-GP neurons expressing ChR2 was high (> 100Hz; **Fig. 4.18D-E**). A flash of blue light (100 ms; 4 mW of total power) produced a strong and transient elevation of their firing which came back to basal resting firing rate when the light was turned off (Light OFF $mean_{FR}$=20.1 ± 2.5 Hz; Light ON $mean_{FR}$ =100.1 ± 28.2; P<0.001 Friedman ANOVA, followed by Dunn's test; n=3/m=2; **Fig. 4.18F-G**).

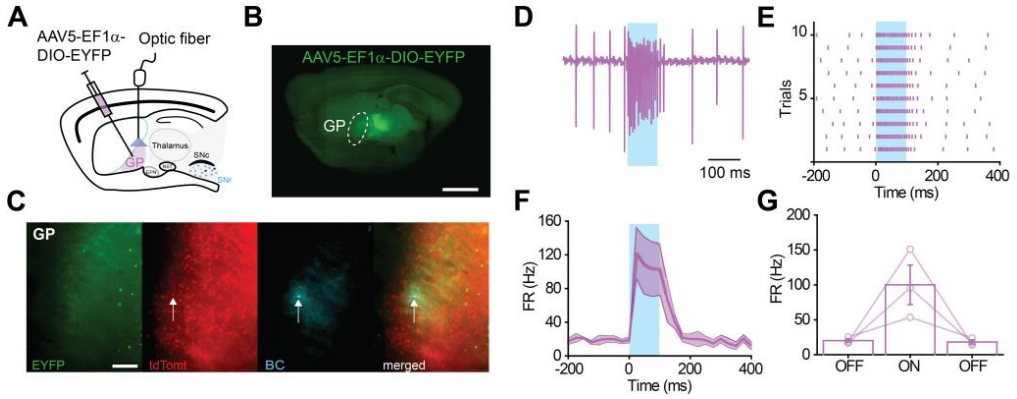

Figure 4.18. Response of PV-expressing GP neurons to light stimulation. A: Scheme showing adeno-associated viral (AAV) vector injection and the fiber optic placement. AAV5-EF1a-DIO (H134R)-EYFP was injected into the GP of PVCre::Ai9T mice. **B:** Fluorescence images of a sagittal section showing ChR2-EYFP transfection (green) 3 weeks after AAV injection. **C:** High-magnification fluorescence images from the (B) GP showing ChR2-EYFP transfection (green), tdTomt (red), biocytin-filled neurons (cyan) and merged. GP neurons which express PV (arrows) are identified by biocytin labeling. **D:** Typical example from a GP-positive neuron depicting the increase of firing activity in response to blue light stimulation (1 pulse of 100ms) in cell-attached configuration. **E:** Raster diagrams of responses to light stimulation for 10 traces. **F:** Average firing rate of PV GP neurons expressing ChR2 (n=3) before, during (time 0) and after 100 ms of 1 light pulse. **G:** Population graph showing the change of firing rate (FR) induced by light stimulation of GP positive neurons. Scale bars: B, 1mm; C, 500 μm.

4.2.3.1. Impact of GP-SNr synapses on PV+ SNr neurons

GP-SNr GABAergic transmission in the SNr in experimental models of PD has not been described yet. To report it, we first administered the virus into the GP, then we waited for 4-5 weeks to ensure the virus expression and finally we proceed to inject 6-OHDA or vehicle into the right MFB (**Fig. 4.19A**).

To study *in vitro* the impact of GP-SNr synapses on the activity of PV+ SNr neurons we placed the optical fiber on top of the SNr with the purpose to stimulate axon terminals projecting to the SNr (**Fig. 4.19B**). Cell-attached voltage clamp recordings from sagittal brain slices were used to record PV+ neurons in the SNr. The patch pipette solution that precluded the electrophysiological identification of neurons also contained biocytin, KGluconate and QX-314. **Figure 4.19C and D**, shows example responses and group averages for these cell subpopulations in sham and 6-OHDA lesioned mice, demonstrating weak firing rate modulation. Besides this, we observed a significant

change in firing rate (P<0.05, Friedman ANOVA) in response to laser stimulation, suggesting that our stimulation conditions could modulate SNr output in these groups (sham, n= 9/m=3; 6-OHDA, n= 8/m=4). In DA-intact mice, stimulation of GP-SNr inputs produced a reduction of firing frequency of 30 ± 3 % (light OFF $mean_{FR}$=16.8 ± 1.7 Hz; Light ON $mean_{FR}$=11.8 ± 1.4 Hz; P=0.0003, Dunn's multiple comparison test; **Fig. 4.19C and E**). Light stimulation in 6-OHDA lesioned mice triggered a decrease in firing rate of 29 ± 4.2 % (light OFF $mean_{FR}$ =8.9 ± 1.3 Hz; Light ON $mean_{FR}$ =6.7 ± 1.1 Hz; P=0.0003 Friedman ANOVA, Dunn's multiple comparison test; **Fig. 4.19D**). The percentage of reduction in firing rate was similar in sham and 6-OHDA conditions (P>0.05; Mann Whitney test; **Fig. 4.19E**).

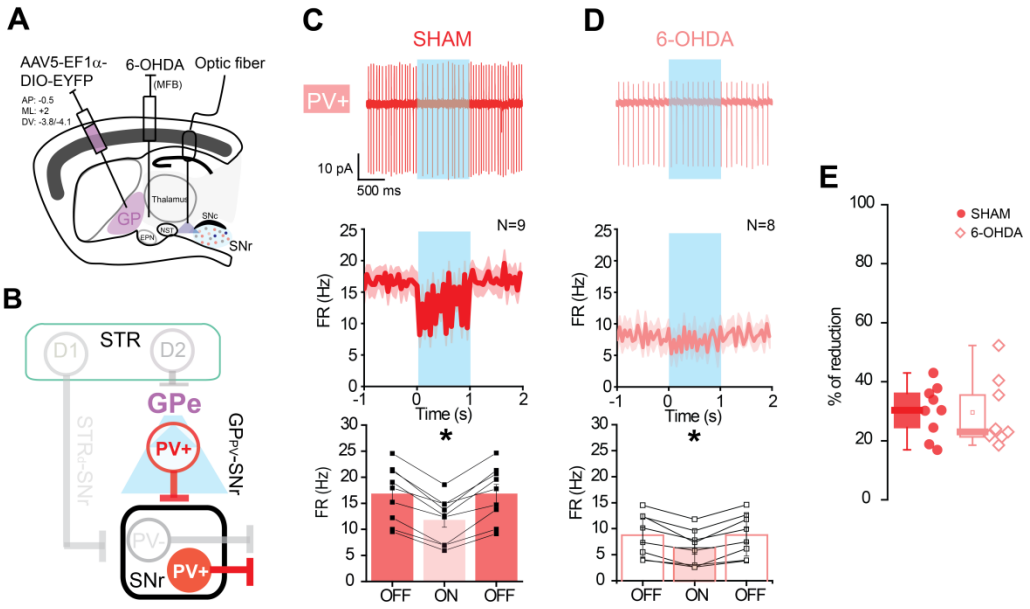

Figure 4.19. Impact of GP-SNr synapses on the activity of PV+ SNr neurons. A: Scheme showing adeno-associated viral (AAV) vector injection into the GP and the optic fiber placement activating the axon terminals of PVCre::Ai9Tmice. First, the virus injection was performed, 15 days later; 6-OHDA injection into the medial forebrain bundle (MFB) was implemented. **B:** Schematic diagram of the optogenetic approach showing the activation of PV-expressing GP neurons and the effect on PV+ SNr neurons. **C:** Top, representative cell-attached recording from a PV+ SNr neuron during light stimulation (10Hz, 1s) of sham mice. Middle, graph showing the average decrease in firing rate of PV+ cells induced by light stimulation (Bin=1000 ms). Bottom, population graphs showing the efficiency of the light stimulus reducing the cell firing rate (30 ± 3%). **D:** Same as C for 6-OHDA PV+ cells. Percentage of firing frequency reduction was similar to sham mice (29 ± 4.2%). *P<0.05; Friedman ANOVA, followed by Dunn's test. **E:** Percentage of inhibition for sham (n=9) and 6-OHDA (n=8) PV+ SNr neurons.

Because cell-attached recordings provide a limited readout of the properties of GP-SNr synapses, we undertook whole-cell voltage-clamp recordings to determine if DA depletion altered the GP-SNr synaptic transmission received by PV+ SNr neurons. These whole-cell recordings were performed in presence of DNQX (20 µM) and D-AP5 (50 µM) to block glutamatergic AMPAR and NMDAR, respectively. SNr neurons were recorded using KGluconate-based internal solution and outward light-evoked IPSC were recorded (as previously for STR-SNr pathway) at a holding potential of -38 mv after junction potential correction which was 13mV in our recording conditions (**Fig. 4.20A**).

We first compared the amplitude of GP-SNr IPSC at 10 Hz of frequency and it was markedly reduced in 6-OHDA compared to sham mice (sham, n=11/m=3; $mean_{amplitude}$=362.9 ± 46.3 pA; 6-OHDA, n=10/m=4; $mean_{amplitude}$= 176.6 ± 22.51 pA; P=0.003; Mann Whitney test; **(Fig. 4.20B**).

We then compared the short-term plasticity dynamics of GP-SNr synapses using train of stimulation (10 pulses, 1ms duration) at various frequencies (5-60 Hz). Representative examples of responses elicited at 10 and 40Hz are presented in **figure 4.20C-D**. The amplitude of the IPSC at 10Hz frequencies was markedly decreased in 6-OHDA mice (**Fig. 4.20C**); (sham, 170.6 ± 18.3 pA; 6-OHDA, 101.3 ± 9.5 pA, P = 0.0015, Mann-Whitney U test). The same result was obtained at 40 Hz frequency (**Fig. 4.20D**); (sham, 135.9 pA ± 22.3; 6-OHDA, 82.4 ± 15.4 pA, P = 0.015, Mann-Whitney U test). Nevertheless, no differences in the paired-pulse ratio (Normalized IPSC) were depicted (P> 0.05 Two-way ANOVA, followed by Sidak's test; **Fig. 4.20E**).

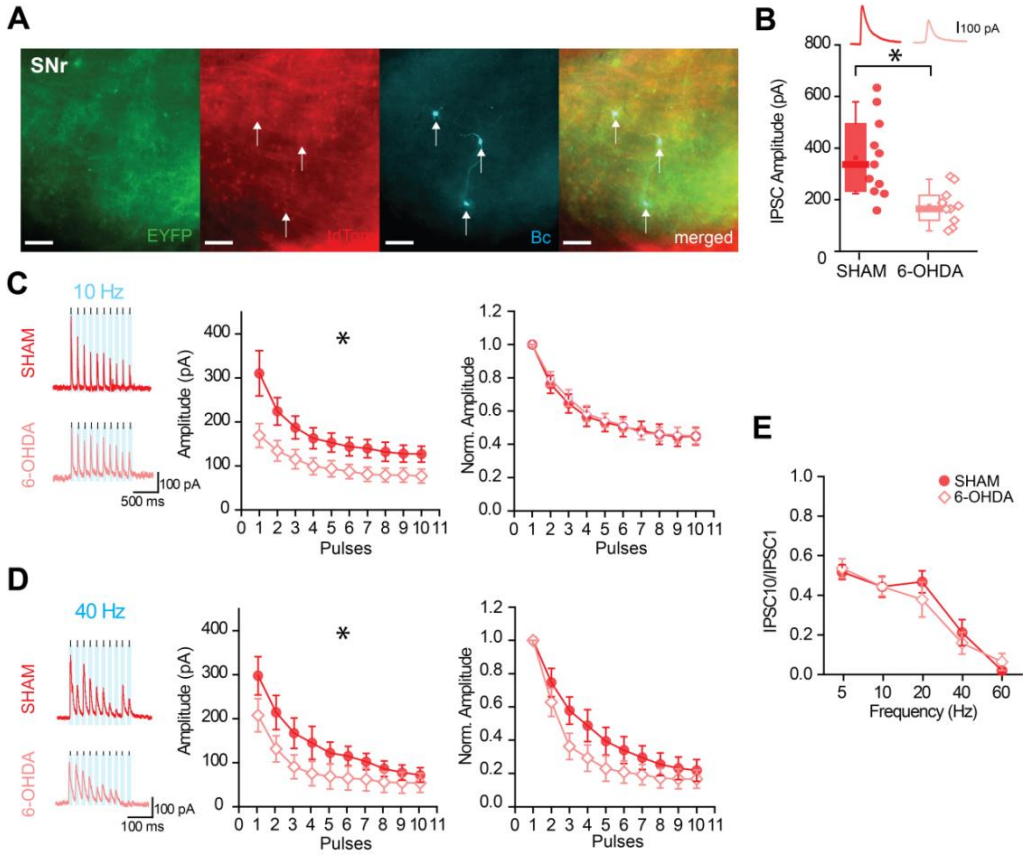

Figure 4.20. Characterization of GP-SNr IPSC short-term plasticity for PV+ neurons in sham and 6-OHDA mice. A: High-magnification images of the SNr from a PVcre::Ai9T mouse showing on the left the virus transfection, tdTomato staining and biocytin-filled neurons in the SNr. Right, overlay displays three biocytin-filled PV+ neurons (arrows) in the transfected zone. **B:** Population graph showing the amplitude of the first STR-SNr IPSC at 10 Hz. Note a decrease in the amplitude after the 6-OHDA lesion (p=0.003; MW-U test). **C:** Examples of GP-SNr IPSCs recorded in sham (red) and 6-OHDA (pink) mice. Amplitude and normalized amplitude is represented at 10 Hz of frequency with a protocol of 10 pulses for 1 ms. Data from sham (n=11) and 6-OHDA (n=10). Note a significant difference in amplitude between sham and 6-OHDA (p=0.0015; MW-U test). **D:** Examples and graphs depicting the amplitude and normalized amplitude at 40 Hz of frequency. Note a significant difference in the amplitude (P=0.015; MW-U test). **E:** Plasticity is represented by dividing the last IPSC by the first not showing differences between groups. Scale bars: 50 μm.

4.2.3.2. Impact of GP-SNr synapses on PV- SNr neurons

For the study of the impact of GP-SNr synapses on the activity of PV- SNr neurons from sham and DA depleted mice, we followed the same experimental procedure described for PV+ neurons (**Fig. 4.21A**). Conversely, this time we focused on PV- SNr neurons (**Fig. 4.21B**). Cell-attached voltage clamp recordings from sagittal brain slices were used to record PV- neurons in the SNr. **Figure 4.21C and D**, show example responses and average data for PV- SNr cell in sham and 6-OHDA lesioned mice. Overall, we observed a significant change in firing rate ($P<0.05$, Friedman ANOVA) in response to laser stimulation, suggesting that our stimulation conditions could modulate SNr output in sham and 6-OHDA conditions (sham, n=13/m= 3, 6-OHDA, n=7/m=4). In DA-intact mice, stimulation of GP-SNr inputs produced a reduction of firing frequency of 20 ± 2 % (**Fig. 4.21C, E**; light OFF $mean_{FR}$=14.4 ± 0.9 Hz; Light ON $mean_{FR}$=10.5 ± 1.1 Hz; $P<0.0001$, Dunn's multiple comparison test; **Fig. 4.21C**). However, the reduction of the firing rate (37 ± 4.2 %; **Fig. 4.21D, E**) was markedly higher in 6-OHDA mice (light OFF $mean_{FR}$=7.8 ± 1.1 Hz; Light ON $mean_{FR}$=5.1 ± 0.9 Hz; $P<0.0001$, Dunn's multiple comparison test; **Fig. 4.21D**). Contrary to what we shown for PV+ SNr neurons, cell-attached recordings from PV- SNr neurons revealed marked differences in the percentage of reduction of autonomous pacemaking after DA denervation ($P=0.002$, Mann Whitney test; **Fig. 4.21F**).

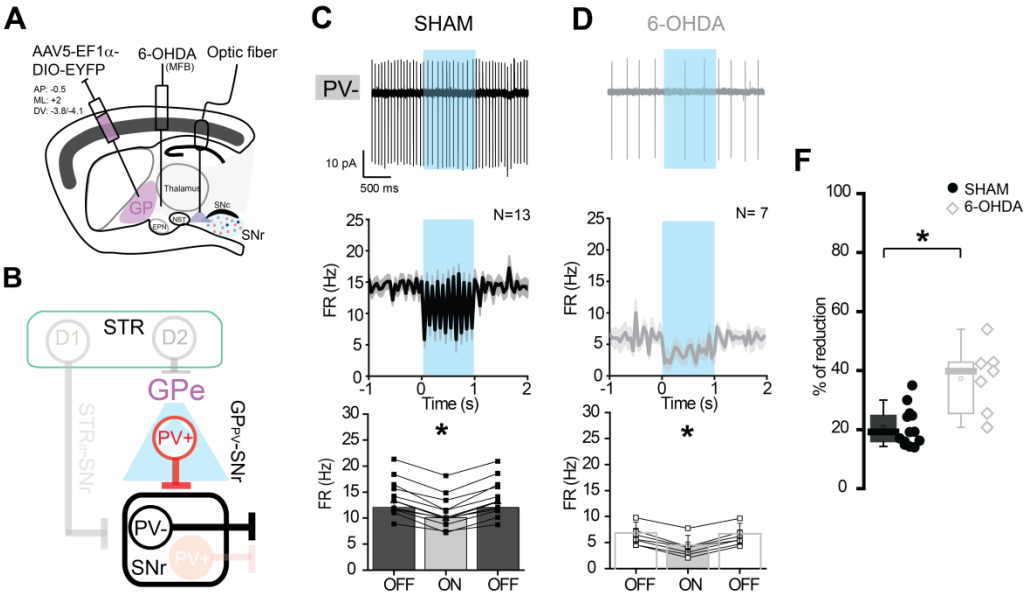

Figure 4.21. Impact of GP-SNr synapses on the activity of PV- SNr neurons. A: Scheme showing the same experimental procedure followed than for PV+ neurons **B:** Diagram of the optogenetic approach showing the activation of PV-expressing GP neurons and the effect on PV- SNr neurons from PVCre::Ai9T mice. **C-E:** Representative cell-attached recording from a PV- SNr neuron during light stimulation (10Hz, 1s) of sham (black) and 6-OHDA (gray) mice. Middle, graph showing the average decrease in firing rate of PV- cells induced by light stimulation (Bin=1000 ms). Bottom, population graphs depicting the reduction in the firing rate during the activation of GP-SNr synapses. The percentage of reduction on firing rate for PV- SNr neurons in sham 20 ± 2% and in 6-OHDA lesioned 37 ± 4.2 %. *P<0.05; Friedman ANOVA, followed by Dunn's test. **F:** Percentage of reduction for sham (n=13) and 6-OHDA (n=7) PV-SNr neurons. Note a significant difference in terms of inhibition between sham and 6-OHDA (*P=0.002; MW-U test).

As for PV+, we undertook whole-cell voltage-clamp recordings to investigate the impact of DA-depletion on the properties of GP-SNr synapses in PV- SNr neurons. These cells were filled with biocytin with the purpose of performing *post-hoc* immunohistochemistry and confirm not only their identity as tdTomato$^-$ but also their location in an area of the SNr receiving GP-SNr inputs (**Fig. 4.22A**). Light-evoked outward $GABA_A$-mediated IPSCs were recorded at a holding potential of -38mV. Contrary to what we observed for PV+ SNr neurons, the amplitude of single IPSCs was markedly increased in DA-depleted mice compared to sham mice (sham, n=13/m=3, $mean_{amplitude}$=67.6 ± 7.7 pA; 6-OHDA, n=10/m=4, $mean_{amplitude}$=121.5 ± 10.5 pA; P=0.0005; Mann Whitney test; **Fig. 4.22B**).

To examine differences in short-term plasticity of GP-SNr inputs received by PV- SNr neurons, we also compared the short-term dynamics of GP-SNr synapses using train of stimulation (10 pulses, 1 ms duration) at various frequency (5-60Hz). Typical responses are depicted at frequencies of 10 Hz (**Fig. 4.22C**) and 40 Hz (**Fig. 4.22D**) in sham and 6-OHDA lesioned mice. The amplitude and paired-pulse ratio (normalized amplitude) of IPSCs was studied for these two frequencies just showing significant differences at 10Hz frequency (P=0.0005; Mann Whitney U test). No differences were depected across the whole range of frequencies tested (**Fig. 4.22E**).

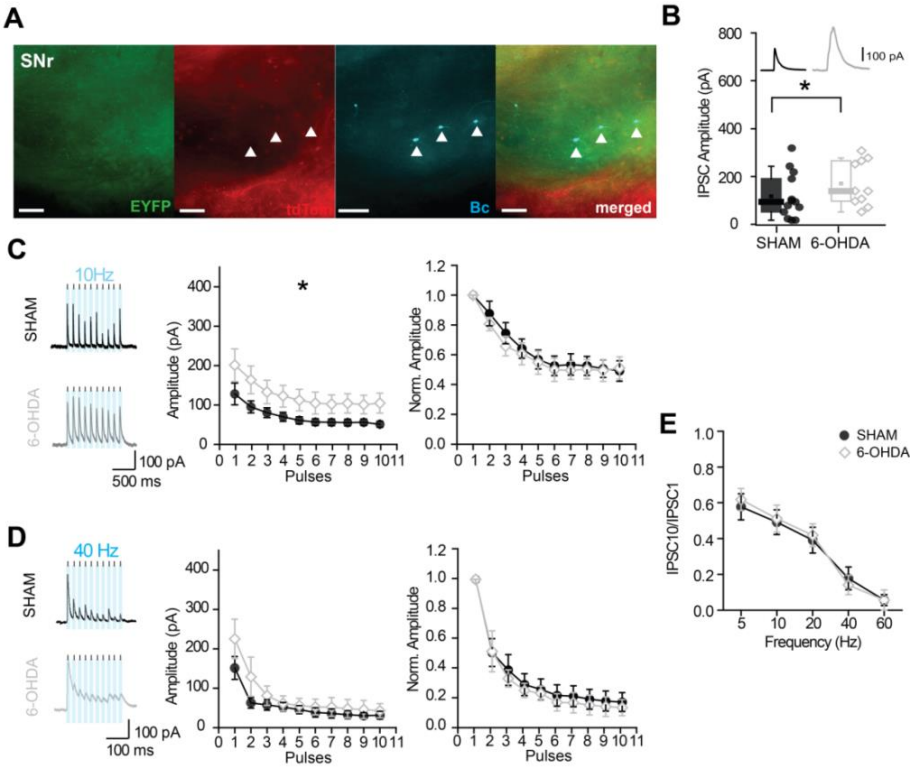

Figure 4.22. Characterization of GP-SNr IPSC short-term plasticity for PV- neurons in sham and 6-OHDA mice. A: Pallidal viral expression in the SNr of a PVcre::Ai9T mouse where viral expression is reported by EYFP (green), Cre expression by tdTomato (red) followed by immunolabelling for neurons stained by biocytin (cyan) and overlay. Immunofluorescence images display many tdTomato$^+$ and tdTomato$^-$ neurons in the SNr including the tdTomato$^-$ recorded neurons (arrowheads). Overlay images depicts the three neurons in the transfected zone. **B:** Population graph showing the amplitude of first STR-SNr IPSC at 10 Hz. Note an increse in amplitude after 6–OHDA lesion (P=0.036; MW-U test). **C:** Examples of GP-SNr IPSCs recorded in sham (black) and 6-OHDA (gray) mice for PV- SNr neurons. Amplitude and normalized amplitude is represented at 10 Hz of frequency with a protocol of 10 pulses for 1 ms. Data from sham (n=13) and 6-OHDA (n=10). Note a significant increase in IPSC amplitude (P=0.0005; MW-U test). **D:** Examples and graphs depicting the amplitude and normalized amplitude at 40 Hz of frequency. **E:** Plasticity is represented by dividing the last IPSC by the first not showing differences between groups. Scale bars: 50 μm.

The following scheme (**Fig. 4.23**) summarize all the results obtained in the study of STR and GP inputs to SNr neurons. Thus, a decrease in firing rate of both subtypes of SNr neurons and an altered STR-SNr transmission onto PV+ neurons as well as a potentiated GP-SNr transmission onto PV- cells after the 6-OHDA lesion are the main results obtained in this STUDY II.

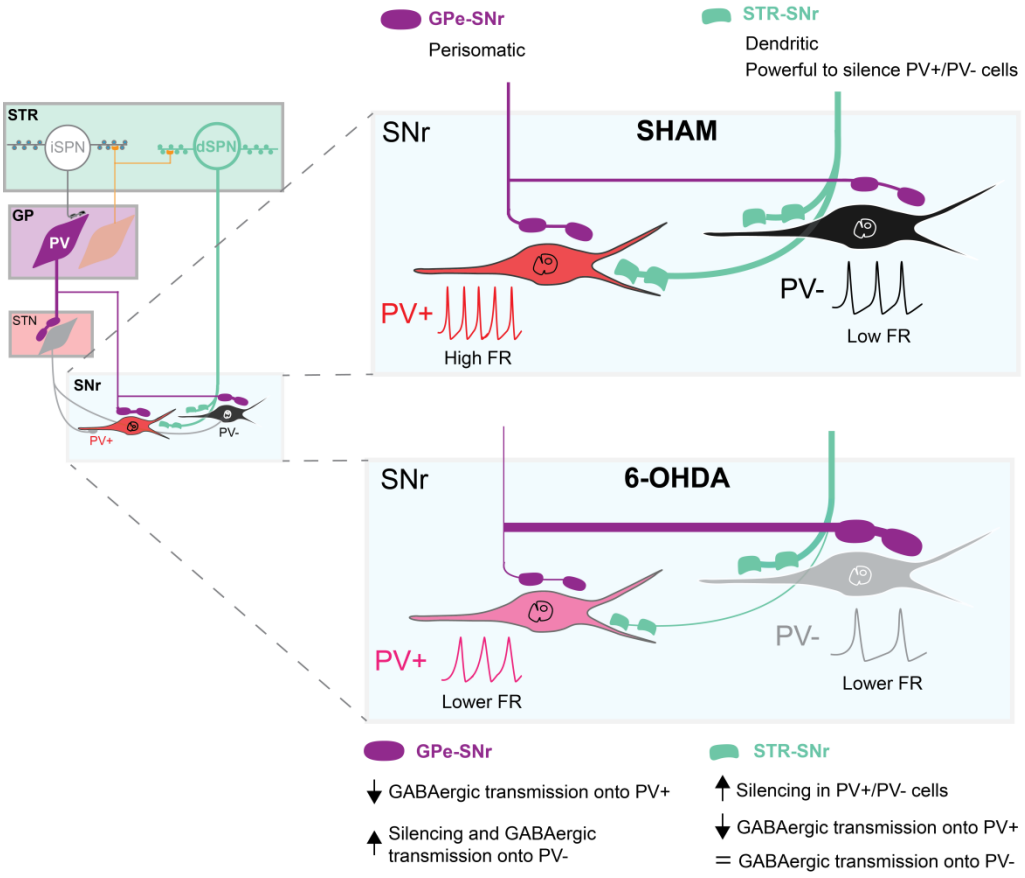

Figure 4.23. Summary of STR-SNr and GP-SNr GABAergic transmission onto PV+ and PV- SNr neurons from sham and DA depleted mice. In normal states, both PV+ and PV- cells in the SNr receive inputs from striatal dSPN and PV-GP neurons. The dentritic inhibition from striatal dSPNs is more efficient silencing the activity of both subtypes of SNr neurons than perisomatic inputs from PV-GP neurons. Indeed, the firing rate is affected in both PV+ and PV- SNr neurons in absence of GABAergic synaptic blockers. Interestingly, the impact of DA loss on STR-SNr synapses reveals an increase of short-term depression only in PV+ cells after the 6-OHDA lesion, suggesting an alteration of STR-SNr transmission onto these neurons. In contrast, augmented GP-SNr transmission is observed onto PV- neurons and the opposite effect in PV+ cells.

4.3. STUDY III. GABAergic extrasynaptic transmission in SNr neurons from control and parkinsonian mice

4.3.1. Distribution of extrasynaptic δ and α5-subunits in $GABA_A$Rs of both subtypes of SNr neurons

In the CNS, tonic inhibition is mediated by extrasynaptic $GABA_A$ receptors composed of δ and α5-subunits that confer high affinity for GABA and slow deactivation and desensitization kinetics. In the SNr, the presence of δ and α5 subunits seems to be controversial due to the low level of protein expression compared to the *thalamus* or the STR (Pirker et al., 2000; Schwarzer et al., 2001).

The expression of δ $GABA_A$R subunit in the SNr, has already been investigated looking at age- and sex- differences (Chudomel et al., 2015). These authors observed a decline in the density of δ subunit in the SNr age related, but no sex-specific changes. However, there are no studies discerning among subpopulations of SNr neurons.

In the first place, we explored δ–subunit expression in the SNr of wild-type ($\delta^{+/+}$) and knock-out ($\delta^{-/-}$) mice. As control nucleus, we selected the *thalamus* which is known to have the highest level of δ–subunit expression in the brain, and where we found a strong labeling (**Fig. 4.24A,** top). To ensure the specificity of our δ–subunit antibody, the same immunohistochemistry protocol was run on δ-KO mice where no labeling was observed (**Fig. 4.24A,** bottom). In the SNr from wild type animals (**Fig. 4.24**, top), δ-subunit labeling was weaker compared to the *thalamus* but was clearly delineating the membrane of both PV+ (**Fig. 4.24B**, arrowhead) and PV- (**Fig. 4.24B**, arrow) SNr neurons. The δ labeling in the SNr from δ–KO mice was totally absent (**Fig. 4.24B,** bottom).

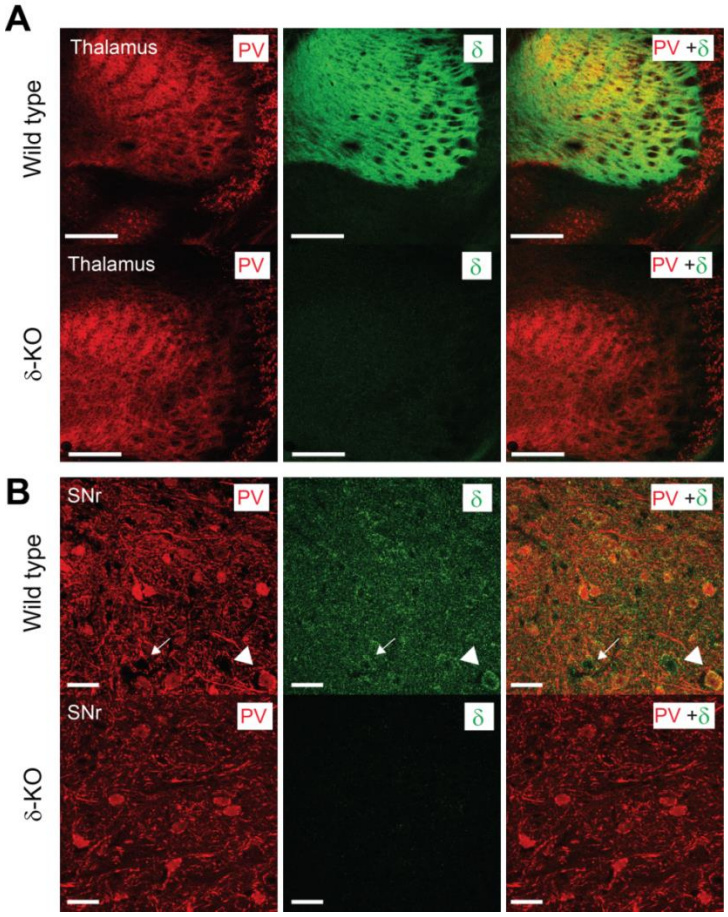

Figure 4.24. $GABA_A$ receptor δ-subunit is expressed in the SNr. A: Coronal sections of the *thalamus* are immunostained for PV (red), delta (green) and overlay. Remark that *thalamus* is the brain area with the highest expression of δ–subunit. Same settings were used for SNr images. Note the lack of staining for δ–subunits in the *thalamus* of $\delta^{-/-}$ mice. **B:** Top, immunostaining for PV, delta and overlay in the SNr from a wild type mouse. Note that both PV+ (arrowhead) and PV- (arrow) SNr neurons express δ–subunit. Bottom, immunostaining in a $\delta^{-/-}$ mouse showing the lack of staining for δ-subunit in the SNr. Scale bars: A, 500 μm; B, 30 μm respectively.

To further elucidate whether δ–$GABA_AR$ subunit was more present in a subtype of SNr neuron than in the other, we looked at the expression of this subunit using the PVcre::Ai9T mouse line to distinguish among PV+ and PV- SNr neurons. We performed immunostaining for PV, δ-subunit and overlay (**Fig. 4.25A-C**), then we did two different

measurements into the SNr of these sham mice (m=2). On the one hand, when analyzing δ-expression in the SNr, as the total of our labelled neurons, we observed that from all cells with δ-subunit expression, 46.5 ± 12.8 % belonged to PV- SNr neurons and 53.5 ± 8.2 % to PV+ cells (**Fig. 4.25D**). On the other hand, when the PV expression was considered as the total of stained neurons, we depicted that only 32.5 ± 10.5 % of PV+ SNr neurons expressed δ-subunit (**Fig. 4.25E**). Because the percentage of PV+ and PV- neurons in the SNr is approximately 50/50, we can estimate that the proportion of PV- neurons expressing δ-subunit is around 30-40%, although NeuN immunostaining would be needed to resolve precisely the percentage of PV- SNr neurons expressing δ-subunit.

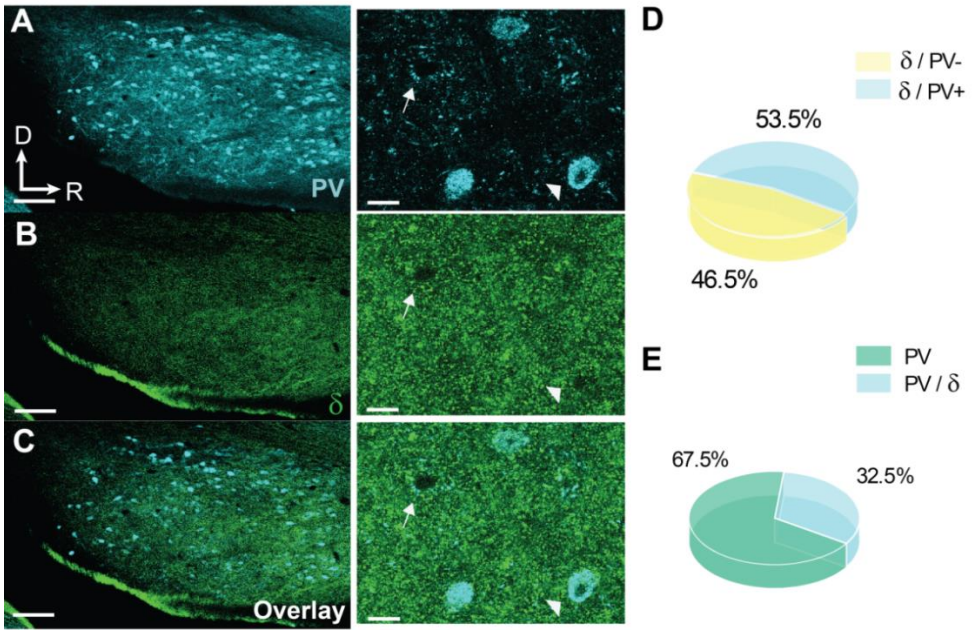

Figure 4.25. Expression profile of GABA$_A$R δ subunit in SNr neurons from PVcre::Ai9T mice. A-C: Micrographs depicting PV (cyan), and δ (green) immunoreactivity in the SNr. On the left, low-magnification images from the SNr of PVcre::Ai9T mouse showing a diffuse δ staining but present in both PV+ (arrowheads) and PV- (arrows) SNr neurons. On the right, high-magnification images showing the co-localization between PV and δ. **D:** Quantification of co-localization to determine the percentage of SNr neurons expressing δ subunit. Note that δ subunit is present equally in both subtypes of SNr neurons. **E:** Quantification of co-localization depicting just the 32.5 % of PV+ SNr neurons expresses δ-subunit. Scale bars: left, 200μm, right, 30 μm.

Here, to determine whether α5-subunit-containing $GABA_A$ receptors were expressed in PV+ and PV- SNr neurons, we performed PV (**Fig. 4.26A**) and α5 (**Fig. 4.26B**) immunohistochemistry using slices from PVcre::Ai9T mice (m=2). Surprisingly, we observed a moderate to strong expression of α5 in the SNr. The overlay of confocal microscopy images was used to estimate the percentages of co-localization between PV and α5 (**Fig. 4.26C**). As we did for the δ-subunit, from the total of α5 positive cells into the SNr the 32.2 ± 11.9% were PV+ cells, while the 67.8 ± 12.1% belonged to PV- SNr neurons (**Fig. 4.26D**). Secondly, we used PV expression as the total of stained SNr neurons and we observed that only the 15.4 ± 13.8 % of PV+ SNr neurons expressed α5-subunit (**Fig. 4.26E**). To obtain the exact percentage of PV- SNr neurons expressing this subunit, NeuN immunostaining would be necessary.

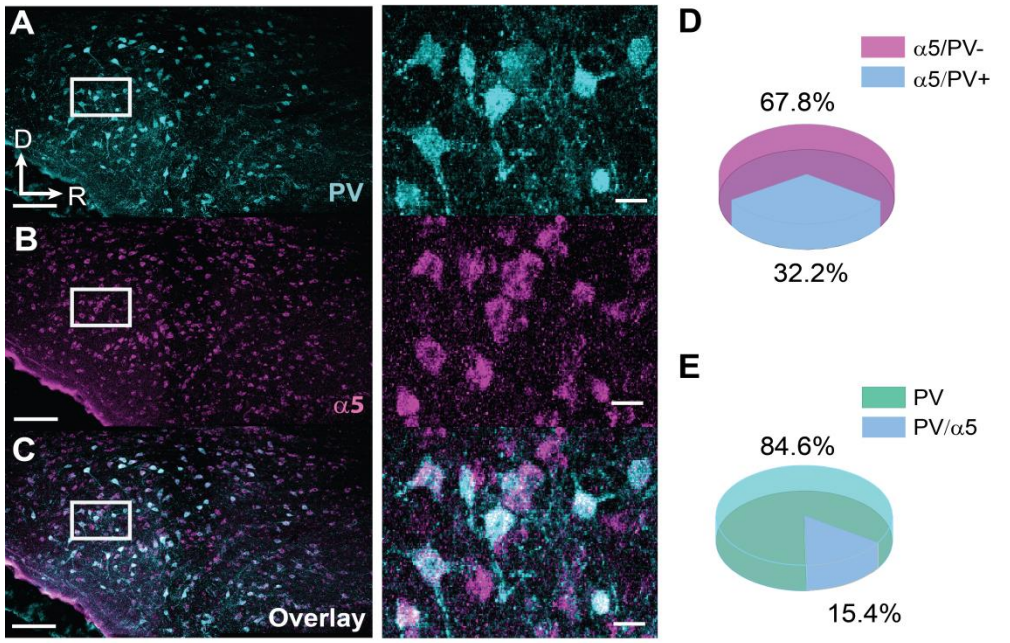

Figure 4.26. Expression profile of $GABA_AR$ α5 subunit in SNr neurons from PVcre::Ai9T mice. A-C: Micrographs depicting PV (cyan) and α5 (magenta) immunoreactivity in the SNr. Left, low-magnification images from the SNr showing strong α5 expression in both PV+ and PV- SNr neurons. On the right, high-magnification images showing the co-localization between PV and α5. **D:** Quantification of co-localization to determine the percentage of SNr neurons expressing α5 subunit. Note that α5 subunit is more present in PV- SNr neurons representing a percentage of 67.8%. **E:** Quantification of co-localization depicting that just the 15.4% of PV+ SNr neurons express α5-subunit. Scale bars: left, 200μm; right, 20μm.

4.3.2. Nigral tonic inhibition is mediated by extrasynaptic $GABA_A$ receptors containing δ and α5-subunits

At the beginning, we wanted to identify whether tonic $GABA_A$ receptor-mediated conductances using PVcre::Ai9T mice to keep differentiating PV+ and PV- SNr subpopulations. We performed whole-cell voltage-clamp recordings from brain sagittal slices. The internal solution of our pipette contained CsCl, QX314 and biocytin and we perfused DNQX (20 µM) and D-AP5 (50 µM) to block glutamatergic transmission. We used the $GABA_AR$ antagonist, GABAzine (SR-95531-20µM) to reveal the presence of tonic inhibition in both subtypes of SNr cells (**Fig. 4.27A-B**) by monitoring a shift in the holding current (consistent with the blockade of extrasynaptic $GABA_A$ channels). SNr neurons were recorded at a holding potential of -64 mV (after JP correction). Under this recording condition, spontaneous IPSC were numerous but their amplitude and frequency were not different between PV+ and PV- SNr neurons (P>0.05 Mann-Whitney U test; **Fig. 4.27D-E**). Application of GABAzine (20µM) produced a complete blockade of spontaneous IPSC, both in PV+ and PV- SNr neurons and induced a significantly bigger shift (ΔI) in the holding current in PV- compared to PV+ SNr neurons (PV+, $mean_{\Delta I}$=6.7 ± 2.5 pA; n=13/m=9; PV-, $mean_{\Delta I}$=25.9 ± 5.3 pA; n=18/ m=9; P=0.002, Mann-Whitney U test; **Fig. 4.27C**). Even if most PV+ cells depicted a discrete tonic current, an small subset of neurons (15.4%) showed a remarkable shift in the holding current.

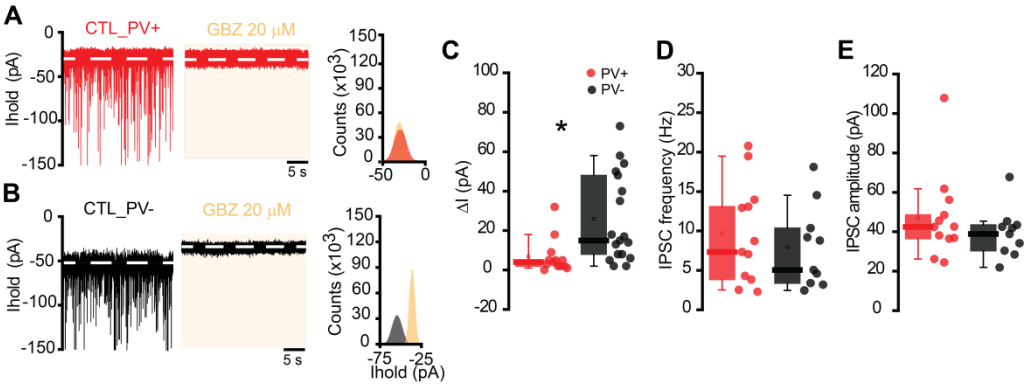

Figure 4.27. $GABA_A$-mediated neurotransmission in SNr neurons from PVcre::Ai9T mice. A-B: Examples of whole-cell voltage-clamp recording of a PV+ (A) and PV- (B) SNr cell before and during the perfusion of GBZ, a selective $GABA_A$ receptor antagonist with the corresponding histogram distributions (A and B). Dashed lines indicate the median currents of all points used to measure shifts in the holding current. **C:** Boxplots depicting the presence of a tonic current only in PV- SNr neurons (PV+, n=13; PV-, n=18). **D-E:** Boxplots showing sIPSC frequency (D) and amplitude (E) in PV+ and PV- SNr neurons. * P<0.05; MW-U test.

Since we detected that tonic inhibition was present in the SNr, mainly in PV- SNr neurons, and our immunohistochemical results showed that both δ and α5-subunits were present in the SNr, we decided to further characterize the subunits responsible for the observed currents in PV- SNr neurons. For that, we combined pharmacological experiments with $\delta^{+/+}$ and $\delta^{-/-}$ mice to test the involvement of this subunit in the extrasynaptic $GABA_A$ receptors present in SNr neurons. We studied the presence/absence of tonic inhibition using whole-cell voltage-clamp recordings from SNr neurons of these $\delta^{+/+}$ (m=2; **Fig. 4.28A**) and $\delta^{-/-}$ (m=2; **Fig. 4.28B**) mice when we perfused 20 μM gabazine. No tonic currents were detectable in δ-/- mice (**Fig. 4.28C**), suggesting that the presence of this subunit is mandatory to have functional extrasynaptic $GABA_A$ receptors in SNr neurons (WT, meanΔI=42.4 ± 15.6 pA, n=7; KO, meanΔI=3 ± 2.5 pA, n=7; P=0.04 Mann-Whitney U test).

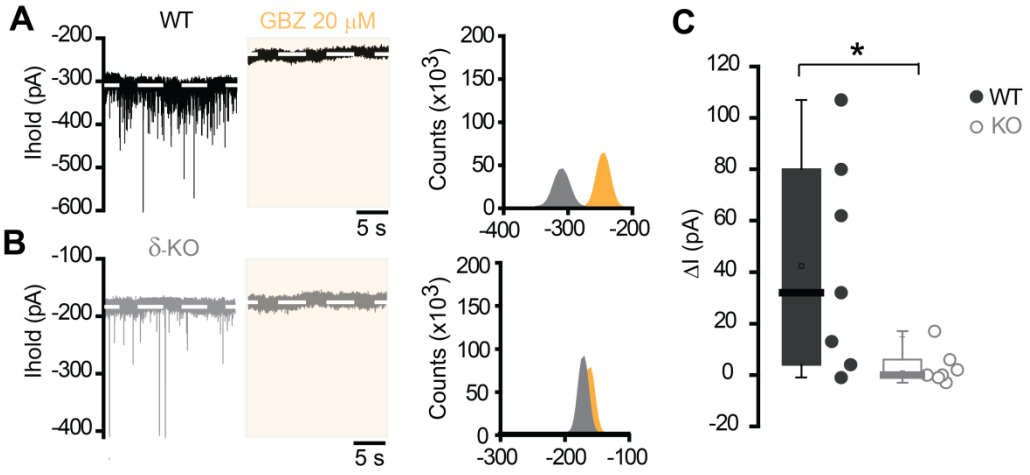

Figure 4.28. Nigral tonic inhibition is mediated by δ–containing extrasynaptic $GABA_A$. A: Whole-cell voltage-clamp recording from a SNr neuron of a wild-type mouse ($\delta^{+/+}$) before and during the perfusion of GBZ. Right, the corresponding all point histogram distribution. **B:** Example of whole-cell recording of a SNr neuron from a knockout ($\delta^{-/-}$) mouse, before and during the perfusion of GBZ with the all-point histogram distribution. **C:** Population graph depicting differences in tonic inhibition between WT (n=7) and δ-KO mice (n=7). Note that δ-subunit containing $GABA_A$ receptor mediates tonic inhibition in the SNr. *P=0.04 MW-U test.

Later, we carried out electrophysiological recordings in PVcre::Ai9T mice to elucidate if δ–subunit containing $GABA_A$ receptors were mediating more tonic inhibition in a subtype of SNr neuron rather than in the other one as we observed staining in both PV+ (**Fig. 4.29A**) and PV- (**Fig. 4.29B**) cells. For this reason, we decided to use the $GABA_A$ agonist, THIP (4,5,6,7-tetrahydoisoxazolo [5,4-c] pyridin-3(2H)-one), a "super-agonist" of $GABA_A$-receptors with preference for δ-subunit (Drasbek et al., 2007; Meera et al., 2011). As it is known that THIP is a useful selective agonist for activation of the tonic current, we performed whole-cell voltage clamp recordings in PV+ and PV- SNr neurons. For that, once our holding current was stabilized, we perfused 1μM of THIP and observed a tiny shift in PV+ SNr neurons ($mean_{\Delta I}$= -8.6 ± 2.7 pA, n=3/m=3) but a much more pronounced effect in PV- SNr neurons ($mean_{\Delta I}$= -28.4 ± 8 pA, n=7/m=3); (**Fig. 4.29C-D, left**). Nevertheless, more patch-clamp recordings will be needed to conclude that δ-containing $GABA_A$ receptor mediates tonic inhibition only in PV- SNr neurons (**Fig. 4.29E**). We also tested the impact of blocking $GABA_A$ receptors (20μm of GBZ) in the holding current after activation of δ-subunits in PV+ and PV- SNr neurons (**Fig. 4.29C-D, right**). We observed an increase in holding current after perfusion of GBZ in both sub-types of SNr neurons (**Fig. 4.29F**; P>0.05 Mann-Whitney U test). From this experiment, it can be concluded that δ-subunit is partially mediating tonic inhibition in PV- SNr neurons while in PV+ cells; it is not contributing to tonic inhibition.

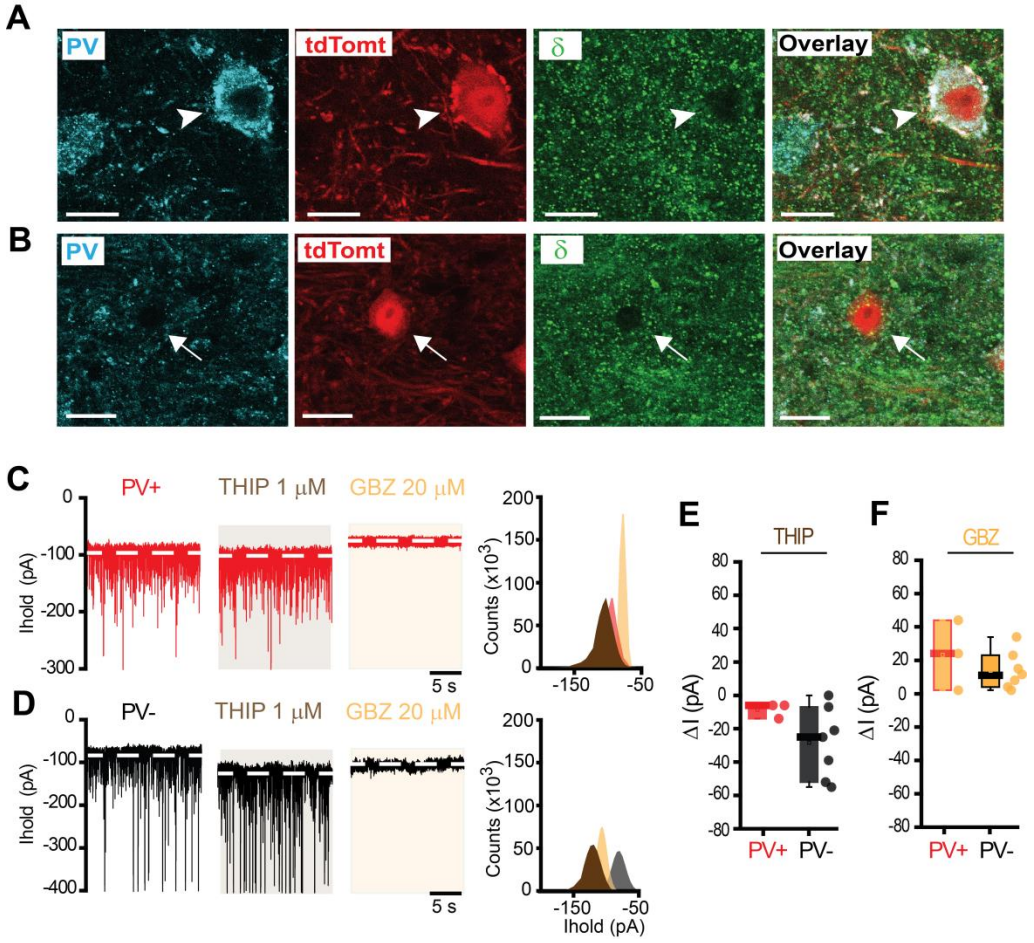

Figure 4.29. Extrasynaptic $GABA_A$ receptors of PV+ and PV- SNr neurons contain δ-subunits in DA-intact mice. A: Representative confocal microscopy images from the SNr of a PVcre::Ai9T transgenic mouse. Immunostaining for PV (cyan), tdTomato (red) and δ–subunit (green) and overlay displaying a PV and tdTomato positive (arrowheads) SNr neuron. Note that δ–subunit staining is surrounding the PV+ neuron. **B:** High-magnification images of the SNr depicting a PV negative neuron (arrows) which expresses tdTomato and δ-subunit. **C-D:** Examples of whole-cell voltage-clamp recordings of a PV+ (red) and PV- (black) SNr neurons from control mice, before and during the perfusion of 1 μM THIP, a selective $GABA_A$-receptor agonist with preference for δ-subunit. Then GBZ was perfused. Note a decreased on holding current during the perfusion of δ-agonist for PV negative SNr neuron with the following shift when 20 μM of GBZ is perfused. Right, the corresponding all point histogram distributions (C-D). **E:** Population graphs depicting the effect of the THIP on PV+ (n=3) and PV- (n=7) SNr neurons. **F:** Box plot graphs depicting the effect of the GBZ after activation of δ-subunit for the neurons represented in E. Scale bars: 10 μm.

Similarly, after demonstrating that α5-subunit was expressed in both PV+ (**Fig. 4.30A**) and PV- (**Fig. 4.30B**) SNr neurons, we tested the contribution of α5 subunit containing $GABA_A$ receptors in nigral tonic inhibition using the α5 inverse agonist L-655,708. Electrophysiological *in vitro* experiments were performed in sagittal brain slices from reported mice (m=8). Whole-cell voltage clamp recordings from PV+ and PV- SNr neurons during the perfusion of 1 μM of L655,708 depicted differences in holding current on PV+ and PV- SNr neurons (**Fig. 4.30C-D, left**). The magnitude of α5-induced currents was significantly smaller in PV+ compared to PV- SNr neurons in control mice (**Fig. 4.30E**; PV+, $mean_{\Delta I}$=0.5 ± 0.9 pA, n=17; PV-, $mean_{\Delta I}$=7.7 ± 1.8 pA, n=14; p=0.002 Mann-Whitney U test). This result suggests that nigral tonic inhibition present in PV- SNr neurons might be mediated by α5-containing $GABA_A$ receptors.

We also tested whether α5-subunit was the only responsible for the tonic inhibition in the SNr. For that, subsequently to L-655,708, we blocked $GABA_A$ receptors (20μm of GBZ) and observed that the magnitude of tonic current was similar in PV+ and PV- SNr neurons (P>0.05 Mann-Whitney U test; **Fig. 4.30F**). This lack of GABAzine effect in holding current suggests that the observed tonic inhibition of PV- SNr neurons was mediated by α5-subunit present in this cell type, however no tonic inhibition mediated by α5 was observed in PV+ SNr neurons.

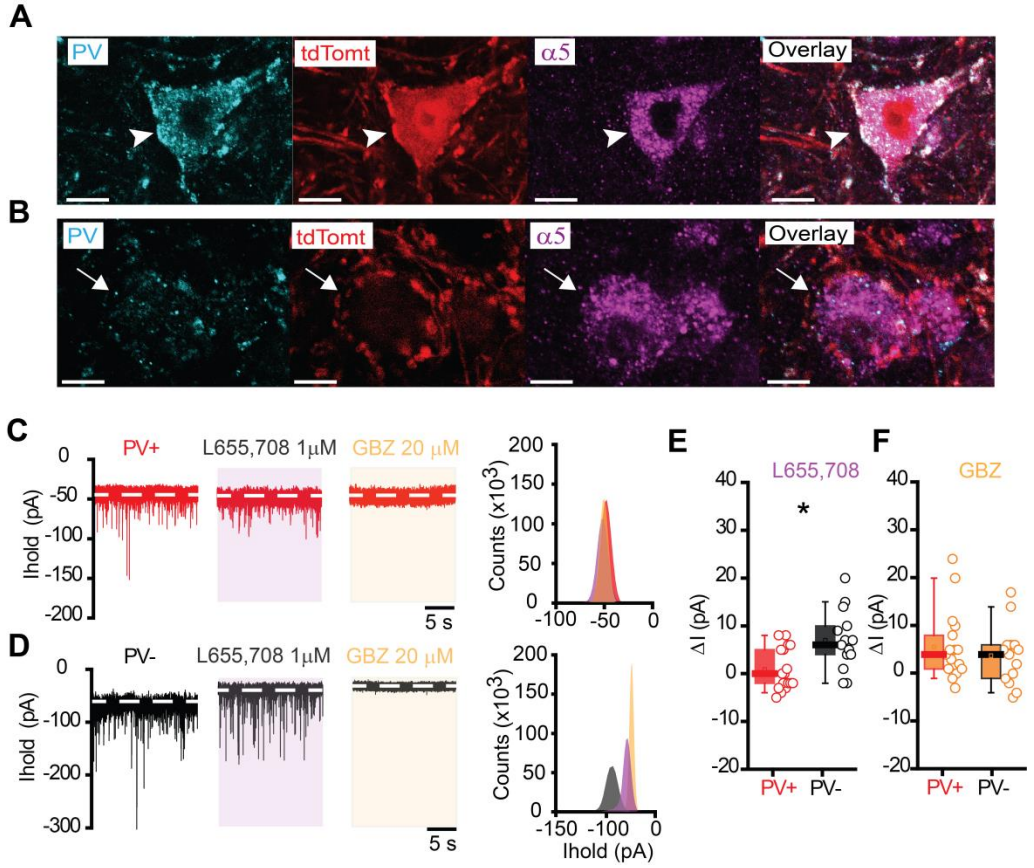

Figure 4.30. Nigral tonic inhibition is mediated by α5-containing extrasynaptic $GABA_A$ receptors in PV- SNr neurons. A: Confocal microscopy images from the SNr of a PVcre::Ai9T transgenic mouse. Immunostaining for PV (cyan), tdTomato (red) and α5-subunit (magenta) and overlay displaying a PV and tdTomato+ (arrowheads) SNr neuron. Note that α5-subunit staining defines the cytoplasm of PV+ neurons. **B:** High-magnification images of the SNr depicting a PV negative neuron (arrows) which expresses tdTomato and α5-subunit. **C-D:** Representative traces of a PV+ (red) and PV- (black) SNr neurons from control mice showing that 1 μM of L-655,708, an inverse agonist of a5-containing containing $GABA_A$, produces a shift in the holding current just on PV negative SNr neurons. Then GBZ was perfused and we observed in almost all cases a shift, meaning that tonic inhibition is not just mediated by α5-subunit containing $GABA_A$ receptors. Right, the corresponding all point histogram distributions. **E:** Population graphs depicting the effect of L-655,708 and GBZ on PV+ (n=17) and PV- (n=14) SNr neurons. Note a significant increase on holding current in PV- SNr neurons suggesting that tonic inhibition is mediated by α5-containing extrasynaptic $GABA_A$ receptors in PV- SNr neurons ($p<0.001$; MW-U test). Scale bar: 10 μm.

4.3.3. Impact of dopamine depletion in nigral tonic inhibition

It is known that basal levels of glutamate and GABA in the GP and SNr are significantly higher in hemiparkinsonian than in intact rats (Windels et al., 2005). For this reason, we decided to investigate whether GABAergic extrasynaptic transmission was altered in PV+ or/and PV- SNr neurons after unilateral 6-OHDA lesion (**Fig. 4.31A and C**). As performed for PVcre::Ai9T control mice, we analyzed the effect of GABAzine (20µM) on the holding current from both subtypes of SNr neurons in 6-OHDA lesioned mice (m=6). Tonic inhibition in control and DD conditions was similar (**Fig. 4.31B**; P>0.05 Mann-Whitney U test), showing prominent tonic current in most PV- cells but only in few PV+ cells (25%). In PV- cells, DA depletion did not modify the magnitude of the shift in holding current compared to DA-intact conditions (sham, n= 18; mean$_{\Delta I}$= 25.9 ± 5.3 pA; 6-OHDA, n=10; mean$_{\Delta I}$= 26.5 ± 9.3 pA; P>0.05, Mann-Whitney U test), meaning that tonic inhibition is still present in this subpopulation (**Fig. 4.31D**) but is not augmented after the 6-OHDA lesion.

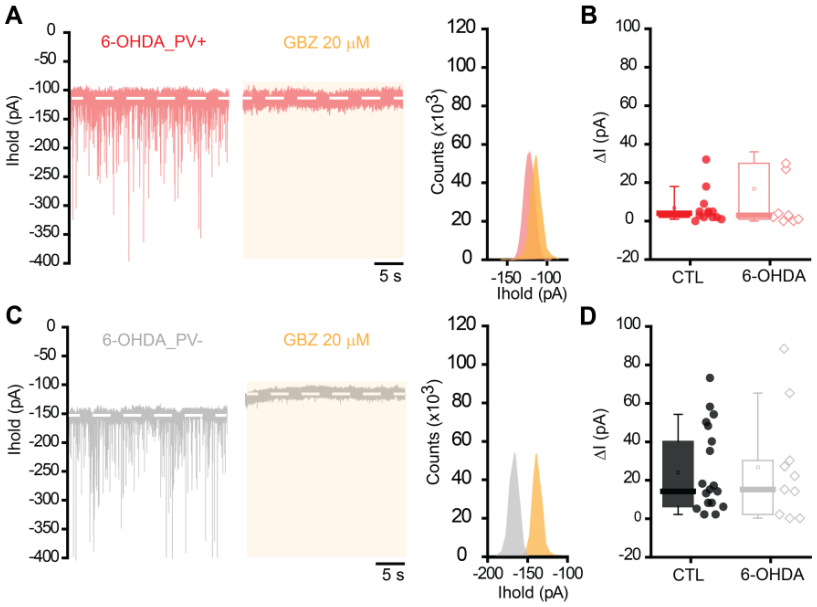

Figure 4.31. Impact of 6-OHDA lesion on GABA$_A$-mediated extrasynaptic transmission in SNr neurons from PVcre::Ai9T mice. A: Whole-cell voltage-clamp recording from a PV+ SNr neuron after DA depletion, before and during the perfusion of GBZ. Right, corresponding histogram distributions. **B:** Population data depicting the amplitude of tonic inhibition for PV+ SNr neurons from control (n=13) and 6-OHDA (n=8) mice. **C:** Example traces from a PV- SNr neuron after 6-OHDA lesion, before and during the perfusion of GBZ. Right, corresponding histogram distributions. **D:** Same as B for PV – SNr (control, n= 18 and 6-OHDA, n=10). Note that tonic inhibition is still present after DA depletion.

Later, we wanted to investigate whether the functioning of δ and/or α5-subunits was affected by DA loss. We first performed triple-labeling techniques from coronal sections to investigate the distribution of δ-subunits in SNr neurons after DA depletion (**Fig. 4.32A**). Subsequently, after proving that δ-subunits were still present in both PV+ and PV- SNr neurons, we characterized the change in holding current (ΔI) produced by THIP in PV+ and PV- from DA depleted mice (**Fig. 4.32B and E, left**). Although it was not statistically significant, it seemed that THIP-induced currents were higher for PV+ cells after DA depletion (control, mean$_{\Delta I}$=8.6 ± 2.6 pA, n=3; 6-OHDA, mean$_{\Delta I}$=32 ± 3 pA, n=2/m=1; P>0.05 Mann Whitney U test, **Fig. 4.32C**). For confirming this effect, a higher number of neurons should be recorded in each condition. The effect that THIP induced in holding current of PV- after 6-OHDA lesion was similar to control values (control, mean$_{\Delta I}$ =28.4 ± 8 pA, n=7; 6-OHDA, mean$_{\Delta I}$=25 ± 2 pA, n=3; P>0.05 Mann Whitney U test; **Fig. 4.32F**). Subsequent to THIP administration, we studied the effect of GABAzine on the holding current in PV+ and PV- SNr neurons (**Fig. 4.32B-E, right**). In this condition, we still perceived an increase in holding current for both sub-types of SNr neurons and conditions (P>0.05 Mann-Whitney U test, **Fig. 4.32D-G**) suggesting the existence of other subunits mediating tonic currents.

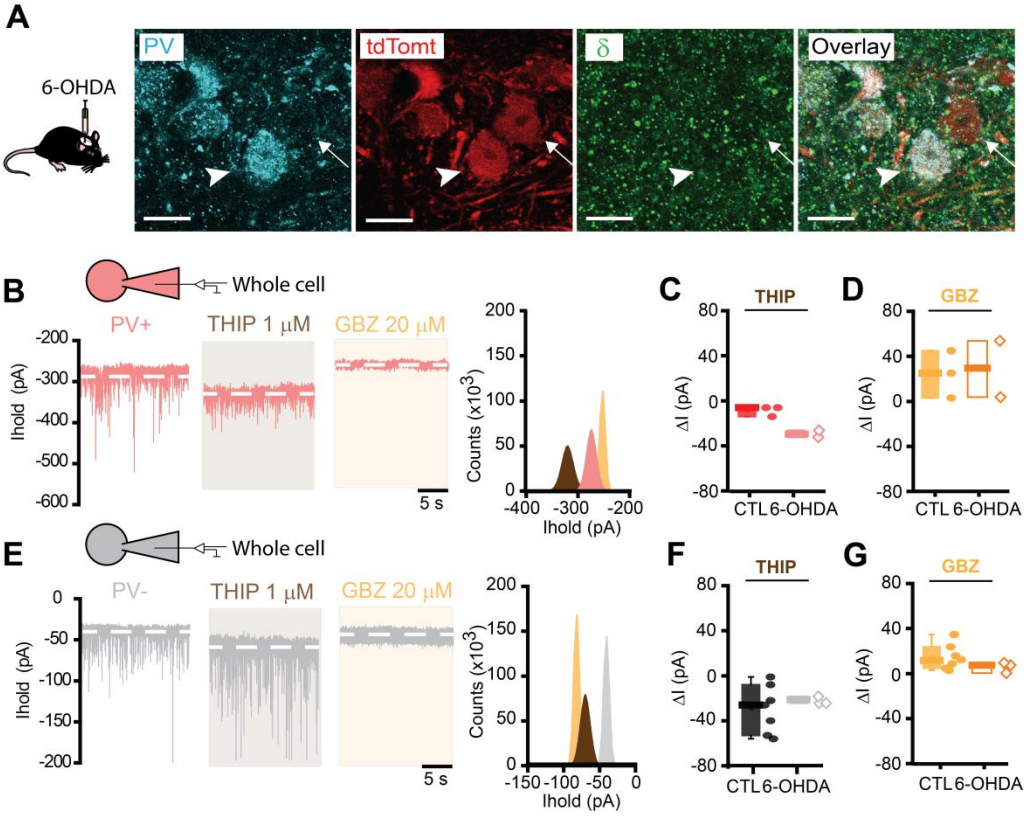

Figure 4.32. Extrasynaptic $GABA_A$ receptors of PV+ and PV- SNr neurons express δ-subunits in DA depleted mice. A: Representative confocal microscopy images from the SNr of a PVcre::Ai9T transgenic mouse. Immunostaining for PV (cyan), tdTomato (red), δ-subunit (green) and overlay displaying a PV+ (arrowheads) and a PV- (arrows) SNr neurons. Note that the staining for δ-subunit is diffuse. **B:** Example of the effect of 1 μM THIP and 20 μM GBZ on the holding current of one PV+ (pink) SNr neuron recorded in a 6-OHDA mouse. Shifts in holding currents are represented by dashed lines in the electrophysiological recordings and by Gaussian fits in all-points histograms (right). **C-D:** Box plots depicting the effect of THIP and GBZ on PV+ cells in control (n=3) and 6-OHDA mice (n=2). **E:** Example of a PV- (gray) SNr neuron recorded from 6-OHDA mice showing the effect of 1 μM THIP and 20 μM GBZ on the holding current. **F-G:** Boxplots representing the effect of THIP and GBZ on PV- SNr neurons in control (n=8) and 6-OHDA mice (n=3). Scale bar: 10 μm.

As previously performed for δ-subunits, we tested if PV+ and PV- SNr neurons were still expressing α5-subunit in 6-OHDA unilaterally lesioned mice. Although, quantification of the subunit expression would be needed to better estimate if α5 subunits were over-expressed in the SNr after DA depletion, we observed that after DA loss there was still expression (**Fig. 4.33A**). In addition, we characterized the change in holding current provoked by L-655,708 perfusion in PV+ and PV- SNr neurons from DA depleted mice (m= 7; **Fig. 4.33B and E, left**). For PV+ SNr neurons we did not depict changes after the 6-OHDA lesion (**Fig. 4.33C**), nevertheless significant differences were reported for PV- cells after DA depletion (control, mean$_{\Delta I}$=7.7 ± 1.8 pA, n=14; 6-OHDA, mean$_{\Delta I}$= 2.1 ± 2.6 pA, n= 10; P= 0.04 Mann Whitney U test, **Fig. 4.33F**). In the same way, when we studied the effect of GABAzine perfusion subsequent to L-655,708 (**Fig. 4.33B-E, right**) we perceived interesting results. We observed that after DA loss, the effect of the α-5 subunit mediating currents was smaller than in control conditions (in PV- cells) and that subsequent application of GBZ further changed the holding current only in the DA depleted mice (**Fig. 4.33G**; control, mean$_{\Delta I}$= 3 ± 1.3 pA; 6-OHDA, mean$_{\Delta I}$= 11.2 ± 3 pA; P= 0.0021 Mann-Whitney U test). These results suggest that after DA depletion α5-subunit might not mediate anymore tonic inhibition in PV- SNr neurons and that other subunits could be supporting these currents.

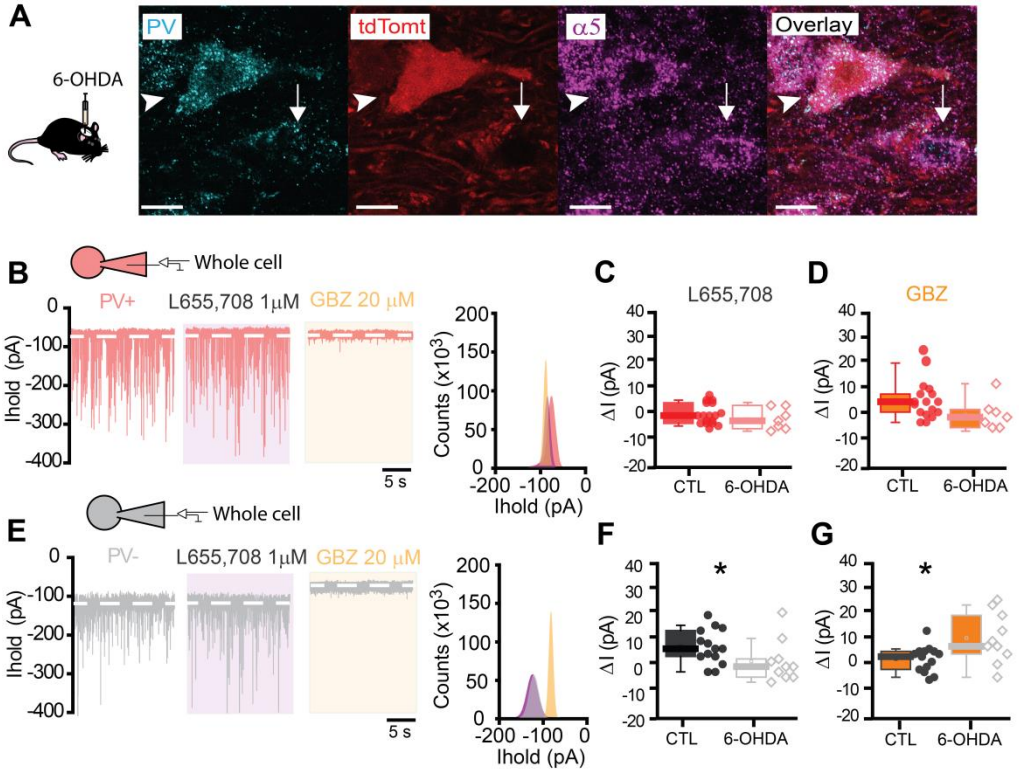

Figure 4.33. Presence of α5-subunit in $GABA_A$ receptors of PV+ and PV- SNr neurons in DA-depleted mice. A: Representative confocal microscopy images from the SNr of a PVcre::Ai9T mouse. Immunostaining for PV (cyan), tdTomato (red) and α5-subunit (magenta) and overlay displaying a PV+ (arrowheads) and a PV negative (arrows) SNr neurons. **B:** Examples of the lack of effect of 1 μM L655,708 and 20 μM GBZ on the holding current of PV+ (pink) SNr neuron recorded from a DA depleted mouse. Right, the corresponding all point histogram distributions. **C-D:** Box plots depicting the effect of L-655,708 and GBZ on PV+ neurons in control (n=17) and in 6-OHDA (n=7) mice. **E:** Example of a PV- (gray) SNr neuron recorded from 6-OHDA mice showing the lack of effect of 1 μM L655,708 and the shift in holding current after 20 μM GBZ. **F-G:** Boxplots representing the effect of the THIP and GBZ on PV- SNr neurons in control (n=14) and 6-OHDA mice (n=10). Highlight a loss of effect for L655,708 after DD (P= 0.04 MW-U test) and a significant increase on holding current after GBZ perfusion (P= 0.0021 MW-U test). Scale bar: 10 μm.

Altogether, this study provides not only the first indication of extrasynaptic $GABA_ARs$ containing α5 subunits in SNr neurons, but also reveal differences in tonic inhibition among PV+ and PV- SNr neurons, confirming once again, the importance of subdividing the SNr into two subpopulations of cells. While PV- SNr neurons, displayed higher tonic currents and expressed higher levels of α5 subunit, the neighboring PV+ SNr neurons showed smaller currents and less expression of this subunit. However, DA depletion did not trigger an increase in tonic inhibition.

5. DISCUSSION

5.1. STUDY I. Intrinsic properties of substantia nigra pars reticulata neurons regarding the expression of Parvalbumin in sham, parkinsonian and dyskinetic mice.

Here, by using a transgenic PVcre::Ai9T mouse line, we have demonstrated that PV+ and PV- SNr neurons are unique in their molecular content, spatial distribution, intrinsic properties and sensitivity to DA depletion and subsequent L-DOPA chronic treatment. For this reason, these two subpopulations should be considered as distinct functional neuron classes. These results converge to support the importance of differentiating distinct cell-types for a better understanding of BG function in normal and disease states.

5.1.1. Molecular evidence for distinct SNr neuron classes

The cellular complexity of the SNr has been a long-standing question. Our analyses afford new insights addressing molecular diversity of SNr cells. Until present, the SNr has been considered a homogeneous nucleus conformed mainly of GABAergic neurons expressing glutamic acid decarboxylase (GAD) and the calcium binding protein PV (Reiner and Anderson, 1993; Rajakumar et al., 1994; González-Hernández and Rodríguez, 2000). However, the presence of glutamatergic neurons expressing VGluT2 in the SNr has also been described (Antal et al., 2014). The evidence demonstrating the existence of several SNr cells subtypes is emerging, overall looking at their distinct projections (Rizzi and Tan, 2019; Liu et al., 2020) Regarding this heterogeneity, transcriptomic studies have revealed up to six clusters of SNr cells subdivided by their neurotransmitter markers (mainly GAD2 for GABAergic neurons and slc17a6 for glutamatergic neurons), current GP markers (PV, Zfpm2 and Foxp1) and novel markers such as *Sema3a, Adarb2, Pax5* or *Pou6f2* among others (Saunders et al., 2018). From this study it is worth mentioning that apart from the novel markers defining SNr subpopulations, they found mainly 4 subtypes of SNr cells which can be grouped into $GAD2^{+}/PV^{-}$, $GAD2^{-}$/slc17a6/PV^{-} (vGluT2), $GAD2^{-}/PV^{+}$ and $GAD2^{-}/PV^{-}$ cells. Other recent publication has depicted that PV and GAD2 are expressed in separate SNr GABAergic populations (Liu et al., 2020). In agreement with these authors, we also

found distinct populations of SNr neurons using PVcre::Ai9T reporter mice. While 46% of the total number of SNr neurons was tdTomato+ cells, nearly 50% were tdTomato- cells, meaning that approximately half of the population expresses PV. It should be pointed out the fact that PV expression is lower in mice than in other species such as rats or primates (Mastro et al., 2014; Abrahao and Lovinger, 2018). Similarly consistent with previous studies (Grace and Onn, 1989; González-Hernández and Rodríguez, 2000; Tepper and Lee, 2007a) we observed scattered groups of dopaminergic neurons within the SNr representing the 5% of total cells in this nucleus.

We also determined the fidelity of cre recombination in PVcre::Ai9T transgenic mice using PV immunohistochemistry and we obtained similar results than other labs (Saunders et al., 2016) with ~77% of cells coexpressing tdTomato/PV in DA-intact and DA-depleted mouse brains. Additionally, it is noteworthy that some tdTomato+ SNr neurons were indeed PV- which could explain some variability observed in our electrophysiological experiments. Our definition of PV+ and PV- expression has particular relevance for understanding the ontogeny of SNr neurons. Besides, our results addressing the topographical distribution of SNr neurons are in concordance with a recent publication (Liu et al., 2020). We observed that PV+ neurons are predominantly located in the lateral SNr, while PV- neurons occupy more medial regions of the nucleus. Moreover, the finding that neurons in the lateral SNr are involved in sensorimotor functions whereas those in the medial SNr are more related to associative functions (Rajakumar et al., 1994; Deniau et al., 1996), allows us to think that probably PV+ and PV- SNr neurons have different physiological or pathological implications. In this sense, PV- but not PV+ cells, have been recently demonstrated to play an specific role in epilepsy (Wicker et al., 2019; Chen et al., 2020).

5.1.2. PV+ and PV- SNr neurons have different intrinsic electrophysiological properties

The electrophysiological properties of SNr neurons have been described both *in vivo* (Sanderson et al., 1986; Gulley et al., 1999; Deransart et al., 2003; Maurice et

al., 2003; Windels and Kiyatkin, 2006a; Sano et al., 2013) and in slice preparations (Wilson et al., 1977; Deniau et al., 1978; Nakanishi et al., 1987; Atherton and Bevan, 2005; Connelly et al., 2010; Seutin and Engel, 2010; Zhou and Lee, 2011; Lutas et al., 2014; Zhou, 2016; Faynveitz et al., 2019) but a rigorous classification scheme has not been yet established. Here, we provide the first working definitions of the *in vitro* intrinsic properties of PV+ and PV- SNr neurons in the DA-intact mouse brain. It is extensively described in the literature that SNr GABA neurons *in vitro* fire spontaneously around 10-20 Hz (Richards et al., 1997; Tepper and Lee, 2007b; Ding et al., 2011a, 2011b). However, our recordings of identified PV+ and PV- GABA SNr neurons provide additional information; whereas PV+ neurons fire at high rates (~20 Hz), PV- neurons fire at markedly lower rates (~10 Hz). The spontaneous activity of these two subtypes of SNr neurons, seems not be affected by the blockade of fast synaptic transmission (D-AP5, DNQX and Picrotoxin), meaning that intrinsic cell properties are responsible for the spontaneous discharge. This feature is consistent with previous results performed in rat SNr neurons *in vitro* (Atherton and Bevan, 2005; Sierra et al., 2015). Electrophysiological experiments performed in the mouse GP, where similar subpopulation distribution is observed, concluded that PV expression confers the ability to fire at higher frequencies than when this protein is lacking (Mastro et al., 2014; Abdi et al., 2015; Hernández et al., 2015; Saunders et al., 2016; Abrahao and Lovinger, 2018). However, we suggest that not only the expression of PV, but also distinct ion channels present on the membrane of these SNr neurons (such as the TRPC3 or NACLN, described below) could be responsible of the observed differences in their pacemaking.

Our patch-clamp recordings from PV+ and PV- SNr neurons revealed differences in several AP parameters. We observed that PV+ cells present a relatively depolarized APth (around -35 mV) whereas PV- cells are noticeably more hyperpolarized (around -45 mV). These results suggest that probably these two populations of SNr neurons exhibit distinct ion channels responsible of cell depolarization. In the literature a persistent sodium current (I_{NaP}), TRPC3 and NALCN channels have been observed in SNr neurons and seem to be in charge of depolarizing these neurons (Atherton and Bevan, 2005; Zhou et al., 2006, 2008; Seutin and Engel, 2010; Lutas et al., 2016). Atherton and Bevan evidenced by blocking sodium channels with TTX that I_{NaP} contributes to depolarize SNr GABA neurons, but these channels are not sufficient to sustain the considerably depolarized membrane potential of these neurons, shown in rats to be around -50 mV (Atherton and Bevan, 2005; Zhou et al.,

2006). Additionally, TRPC3 channels have been shown to contribute to tonically depolarize SNr neurons toward their APth (Zhou et al., 2008). All these findings lead to hypothesize that PV+ cells in the SNr may exhibit higher levels of I_{NaP} and TRPC3 channels than PV- neurons or that they are just tonically more active in these neurons. The participation of TRPC3 channels in the pacemaking of SNr neurons have, however, been questioned by some authors that demonstrated that genetic deletion of these channels did not affect their spontaneous firing activity (Lutas et al., 2014). Additionally, the activity of NALCN is strongly dependent upon glycolysis and alterations in this metabolic pathway cannot only impair autonomous pacemaking in SNr neurons, but also regulate SNr neuron excitability (Lutas et al., 2014, 2016). In this way, we suggest that PV- SNr neurons might express lower levels of NALCN or maybe that their functionality is different in this subpopulation of SNr neurons. Interestingly hippocampal neurons from NALCN knockout mice show significantly hyperpolarized membrane potentials (Lu et al., 2007), which points out the key function of NALCN in maintaining depolarized membrane potentials, as we have observed for PV+ SNr neurons. In addition to TRPC3 and NALCN channels, SNr GABA neurons have revealed to present high density of transient voltage-gated sodium current (I_{NaT}) contributing to high frequency firing (Ding et al., 2011b; Seutin and Engel, 2010). Indeed, once depolarization subthreshold is reached by I_{NaP} and TRPC3 channels, at or slightly below −50 mV, I_{NaT} is activated, triggering the regenerative fast rising phase of the AP (Bean, 2007; Zhou and Lee, 2011). These findings, together with the fact that PV+ cells in the SNr fire at relatively higher frequency than PV- neurons, suggest that the density or kinetics of I_{NaT} among these two SNr neuron types could be different, expecting higher density of I_{NaT} on PV+ neurons.

Specific techniques will be needed to further elucidate which ion channels are responsible of the distinct APth and firing properties shown among PV+ and PV- SNr neurons. Single-cell RT-PCR looking at the expression of Na_V, TRPC3 and NALCN could be useful to detect differences between PV+ and PV- cells. Additionally, electrophysiological strategies such as the use of the Na_V channel blocker TTX and Na replacement can be useful to study I_{NaP} (Atherton and Bevan, 2005). The steeper voltage-dependent I_{NaT} activation, could contribute to further elucidate whether increasing depolarization triggers different kinetics of I_{NaT} conductance in both subtypes of SNr neurons (Ding et al., 2011b). The blockade of TRPC3 channels by bath-application of flufenamic acid or intracellular TRPC3 antibody (Zhou et al., 2008) would also address their functionality into PV+ and/or PV- cells. Finally, for studying the

expression of nonselective cation channel NALCN in both subtypes of SNr cells, the use of the trivalent cation gadolinium (Gd^{3+}) to block these channels could help to further elucidate their contribution (Lu et al., 2007).

Considering our results, another AP parameter such as the AHP peak, also showed marked differences between PV+ and PV- SNr neurons, being a few mV more negative in PV- cells. This result could be explained by changes on calcium-activated potassium SK channels which have been shown to be responsible for the AHP peak and thus play an important role in the maintenance of the frequency and precision of single-spike firing in SNr GABA neurons, as already described for GP and STN neurons (Wilson et al., 2004; Ramanathan et al., 2008; Deister et al., 2009). It may happen that, the distribution, expression or functionality of SK channels was minor in PV- neurons of the SNr explaining that these cells fire at lower rates than PV+ cells. The blockade of SK channels in PV+ and PV- neurons can be tested by using apamin. In the SNr, the effects of this blockade, thought to be coupled to the entry of Ca^{2+} ions into SNr neurons through Cav2.2 channels, cause activation of K_{Ca} channels and reduce the frequency of firing of SNr neurons by reducing the single spike AHP (Atherton and Bevan, 2005).

The rising phase of the AP triggers the activation of voltage-activated K^+ (Kv) channels which are important for controlling spike frequency and duration (Bean, 2007). In mammalian brain, four Kv channels families (Kv1–Kv4) and multiple subtypes have been described (see review, Zhou and Lee, 2011). As a result of their fast activation and slow inactivation kinetics, Kv3 channels have been associated to fast-spiking SNr GABA neurons whereas slow-spiking nigral DA neurons express more kv4 mRNA. However in these studies they considered the SNr as a homogeneous nucleus containing mainly GABA neurons (Ding et al., 2011a). Our results did not show differences in AP waveforms or magnitude between PV+ and PV- SNr, suggesting that probably other channel or protein content is more relevant for observed changes in firing rate.

Our electrophysiological recordings also shown that both PV+ and PV- SNr neurons displayed moderate I_h-induced sag in response to hyperpolarizing current injection, which is mediated by HCN channels (Biel et al., 2009). These results are in agreement with previous studies showing that SNr GABA neurons recorded *in vitro* exhibit small I_h-sag and that HCN channels poorly contributes to the generation of spontaneous activity in control conditions (Atherton and Bevan, 2005; Zhou et al., 2006, 2008; Tepper and Lee, 2007a; Ding et al., 2011b). For this reason, our results sustain

not only that both subtypes of SNr neurons are GABAergic neurons in the SNr, but also assume that the subunit composition, density, and/or distribution of HCN channels along the somatodendritic membranes of PV+ and PV- SNr cells is similar. In other brain regions such as hippocampal interneurons (Maccaferri and McBain, 1996), striatal cholinergic interneurons (Bennett et al., 2000) and neurons in the external GPe (Chan et al., 2004), I_h considerably contributes to the generation of spontaneous activity.

In addition to all described differences in the studied parameters, we observed that PV- neurons in the SNr were slightly (not significant) more responsive to current injection (i.e. excitatory inputs) based on the F-I curves. This result is supported by the calculated firing gain revealing a better capacity of PV- cells to fire high frequency spikes. These differences could be related to the amount of expression of Ca_V channels among PV+ and PV- neurons, suggesting a greater expression in PV- cells. The presence of Ca_V channels among the membrane of SNr neurons and their influence in the excitability of these neurons have been widely described (Atherton and Bevan, 2005; Yanovsky et al., 2005). The entry of calcium through N-type calcium channels ($Ca_V2.2$) activates K_{Ca} channels that in turn decrease the firing rate and increase the regularity of firing in SNr GABA neurons which could explain indeed the lower firing rate observed in PV- neurons. The blockade of $Ca_V2.2$ channels with ω-conotoxin GVIA could be useful to test their contribution.

We conclude that PV expression together with probably distinct ion channel content, as Na_V, TRPC3, NALCN, $Ca_V2.2$, could be responsible for the different electrophysiological characteristics of PV+ and PV+ SNr neurons. These cells show different neurochemical, topographical and electrophysiological profiles which thereby, can influence their susceptibility in BG disorders as PD and/or L-DOPA induced dyskinesias.

5.1.3. Divergent effect of DA loss and L-DOPA treatment on the excitability of PV+ and PV- SNr neurons

In our experimental conditions, the 6-OHDA lesion and subsequent L-DOPA treatment induced major changes in PV+ than in PV- SNr neurons. Our results mainly showed a marked reduction in the firing rate of PV+ cells from DA-depleted and dyskinetic mice. Indeed, the excitability of PV+ SNr neurons was affected by DA loss

and only partially rescued by L-DOPA treatment in dyskinetic mice (F-I curves). Concerning PV- cells, no changes on spontaneous firing properties were detected after DA loss or L-DOPA treatment. However, we observed that the responsiveness to current injection of these neurons was reduced in DA-depleted conditions and then rescued by L-DOPA treatment (F-I curves), suggesting subtle alterations in voltage-gated ion channels.

In the literature, some authors have described a burst firing pattern in GABAergic neurons in the SNr of anaesthetized 6-OHDA lesioned rats (Burbaud et al., 1995; Murer et al., 1997; Rohlfs et al., 1997; Lee et al., 2001; Rodríguez Díaz et al., 2003; Wang et al., 2010; Seeger-Armbruster and Von Ameln-Mayerhofer, 2013; Lobb and Jaeger, 2015; Aristieta et al., 2016) primates (Wichmann and Soares, 2006), awake mice (Willard et al., 2019) and in slice preparations obtained from rats following the application of D1 and D2 antagonists to block STR-SNr and GP-SNr inputs (Ibáñez-Sandoval et al., 2007; Aceves et al., 2011a). These authors also observed that STN-SNr inputs contributed to this burst firing and the blockade of these glutamatergic transmission returned SNr neurons to a tonic firing pattern. In line with this and in agreement with other authors (Faynveitz et al., 2019) we did not encounter bursting activity neither in PV+ nor in PV- SNr neurons probably due to different recording conditions during our electrophysiological experiments.

The reduction in firing rate observed in PV+ SNr neurons after the 6-OHDA lesion agrees with other studies performed in anesthetized rats (MacLeod et al., 1990; Murer et al., 1997; Rohlfs et al., 1997; Delaville et al., 2012), awake mice (Sano and Nambu, 2019) as well as *in vitro* recordings from rats (Faynveitz et al., 2019). By contrast, other authors evidenced an increase in firing rate (Burbaud et al., 1995; Breit et al., 2008) or even no changes (Tai et al., 2003; Aristieta et al., 2016) after the 6-OHDA lesion. In the literature, the controversy in the results was attributed to varying recording sites within the SNr (lateral and medial regions) or 6-OHDA lesions into the SNc or MFB (Wang et al., 2010) as well as post lesion recordings time (MacLeod et al., 1990). Another reason for discrepant results could also be the fact that SNr subpopulations were not separately studied, as we did here. To the best of our knowledge, there is only one publication in which the authors subdivided GABAergic SNr cells according to their firing activity and GAD levels revealing distinct modifications in the firing patterns induced by 6-OHDA lesion for GAD65 and GAD67 SNr cells

(Rodríguez Díaz et al., 2003). However, they were not able to attribute evident changes in their firing activity only regarding the expression of GAD.

Here, we propose that one of the possible mechanisms underlying the decrease in the excitability of PV+ SNr cells after the 6-OHDA lesion could be a loss of D1 and D5 receptors modulation which is lost in an experimental rat model of PD (Zhou et al., 2009). These D1/D5Rs are present on SNr neurons and coupled to tonically active TRPC3 channels. Under physiological conditions, D1/5R are activated by DA released from the so-called ultra-short DA SNc-SNr pathway, and positively modulate TRPC3 channels leading to increase firing activity in SNr neurons (Zhou et al., 2009; Kliem et al., 2010). In PD, this ultra-short DA pathway is lost which could be responsible of the spontaneous firing rate decreased observed mainly in PV+ SNr cells. As we reported previously, the NALCN channels could also contribute to the observed changes (Lutas et al., 2016). Another possibility could be a form of adaptation/compensation to the hyperactivity of STN neurons. To address the potential tonic D1/D5 receptor activity, it would be needed first to block fast GABA- and glutamate-mediated synaptic transmission and after block D1 and D5 receptors pharmacologically, similarly the use of D1 KO mice and D5 KO mice could be useful to study their involvement in control and pathological PD states on these SNr neurons. To prove whether PV+ cells exhibit a compensatory mechanism to hyperactivity of STN neurons, not blocking glutamatergic transmission could address this hypothesis.

Similarly, the decreased in firing rate observed in PV+ cells from dyskinetic mice can be attributed to the involvement of other channels. We observed a significant decrease of the AHP peak on these neurons suggesting probably modifications in the expression profile of SK channels after L-DOPA treatment (Atherton and Bevan, 2005). We also observed the strong I_h exhibited in these neurons after L-DOPA treatment, suggesting a compensatory, but unsuccessful, phenomenon to restore normal level of activity in PV+ SNr neurons. In the literature, only few and controversial data are available regarding changes of spontaneous firing rate of SNr neurons in L-DOPA treated rats. Some authors using anesthetized rats have shown that the firing rate in the SNr was increased in L-DOPA chronic treated PD models compared to control (Meissner et al., 2006; Aristieta et al., 2016). However, Aristieta and colleagues also shown that after an acute challenge of L-DOPA the firing of these SNr neurons was decreased which sustain our data obtained from brain slices 20–120 min after the last injection of L-DOPA (the time period of intense dyskinetic behavior). Furthermore, these

results are also in agreement with the concept that LID are associated with hypoactivity of the BG output nuclei (Obeso et al., 2002).

The slight (non significant) reduction in the firing rate properties of PV- neurons after the 6-OHDA lesion or subsequent L-DOPA treatment, suggest no changes in the intrinsic properties of this subpopulation of SNr by DA loss. However, the F-I curve of these neurons was reduced after the 6-OHDA lesion and rescued to basal levels by L-DOPA treatment, indicating that DA-depletion influences this cell population in a lesser extent than PV+ SNr neurons.

Taking into account all these results, together with the observed dysfunction of PV+ SNr cells after DA loss (partially rescued by L-DOPA treatment) and their dorsolateral preferential distribution within the SNr, we propose that PV+ neurons may be involved in sensorimotor functions, the reason why they are mostly affected in PD states, while the neighboring PV- cells are more related to associative functions as suggested by their differential axonal targets (Liu et al., 2020). Indeed, the fact that PV+ neurons are known to degenerate in a late stage of PD (Hardman et al., 1996) further support the divergent impact on the activity of PV+ and PV- SNr neurons that we have observed in parkinsonian and dyskinetic mice and reiterates the importance to consider neuronal diversity in the SNr to study BG functions and dysfunctions. We also highlight the impact of specific manipulation of PV+ SNr neurons to improve motor symptoms, as well as PV- neurons to ameliorate non-motor PD symptoms.

5.2. STUDY II. Striato-nigral and pallido-nigral GABAergic synaptic transmission in sham and parkinsonian mice

Using selective *in vitro* optogenetic stimulation of STR-SNr and GP-SNr synapses and employing sham and DA-depleted PVcre::Ai9T mice, we first observed that both PV+ and PV- cells in the SNr received inputs from striatal dSPN and PV-GP neurons. In addition, we showed several differences in the effects of DA loss on these two converging inhibitory pathways impinging on PV+ and PV- neurons in the SNr.

5.2.1. Striatal and pallidal inputs to the SNr innervate PV+ and PV- neurons

First of all, our optogenetics results from *in vitro* electrophysiological recordings in PVcre::Ai9T mice, have revealed that both PV+ and PV- in the SNr received inputs from the STR and the GP. These results are novel, as there is no existing publication regarding the electrophysiological characterization of these inputs in respect with several populations of SNr neurons. By using optogenetic stimulation of the STR and GP, we detected short-term plasticity representative of synapses with high release probability; specifically we observed short-term depression at both STR-SNr and GP-SNr synapses on PV+ and PV- SNr neurons. These results are partially in disagreement with some authors who used electrical stimulation and C57/BL6 mice and described short-term facilitation for STR-SNr synapses, whereas GP-SNr synapses displayed short-term depression (Miyazaki and Lacey, 1998; Connelly et al., 2010). This controversy could be due to the different methodological approach used among the studies. Connelly and colleagues used electrical stimulation which is known to be less selective than the optical one, making more complicate to trigger specific STR-SNr/GP-SNr GABA release. The use of optogenetic tools is therefore more convenient, but not absent of drawbacks, as some studies have also reported that ChR2 and AAVs used for gene delivery could increase the release probability of synapses (Zhang and Oertner, 2007; Jackman et al., 2014). It is also known that short-term synaptic plasticity decreases considerably with animal's aging (Mori-Kawakami et al., 2003; Fedchyshyn and Wang, 2005). In this sense, electrical stimulation studies were achieved in juvenile mice (postnatal day 14 to 20) whereas our experiments were performed in adult mice (P50-60).

Our results, partially in agreement with anatomical and electrical previous studies (Smith et al., 1998; Connelly et al., 2010) shown that the dendritic inhibition from striatal dSPNs was more powerful to silence the activity of PV+ and PV- SNr neurons (~70-80%) than inputs from PV-GP neurons targeting SNr cells (~20-40%). These results can be explained by the anatomical description that Smith and colleagues achieved revealing that 48 striatal neurons innervate only one SNr neuron. Besides, considering that a single striatal neuron makes synaptic contact with several neurons in the SNr, the degree of convergence of this STR-SNr input is expected to be much higher than the one displayed by GP-SNr synapses. Besides, the GP-SNr input is very much sparse making contacts with the perikarya (59%) but also with proximal (37%) and distal (4%) dendrites of SNr neurons (Smith and Bolam, 1989). Some studies analyzed morphologically and electrophysiologically PV-GP axons in the SNr and revealed that PV-GP neurons formed dense axon varicosities with PV+ cells in the SNr, however they did not look at PV- SNr cells (Mastro et al., 2014; Oh et al., 2017). Interestingly, the Fujiyama's group also observed that PV-GP axonal boutons were concentrated around the cell bodies of PV+ SNr neurons (Oh et al., 2017).

5.2.2. Striato-nigral synaptic changes after dopamine depletion

In relation to STR-SNr synapses and bearing in mind that the firing rate of both, PV+ and PV- neurons decreased after DA-depletion (without blocking GABAergic transmission), we observed that the silencing of both PV+ and PV- neurons by these synapses tended to be more efficient after DA loss. However, we only observed an increase of short-term depression after the 6-OHDA lesion in PV+ SNr cells, suggesting an alteration of STR-SNr transmission onto this cell type. By contrast, this GABAergic transmission was unaffected in PV- SNr neurons after DA-depletion. Under my knowledge there is only one publication in which authors investigated the impact of DA loss on STR-SNr synapses and provided the first sign that DA loss increased GABA transmission in the SNr by presynaptic enhancement of GABA release (Borgkvist et al., 2015). This finding is in disagreement with our results for PV+ SNr neurons where we observed a reduction of STR-SNr transmission onto this cell subtype. However, this result is agreement with Aceves's pharmacological experiments on the STR-SNr synapse where application of D1-receptor antagonists greatly decreased STR-SNr IPSCs (Aceves et al., 2011a). Similar results were obtained in Lavian's study on the synapse of STR and EPN, the parallel output nuclei (Lavian et al., 2017). The work of

Borgskvist and colleagues, besides, reported conflicting results. On the one hand, by using electrical stimulation they observed short-term facilitation in sham and 6-OHDA lesioned mice and a potentiated STR-SNr pathway after DA loss associated to a reduction of presynaptic $GABA_B$ response. By contrast, using selective optogenetic stimulation in D1-cre mice, they observed this facilitation only in sham mice while in 6-OHDA lesioned animals showed short-term depression, as we did for this pathway in sham and 6-OHDA animals. Another discrepancy is that these authors did not reveal changes in the firing properties of SNr neurons after DA loss, while we and others (Faynveitz et al., 2019) have consistently demonstrated that the overall firing frequency in the SNr is reduced in experimental parkinsonism.

It is worth to highlight the role that local plasticity plays on STR-SNr synapses which has been recently observed after optogenetic stimulation of STR-SNr terminals in 6-OHDA lesioned mice (Keifman et al., 2019). These authors by optostimulation of STR-SNr terminals were able to inhibit SNr neurons and thereby induce dyskinesias in DA depleted mice. This finding points at the manipulation of these STR-SNr synapses as an attractive target for managing LID and could be considered one of the future directions of this research project. However, the fact that other authors showed that co-activation of dSPN and iSPN is necessary to manipulate dyskinesias (Alcacer et al., 2017) exposes the complexity of the BG circuit which indeed, has distinct subpopulations of neurons with diverse intrinsic properties and functional implications.

5.2.3. Pallido-nigral synaptic changes after dopamine depletion

Concerning the inhibitory synaptic connections between PV+ neurons in the GP and PV+ or PV- cells in the SNr, we studied the synaptic alterations triggered by DA-depletion. We considered important to further explore this pathway, as a recent publication by Mastro and colleagues has demonstrated that the specific manipulation of PV-GP cells restores normal movement in DA-depleted mice (Mastro et al., 2017). The optogenetic stimulation of PV-GP neurons in our experiments with 6-OHDA lesioned mice, revealed opposite effects in PV+ and PV- SNr neurons. We observed that GP-SNr transmission was decreased in PV+ SNr neurons but significantly increased in PV- SNr cells. The former results are partially in agreement with the recent paper from the Korngreen's group performed in 6-OHDA lesioned rats into the medial SN (Faynveitz et al., 2019). These authors observed an increase in the IPSC amplitude

after DA depletion, consistent with the up-regulation of $GABA_AR$ gene expression in DA depleted rats (Chadha et al., 2000). We also detected an increase in the IPSC amplitude in PV- SNr neurons after DA loss, while in PV+ cells the amplitude of the IPSC was decreased. Probably the fact of differentiating among two subpopulations of SNr neurons could justify the discrepancy of our results respect to those of Faynveitz and colleagues (Faynveitz et al., 2019). In line with this, considering that synaptic changes are related to modification in the response of SNr neurons to GABA release, we suggest a decrease in the density of somatic $GABA_A$ receptors mediating inhibition on PV+ SNr neurons after DA depletion as the possible mechanism addressing the decrease in the IPSC amplitude observed in this synapses. These results together with the reduced STR-SNr transmission onto PV+ cells after the 6-OHDA lesion lead to hypothesize that the changes observed in firing rate of PV+ SNr neurons after DA loss, are mainly due to alterations in the intrinsic properties of these neurons as we reported in the Study I and exclude a potentiated STR-SNr/GP-SNr transmission onto these PV+ neurons as the mechanism responsible of the decrease in firing rate.

By contrast, the potentiated impact of GP-SNr synapses on the activity of PV- SNr neurons reported after DA loss, along with the larger IPSCs after the 6-OHDA lesion could explain the decrease in firing rate observed in PV- cells after DA loss (without blocking GABAergic transmission). Probably an up-regulation of $GABA_A$ receptor gene expression in parkinsonian mice or an increase in the number of postsynaptic receptors on these PV- SNr cells could be expected (Chadha et al., 2000).

Some authors who discerned among PV+ and PV- neurons in the SNr, showed that PV+ SNr neurons display $GABA_A$ receptor $\alpha 1$ subunits and at least two subtypes of the $GABA_B$ receptor (type I,II) presynaptically at PV+ synapses, while PV- cells displayed $GABA_A$ $\alpha 1$ and $GABA_BR1$ (Ng and Yung, 2000, 2001) but the physiological roles of $GABA_BRs$ receptors in the reticulata neurons await further investigated. Furthermore, Fujiyama and colleagues demonstrated that $\alpha 1$, $\beta 2/3$ and/or $\gamma 2$ subunits are present on symmetrical synapses formed by STR and GP terminals but they did not look at distinct SNr population of neurons (Fujiyama et al., 2002) nor to changes after DA depletion.

The observed changes on synaptic transmission could be confirmed by immunostaining for the inhibitory presynaptic marker vGAT and subsequent analysis of density or distribution of $GABA_A$ receptor subunits after DA loss in PV+ or PV- SNr

neurons. This procedure was undertaken previously by Faynveitz and colleagues (Faynveitz et al., 2019) revealing an increase in the density of vGAT in the SNr from DA depleted slices, but considering the SNr as an homogeneous nucleus.

Interestingly, it is well-known that intranigral microcircuit (i.e. axon collaterals) is sufficient to provide robust feedback inhibition to the activity of SNr neurons (Brown et al., 2014) but, it is unknown whether GABA release from axon collaterals of SNr neurons is affected by the DA denervation itself. Considering the findings from Miguelez and colleagues in GP-GP synapses (potentiated after DA loss), we hypothesize that the SNr could present similar homeostatic response to the known hyperactivity of the STN in 6-OHDA animals (Miguelez et al., 2012). It may happen that chronic DA-depletion induces a postsynaptic increase in the potency of GABAergic transmission among PV+ and PV- SNr neurons thereby contributing to the altered activity of these both subtypes of SNr cells. Meanwhile, it would be of great interest to investigate whether PV+ and PV- SNr are connected to each other and if so, whether this connection is enhanced after DA depletion.

All these findings and discrepancies could be explained by subdivision of the SNr into PV+ and PV- neurons. Nevertheless, DA has complex effects on the activity of SNr neurons *in vitro* probably because it acts in a distinct manner on PV+ and PV- SNr neurons and on both presynaptic and postsynaptic elements, thereby controlling synaptic weight and neuronal excitability.

5.3. STUDY III. GABAergic extrasynaptic transmission in SNr neurons from control and parkinsonian mice

In this study, we demonstrated that both subtypes of SNr neurons express $GABA_A$ extrasynaptic receptors containing α5 and δ subunits. However, our data reveal that the subunit composition of extrasynaptic $GABA_A$ receptors is different among PV+ and PV- neurons in the SNr. Moreover, our electrophysiological recordings revealed that PV- neurons display larger $GABA_A$ receptor-mediated tonic currents than PV+ neurons in the SNr; nevertheless, tonic inhibition did not increase in DA depleted mice.

5.3.1. Extrasynaptic α5 and δ subunits expressed in the SNr

In the CNS, tonic inhibition is mediated by extrasynaptic $GABA_A$ receptors composed of specific subunits that confer high affinity for GABA and slow deactivation and desensitization kinetics. These extrasynaptic receptors frequently contain α5 and δ $GABA_A$ subunits (Stell et al., 2003; Caraiscos et al., 2004a; Glykys et al., 2008; Bright et al., 2011), the reason for studying more in detail these two subunits in the SNr. The presence of δ and α5 subunits in the SNr seems to be controversial due to the low level of protein expression compared to the *thalamus* or the STR (Pirker et al., 2000). Here, we performed immunohistochemical experiments with δ-/- and δ+/+ mice (males and females) to test the expression of δ-subunit in the SNr. As a result, no staining was found in the SNr of δ-KO mice supporting the specificity of our δ labeling in wild-type mice. Nevertheless, we wanted to clarify whether this δ-subunit was more often present in a subpopulation of SNr neurons rather than in the other one, in consequence, we used the PVcre::Ai9T mouse line. The expression profile of δ-subunit in the SNr of these mice was diffuse and similarly present in both PV+ and PV- SNr neurons. In the literature, δ-subunit containing $GABA_A$ receptors are known by their ability to generate a persistent, "tonic" current that strongly affects neuronal excitability as well as their ability to regulate memory, anxiety and nociception or their dynamic changes in expression levels under normal and pathological conditions (for review see, Whissell et al., 2015). In addition, we looked at the expression profile of $GABA_ARs$ containing α5-subunits in the SNr, revealing a strong expression of this subunit preferentially surrounding PV- cells. Some promising studies exposed that mice lacking α5-$GABA_ARs$, improved performance in associative learning and memory tasks (Collinson

et al., 2002; Crestani et al., 2002; Yee et al., 2004). Altogether, we decided to further investigate by electrophysiological recordings whether δ or α5 subunits were mediating bigger currents in a subtype or SNr neurons rather than in the other one.

5.3.2. Extrasynaptic $GABA_A$ receptors mediates tonic inhibition mainly in PV- SNr cells

In our voltage-clamp recordings in whole-cell configuration, we used CsCl as internal solution which facilitates the detection of spontaneous IPSCs. The Cs-based internal solution has been widely employed in the STR or GP to permit easy sIPSCs detection (Ade et al., 2008; Chazalon et al., 2018). Our recordings in the SNr of PV::creAi9T mice from PV+ and PV- neurons, in presence of glutamatergic blockers, revealed inward currents that were blocked by the $GABA_A$ receptor antagonist GABAzine, confirming their identity as $GABA_A$-mediating sIPSCs in both PV+ and PV- SNr neurons. However, the blockade of extrasynaptic $GABA_A$Rs revealed a bigger effect on PV- cells suggesting that these neurons are more sensitive to low doses of GABA than PV+ neurons in the SNr. These results together with the demonstration in the GP that artificial elevation of GABAergic transmission induces a reduction of neuron firing discharge in these neurons (Chazalon et al., 2018), lead to suggest that tonic inhibition can also contribute to the low firing rates of PV- cells. This supposition could be in agreement with previous studies in the cerebellum and *thalamus* in which blockade of tonic GABA currents increases AP firing rate in response to depolarizing current injections (Semyanov et al., 2003; Cope et al., 2005; Farrant and Nusser, 2005). Our results did not report differences in the sIPSC frequency or amplitude between populations of SNr neurons with CsCl as internal solution (data not shown) meaning that probably the number of synaptic $GABA_A$Rs is similar in both populations of SNr neurons (Nusser et al., 1997).

The differences observed in $GABA_A$-mediated tonic current between PV+ and PV- SNr neurons could be due to divergent GABA transporters (GAT) distribution in respect with each cell subtypes. GATs are the main buffering system to control extracellular levels of GABA and thereby regulate GABAergic transmission (Scimemi, 2014). In the SNr, the regulatory functions of GATs on synaptic transmission have not been investigated as well as in the GP, STR or *thalamus* (Jin et al., 2011). In the rat SNr, GAT-1 and GAT-3 mRNAs have been detected in control conditions, however it

seems that GAT-1 expression is stronger in dopaminergic neurons than in GABAergic nigral cells (Durkin et al., 1995; Yasumi et al., 1997). Electron microscopy analysis in the monkey has revealed that in the SNr, GAT-3 is mainly associated with astrocytes (Ng et al., 2000). In the same way, other authors shown that GAT-1 blockade significantly reduced GABA uptake in synaptosomes generating an increase of extracellular GABA levels in the rat SNr (Fink-Jensen et al., 1992; Bahena-Trujillo and Arias-Montaño, 1999). In other brain regions such as the STR, GP or the hippocampus GAT-3 regulates GABA levels (Allen et al., 2004; Wu et al., 2014; Chazalon et al., 2018). In the *thalamus* but also in the GP, GAT-1 contributes to tonic inhibition in control conditions (Cope et al., 2009; Errington et al., 2011; Pirttimaki et al., 2013; Chazalon et al., 2018). All these findings lead to suggest that probably an increased activity of GATs or distinct subtypes of GATs working in the uptake of GABA from the synaptic clefts of PV+ cells can be responsible for the absence of changes in tonic inhibition exhibited on this neuron subtype.

It should be noted that the involvement of extrasynaptic δ-$GABA_A$Rs mediating tonic inhibition in the SNr seems to be sex- and age- related. Our experiments were performed in adult mice (PN 40-50 days) and $GABA_A$R-mediated tonic inhibition reduces while age increases (Garant et al., 1995; Chudomel et al., 2009, 2015), inducing greater tonic responses in postnatal day 5-9 rats than in older 25-32 days rats (Chudomel et al., 2015). The age-related decline observed by these authors correlated with the reduction in δ subunit in the SNr. Although we didn't differentiate between male and females, sex differences have been reported in the expression of $GABA_A$Rs containing α1 subunit in the rats SNr being higher in females compared to males (Ravizza et al., 2003). Interestingly, some studies have also differentiated two regions into the SNr revealing lower densities of $GABA_A$Rs containing α1 subunits in the posterior SNr compared to the anterior part of the SNr (Veliskova et al., 1998). However, these studies were performed while considering the SNr as a homogeneous nucleus and our electrophysiological recordings hope to elucidate novel findings.

Later, we explored which subunit mediated these tonic currents mainly observed in PV- SNr neurons. We combined pharmacological experiments with δ-/- mice to test for the involvement of this subunit in the extrasynaptic receptors present in SNr neurons. The fact that no tonic currents were detectable in these mice suggested that the presence of this subunit is needed to present functional extrasynaptic $GABA_A$ receptors in SNr neurons. With the proposal of examining whether this δ-subunit was

more present in PV+ rather than PV- SNr neurons, we employed the PVcre::Ai9T mouse line. Our electrophysiological recordings shown that the δ-selective drug THIP, induced a major tonic current in PV- neurons but the number of registered cells is a bit limiting to get conclusions. THIP has been widely used for activation of the tonic current in other brain regions (Cope et al., 2005; Drasbek and Jensen, 2006; Drasbek et al., 2007; Ade et al., 2008; Chazalon et al., 2018). The estimated concentration of this drug to selectively activate δ-containing $GABA_A$ receptors is 1 μM, which was the used dose for our electrophysiological recordings in the SNr (Drasbek et al., 2007; Meera et al., 2011).

In the same way, several studies have shown that α5-subunit-containing $GABA_A$ receptors mediate tonic inhibition in several brain regions such as the STR (Ade et al., 2008), cortex (Yamada et al., 2007b; Clarkson et al., 2010) and hipocampos (Scimemi et al., 2005; Wu et al., 2014). For this reason, together with the demonstrated presence of this subunit in the SNr by some authors (Pirker et al., 2000) and also verified by us, we decided to investigate the effect that a selective inverse agonist of α5-$GABA_A$Rs had on both PV+ and PV- SNr neurons. This drug was able to modify the holding current of PV+ and PV- neurons reporting a marked bigger effect on PV- SNr cells. These results provide the first indication of α5-subunit contribution to tonic inhibition in the SNr, mainly settled to PV- cells. Differences in tonic currents among neurons within the same BG nucleus, the STR, have also been reported (Ade et al., 2008). These authors showed that D2+ SPNs displayed greater $GABA_A$ receptor-mediated tonic currents containing α5-subunits than D1+ SPNs. The concentration of 1 μM (that we employed here) is the one chosen in the majority of brain slice physiology studies (Scimemi et al., 2005; Yamada et al., 2007b; Chazalon et al., 2018). Interestingly, Ade and colleagues shown that 50 nM L655,708 was as efficacious in antagonizing tonic currents in D2+ SPNs as higher concentrations (10 μM). However, tonic currents in D1+ SPNs were not significantly reduced by either 50 nM or 10 μM of L655,708 (Ade et al., 2008). In this line it would be interesting also to test distinct concentrations in PV+ and PV- SNr neurons.

5.3.3. Tonic inhibition remains unaltered after the 6-OHDA lesion in SNr neurons

In the SNr, extracellular GABA and glutamate concentrations are abnormally elevated in the DA depleted condition (Windels et al., 2005), although some ongoing experiments (unpublished data) from our laboratory do not support this hypothesis. For this reason we decided to further investigate whether GABAergic extrasynaptic transmission was altered in PV+ or PV- SNr neurons after the 6-OHDA lesion. So far, we discovered that DA loss did not modify the magnitude of tonic current induced either in PV+ or in PV- cells. Other publications using this animal model, showed aberrant form of GABAergic inhibition in the GP, due to a downregulation of GAT-3 in GP astrocytes without alteration of GAT-1 or extrasynaptic receptors functions (Chazalon et al., 2018).

In our study, we tested whether THIP induced tonic current of similar magnitude in both PV+ and PV- neurons in DA-depleted mice. As expected, tonic currents were of similar magnitude after DA loss in both PV+ and PV- cells excluding an increased expression of δ subunits following chronic DA depletion. In the same way, we used L655,708 in DA depleted mice to test the contribution of α5 subunits mediating tonic currents after the 6-OHDA lesion, surprisingly this pharmacological approaches failed to modify the holding current in PV- neurons contrary to what we observed in control conditions. However, GABAzine administration revealed tonic inhibition which lead to hypothesize about a downregulation of α5-subunit in DA depleted mice and excludes *de novo* expression of this subunit in the SNr following DA depletion. In the same way, these results could indicate that other subunit might compensate for the loss. Nevertheless, the number of recorded neurons is limiting to get conclusions so further experiments would be needed to confirm these results. Besides, some authors did not succeed antagonizing tonic currents until 10 μM of concentration in the STR (Ade et al., 2008) which suggests that increasing the concentration of L655,708 could address the contribution of these subunits in pathological states.

In the same way, it would be of great interest to examine the changes in the amplitude and frequency of sIPCSs between control and 6-OHDA lesioned mice for PV+ and PV- SNr. As changes in the frequency of synaptic events reflect presynaptic alterations in synaptic strength, perhaps an increased frequency of sIPSCs in DA depleted mice would reflect an enhancement of presynaptic GABA release. Certainly, this theory has already been confirmed by Borgkvist et al., 2015 leading us to suggest

that the changes on the activity of PV+ and PV- cells that we observed after DA loss, can be due to alterations in the intrinsic properties of these neurons, in GABAergic synaptic transmission or both.

Overall, our results suggest that PV- SNr neurons have higher expression of extrasynaptic $GABA_A$ receptors containing α5 subunit than the neighboring PV+ SNr neurons. Despite DA depletion did not trigger an increase of tonic inhibition in neither subtype of SNr neurons; we put forward the importance of subdividing the SNr into these two populations. Furthermore, because tonic inhibitory currents provide a powerful mechanism to regulate cell excitability, targeting α5 subunits in PV- SNr neurons may serve as a novel therapeutic tool for ameliorating associative disturbances associated with PD.

6. CONCLUSIONS AND PERSPECTIVES

CONCLUSIONS

The different results obtained in the aforementioned studies lead us to the following conclusions:

I. In this study we confirmed that the PVcre::Ai9T transgenic mouse line is a useful tool to identify distinct SNr neurons based on the expression of PV and has potential to investigate different roles of PV+ and PV- cells in BG function.

II. In control and DA-depleted conditions, PV+ and PV- cells are present in equal proportions in the SNr but differently distributed. Thus, while PV+ neurons are predominantly located in the lateral SNr, PV- cells are found in the medial portion of the nucleus.

III. Electrophysiologically, PV+ and PV SNr neurons show different intrinsic properties depicting, in average, higher firing frequencies in PV+ cells in control mice. PV- cells exhibit lower firing rates and more hyperpolarized APth, probably related to lower I_{NAP}, I_{NAT} currents or lower expression of TRPC3 or NALCN channels than the neighboring PV+ SNr neurons.

IV. DA loss and subsequent L-DOPA treatment strongly influence electrical intrinsic properties in PV+ SNr neurons, showing significantly reduced firing frequency and altered excitability. By contrast, DA loss or pharmacological replacement does not produce relevant changes in the PV- subpopulation.

V. The optogenetic manipulation of STR-SNr and GP-SNr pathways revealed not only that both PV+ and PV- SNr neurons receive equivalent inputs from these two nuclei but also that inhibition from dSPN is more powerful to silence the activity of both subtypes of SNr neurons in DA-intact mice.

VI. DA loss affects GABA transmission in a different manner in PV+ and PV- SNr cells. Whereas PV+ neurons are more sensible to striatal synaptic inhibition; PV-GP transmission is increased in PV- cells after the 6-OHDA lesion. This latter result may explain the decrease firing rate observed in PV- SNr subpopulation when GABAergic transmission is not blocked.

VII. The immunohistochemical assays, revealed expression of $GABA_A$ extrasynaptic receptors containing δ and $\alpha5$ subunits in PV+ and PV- SNr neurons from control mice. However, GABAergic tonic extrasynaptic transmission is more prominent in PV- compared to PV+ SNr neurons, probably attributable to the major presence of $\alpha5$-subunits on these cells.

VIII. Contrary to our expectations, DA-depletion does not modify tonic extrasynaptic transmission in any SNr subpopulation, although compensatory mechanisms may take place in PV- cells from parkinsonian mice.

In summary, the present study provides for the first time a valuable characterization of PV+ and PV- SNr neurons in physiological and parkinsonian conditions. In addition, we confirmed that GABAergic synaptic and extrasynaptic transmissions are influenced by DA content and differentially expressed in SNr neuron subpopulations. Therefore, this study highlights the importance of discriminating among SNr neurons types for better understanding the involvement of this nucleus in sensorimotor or associative functions and for developing new pharmacological cell-specific tools to treat PD.

PERSPECTIVES

Here, we propose potential future directions for our investigation, which could properly address some of the unsolved questions and strength the obtained results.

Channels involved in the pacemaking of PV+ and PV- cells

After proving that PV+ and PV- neurons exhibited markedly distinct firing rates, we consider of great importance the study of the channels responsible for these observed differences. In the literature, multiple ion channels have been described in SNr neurons and seem to be responsible of the sustained high firing of these neurons; however these studies were carried out considering the SNr as a homogeneous nucleus. For this reason, it would be interesting to further investigate more precisely TRPC3, NALCN or SK channels along with I_{NaP} (Atherton and Bevan, 2005; Zhou et al., 2006, 2008; Seutin and Engel, 2010; Lutas et al., 2016).

Overall, as we described previously during the discussion, we expect that differences in the density, distribution or kinetics of these channels could be found among PV+ and PV- cells, thereby contributing to clarify the mechanisms involved in the distinct firing rates observed in these two cell subtypes of SNr neurons.

Characterization of STR-SNr and GP-SNr pathways in L-DOPA treated mice

After demonstration by some authors that selective optogenetic activation of the dorsolateral STR induces dyskinesias in the 6-OHDA rat model of PD (Hernández et al., 2017; Girasole AE., 2018) along with the finding that optostimulation of STR-SNr terminals inhibits SNr neurons and induces dyskinesia in DA depleted mice (Keifman et al., 2019), we consider of great interest to explore the impact that optogenetic manipulation of STR-SNr and GP-SNr inputs can have on the activity of both PV+ and PV- SNr neurons in dyskinetic PVcre::Ai9T mice. For that, it would be needed to treat a group of 6-OHDA lesioned mice (2 weeks after the surgery) with L-DOPA (6 mg/kg) + Benserazide (12 mg/kg) during 15 days and follow the same experimental procedure we used for the characterization of STR-SNr and GP-SNr pathways. More precisely, taking into account these previous findings (Hernández et al., 2017; Keifman et al., 2019) and our results, we could expect that dyskinetic mice showed the opposite effect to those obtained here for 6-OHDA lesioned mice. This is, we could expect potentiated STR-SNr and GP-SNr transmissions on PV+ neurons, which is the SNr neuron subtype related to sensorimotor functions. This selective enhanced transmission in PV+ SNr neurons could be some of the mechanisms responsible of dyskinesia manifestation. Thereby, the selective manipulation of these pathways onto PV+ SNr neurons could be useful for the treatment of LID.

Behavioral experiments

It would be worthwhile to complete our anatomical and electrophysiological findings with behavioral experiments in control, parkinsonian and more ambitiously in dyskinetic mice. Recent publications discerning two subpopulations of SNr neurons

have well characterized the inputs/outputs of these neurons (Assaf and Schiller, 2019; Liu et al., 2020). Indeed, the subdivision of SNr neurons described by Liu and colleagues is analogous to ours, discriminating between PV+ and PV- SNr neurons. These authors have shown that PV+ neurons receive inputs mainly from BG nuclei and project to motor-control regions, however PV- neurons integrate a much extensive range of inputs, including BG nuclei but also *hypothalamus* and midbrain regions, and project broadly to brain-state as well as motor-control regions.

One interesting experiment to perform would be to selectively modulate the activity of PV+ and PV- SNr neurons by using chemogenetic/optogenetic approaches not only in control mice, already studied by the groups of Chiller and Dan in their recent publications (Assaf and Schiller, 2019; Liu et al., 2020), but more stirringly in parkinsonian and dyskinetic mice. Consequently, behavioral tests would be required to monitor the impact of selective manipulation of these subtypes of SNr neurons in different behavioral motor components as well as associative behaviors, also affected in PD after DA loss.

In recent years the use of chemogenetic tools is emerging and could be useful to selectively modulate the activity of PV+/PV- SNr neurons. Indeed, considering our electrophysiological recordings from 6-OHDA lesioned and L-DOPA treated mice showing a major influence on PV+ cells (involved in sensorimotor functions), along with the well-described hyperactivity of BG output nuclei in PD *in vivo* (Lanciego et al., 2012; DeLong and Wichmann, 2015), one could hypothesize that suppressing the activity of PV+ SNr neurons in 6-OHDA models of PD would improve motor symptoms related to PD. To test this theory, we should use the PVcre::Ai9T mouse line and inject into the SNr an AAV-DIO-hM4Di-mCherry, a double floxed inverted open reading frame adeno associated virus (AAV-DIO) that expresses, in a Cre-dependent manner, an engineered Gi-coupled receptor hM4Di, inhibitory (the designer receptor exclusively activated by designer drug, “DREADD”) tagged with a fluorescent protein mCherry (hM4Di-mCherry). Similarly, we could use the excitatory Gq DREADDs (AAV-hSyn-DIO-hM3D(Gq)-mCherry) to enhance the activity of PV+ SNr neurons in L-DOPA treated mice. Equally interesting would be the selective manipulation of PV- SNr neurons to further investigate their associative functions and damage after DA loss or subsequent L-DOPA treatment. For that, the use of a $Gad2^{Cre}$ mouse line that mainly label PV- cells would be required. Generally, viral vectors and 6-OHDA should be injected in the same session.

To investigate the effect of DREADDs activation/inhibition, we should inject intraperitoneally either clozapine-N-oxide (CNO) or normal saline (0.9% NaCl) in a random order. Behavioral tests will be performed approximately 20 to 30 minutes after intraperitoneal drug administration. We propose the Open-Field Test and the Skill-Reaching Task (SRT) for a better evaluation of motor functions after manipulation of PV+ neurons in 6-OHDA lesioned or dyskinetic mice. To test the impact of PV- cells manipulation, it could be useful the Novel Object Recognition (NOR), widely used to evaluate cognition, particularly recognition memory, in rodent models of CNS disorders.

Optogenetic stimulation of PV+ and PV- SNr neurons *in vivo* under anesthesia could also be advantageous to confirm the data from chemogenetic experiments. For that, it would be needed to inject the virus into the SNr and then implant optic fibers (Sparta et al., 2012) above each SNr to achieve local soma photo-stimulation. Bearing in mind the high baseline firing rate of SNr neurons, we should use a 50-Hz light protocol with the proposal to increase the activity of these neurons as recently did Rizzi and colleagues in control mice (Rizzi and Tan, 2019).

However, as we observed changes in STR-SNr and GP-SNr pathways after DA loss, we consider interesting the selective manipulation of these pathways as previously did Kravitz and colleagues showing that movement can be rescued during D1-ChR2 stimulation in the 6-OHDA model of PD (Kravitz et al., 2010). Similarly, Mastro and colleagues revealed that elevating the activity of PV-GPe neurons restores movement in DA depleted mice (Mastro et al., 2017).

Altogether, this PhD project represents a forward step toward a more comprehensive understanding of the SNr anatomy, nevertheless the selective manipulation of either PV+ or PV- SNr neurons along with behavioral tests, would be beneficial to further characterize the functionality of these subtypes of SNr neurons within the BG circuit in control and PD conditions.

7. BIBLIOGRAPHY

Abdi A, Mallet N, Mohamed FY, Sharott A, Dodson PD, Nakamura KC, Suri S, Avery S V., Larvin JT, Garas FN, Garas SN, Vinciati F, Morin S, Bezard E, Baufreton J, Magill PJ (2015) Prototypic and arkypallidal neurons in the dopamine-intact

external globus pallidus. J Neurosci 35:6667–6688.

Abercrombie ED, Bonatz AE, Zigmond MJ (1990) Effects of l-DOPA on extracellular dopamine in striatum of normal and 6-hydroxydopamine-treated rats. Brain Res 525:36–44.

Abrahao KP, Lovinger DM (2018) Classification of GABAergic neuron subtypes from the globus pallidus using wild-type and transgenic mice. J Physiol 596:4219–4235.

Aceves J de J, Rueda-Orozco PE, Hernández R, Plata V, Ibañez-Sandoval O, Galarraga E, Bargas J (2011a) Dopaminergic presynaptic modulation of nigral afferents: Its role in the generation of recurrent bursting in substantia nigra pars reticulata neurons. Front Syst Neurosci 5:1–10.

Aceves JJ, Rueda-Orozco PE, Hernandez-Martinez R, Galarraga E, Bargas J (2011b) Bidirectional plasticity in striatonigral synapses: A switch to balance direct and indirect basal ganglia pathways. Learn Mem 18:764–773.

Adams RN, Murrill E, McCreery R, Blank L, Karolczak M (1972) 6-Hydroxydopamine, a new oxidation mechanism. Eur J Pharmacol 17:287–292.

Ade KK, Janssen MJ, Ortinski PI, Vicini S (2008) Differential Tonic GABA Conductances in Striatal Medium Spiny Neurons. J Neurosci 28:1185–1197.

Albert AP, Pucovský V, Prestwich SA, Large WA (2006) TRPC3 properties of a native constitutively active Ca2+-permeable cation channel in rabbit ear artery myocytes. J Physiol 571:361–369.

Albin RL, Young AB, Penney JB, Roger LA, Young BB (1989) The functional anatomy of basal ganglia disorders. Trends Neurosci 12:366–375.

Alcacer C, Andreoli L, Sebastianutto I, Jakobsson J, Fieblinger T, Cenci MA (2017) Chemogenetic stimulation of striatal projection neurons modulates responses to Parkinson's disease therapy. J Clin Invest 127:720–734.

AlDakheel A, Kalia L V., Lang AE (2014) Pathogenesis-Targeted, Disease-Modifying Therapies in Parkinson Disease. Neurotherapeutics 11:6–23.

Alicia M. Pickrell and Richard J. Youle (2015) The Roles of PINK1, Parkin and Mitochondrial Fidelity in Parkinson's Disease. Neuron 85(2):257–273.

Allen NJ, Rossi DJ, Attwell D (2004) Sequential Release of GABA by Exocytosis and Reversed Uptake Leads to Neuronal Swelling in Simulated Ischemia of Hippocampal Slices. J Neurosci 24:3837–3849.

Alzheimer C, Schwindt PC, Crill WE (1993) Modal gating of Na+ channels as a mechanism of persistent Na+ current in pyramidal neurons from rat and cat sensorimotor cortex. J Neurosci 13:660–673.

Amaral MD, Pozzo-Miller L (2007) TRPC3 channels are necessary for brain-derived neurotrophic factor to activate a nonselective cationic current and to induce dendritic spine formation. J Neurosci 27:5179–5189.

Ammari R, Lopez C, Bioulac B, Garcia L, Hammond C (2010) Subthalamic nucleus

evokes similar long lasting glutamatergic excitations in pallidal, entopeduncular and nigral neurons in the basal ganglia slice. Neuroscience 166:808–818.

Antal M, Beneduce BM, Regehr WG (2014) The substantia nigra conveys target-dependent excitatory and inhibitory outputs from the basal ganglia to the thalamus. J Neurosci 34:8032–8042.

Appell PP, Behan M (1990) Sources of subcortical GABAergic projections to the superior colliculus in the cat. J Comp Neurol 302:143–158.

Aquino CC, Fox SH (2015) Clinical spectrum of levodopa-induced complications. Mov Disord 30:80–89.

Aristieta A, Azkona G, Sagarduy A, Miguelez C, Ruiz-Ortega JÁ, Sanchez-Pernaute R, Ugedo L (2012) The role of the subthalamic nucleus in L-DOPA induced dyskinesia in 6-hydroxydopamine lesioned rats. PLoS One 7:1–14.

Aristieta A, Ruiz-Ortega JA, Miguelez C, Morera-Herreras T, Ugedo L (2016) Chronic L-DOPA administration increases the firing rate but does not reverse enhanced slow frequency oscillatory activity and synchronization in substantia nigra pars reticulata neurons from 6-hydroxydopamine-lesioned rats. Neurobiol Dis 89:88–100.

Arjona V et al. (2003) Autotransplantation of human carotid body cell aggregates for treatment of Parkinson's disease. Neurosurgery 53:321–330.

Asanuma M, Miyazaki I, Ogawa N (2003) Dopamine- or L-DOPA-induced neurotoxicity: The role of dopamine quinone formation and tyrosinase in a model of Parkinson's disease. Neurotox Res 5:165–176.

Assaf F, Schiller Y (2019) A chemogenetic approach for treating experimental Parkinson's disease. Mov Disord 34:469–479.

Atack JR (2011) GABAA Receptor Subtype-Selective Modulators. II. a5-Selective Inverse Agonists for Cognition Enhancement. Curr Top Med Chem 11:1203–1214.

Atherton JF, Bevan MD (2005) Ionic mechanisms underlying autonomous action potential generation in the somata and dendrites of GABAergic substantia nigra pars reticulata neurons in vitro. J Neurosci 25:8272–8281.

Aubert I, Guigoni C, Håkansson K, Li Q, Dovero S, Barthe N, Bioulac BH, Gross CE, Fisone G, Bloch B, Bezard E (2005) Increased D1 dopamine receptor signaling in levodopa-induced dyskinesia. Ann Neurol 57:17–26.

Bahena-Trujillo R, Arias-Montaño JA (1999) [3H] γ-aminobutyric acid transport in rat substantia nigra pars reticulata synaptosomes: Pharmacological characterization and phorbol ester-induced inhibition. Neurosci Lett 274:119–122.

Baldereschi M, Di Carlo A, Rocca WA, Vanni P, Maggi S, Perissinotto E, Grigoletto F, Amaducci L, Inzitari D (2000) Parkinson's disease and parkinsonism in a longitudinal study: two-fold higher incidence in men. ILSA Working Group. Italian Longitudinal Study on Aging. Neurology 55:1358–1363.

Ballard TM, Knoflach F, Prinssen E, Borroni E, Vivian JA, Basile J, Gasser R, Moreau JL, Wettstein JG, Buettelmann B, Knust H, Thomas AW, Trube G, Hernandez MC (2009) RO4938581, a novel cognitive enhancer acting at GABAA α5 subunit-containing receptors. Psychopharmacology (Berl) 202:207–223.

Bant JS, Raman IM (2010) Control of transient, resurgent, and persistent current by open-channel block by Na channel β4 in cultured cerebellar granule neurons. Proc Natl Acad Sci U S A 107:12357–12362.

Baranauskas G, Tkatch T, Nagata K, Yeh JZ, Surmeier DJ (2003) Kv3.4 subunits enhance the repolarizing efficiency of Kv3.1 channels in fast-spiking neurons. Nat Neurosci 6:258–266.

Barker RA, Barrett J, Mason SL, Björklund A (2013) Fetal dopaminergic transplantation trials and the future of neural grafting in Parkinson's disease. Lancet Neurol 12:84–91.

Barker RA, Parmar M, Studer L, Takahashi J (2017) Human Trials of Stem Cell-Derived Dopamine Neurons for Parkinson's Disease: Dawn of a New Era. Cell Stem Cell 21:569–573.

Baron MS, Vitek JL, Bakay RAE, Green J, Kaneoke Y, Hashimoto T, Turner RS, Woodard JL, Cole SA, McDonald WM, DeLong MR (1996) Treatment of advanced Parkinson's disease by posterior GPi pallidotomy: 1-Year results of a pilot study. Ann Neurol 40:355–366.

Barter JW, Castro S, Sukharnikova T, Rossi MA, Yin HH (2014) The role of the substantia nigra in posture control. Eur J Neurosci 39:1465–1473.

Barter JW, Li S, Sukharnikova T, Rossi MA, Bartholomew RA, Yin HH (2015) Basal ganglia outputs map instantaneous position coordinates during behavior. J Neurosci 35:2703–2716.

Basso MA, Wurtz RH (2002) Neuronal activity in substantia nigra pars reticulata during target selection. J Neurosci 22:1883–1894.

Baufreton J, Atherton JF, Surmeier DJ, Bevan MD (2005) Enhancement of excitatory synaptic integration by GABAergic inhibition in the subthalamic nucleus. J Neurosci 25:8505–8517.

Baufreton J, Kirkham E, Atherton JF, Menard A, Magill PJ, Bolam JP, Bevan MD (2009) Sparse but selective and potent synaptic transmission from the globus pallidus to the subthalamic nucleus. J Neurophysiol 102:532–545.

Bean BP (2007) The action potential in mammalian central neurons. Nat Rev Neurosci 8:451–465.

Benabid AL, Chabardes S, Mitrofanis J, Pollak P (2009) Deep brain stimulation of the subthalamic nucleus for the treatment of Parkinson's disease. Lancet Neurol 8:67–81.

Benarroch EE (2008) Subthalamic nucleus and its connections. Neurology:1991–1996.

Bennett BD, Callaway JC, Wilson CJ (2000) Intrinsic membrane properties underlying spontaneous tonic firing in neostriatal cholinergic interneurons. J Neurosci 20:8493–8503.

Berg D et al. (2015) MDS research criteria for prodromal Parkinson's disease. Mov Disord 30:1600–1611.

Bergman H, Wichmann T, Karmon B, DeLong MR (1994) The primate subthalamic nucleus. II. Neuronal activity in the MPTP model of parkinsonism. J Neurophysiol 72:507–520.

Berton O, Guigoni C, Li Q, Bioulac BH, Aubert I, Gross CE, DiLeone RJ, Nestler EJ, Bezard E (2009) Striatal Overexpression of ΔJunD Resets L-DOPA-Induced Dyskinesia in a Primate Model of Parkinson Disease. Biol Psychiatry 66:554–561.

Betarbet R, Sherer TB, MacKenzie G, Garcia-Osuna M, Panov A V., Greenamyre JT (2000) Chronic systemic pesticide exposure reproduces features of Parkinson's disease. Nat Neurosci 3:1301–1306.

Bevan MD, Atherton JF, Baufreton J (2006) Cellular principles underlying normal and pathological activity in the subthalamic nucleus. Curr Opin Neurobiol 16:621–628.

Bevan MD, Clarke NP, Bolam JP (1997) Synaptic integration of functionally diverse pallidal information in the entopeduncular nucleus and subthalamic nucleus in the rat. J Neurosci 17:308–324.

Bevan MD, Magill PJ, Hallworth NE, Bolam JP, Wilson CJ (2002a) Regulation of the timing and pattern of action potential generation in rat subthalamic neurons in vitro by GABA-A IPSPs. J Neurophysiol 87:1348–1362.

Bevan MD, Magill PJ, Terman D, Bolam JP, Wilson CJ (2002b) Move to the rhythm: Oscillations in the subthalamic nucleus-external globus pallidus network. Trends Neurosci 25:525–531.

Bevan MD, Smith AD, Bolam JP (1996) The substantia nigra as a site of synaptic integration of functionally diverse information arising from the ventral pallidum and the globus pallidus in the rat. Neuroscience 75:5–12.

Bezard E, Brotchie JM, Gross CE (2001) Pathophysiology of levodopa-induced dyskinesia: potential for new therapies. Nat Rev Neurosci 2:577–588.

Bézard E, Ferry S, Mach U, Stark H, Leriche L, Boraud T, Gross C, Sokoloff P (2003) Attenuation of levodopa-induced dyskinesia by normalizing dopamine D3 receptor function. Nat Med 9:762–767.

Bianchi L, Galeffi F, Bolam JP, Della Corte L (2003) The effect of 6-hydroxydopamine lesions on the release of amino acids in the direct and indirect pathways of the basal ganglia: A dual microdialysis probe analysis. Eur J Neurosci 18:856–868.

Biel M, Wahl-Schott C, Michalakis S, Zong X (2009) Hyperpolarization-activated cation channels: From genes to function. Physiol Rev 89:847–885.

Blandini F, Nappi G, Tassorelli C, Martignoni E (2000) Functional changes of the basal

ganglia circuitry in Parkinson's disease. Prog Neurobiol 62:63–88.

Blin O, Desnuelle C, Rascol O, Borg M, Paul HP Saint, Azulay JP, Billé F, Figarella D, Coulom F, Pellissier JF, Montastruc JL, Chatel M, Serratrice G (1994) Mitochondrial respiratory failure in skeletal muscle from patients with Parkinson's disease and multiple system atrophy. J Neurol Sci 125:95–101.

Bolam JP, Hanley JJ, Booth PAC, Bevan MD (2000) Synaptic organisation of the basal ganglia. J Anat 196:527–542.

Bonin RP, Labrakakis C, Eng DG, Whissell PD, Koninck Y De, Orser BA (2011) Pharmacological enhancement of δ-subunit-containing GABAA receptors that generate a tonic inhibitory conductance in spinal neurons attenuates acute nociception in mice. Pain 152:1317–1326.

Bonsi P, Cuomo D, Martella G, Madeo G, Schirinzi T, Puglisi F, Ponterio G, Pisani A (2011) Centrality of striatal cholinergic transmission in basal ganglia function. Front Neuroanat 5:1–9.

Bordia T, Perez XA, Heiss JE, Zhang D, Quik M (2016) Optogenetic activation of striatal cholinergic interneurons regulates L-dopa-induced dyskinesias. Neurobiol Dis 91:47–58.

Borgkvist A, Avegno EM, Wong MY, Kheirbek MA, Sonders MS, Hen R, Sulzer D (2015) Loss of Striatonigral GABAergic Presynaptic Inhibition Enables Motor Sensitization in Parkinsonian Mice. Neuron 87:976–988.

Bose A, Beal MF (2016) Mitochondrial dysfunction in Parkinson's disease. J Neurochem:216–231.

Bottcher J (1975) Morphology of the basal ganglia in Parkinson's disease. Acta Neurol Scand Suppl 62:1–87.

Boulet S, Lacombe E, Carcenac C, Feuerstein C, Sgambato-Faure V, Poupard A, Savasta M (2006) Subthalamic stimulation-induced forelimb dyskinesias are linked to an increase in glutamate levels in the substantia nigra pars reticulata. J Neurosci 26:10768–10776.

Bowery NG (2007) GABA-B receptor. xPharm Compr Pharmacol Ref:1–8.

Bowery NG, Hill DR, Hudson AL (1997) Characteristics of GABAB receptor binding sites on rat whole brain synaptic membranes. Br J Pharmacol 120:452–467.

Bowery NG, Hudson AL, Price GW (1987) GABAA and GABAB receptor site distribution in the rat central nervous system. Neuroscience 20:365–383.

Boyes J, Bolam JP (2003) The subcellular localization of GABA. Neuroscience 18:3279–3293.

Breit S, Bouali-Benazzouz R, Popa RC, Gasser T, Benabid AL, Benazzouz A (2007) Effects of 6-hydroxydopamine-induced severe or partial lesion of the nigrostriatal pathway on the neuronal activity of pallido-subthalamic network in the rat. Exp Neurol 205:36–47.

Breit S, Martin A, Lessmann L, Cerkez D, Gasser T, Schulz JB (2008) Bilateral changes in neuronal activity of the basal ganglia in the unilateral 6-hydroxydopamine rat model. J Neurosci Res 86:1388–1396.

Brickley SG, Mody I (2012) Extrasynaptic GABA A Receptors: Their Function in the CNS and Implications for Disease. Neuron 73:23–34.

Bright DP, Renzi M, Bartram J, McGee TP, MacKenzie G, Hosie AM, Farrant M, Brickley SG (2011) Profound desensitization by ambient GABA limits activation of δ-containing GABAA receptors during spillover. J Neurosci 31:753–763.

Brotchie JM (2005) Nondopaminergic mechanisms in levodopa-induced dyskinesia. Mov Disord 20:919–931.

Brown J, Pan WX, Dudman JT at. (2014) The inhibitory microcircuit of the substantia nigra provides feedback gain control of the basal ganglia output. Elife 3:e02397.

Burbaud P, Gross C, Benazzouz A, Coussemacq M, Bioulac B (1995) Reduction of apomorphine-induced rotational behaviour by subthalamic lesion in 6-OHDA lesioned rats is associated with a normalization of firing rate and discharge pattern of pars reticulata neurons. Exp Brain Res 105:48–58.

Cáceres-Chávez VA, Hernández-Martínez R, Pérez-Ortega J, Herrera-Valdez MA, Aceves JJ, Galarraga E, Bargas J (2018) Acute dopamine receptor blockade in substantia nigra pars reticulata: A possible model for drug-induced parkinsonism. J Neurophysiol 120:2922–2938.

Cajal SR (1911) Sistème Nerveux de l'homme & des vertébrés. Ed FRANÇAISE Rev MISE A JOUR PAR L'AUTEUR Meloine A, Paris.

Calabresi P, Di Filippo M, Ghiglieri V, Picconi B (2008) Molecular mechanism underlying levodopa-induced dyskinesia. Mov Disord 23:570–579.

Calabresi P, Filippo M Di, Ghiglieri V, Tambasco N, Picconi B (2010) Levodopa-induced dyskinesias in patients with Parkinson's disease: Filling the bench-to-bedside gap. Lancet Neurol 9:1106–1117.

Caraiscos VB, Elliott EM, You-Ten KE, Cheng VY, Belelli D, Newell JG, Jackson MF, Lambert JJ, Rosahl TW, Wafford KA, MacDonald JF, Orser BA (2004a) Tonic inhibition in mouse hippocampal CA1 pyramidal neurons is mediated by α5 subunit-containing γ-aminobutyric acid type A receptors. PNAS 101:3662–3667.

Caraiscos VB, Newell JG, You-Ten KE, Elliott EM, Rosahl TW, Wafford KA, MacDonald JF, Orser BA (2004b) Selective enhancement of tonic GABAergic inhibition in murine hippocampal neurons by low concentrations of the volatile anesthetic isoflurane. J Neurosci 24:8454–8458.

Carta M, Carlsson T, Kirik D, Björklund A (2007) Dopamine released from 5-HT terminals is the cause of L-DOPA-induced dyskinesia in parkinsonian rats. Brain 130:1819–1833.

Carter DA, Fibiger HC (1978) The projections of the entopeduncular nucleus and globus pallidus in rat as demonstrated by autoradiography and horseradish peroxidase

histochemistry. J Comp Neurol 177:113–123.

Cazorla M, DeCarvalho FD, Chohan MO, Shegda M, Chuhma N, Rayport S, Ahmari SE, Moore H, Kellendonk C (2014) Dopamine d2 receptors regulate the anatomical and functional balance of basal ganglia circuitry. Neuron 81:153–164.

Cebrián C, Parent A, Prensa L (2005) Patterns of axonal branching of neurons of the substantia nigra pars reticulata and pars lateralis in the rat. J Comp Neurol 492:349–369.

Cebrián C, Parent A, Prensa L (2007) The somatodendritic domain of substantia nigra pars reticulata projection neurons in the rat. Neurosci Res 57:50–60.

Cenci MA, Lundblad M (2007) Ratings of L -DOPA-Induced Dyskinesia in the Unilateral 6-OHDA Lesion Model of Parkinson's Disease in Rats and Mice . Curr Protoc Neurosci:1–23.

Cepeda C, André VM, Yamazaki I, Wu N, Kleiman-Weiner M, Levine MS (2008) Differential electrophysiological properties of dopamine D1 and D2 receptor-containing striatal medium-sized spiny neurons. Eur J Neurosci 27:671–682.

Chadha A, Dawson LG, Jenner PG, Duty S (1999) Effect of unilateral 6-hydroxydopamine lesions of the nigrostriatal pathway on GABA(A) receptor subunit gene expression in the rodent basal ganglia and thalamus. Neuroscience 95:119–126.

Chambers MS, Atack JR, Carling RW, Collinson N, Cook SM, Dawson GR, Ferris P, Hobbs SC, O'Connor D, Marshall G, Rycroft W, MacLeod AM (2004) An orally bioavailable, functionally selective inverse agonist at the benzodiazepine site of GABAA α5 receptors with cognition enhancing properties. J Med Chem 47:5829–5832.

Chan CS, Shigemoto R, Mercer JN, Surmeier DJ (2004) HCN2 and HCN1 channels govern the regularity of autonomous pacemaking and synaptic resetting in globus pallidus neurons. J Neurosci 24:9921–9932.

Chang et al. 2007 (2008) Age-Dependent Effect of Nitric Oxide on Subventricular Zone and Olfactory Bulb. J Comp Neurol 346:339–346.

Charara A, Heilman C, Levey AI, Smith Y (1999) Pre- and postsynaptic localization of GABA(B) receptors in the basal ganglia in monkeys. Neuroscience 95:127–140.

Chazalon M, Paredes-Rodriguez E, Morin S, Martinez A, Cristóvão-Ferreira S, Vaz S, Sebastiao A, Panatier A, Boué-Grabot E, Miguelez C, Baufreton J (2018) GAT-3 Dysfunction Generates Tonic Inhibition in External Globus Pallidus Neurons in Parkinsonian Rodents. Cell Rep 23:1678–1690.

Chen B, Xu C, Wang Y, Lin W, Wang Y, Chen L, Cheng H, Xu L, Hu T, Zhao J, Dong P, Guo Y, Zhang S, Wang S, Zhou Y, Hu W, Duan S, Chen Z (2020) A disinhibitory nigra-parafascicular pathway amplifies seizure in temporal lobe epilepsy. Nat Commun 11:923:1–16.

Chudomel O, Hasson H, Bojar M, Moshe SL, Galanopoulou AS (2015) Age- and Sex-

Related Characteristics of Tonic Gaba Currents in the Rat Substantia Nigra Pars Reticulata. Neurochem Res 40:747–757.

Chudomel O, Herman H, Nair K, Moshé SL, Galanopoulou AS (2009) Age- and gender-related differences in GABAA receptor-mediated postsynaptic currents in GABAergic neurons of the substantia nigra reticulata in the rat. Neuroscience 163:155–167.

Chuhma N, Tanaka KF, Hen R, Rayport S (2011) Functional connectome of the striatal medium spiny neuron. J Neurosci 31:1183–1192.

Ciliax BJ, Nash N, Heilman C, Sunahara R, Hartney A, Tiberi M, Rye DB, Caron MG, Niznik HB LA (2000) Dopamin D5 Receptor Immunocolocalization in Rat Brain and Monkey Brain. Synapse 37:125–145.

Clarkson AN, Huang BS, MacIsaac SE, Mody I, Carmichael ST (2010) Reducing excessive GABA-mediated tonic inhibition promotes functional recovery after stroke. Nature 468:305–309.

Coetzee WA, Amarillo Y, Chiu J, Chow A, Lau D, McCormack T, Moreno H, Nadal MS, Ozaita A, Pountney D, Saganich M, Vega-Saenz De Miera E, Rudy B (1999) Molecular diversity of K+ channels. Ann N Y Acad Sci 868:233–285.

Collinson N, Kuenzi FM, Jarolimek W, Maubach KA, Cothliff R, Sur C, Smith A, Otu FM, Howell O, Atack JR, McKernan RM, Seabrook GR, Dawson GR, Whiting PJ, Rosahl TW (2002) Enhanced learning and memory and altered GABAergic synaptic transmission in mice lacking the α5 subunit of the GABAA receptor. J Neurosci 22:5572–5580.

Collomb-Clerc A, Welter ML (2015) Effects of deep brain stimulation on balance and gait in patients with Parkinson's disease: A systematic neurophysiological review. Neurophysiol Clin 45:371–388.

Connelly WM, Schulz JM, Lees G, Reynolds JNJ (2010) Differential Short-Term Plasticity at Convergent Inhibitory Synapses to the Substantia Nigra Pars Reticulata. J Neurosci 30:14854–14861.

Cope DW, Di Giovanni G, Fyson SJ, Orbán G, Errington AC, Lrincz ML, Gould TM, Carter DA, Crunelli V (2009) Enhanced tonic GABA A inhibition in typical absence epilepsy. Nat Med 15:1392–1398.

Cope DW, Hughes SW, Crunelli V (2005) GABAA receptor-mediated tonic inhibition in thalamic neurons. J Neurosci 25:11553–11563.

Cossette M, Lévesque M, Parent A (1999) Extrastriatal dopaminergic innervation of human basal ganglia. Neurosci Res 34:51–54.

Cotzias GC, Papavasiliou PS GR (1969) Modification of parkinsonism - Chronic treatment with L-DOPA, Cotzias et al, 1969. N Engl J Med 280:337–345.

Cowan RL, Wilson CJ, Emson PC, Heizmann CW (1990) Parvalbumin-containing gabaergic interneurons in the rat neostriatum. J Comp Neurol 302:197–205.

Crestani F, Keist R, Fritschy JM, Benke D, Vogt K, Prut L, Blüthmann H, Möhler H, Rudolph U (2002) Trace fear conditioning involves hippocampal α5 GABAA receptors. Proc Natl Acad Sci U S A 99:8980–8985.

Crittenden JR, Cantuti-Castelvetri I, Saka E, Keller-McGandy CE, Hernandez LF, Kett LR, Young AB, Standaert DG, Graybiel AM (2009) Dysregulation of CalDAG-GEFI and CalDAG-GEFII predicts the severity of motor side-effects induced by anti-parkinsonian therapy. Proc Natl Acad Sci U S A 106:2892–2896.

Crossman AR (1987) Primate models of dyskinesia: The experimental approach to the study of basal ganglia-related involuntary movement disorders. Neuroscience 21:1–40.

Crossman AR, Mitchell IJ, Sambrook MA, Jackson A (1988) Chorea and myoclonus in the monkey induced by gamma-aminobutyric acid antagonism in the lentiform complex: The site of drug action and a hypothesis for the neural mechanisms of chorea. Brain 111:1211–1233.

Cui G, Jun SB, Jin X, Pham MD, Vogel SS, Lovinger DM, Costa RM (2013) Concurrent activation of striatal direct and indirect pathways during action initiation. Nature 494:238–242.

Cury RG, Barbosa ER, De Andrade DC (2015) Subthalamic nucleus deep brain stimulation in Parkinson disease. JAMA Neurol 72:948.

Cushman JD, Moore MD, Olsen RW, Fanselow MS (2014) The role of the δ GABA(A) receptor in ovarian cycle-linked changes in hippocampus-dependent learning and memory. Neurochem Res 39:1140–1146.

Da Prada M, Kettler R, Zurcher G, Schaffner R HW (1987) Inhibition of decarboxylase and levels of dopa and 3-o-methyldopa: a comparative study of benserazide versus carbidopa in rodents and of Madopar standard versus Madopar HBS in volunteers. Eur Neurol 27:9–20.

Darmopil S, Martín AB, De Diego IR, Ares S, Moratalla R (2009) Genetic Inactivation of Dopamine D1 but Not D2 Receptors Inhibits L-DOPA-Induced Dyskinesia and Histone Activation. Biol Psychiatry 66:603–613.

Das K, Benzil DL, Rovit RL, Murali R, Couldwell WT (1998) Irving S. Cooper (1922-1985): a pioneer in functional neurosurgery. J Neurosurg 89:865–873.

Dawson GR, Maubach KA, Collinson N, Cobain M, Everitt BJ, Macleod AM, Choudhury HI, Mcdonald LM, Pillai G, Rycroft W, Smith AJ, Sternfeld F, Tattersall FD, Wafford KA, Reynolds DS, Seabrook GR, Atack JR (2006) An Inverse Agonist Selective for ⌴ 5 Subunit-Containing GABA. J Pharmacol Exp Ther 316:1335–1345.

de Lau LML, Breteler MMB (2006) Epidemiology of Parkinson's disease. Lancet Neurol 5:525–535.

Deister CA, Chan CS, Surmeier DJ, Wilson CJ (2009) Calcium-activated SK channels influence voltage-gated ion channels to determine the precision of firing in globus pallidus neurons. J Neurosci 29:8452–8461.

Delaville C, Navailles S, Benazzouz A (2012) Effects of noradrenaline and serotonin depletions on the neuronal activity of globus pallidus and substantia nigra pars reticulata in experimental parkinsonism. Neuroscience 202:424–433.

DeLong MR (1990) Primate models of movement disorders of basal ganglia origin. Trends Neurosci 13:281–285.

DeLong MR, Crutcher MD, Georgopoulos AP (1983) Relations between movement and single cell discharge in the substantia nigra of the behaving monkey. J Neurosci 3:1599–1606.

DeLong MR, Wichmann T (2015) Basal ganglia circuits as targets for neuromodulation in Parkinson disease. JAMA Neurol 72:1354–1360.

Deniau JM, Chevalier G (1992) The lamellar organization of the rat substantia nigra pars reticulata: Distribution of projection neurons. Neuroscience 46:361–377.

Deniau JM, Hammond C, Riszk A, Feger J (1978) Electrophysiological properties of identified output neurons of the rat substantia nigra (pars compacta and pars reticulata): Evidences for the existence of branched neurons. Exp Brain Res 32:409–422.

Deniau JM, Mailly P, Maurice N, Charpier S (2007) The pars reticulata of the substantia nigra: a window to basal ganglia output. Prog Brain Res 160:151–172.

Deniau JM, Menetrey A, Charpier S (1996) The lamellar organization of the rat substantia nigra pars reticulata: Segregated patterns of striatal afferents and relationship to the topography of corticostriatal projections. Neuroscience 73:761–781.

Deransart C, Hellwig B, Heupel-Reuter M, Léger JF, Heck D, Lücking CH (2003) Single-unit Analysis of Substantia Nigra Pars Reticulata Neurons in Freely Behaving Rats with Genetic Absence Epilepsy. Epilepsia 44:1513–1520.

Dias V, Junn E, Mouradian MM (2013) The role of oxidative stress in parkinson's disease. J Parkinsons Dis 3:461–491.

Diaz MR, Vollmer CC, Zamudio-Bulcock PA, Vollmer W, Blomquist SL, Morton RA, Everett JC, Zurek AA, Yu J, Orser BA, Valenzuela CF (2014) Repeated intermittent alcohol exposure during the third trimester-equivalent increases expression of the GABAA receptor δ subunit in cerebellar granule neurons and delays motor development in rats. Neuropharmacology 79:262–274.

Dickson DW, Braak H, Duda JE, Duyckaerts C, Gasser T, Halliday GM, Hardy J, Leverenz JB, Del Tredici K, Wszolek ZK, Litvan I (2009) Neuropathological assessment of Parkinson's disease: refining the diagnostic criteria. Lancet Neurol 8:1150–1157.

Ding S, Li L, Zhou FM (2013) Presynaptic Serotonergic gating of the subthalamonigral glutamatergic projection. J Neurosci 33:4875–4885.

Ding S, Li L, Zhou FM (2015a) Robust presynaptic serotonin 5-HT1B receptor inhibition of the striatonigral output and its sensitization by chronic fluoxetine treatment. J

Neurophysiol 113:3397–3409.

Ding S, Li L, Zhou FM (2015b) Nigral dopamine loss induces a global upregulation of presynaptic dopamine D1 receptor facilitation of the striatonigral GABAergic output. J Neurophysiol 113:1697–1711.

Ding S, Matta SG, Zhou FM (2011a) Kv3-like potassium channels are required for sustained high-frequency firing in basal ganglia output neurons. J Neurophysiol 105:554–570.

Ding S, Wei W, Zhou FM (2011b) Molecular and functional differences in voltage-activated sodium currents between GABA projection neurons and dopamine neurons in the substantia nigra. J Neurophysiol 106:3019–3034.

Do MTH, Bean BP (2003) Subthreshold sodium currents and pacemaking of subthalamic neurons: Modulation by slow inactivation. Neuron 39:109–120.

Dodson PD, Larvin JT, Duffell JM, Garas FN, Doig NM, Kessaris N, Duguid IC, Bogacz R, Butt SJB, Magill PJ (2015) Distinct developmental origins manifest in the specialized encoding of movement by adult neurons of the external globus pallidus. Neuron 86:501–513.

Doshi PK (2011) Long-term surgical and hardware-related complications of deep brain stimulation. Stereotact Funct Neurosurg 89:89–95.

Drasbek KR, Hoestgaard-Jensen K, Jensen K (2007) Modulation of extrasynaptic THIP conductances by GABAa-receptor modulators in mouse neocortex. J Neurophysiol 97:2293–2300.

Drasbek KR, Jensen K (2006) THIP, a hypnotic and antinociceptive drug, enhances an extrasynaptic GABAA receptor-mediated conductance in mouse neocortex. Cereb Cortex 16:1134–1141.

Du Z, Tertrais M, Courtand G, Leste-Lasserre T, Cardoit L, Masmejean F, Halgand C, Cho YH, Garret M (2017) Differential alteration in expression of striatal GABAA R subunits in mouse models of huntington's disease. Front Mol Neurosci 10:1–16.

Dudman JT, Gerfen CR (2015) The Basal Ganglia.

Dupuis JP, Feyder M, Miguelez C, Garcia L, Morin S, Choquet D, Hosy E, Bezard E, Fisone G, Bioulac BH, Baufreton J (2013) Dopamine-dependent long-term depression at subthalamo-nigral synapses is lost in experimental parkinsonism. J Neurosci 33:14331–14341.

Durkin MM, Smith KE, Borden LA, Weinshank RL, Branchek TA, Gustafson EL (1995) Localization of messenger RNAs encoding three GABA transporters in rat brain: an in situ hybridization study. Mol Brain Res 33:7–21.

Dybdal D, Forcelli PA, Dubach M, Oppedisano M, Holmes A, Malkova L, Gale K (2013) Topography of dyskinesias and torticollis evoked by inhibition of substantia nigra pars reticulata. Mov Disord 28:460–468.

Eid L, Parent M (2016) Chemical anatomy of pallidal afferents in primates. Brain Struct

Funct 221:4291–4317.

Erlij D, Acosta-García J, Rojas-Márquez M, González-Hernández B, Escartín-Perez E, Aceves J, Florán B (2012) Dopamine D4 receptor stimulation in GABAergic projections of the globus pallidus to the reticular thalamic nucleus and the substantia nigra reticulata of the rat decreases locomotor activity. Neuropharmacology 62:1111–1118.

Errington AC, Cope DW, Crunelli V (2011) Augmentation of tonic GABAA inhibition in absence epilepsy: Therapeutic value of inverse agonists at extrasynaptic GABAA receptors. Adv Pharmacol Sci 2011.

Etherington LA, Mihalik B, Pálvölgyi A, Ling I, Pallagi K, Kertész S, Varga P, Gunn BG, Brown AR, Livesey MR, Monteiro O, Belelli D, Barkóczy J, Spedding M, Gacsályi I, Antoni FA, Lambert JJ (2017) Selective inhibition of extra-synaptic α5-GABAA receptors by S44819, a new therapeutic agent. Neuropharmacology 125:353–364.

F. Hernández L, Castela I, Ruiz-DeDiego I, Obeso JA, Moratalla R (2017) Striatal activation by optogenetics induces dyskinesias in the 6-hydroxydopamine rat model of Parkinson disease. Mov Disord 32:530–537.

Fahn S (2008) The history of dopamine and levodopa in the treatment of Parkinson's disease. Mov Disord 23.

Fahn S (2015) The medical treatment of Parkinson disease from James Parkinson to George Cotzias. Mov Disord 30:4–18.

Falowski SM, Ooi YC, Bakay RAE (2015) Long-Term Evaluation of Changes in Operative Technique and Hardware-Related Complications with Deep Brain Stimulation. Neuromodulation 18:670–676.

Fan D, Rossi MA, Yin HH (2012) Mechanisms of action selection and timing in substantia nigra neurons. J Neurosci 32:5534–5548.

Farrant M, Nusser Z (2005) Variations on an inhibitory theme: Phasic and tonic activation of GABA A receptors. Nat Rev Neurosci 6:215–229.

Faynveitz A, Lavian H, Jacob A, Korngreen A (2019) Proliferation of Inhibitory Input to the Substantia Nigra in Experimental Parkinsonism. Front Cell Neurosci 13:1–11.

Fedchyshyn MJ, Wang LY (2005) Developmental transformation of the release modality at the calyx of held synapse. J Neurosci 25:4131–4140.

Ferreira M, Massano J (2017) An updated review of Parkinson's disease genetics and clinicopathological correlations. Acta Neurol Scand 135:273–284.

Feyder M, Bonito-Oliva A, Fisone G (2011) L-DOPA-induced dyskinesia and abnormal signaling in striatal medium spiny neurons: Focus on dopamine D1 receptor-mediated transmission. Front Behav Neurosci 5:1–11.

Ficalora AS, Mize RR (1989) The neurons of the substantia nigra and zona incerta which project to the cat superior colliculus are GABA immunoreactive: A double-label study using GABA immunocytochemistry and lectin retrograde transport.

Neuroscience 29:567–581.

Fieblinger T, Graves SM, Sebel LE, Alcacer C, Plotkin JL, Gertler TS, Chan CS, Heiman M, Greengard P, Cenci MA, Surmeier DJ (2014) Cell type-specific plasticity of striatal projection neurons in parkinsonism and L-DOPA-induced dyskinesia. Nat Commun 5:1–15.

Fink-Jensen A, Suzdak PD, Swedberg MDB, Judge ME, Hansen L, Nielsen PG (1992) The γ-aminobutyric acid (GABA) uptake inhibitor, tiagabine, increases extracellular brain levels of GABA in awake rats. Eur J Pharmacol 220:197–201.

Foley PB, Macquarie BSH, Würzburg MA (2001) Beans , roots and leaves A History of the Chemical Therapy of Parkinsonism by. Therapy.

Fox SH, Chuang R, Brotchie JM (2009) Serotonin and Parkinson's disease: On movement, mood, and madness. Mov Disord 24:1255–1266.

Fox SH, Katzenschlager R, Lim SY, Ravina B, Seppi K, Coelho M, Poewe W, Rascol O, Goetz CG, Sampaio C (2011) The movement disorder society evidence-based medicine review update: Treatments for the motor symptoms of Parkinson's disease. Mov Disord 26:2–41.

Freed CR, Greene PE, Breeze RE, Tsai W-Y, Dumouchel W (2010) Transplantation of Embryonic Dopamine Neurons for Severe. N Engl J Med 344:710–719.

Freeze BS, Kravitz A V., Hammack N, Berke JD, Kreitzer AC (2013) Control of basal ganglia output by direct and indirect pathway projection neurons. J Neurosci 33:18531–18539.

Freitas ME, Fox SH (2016) Nondopaminergic treatments for Parkinson's disease: current and future prospects. Neurodegener Dis Manag 6:249–268.

Friend DM, Kravitz A V. (2014) Working together: Basal ganglia pathways in action selection. Trends Neurosci 37:301–303.

Fujiyama F, Nakano T, Matsuda W, Furuta T, Udagawa J, Kaneko T (2016) A single-neuron tracing study of arkypallidal and prototypic neurons in healthy rats. Brain Struct Funct 221:4733–4740.

Fujiyama F, Stephenson FA, Bolam JP (2002) Synaptic localization of GABAA receptor subunits in the substantia nigra of the rat: Effects of quinolinic acid lesions of the striatum. Eur J Neurosci 15:1961–1975.

Gagnon D, Petryszyn S, Sanchez MG, Bories C, Beaulieu JM, De Koninck Y, Parent A, Parent M (2017) Striatal Neurons Expressing D1 and D2 Receptors are Morphologically Distinct and Differently Affected by Dopamine Denervation in Mice. Sci Rep 7:9–17.

Galvan A, Wichmann T (2008) Pathophysiology of Parkinsonism. Clin Neurophysiol 119:1459–1474.

Garant DS, Xu SG, Sperber EF, Moshé SL (1995) Age-Related Differences in the Effects of GABA, Agonists Microinjected Into Rat Substantia Nigra: Pro- and

Anticonvulsant Actions. Epilepsia 36:960–965.

Gauthier J, Parent M, Lévesque M, Parent A (1999) The axonal arborization of single nigrostriatal neurons in rats. Brain Res 834:228–232.

George S, Rey NL, Reichenbach N, Steiner JA, Brundin P (2013) α-Synuclein: The long distance runner. Brain Pathol 23:350–357.

Gerashchenko D, Blanco-Centurion CA, Miller JD, Shiromani PJ (2006) Insomnia following hypocretin2-saporin lesions of the substantia nigra. Neuroscience 137:29–36.

Gerfen CR, Engber TM, Mahan LC, Susel Z, Chase TN, Monsma FJ SD (1990) D1 and D2 dopamine receptor-regulated gene expression of striatonigral and striatopallidal neurons. Science (80-) 250:1429–1432.

Gerfen CR (1985) The neostriatal mosaic. I. compartmental organization of projections from the striatum to the substantia nigra in the rat. J Comp Neurol 236:454–476.

Gerfen CR, Surmeier DJ (2011) Modulation of Striatal Projection Systems by Dopamine. Annu Rev Neurosci 34:441–466.

Gertler TS, Chan CS, Surmeier DJ (2008) Dichotomous anatomical properties of adult striatal medium spiny neurons. J Neurosci 28:10814–10824.

Girasole AE, Lum MY, Nathaniel D, Bair-Marshall CJ, Guenthner CJ, Luo L, Kritzer AC NA (2018) A Subpopulation of Striatal Neurons Mediates Levodopa- Induced Dyskinesia. Neuron 97(4):787–795.

Gittis AH, Hang GB, LaDow ES, Shoenfeld LR, Atallah B V., Finkbeiner S, Kreitzer AC (2011) Rapid target-specific remodeling of fast-spiking inhibitory circuits after loss of dopamine. Neuron 71:858–868.

Gittis AH, Kreitzer AC (2012) Striatal microcircuitry and movement disorders. Trends Neurosci 35:557–564.

Glykys J, Mann EO, Mody I (2008) Which GABAA receptor subunits are necessary for tonic inhibition in the hippocampus? J Neurosci 28:1421–1426.

Goedert M, Compston A (2018) Parkinson's disease - The story of an eponym. Nat Rev Neurol 14:57–63.

Golbe LI (1991) Young-onset parkinson's disease: A clinical review. Neurology 41:168–173.

González-Hernández T, Rodríguez M (2000) Compartmental organization and chemical profile of dopaminergic and GABAergic neurons in the substantia nigra of the rat. J Comp Neurol 421:107–135.

Grace AA, Onn SP (1989) Morphology and electrophysiological properties of immunocytochemistry identified rat dopamine neurons recorded in vitro. J Neurosci 9:3463–3481.

Gratwicke J, Zrinzo L, Kahan J, Peters A, Beigi M, Akram H, Hyam J, Oswal A, Day B,

Mancini L, Thornton J, Yousry T, Limousin P, Hariz M, Jahanshahi M, Foltynie T (2018) Bilateral deep brain stimulation of the nucleus basalis of meynert for Parkinson disease dementia a randomized clinical trial. JAMA Neurol 75:169–178.

Graybiel AM, Smith KS (2014) Good habits, bad habits. Sci Am 310:38–43.

Grofova I, Deniau JM, Kitai ST (1982) Morphology of the substantia nigra pars reticulata projection neurons intracellularly labeled with HRP. J Comp Neurol 208:352–368.

Gu M, Owen AD, Toffa SEK, Cooper JM, Dexter DT, Jenner P, Marsden CD, Schapira AHV (1998) Mitochondrial function, GSH and iron in neurodegeneration and Lewy body diseases. J Neurol Sci 158:24–29.

Gulley JM, Kuwajima M, Mayhill E, Rebec G V. (1999) Behavior-related changes in the activity of substantia nigra pars reticulata neurons in freely moving rats. Brain Res 845:68–76.

Gulley JM, Reed JL, Kuwajima M, Rebec G V. (2004) Amphetamine-induced behavioral activation is associated with variable changes in basal ganglia output neurons recorded from awake, behaving rats. Brain Res 1012:108–118.

Guzman JN, Sánchez-Padilla J, Chan CS, Surmeier DJ (2009) Robust pacemaking in substantia nigra dopaminergic neurons. J Neurosci 29:11011–11019.

Haas RH, Nasirian F, Nakano K, Ward D, Pay M, Hill R, Shults CW (1995) Low platelet mitochondrial complex I and complex II/III activity in early untreated parkinson's disease. Ann Neurol 37:714–722.

Haber SN, Knutson B (2010) The reward circuit: Linking primate anatomy and human imaging. Neuropsychopharmacology 35:4–26.

Halje P, Tamtè M, Richter U, Mohammed M, Angela Cenci M, Petersson P (2012) Levodopa-induced dyskinesia is strongly associated with resonant cortical oscillations. J Neurosci 32:16541–16551.

Halliday GM, Holton JL, Revesz T, Dickson DW (2011) Neuropathology underlying clinical variability in patients with synucleinopathies. Acta Neuropathol 122:187–204.

Hamani C, Saint-Cyr JA, Fraser J, Kaplitt M, Lozano AM (2004) The subthalamic nucleus in the context of movement disorders. Brain 127:4–20.

Hardman CD, McRitchie DA, Halliday GM, Cartwright HR, Morris JGL (1996) Substantia nigra pars reticulata neurons in Parkinson's disease. Neurodegeneration 5:49–55.

Hassani OK, Mouroux M, Féger J (1996) Increased subthalamic neuronal activity after nigral dopaminergic lesion independent of disinhibition via the globus pallidus. Neuroscience 72:105–115.

Haynes WIA, Haber SN (2013) The organization of prefrontal-subthalamic inputs in primates provides an anatomical substrate for both functional specificity and integration: Implications for basal ganglia models and deep brain stimulation. J Neurosci 33:4804–4814.

Hegeman DJ, Hong ES, Hernández VM, Chan CS (2016) The external globus pallidus: Progress and perspectives. Eur J Neurosci 43:1239–1265.

Hernandez LF, Kubota Y, Hu D, Howe MW, Lemaire N, Graybiel AM (2013) Selective effects of dopamine depletion and L-DOPA therapy on learning-related firing dynamics of striatal neurons. J Neurosci 33:4782–4795.

Hernández VM, Hegeman DJ, Cui Q, Kelver DA, Fiske MP, Glajch KE, Pitt JE, Huang TY, Justice NJ, Savio Chan C (2015) Parvalbumin + neurons and Npas1 + neurons are distinct neuron classes in the mouse external globus pallidus. J Neurosci 35:11830–11847.

Hidalgo-Figueroa M, Bonilla S, Gutiérrez F, Pascual A, López-Barneo J (2012) GDNF is predominantly expressed in the PV+ neostriatal interneuronal ensemble in normal mouse and after injury of the nigrostriatal pathway. J Neurosci 32:864–872.

Hikosaka O (2007) GABAergic output of the basal ganglia. Prog Brain Res 160:209–226.

Hikosaka O, Kim HF, Amita H, Yasuda M, Isoda M, Tachibana Y, Yoshida A (2019) Direct and indirect pathways for choosing objects and actions. Eur J Neurosci 49:637–645.

Hikosaka O, Kim HF, Yasuda M, Yamamoto S (2014) Basal Ganglia Circuits for Reward Value–Guided Behavior. Annu Rev Neurosci 37:289–306.

Hikosaka O, Takikawa Y, Kawagoe R (2000) Role of the basal ganglia in the control of purposive saccadic eye movements. Physiol Rev 80:953–978.

Hirsch EC, Hunot S (2009) Neuroinflammation in Parkinson's disease: a target for neuroprotection? Lancet Neurol 8:382–397.

Holper L, Ben-Shachar D, Mann J (2019) Multivariate meta-analyses of mitochondrial complex I and IV in major depressive disorder, bipolar disorder, schizophrenia, Alzheimer disease, and Parkinson disease. Neuropsychopharmacology 44:837–849.

Hontanilla B, Parent A, Giménez-Amaya JM (1997) Parvalbumin and calbindin D-28k in the entopeduncular nucleus, subthalamic nucleus, and substantia nigra of the rat as revealed by double- immunohistochemical methods. Synapse 25:359–367.

Hutchison WD, Levy R, Dostrovsky JO, Lozano AM, Lang AE (1997) Effects of apomorphine on globus pallidus neurons in parkinsonian patients. Ann Neurol 42:767–775.

Hyland BI, Reynolds JNJ, Hay J, Perk CG, Miller R (2002) Firing modes of midbrain dopamine cells in the freely moving rat. Neuroscience 114:475–492.

Ibáñez-Sandoval O, Carrillo-Reid L, Galarraga E, Tapia D, Mendoza E, Gomora JC, Aceves J, Bargas J (2007) Bursting in substantia nigra pars reticulata neurons in vitro: Possible relevance for Parkinson disease. J Neurophysiol 98:2311–2323.

Ibañez-Sandoval O, Hernández A, Florán B, Galarraga E, Tapia D, Valdiosera R, Erlij D, Aceves J, Bargas J (2006) Control of the subthalamic innervation of substantia nigra pars reticulata by D1 and D2 dopamine receptors. J Neurophysiol 95:1800–1811.

Inchul P, Amano N, Satoda T, Murata T, Kawagishi S, Yoshino K, Tanaka K (2005) Control of oro-facio-lingual movements by the substantia nigra pars reticulata: High-frequency electrical microstimulation and GABA microinjection findings in rats. Neuroscience 134:677–689.

Jackman SL, Beneduce BM, Drew IR, Regehr WG (2014) Achieving High-Frequency Optical Control of Synaptic Transmission. 34:7704–7714.

Jankovic J, Lai E, Ben-Arie L, Krauss JK, Grossman R (1999) Levodopa-induced dyskinesias treated by pallidotomy. J Neurol Sci 167:62–67.

Jin XT, Galvan A, Wichmann T, Smith Y (2011) Localization and function of GABA transporters GAT-1 and GAT-3 in the basal ganglia. Front Syst Neurosci 5:1–10.

Jones KA et al. (1998) GABA(B) receptors function as a heteromeric assembly of the subunits GABA(B)R1 and GABA(B)R2. Nature 396:674–679.

Kang MG, Nuriya M, Guo Y, Martindale KD, Lee DZ, Huganir RL (2012) Proteomic analysis of α-amino-3-hydroxy-5-methyl-4-isoxazole propionate receptor complexes. J Biol Chem 287:28632–28645.

Katz J, Nielsen KM, Soghomonian JJ (2005) Comparative effects of acute or chronic administration of levodopa to 6-hydroxydopamine-lesioned rats on the expression of glutamic acid decarboxylase in the neostriatum and GABAA receptors subunits in the substantia nigra, pars reticulata. Neuroscience 132:833–842.

Kaupmann K, Malitschek B, Schuler V, Heid J, Froestl W, Beck P, Mosbacher J, Bischoff S, Kulik A, Shigemoto R, Karschin A, Bettler B (1998) GABA(B)-receptor subtypes assemble into functional heteromeric complexes. Nature 396:683–687.

Kaushik S, Cuervo AM (2015) Proteostasis and aging. Nat Med 21:1406–1415.

Kawaguchi Y (1993) Physiological, morphological, and histochemical characterization of three classes of interneurons in rat neostriatum. J Neurosci 13:4908–4923.

Kawaguchi Y, Wilson CJ, Emson PC (1990) Projection subtypes of rat neostriatal matrix cells revealed by intracellular injection of biocytin. J Neurosci 10:3421–3438.

Keifman E, Ruiz-DeDiego I, Pafundo DE, Paz RM, Solís O, Murer MG, Moratalla R (2019) Optostimulation of striatonigral terminals in substantia nigra induces dyskinesia that increases after L-DOPA in a mouse model of Parkinson's disease. Br J Pharmacol 176:2146–2161.

Kha et al. 2001, Halat TJ, El-Maghrabi R, O'Neal MH (2001) Projections from the substantia nigra pars reticulata to the motor thalamus of the rat: Single axon reconstructions and immunohistochemical study. J Comp Neurol 440:20–30.

Kim H, Kim M, Im S-K, Fang S (2018) Mouse Cre-LoxP system: general principles to

determine tissue-specific roles of target genes. Lab Anim Res 34:147.

Kincaid AE, Albin RL, Newman SW, Penney JB, Young AB (1992) 6-Hydroxydopamine lesions of the nigrostriatal pathway alter the expression of glutamate decarboxylase messenger RNA in rat globus pallidus projection neurons. Neuroscience 51:705–718.

Kirkeby A, Grealish S, Wolf DA, Nelander J, Wood J, Lundblad M, Lindvall O, Parmar M (2012) Generation of Regionally Specified Neural Progenitors and Functional Neurons from Human Embryonic Stem Cells under Defined Conditions. Cell Rep 1:703–714.

Kita H, Kitai ST (1987) Efferent projections of the subthalamic nucleus in the rat: Light and electron microscopic analysis with the PHA-L method. J Comp Neurol 260:435–452.

Kita H, Kitai ST (1991) Intracellular study of rat globus pallidus neurons: membrane properties and responses to neostriatal, subthalamic and nigral stimulation. Brain Res 564:296–305.

Kita H, Tokuno H, Nambu A (1999) Monkey globus pallidus external segment neurons projecting to the neostriatum. Neuroreport 10:1467–1472.

Kliem MA, Pare JF, Khan ZU, Wichmann T, Smith Y (2010) Ultrastructural localization and function of dopamine D1-like receptors in the substantia nigra pars reticulata and the internal segment of the globus pallidus of parkinsonian monkeys. Eur J Neurosci 31:836–851.

Koós T, Tepper JM (1999) Inhibitory control of neostriatal projection neurons by GABAergic interneurons. Nat Neurosci 2:467–472.

Koyama S, Appel SB (2006) A-type K+ current of dopamine and GABA neurons in the ventral tegmental area. J Neurophysiol 96:544–554.

Krack P, Limousin P, Benabid AL, Pollak P (1997) Chronic stimulation of subthalamic nucleus improves levodopa-induced dyskinesias in Parkinson's disease. Lancet 350:1676.

Krause M, Fogel W, Heck A, Hacke W, Bonsanto M, Trenkwalder C, Tronnier V (2001) Deep brain stimulation for the treatment of Parkinson's disease: Subthalamic nucleus versus globus pallidus internus. J Neurol Neurosurg Psychiatry 70:464–470.

Kravitz A V., Freeze BS, Parker PRL, Kay K, Thwin MT, Deisseroth K, Kreitzer AC (2010) Regulation of parkinsonian motor behaviours by optogenetic control of basal ganglia circuitry. Nature 466:622–626.

Kriks S, Shim JW, Piao J, Ganat YM, Wakeman DR, Xie Z, Carrillo-Reid L, Auyeung G, Antonacci C, Buch A, Yang L, Beal MF, Surmeier DJ, Kordower JH, Tabar V, Studer L (2011) Dopamine neurons derived from human ES cells efficiently engraft in animal models of Parkinson's disease. Nature 480:547–551.

Kuhn DM, Arthur RE, Thomas DM, Elferink LA (1999) Tyrosine hydroxylase is

inactivated by catechol-quinones and converted to a redox-cycling quinoprotein: Possible relevance to Parkinson's disease. J Neurochem 73:1309–1317.

Lacey MG, Mercuri NB, North RA (1989) Two cell types in rat substantia nigra zona compacta distinguished by membrane properties and the actions of dopamine and opioids. J Neurosci 9:1233–1241.

Lacombe E, Khaindrava V, Melon C, Oueslati A, Kerkerian-Le Goff L, Salin P (2009) Different functional basal ganglia subcircuits associated with anti-akinetic and dyskinesiogenic effects of antiparkinsonian therapies. Neurobiol Dis 36:116–125.

Laitinen L V., Bergenheim AT, Hariz MI (1992) Leksell's posteroventral pallidotomy in the treatment of Parkinson's disease. J Neurosurg 76:53–61.

Lanciego JL, Luquin N, Obeso JA (2012) Functional neuroanatomy of the basal ganglia. Cold Spring Harb Perspect Med 2.

Langston J, Ballard P, Tetrud J, Irwin I (1983) Chronic Parkinsonism in humans due to a product of meperidine-analog synthesis. Science (80-) 219:979–980.

Laprade N, Soghomonian JJ (1999) Gene expression of the GAD67 and GAD65 isoforms of glutamate decarboxylase is differentially altered in subpopulations of striatal neurons in adult rats lesioned with 6-OHDA as neonates. Synapse 33:36–48.

Lavian H, Almog M, Madar R, Loewenstern Y, Bar-Gad I, Okun E, Korngreen A (2017) Dopaminergic modulation of synaptic integration and firing patterns in the rat entopeduncular nucleus. J Neurosci 37:7177–7187.

Lavian H, Korngreen A (2016) Inhibitory short-term plasticity modulates neuronal activity in the rat entopeduncular nucleus in vitro. Eur J Neurosci 43:870–884.

Lee CR, Tepper JM. (2007) A calcium-activated nonselective cation conductance underlies the plateau potential in rat substantia nigra GABAergic neurons. J Neurosci 27:6531–6541.

Lee J Il, Shin HJ, Nan DH, Kim JS, Hong SC, Shin HJ, Park K, Eoh W, Kim JH, Lee WY (2001) Increased burst firing in substantia nigra pars reticulata neurons and enhanced response to selective D2 agonist in hemiparkinsonian rats after repeated administration of apomorphine. J Korean Med Sci 16:636–642.

Lee V, Maguire J (2014) The impact of tonic GABAA receptor-mediated inhibition on neuronal excitability varies across brain region and cell type. Front Neural Circuits 8:1–27.

Liang CL, Sinton CM, German DC (1996) Midbrain dopaminergic neurons in the mouse: Co-localization with calbindin-D(28K) and calretinin. Neuroscience 75:523–533.

Liu D, Li W, Ma C, Zheng W, Yao Y, Tso CF, Zhong P, Chen X, Song JH, Choi W, Paik S-B, Han H, Dan Y (2020) A common hub for sleep and motor control in the substantia nigra. Science (80-) 367:440–445.

Lobb CJ, Jaeger D (2015) Bursting activity of substantia nigra pars reticulata neurons

in mouse parkinsonism in awake and anesthetized states. Neurobiol Dis 75:177–185.

Lu B, Su Y, Das S, Liu J, Xia J, Ren D (2007) The Neuronal Channel NALCN Contributes Resting Sodium Permeability and Is Required for Normal Respiratory Rhythm. Cell 129:371–383.

Lundblad M, Picconi B, Lindgren H, Cenci MA (2004) A model of L-DOPA-induced dyskinesia in 6-hydroxydopamine lesioned mice: Relation to motor and cellular parameters of nigrostriatal function. Neurobiol Dis 16:110–123.

Luo R, Partridge JG, Vicini S (2013) Distinct roles of synaptic and extrasynaptic GABAAreceptors in striatal inhibition dynamics. Front Neural Circuits 7:1–7.

Lutas A, Birnbaumer L, Yellen G (2014) Metabolism regulates the spontaneous firing of substantia nigra pars reticulata neurons via KATPand nonselective cation channels. J Neurosci 34:16336–16347.

Lutas A, Lahmann C, Soumillon M, Yellen G (2016) The leak channel NALCN controls tonic firing and glycolytic sensitivity of substantia nigra pars reticulata neurons. Elife 5:1–19.

M von K, Y S, JP B, AD S (1992) From the Striatum and the Globus Pallidus Onto Neurons in the Substantia Nigra and Retrorubral Field Which Project To the. 50:531–549.

Maccaferri G, McBain CJ (1996) The hyperpolarization-activated current (I(h)) and its contribution to pacemaker activity in rat CA1 hippocampal stratum oriens-alveus interneurones. J Physiol 497:119–130.

MacLeod NK, Ryman A, Arbuthnott GW (1990) Electrophysiological properties of nigrothalamic neurons after 6-hydroxydopamine lesions in the rat. Neuroscience 38:447–456.

Magill PJ, Bolam JP, Bevan MD (2001) Dopamine modulates the impact of the cerebral cortex on the Subthalamic nucelus-Globus Pallidus network. Neuroscience 106:313–330.

Maguire J, Ferando I, Simonsen C, Mody I (2009) Excitability changes related to GABAA receptor plasticity during pregnancy. J Neurosci 29:9592–9601.

Maguire J, Mody I (2008) GABAAR Plasticity during Pregnancy: Relevance to Postpartum Depression. Neuron 59:207–213.

Mahlknecht P, Seppi K, Poewe W (2015) The concept of prodromal Parkinson's disease. J Parkinsons Dis 5:681–697.

Mailly P, Charpier S, Mahon S, Menetrey A, Thierry AM, Glowinski J, Deniau JM (2001) Dendritic arborizations of the rat substantia nigra pars reticulata neurons: Spatial organization and relation to the lamellar compartmentation of striato-nigral projections. J Neurosci 21:6874–6888.

Mailly P, Charpier S, Menetrey A, Deniau JM (2003) Three-dimensional organization of

the recurrent axon collateral network of the substantia nigra pars reticulata neurons in the rat. J Neurosci 23:5247–5257.

Mallet N, Delgado L, Chazalon M, Miguelez C, Baufreton J (2019) Cellular and Synaptic Dysfunctions in Parkinson's Disease: Stepping out of the Striatum. Cells 8:1005.

Mallet N, Le Moine C, Charpier S, Gonon F (2005) Feedforward inhibition of projection neurons by fast-spiking GABA interneurons in the rat striatum in vivo. J Neurosci 25:3857–3869.

Mallet N, Micklem BR, Henny P, Brown MT, Williams C, Bolam JP, Nakamura KC, Magill PJ (2012) Dichotomous Organization of the External Globus Pallidus. Neuron 74:1075–1086.

Mallet N, Schmidt R, Leventhal D, Chen F, Amer N, Boraud T, Berke JD (2016) Arkypallidal Cells Send a Stop Signal to Striatum. Neuron 89:308–316.

Mango D, Bonito-Oliva A, Ledonne A, Nisticò R, Castelli V, Giorgi M, Sancesario G, Fisone G, Berretta N, Mercuri NB (2014) Phosphodiesterase 10A controls D1-mediated facilitation of GABA release from striato-nigral projections under normal and dopamine-depleted conditions. Neuropharmacology 76:127–136.

Marsden CD, Obeso JA (1994) The functions of the basal ganglia and the paradox of stereotaxic surgery in parkinson's disease. Brain 117:877–897.

Martin LJ, Bonin RP, Orser BA (2009) The physiological properties and therapeutic potential of α5-GABAA receptors. Biochem Soc Trans 37:1334–1337.

Martina M, Jonas P (1997) Functional differences in Na+ channel gating between fast-spiking interneurones and principal neurones of rat hippocampus. J Physiol 505:593–603.

Martínez-Murillo R, Villalba RM, Rodrigo J (1989) Electron microscopic localization of cholinergic terminals in the rat substantia nigra: An immunocytochemical study. Neurosci Lett 96:121–126.

Martinez A, Cristovao-ferreira S, Paredes-rodriguez E, Boue-grabot E (n.d.) Cell Reports GAT-3 dysfunction generates tonic inhibition in external globus pallidus neurons in Parkinsonian rodents.

Mastro et al. 2014 (2017) Cell-Specific Pallidal Intervention Induces Long-Lasting Motor Recovery in Dopamine Depleted Mice. Physiol Behav 176:139–148.

Mastro KJ, Bouchard RS, Holt HAK, Gittis AH (2014) Transgenic mouse lines subdivide external segment of the globus pallidus (GPe) neurons and reveal distinct GPe output pathways. J Neurosci 34:2087–2099.

Matsuda W, Furuta T, Nakamura KC, Hioki H, Fujiyama F, Arai R, Kaneko T (2009) Single nigrostriatal dopaminergic neurons form widely spread and highly dense axonal arborizations in the neostriatum. J Neurosci 29:444–453.

Maurice N, Thierry AM, Glowinski J, Deniau JM (2003) Spontaneous and Evoked Activity of Substantia Nigra Pars Reticulata Neurons during High-Frequency

Stimulation of the Subthalamic Nucleus. J Neurosci 23:9929–9936.

McGeer PL, Itagaki S, Boyes BE, McGeer EG (1988) Reactive microglia are positive for HLA-DR in the: Substantia nigra of Parkinson's and Alzheimer's disease brains. Neurology 38:1285–1291.

McRitchie DA, Hardman CD, Halliday GM (1996) Cytoarchitectural distribution of calcium binding proteins in midbrain dopaminergic regions of rats and humans. J Comp Neurol 364:121–150.

Meera P, Wallner M, Otis TS (2011) Molecular basis for the high THIP/gaboxadol sensitivity of extrasynaptic GABA A receptors. J Neurophysiol 106:2057–2064.

Meissner W, Ravenscroft P, Reese R, Harnack D, Morgenstern R, Kupsch A, Klitgaard H, Bioulac B, Gross CE, Bezard E, Boraud T (2006) Increased slow oscillatory activity in substantia nigra pars reticulata triggers abnormal involuntary movements in the 6-OHDA-lesioned rat in the presence of excessive extracelullar striatal dopamine. Neurobiol Dis 22:586–598.

Mela F, Marti M, Dekundy A, Danysz W, Morari M, Cenci MA (2007) Antagonism of metabotropic glutamate receptor type 5 attenuates L-DOPA-induced dyskinesia and its molecular and neurochemical correlates in a rat model of Parkinson's disease. J Neurochem 101:483–497.

Mena-Segovia J, Winn P, Bolam JP (2008) Cholinergic modulation of midbrain dopaminergic systems. Brain Res Rev 58:265–271.

Mendez MA, Horder J, Myers J, Coghlan S, Stokes P, Erritzoe D, Howes O, Lingford-Hughes A, Murphy D, Nutt D (2013) The brain GABA-benzodiazepine receptor alpha-5 subtype in autism spectrum disorder: A pilot [11C]Ro15-4513 positron emission tomography study. Neuropharmacology 68:195–201.

Mercer JN, Chan CS, Tkatch T, Held J, Surmeier DJ (2007) Nav1.6 sodium channels are critical to pacemaking and fast spiking in globus pallidus neurons. J Neurosci 27:13552–13566.

Mercuri NB, Bernardi G (2005) The 'magic' of L-dopa: Why is it the gold standard Parkinson's disease therapy? Trends Pharmacol Sci 26:341–344.

Mercuri NB, Bonci A, Calabresi P, Stefani A, Bernardi G (1995) Properties of the Hyperpolarization-activated Cation Current Ih in Rat Midbrain Dopaminergic Neurons. Eur J Neurosci 7:462–469.

Merello M, Balej J, Delfino M, Cammarota A, Betti O, Leiguarda R (1999) Apomorphine induces changes in GPi spontaneous outflow in patients with Parkinson's disease. Mov Disord 14:45–49.

Middleton FA, Strick PL (2000) Basal ganglia and cerebellar loops: Motor and cognitive circuits. Brain Res Rev 31:236–250.

Miguelez C, Morin S, Martinez A, Goillandeau M, Bezard E, Bioulac B, Baufreton J (2012) Altered pallido-pallidal synaptic transmission leads to aberrant firing of globus pallidus neurons in a rat model of Parkinson's disease. J Physiol 590:5861–

5875.

Milosevic J, Schwarz SC, Ogunlade V, Meyer AK, Storch A, Schwarz J (2009) Emerging role of LRRK2 in human neural progenitor cell cycle progression, survival and differentiation. Mol Neurodegener 4:25:1–9.

Mink JW (1996) The Basal Ganglia: Focused selection and inhibition of competing motor programs. Prog Neurobiol 50:381–425.

Miyamoto Y, Fukuda T (2015) Immunohistochemical study on the neuronal diversity and three-dimensional organization of the mouse entopeduncular nucleus. Neurosci Res 94:37–49.

Miyazaki T, Lacey MG (1998) Presynaptic inhibition by dopamine of a discrete component of GABA release in rat substantia nigra pars reticulata. J Physiol 513:805–817.

Mizuno Y, Suzuki K, Ohta S (1990) Postmortem changes in mitochondrial respiratory enzymes in brain and a preliminary observation in Parkinson's disease. J Neurol Sci 96:49–57.

Monteggia LM, Eisch AJ, Tang MD, Kaczmarek LK, Nestler EJ (2000) Cloning and localization of the hyperpolarization-activated cyclic nucleotide-gated channel family in rat brain. Mol Brain Res 81:129–139.

Monville C, Torres EM, Pekarik V, Lane EL, Dunnett SB (2009) Genetic, temporal and diurnal influences on L-dopa-induced dyskinesia in the 6-OHDA model. Brain Res Bull 78:248–253.

Moore MD, Cushman J, Chandra D, Homanics GE, Olsen RW, Fanselow MS (2010) Trace and contextual fear conditioning is enhanced in mice lacking the α4 subunit of the GABAA receptor. Neurobiol Learn Mem 93:383–387.

Mori-Kawakami F, Kobayashi K, Takahashi T (2003) Developmental decrease in synaptic facilitation at the mouse hippocampal mossy fibre synapse. J Physiol 553:37–48.

Morris et al. 2012 (2012) 基因的改变NIH Public Access. Bone 23:1–7.

Moshé SL, Brown LL, Kubová H, Velíšková J, Zukin RS, Sperber EF (1994) Maturation and segregation of brain networks that modify seizures. Brain Res 665:141–146.

Mrzljak L, Bergson C, Pappy M, Huff R, Levenson R, Goldman-Rakic PS (1996) Localization of dopamine D4 receptors in GABAergic neurons of the primate brain. Nature 381:245–248.

Müller T (2015) Catechol-O-methyltransferase inhibitors in Parkinson's disease. Drugs 75:157–174.

Murer MG, Moratalla R (2011) Striatal signaling in L-DOPA-induced dyskinesia: Common mechanisms with drug abuse and long term memory involving D1 dopamine receptor stimulation. Front Neuroanat 5:1–12.

Murer MG, Riquelme LA, Tseng KY, Pazo JH (1997) Substantia nigra pars reticulata

single unit activity in normal and 60HDA-lesioned rats: Effects of intrastriatal apomorphine and subthalamic lesions. Synapse 27:278–293.

Nagai T, McGeer PL, McGeer EG (1983) Distribution of GABA-T-Intensive neurons in the hat forebrain and midbrain. J Comp Neurol 218:220–238.

Nagatomo K, Suga S, Saitoh M, Kogawa M, Kobayashi K, Yamamoto Y, Yamada K (2017) Dopamine D1 receptor immunoreactivity on fine processes of GFAP-positive astrocytes in the substantia nigra pars reticulata of adult mouse. Front Neuroanat 11:1–11.

Nakanishi H, Kita H, Kitai ST (1987) Intracellular study of rat substantia nigra pars reticulata neurons in an in vitro slice preparation: electrical membrane properties and response characteristics to subthalamic stimulation. Brain Res 437:45–55.

Nambu A (2007) Globus pallidus internal segment. Prog Brain Res 160:135–150.

Nambu A, Tokuno H, Takada M (2002) Functional significance of the cortico-subthalamo-pallidal 'hyperdirect' pathway. Neurosci Res 43:111–117.

Navailles S, Bioulac B, Gross C, De Deurwaerdère P (2010) Serotonergic neurons mediate ectopic release of dopamine induced by l-DOPA in a rat model of Parkinson's disease. Neurobiol Dis 38:136–143.

Navarro JF, Burón E, Martín-López M (2002) Anxiogenic-like activity of L-655,708, a selective ligand for the benzodiazepine site of GABAA receptors which contain the alpha-5 subunit, in the elevated plus-maze test. Prog Neuro-Psychopharmacology Biol Psychiatry 26:1389–1392.

Nevet A, Morris G, Saban G, Fainstein N, Bergman H (2004) Discharge rate of substantia nigra pars reticulata neurons is reduced in non-Parkinsonian monkeys with apomorphine-induced orofacial dyskinesia. J Neurophysiol 92:1973–1981.

Ng CH, Wang XS, Ong WY (2000) A light and electron microscopic study of the GABA transporter GAT-3 in the monkey basal ganglia and brainstem. J Neurocytol 29:595–603.

Ng TKY, Yung KKL (2000) Distinct cellular distribution of GABA(B)R1 and GABA(A)α1 receptor immunoreactivity in the rat substantia nigra. Neuroscience 99:65–76.

Ng TKY, Yung KKL (2001) Subpopulations of neurons in rat substantia nigra display GABABR2 receptor immunoreactivity. Brain Res 920:210–216.

Nicholas AP, Lubin FD, Hallett PJ, Vattem P, Ravenscroft P, Bezard E, Zhou S, Fox SH, Brotchie JM, Sweatt JD, Standaert DG (2008) Striatal histone modifications in models of levodopa-induced dyskinesia. J Neurochem 106:486–494.

Nicholson LFB, Faull RLM, Waldvogel HJ, Dragunow M (1992) The regional, cellular and subcellular localization of GABAA/benzodiazepine receptors in the substantia nigra of the rat. Neuroscience 50:355–370.

Nikam S, Nikam P, Ahaley SK, Sontakke A V. (2009) Oxidative stress in Parkinson's disease. Indian J Clin Biochem 24:98–101.

Nilsson MH, Törnqvist AL, Rehncrona S (2005) Deep-brain stimulation in the subthalamic nuclei improves balance performance in patients with Parkinson's disease, when tested without anti-parkinsonian medication. Acta Neurol Scand 111:301–308.

Notomi T, Shigemoto R (2004) Immunohistochemical Localization of Ih Channel Subunits, HCN1-4, in the Rat Brain. J Comp Neurol 471:241–276.

Nusser Z, Cull-Candy S, Farrant M (1997) Differences in synaptic GABA(A) receptor number underlie variation in GABA mini amplitude. Neuron 19:697–709.

Nusser Z, Sieghart W, Somogyi P (1998) Segregation of different GABA(A) receptors to synaptic and extrasynaptic membranes of cerebellar granule cells. J Neurosci 18:1693–1703.

Nutt J.G (2001) Levodopa, motor fluctuations and dyskinesia in Parkinson's disease. Park Relat Disord 8:101–108.

O'Regan G, Desouza RM, Balestrino R, Schapira AH (2017) Glucocerebrosidase Mutations in Parkinson Disease. J Parkinsons Dis 7:411–422.

Obeso JA, Rodríguez-Oroz MC, Benitez-Temino B, Blesa FJ, Guridi J, Marin C, Rodriguez M (2008) Functional organization of the basal ganglia: Therapeutic implications for Parkinson's disease. Mov Disord 23:548–559.

Obeso JA, Rodríguez-Oroz MC, Rodríguez M, Arbizu J, Giménez-Amaya JM (2002) The basal ganglia and disorders of movement: Pathophysiological mechanisms. News Physiol Sci 17:51–55.

Ochi M, Shiozaki S, Kase H (2004) L-DOPA-Induced Modulation of GABA and Glutamate Release in Substantia Nigra Pars Reticulata in a Rodent Model of Parkinson's Disease. Synapse 52:163–165.

Oh YM, Karube F, Takahashi S, Kobayashi K, Takada M, Uchigashima M, Watanabe M, Nishizawa K, Kobayashi K, Fujiyama F (2017) Using a novel PV-Cre rat model to characterize pallidonigral cells and their terminations. Brain Struct Funct 222:2359–2378.

Olanow CW, Stern MB SK (2009) The scientific and clinical basis for the treatment of Parkinson disease (2009). Neurology 72:S1–S136.

Olanow CW, Goetz CG, Kordower JH, Stoessl AJ, Sossi V, Brin MF, Shannon KM, Nauert GM, Perl DP, Godbold J, Freeman TB (2003) A double-blind controlled trial of bilateral fetal nigral transplantation in Parkinson's disease. Ann Neurol 54:403–414.

Olanow CW, Obeso JA, Stocchi F (2006) Continuous dopamine-receptor treatment of Parkinson's disease: scientific rationale and clinical implications. Lancet Neurol 5:677–687.

Olmos-Serrano JL, Corbin JG, Burns MP (2011) The GABA A receptor agonist THIP ameliorates specific behavioral deficits in the mouse model of fragile X syndrome. Dev Neurosci 33:395–403.

Olsen RW, Sieghart W (2009) GABAA receptors: Subtypes provide diversity of function and pharmacology. Neuropharmacology 56:141–148.

Oorschot DE (1996) Total number of neurons in the neostriatal, pallidal, subthalamic, and substantia nigral nuclei of the rat basal ganglia: A stereological study using the cavalieri and optical disector methods. J Comp Neurol 366:580–599.

Ottersen OP, Storm-Mathisen J (1984) Glutamate- and GABA-containing neurons in the mouse and rat brain, as demonstrated with a new immunocytochemical technique. J Comp Neurol 229:374–392.

Oueslati A, Sgambato-Faure V, Melon C, Kachidian P, Gubellini P, Amri M, Goff LK Le, Salin P (2007) High-frequency stimulation of the subthalamic nucleus potentiates L-DOPA-induced neurochemical changes in the striatum in a rat model of Parkinson's disease. J Neurosci 27:2377–2386.

Overstreet LS, Westbrook GL (2003) Synapse density regulates independence at unitary inhibitory synapses. J Neurosci 23:2618–2626.

Ozaita A, Martone ME, Ellisman MH, Rudy B (2002) Differential subcellular localization of the two alternatively spliced isoforms of the Kv3.1 potassium channel subunit in brain. J Neurophysiol 88:394–408.

Paladini CA, Tepper JM (1999) GABA(A) and GABA(B) antagonists differentially affect the firing pattern of substantia nigra dopaminergic neurons in vivo. Synapse 32:165–176.

Pan HS, Penney JB, Young AB (1985) γ-Aminobutyric Acid and Benzodiazepine Receptor Changes Induced by Unilateral 6-Hydroxydopamine Lesions of the Medial Forebrain Bundle. J Neurochem 45:1396–1404.

Papa SM, Desimone R, Fiorani M, Oldfield EH (1999) Internal globus pallidus discharge is nearly suppressed during levodopa- induced dyskinesias. Ann Neurol 46:732–738.

Parent A, Hazrati LN (1995) Functional anatomy of the basal ganglia. II. The place of subthalamic nucleus and external pallidium in basal ganglia circuitry. Brain Res Rev 20:128–154.

Périer C, Marin C, Jimenez A, Bonastre M, Tolosa E, Hirsch EC (2003) Effect of subthalamic nucleus or entopeduncular nucleus lesion on levodopa-induced neurochemical changes within the basal ganglia and on levodopa-induced motor alterations in 6-hydroxydopamine-lesioned rats. J Neurochem 86:1328–1337.

Picconi B, Centonze D, Håkansson K, Bernardi G, Greengard P, Fisone G, Cenci MA, Calabresi P (2003) Loss of bidirectional striatal synaptic plasticity in L-DOPA-induced dyskinesia. Nat Neurosci 6:501–506.

Pierre SR, Lemmens MAM, Figueiredo-Pereira ME (2009) Subchronic infusion of the product of inflammation prostaglandin J2 models sporadic Parkinson's disease in mice. J Neuroinflammation 6:1–12.

Pinna A, Volpini R, Cristalli G, Morelli M (2005) New adenosine A2A receptor

antagonists: Actions on Parkinson's disease models. Eur J Pharmacol 512:157–164.

Pirker et al. (2000) GABAA Receptors: Immunocytochemical distribution of 13 subunits in the adult rat brain. Neuroscience 101:815–850.

Pirttimaki T, Parri HR, Crunelli V (2013) Astrocytic GABA transporter GAT-1 dysfunction in experimental absence seizures. J Physiol 591:823–833.

Poewe W, Seppi K, Tanner CM, Halliday GM, Brundin P, Volkmann J, Schrag AE, Lang AE (2017) Parkinson disease. Nat Rev Dis Prim 3:1–21.

Postuma RB, Berg D, Stern M, Poewe W, Olanow CW, Oertel W, Obeso J, Marek K, Litvan I, Lang AE, Halliday G, Goetz CG, Gasser T, Dubois B, Chan P, Bloem BR, Adler CH, Deuschl G (2015) MDS clinical diagnostic criteria for Parkinson's disease. Mov Disord 30:1591–1601.

Qiu MH, Vetrivelan R, Fuller PM, Lu J (2010) Basal ganglia control of sleep-wake behavior and cortical activation. Eur J Neurosci 31:499–507.

Quirk K, Blurton P, Fletcher S, Leeson P, Tang F, Mellilo D, Ragan CI, McKernan RM (1996) [3H]L-655,708, a novel ligand selective for the benzodiazepine site of GABA(A) receptors which contain the α5 subunit. Neuropharmacology 35:1331–1335.

Radnikow G, Misgeld U (1998) Dopamine D1 receptors facilitate GABAA synaptic currents in the rat substantia nigra pars reticulata. J Neurosci 18:2009–2016.

Rajakumar N, Elisevich K, Flumerfelt BA (1994) Parvalbumin-containing GABAergic neurons in the basal ganglia output system of the rat. J Comp Neurol 350:324–336.

Ramanathan S, Tkatch T, Atherton JF, Wilson CJ, Bevan MD (2008) D2-like dopamine receptors modulate SKCa channel function in subthalamic nucleus neurons through inhibition of Cav2.2 channels. J Neurophysiol 99:442–459.

Rangel-Barajas C, Silva I, García-Ramírez M, Sánchez-Lemus E, Floran L, Aceves J, Erlij D, Florán B (2008) 6-OHDA-induced hemiparkinsonism and chronic l-DOPA treatment increase dopamine D1-stimulated [3H]-GABA release and [3H]-cAMP production in substantia nigra pars reticulata of the rat. Neuropharmacology 55:704–711.

Rascol O, Brooks DJ, Melamed E, Oertel W, Poewe W, Stocchi F, Tolosa E (2005) Rasagiline as an adjunct to levodopa in patients with Parkinson's disease and motor fluctuations (LARGO, Lasting effect in Adjunct therapy with Rasagiline Given Once daily, study): A randomised, double-blind, parallel-group trial. Lancet 365:947–954.

Ravizza T, Friedman LK, Moshé SL, Velíšková J (2003) Sex differences in GABAAergic system in rat substantia nigra pars reticulata. Int J Dev Neurosci 21:245–254.

Redgrave P, Marrow L, Dean P (1992) Topographical organization of the nigrotectal projection in rat: Evidence for segregated channels. Neuroscience 50:571–595.

Reichel JM, Nissel S, Rogel-Salazar G, Mederer A, Käfer K, Bedenk BT, Martens H, Anders R, Grosche J, Michalski D, Härtig W, Wotjak CT (2015) Distinct behavioral consequences of short-term and prolonged GABAergic depletion in prefrontal cortex and dorsal hippocampus. Front Behav Neurosci 8:1–16.

Reiner A, Anderson KD (1993) Co-occurrence of γ-aminobutyric acid, parvalbumin and the neurotensin-related neuropeptide LANT6 in pallidal, nigral and striatal neurons in pigeons and monkeys. Brain Res 624:317–325.

Rice ME, Patel JC (2015) Somatodendritic dopamine release: Recent mechanistic insights. Philos Trans R Soc B Biol Sci 370:1–14.

Richards CD, Shiroyama T, Kitai ST (1997) Electrophysiological and immunocytochemical characterization of GABA and dopamine neurons in the substantia nigra of the rat. Neuroscience 80:545–557.

Rizzi G, Tan KR (2019) Synergistic Nigral Output Pathways Shape Movement. Cell Rep 27:2184-2198.e4.

Robertson GS, Robertson HA (1989) Evidence that L-dopa-induced rotational behavior is dependent on both striatal and nigral mechanisms. J Neurosci 9:3326–3331.

Rodríguez Díaz M, Barroso-Chinea P, Acevedo A, González-Hernández T (2003) Effects of dopaminergic cell degeneration on electrophysiological characteristics and GAD65/GAD67 expression in the substantia nigra: Different action on GABA cell subpopulations. Mov Disord 18:254–266.

Rodríguez M, González-Hernández T (1999) Electrophysiological and morphological evidence for a GABAergic nigrostriatal pathway. J Neurosci 19:4682–4694.

Rohlfs A, Nikkhah G, Rosenthal C, Rundfeldt C, Brandis A, Samii M, Löscher W (1997) Hemispheric asymmetries in spontaneous firing characteristics of substantia nigra pars reticulata neurons following a unilateral 6- hydroxydopamine lesion of the rat nigrostriatal pathway. Brain Res 761:352–356.

Rottach A, Kremmer E, Nowak D, Boisguerin P, Volkmer R, Cardoso MC, Leonhardt H, Rothbauer U (2008) Generation and characterization of a rat monoclonal antibody specific for PCNA. Hybridoma 27:91–98.

Rudolph U, Möhler H (2014) GABA A Receptor Subtypes: Therapeutic Potential in Down Syndrome, Affective Disorders, Schizophrenia, and Autism . Annu Rev Pharmacol Toxicol 54:483–507.

Rudy B, McBain CJ (2001) Kv3 channels: Voltage-gated K+ channels designed for high-frequency repetitive firing. Trends Neurosci 24:517–526.

Sakamoto M, Hikosaka O (1989) Eye movements induced by microinjection of GABA agonist in the rat substantia nigra pars reticulata. Neurosci Res 6:216–233.

Salin P, López IP, Kachidian P, Barroso-Chinea P, Rico AJ, Gómez-Bautista V, Coulon P, Kerkerian-Le Goff L, Lanciego JL (2009) Changes to interneuron-driven striatal microcircuits in a rat model of Parkinson's disease. Neurobiol Dis 34:545–552.

Salin P, Manrique C, Forni C, Kerkerian-Le Goff L (2002) High-Frequency Stimulation of the Subthalamic Nucleus Selectively Reverses Dopamine Denervation-Induced Cellular Defects in the Output Structures of the Basal Ganglia in the Rat. J Neurosci 22:5137–5148.

Sanderson P, Mavoungou R, Albe-Fessard D (1986) Changes in substantia nigra pars reticulata activity following lesions of the substantia nigra pars compacta. Neurosci Lett 67:25–30.

Sano H, Chiken S, Hikida T, Kobayashi K, Nambu A (2013) Signals through the striatopallidal indirect pathway stop movements by phasic excitation in the substantia nigra. J Neurosci 33:7583–7594.

Sano H, Nambu A (2019) The effects of zonisamide on L-DOPA–induced dyskinesia in Parkinson's disease model mice. Neurochem Int 124:171–180.

Sano T (1910) Beitrag zur vergleichenden anatomie der substantia nigra, des corpus luysii und der zona incerta. Eur Neurol 27:274–283.

Santini E, Valjent E, Usiello A, Carta M, Borgkvist A, Girault JA, Hervé D, Greengard P, Fisone G (2007) Critical involvement of cAMP/DARPP-32 and extracellular signal-regulated protein kinase signaling in L-DOPA-induced dyskinesia. J Neurosci 27:6995–7005.

Santoro B, Chen S, Lüthi A, Pavlidis P, Shumyatsky GP, Tibbs GR, Siegelbaum SA (2000) Molecular and functional heterogeneity of hyperpolarization-activated pacemaker channels in the mouse CNS. J Neurosci 20:5264–5275.

Sarkar J, Wakefield S, MacKenzie G, Moss SJ, Maguire J (2011) Neurosteroidogenesis is required for the physiological response to stress: Role of neurosteroid-sensitive GABA A receptors. J Neurosci 31:18198–18210.

Sauer B (1998) Inducible Gene Targeting in Mice Using the Cre/lox System. A Companion to Methods Enzymol 392:381–392.

Saunders A, Huang KW, Sabatini BL (2016) Globus Pallidus Externus Neurons Expressing parvalbumin Interconnect the Subthalamic Nucleus and Striatal Interneurons. PLoS One 11:1–20.

Saunders A, Macosko EZ, Wysoker A, Goldman M, Krienen FM, de Rivera H, Bien E, Baum M, Bortolin L, Wang S, Goeva A, Nemesh J, Kamitaki N, Brumbaugh S, Kulp D, McCarroll SA (2018) Molecular Diversity and Specializations among the Cells of the Adult Mouse Brain. Cell 174:1015-1030.e16.

Saunders A, Oldenburg IA, Berezovskii VK, Johnson CA, Kingery ND, Elliott HL, Xie T, Gerfen CR, Sabatini BL (2015) A direct GABAergic output from the basal ganglia to frontal cortex. Nature 521:85–89.

Schapira AHV (2007) Mitochondrial dysfunction in Parkinson's disease. Cell Death Differ 14:1261–1266.

Schumacher JM, Ellias SA, Palmer EP, Kott HS, Dinsmore J, Dempsey PK, Fischman AJ, Thomas C, Feldman RG, Kassissieh S, Raineri R, Manhart C, Penney D, Fink

JS, Isacson O (2000) Transplantation of embryonic porcine mesencephalic tissue in patients with PD. Neurology 54:1042–1050.

Schwarzer C, Berresheim U, Pirker S, Wieselthaler A, Fuchs K, Sieghart W, Sperk G (2001) Distribution of the major γ-aminobutyric acidA receptor subunits in the basal ganglia and associated limbic brain areas of the adult rat. J Comp Neurol 433:526–549.

Scimemi A (2014) Structure,function,and plasticity of GABA transporters. Front Cell Neurosci 8:1–14.

Scimemi A, Semyanov A, Sperk G, Kullmann DM, Walker MC (2005) Multiple and plastic receptors mediate tonic GABAA receptor currents in the hippocampus. J Neurosci 25:10016–10024.

Seeger-Armbruster S, Von Ameln-Mayerhofer A (2013) Short- and long-term unilateral 6-hydroxydopamine lesions in rats show different changes in characteristics of spontaneous firing of substantia nigra pars reticulata neurons. Exp Brain Res 224:15–24.

Segura-Aguilar J, Paris I, Muñoz P, Ferrari E, Zecca L, Zucca FA (2014) Protective and toxic roles of dopamine in Parkinson's disease. J Neurochem 129:898–915.

Semyanov A, Walker MC, Kullmann DM (2003) GABA uptake regulates cortical excitability via cell type-specific tonic inhibition. Nat Neurosci 6:484–490.

Semyanov A, Walker MC, Kullmann DM, Silver RA (2004) Tonically active GABAA receptors: Modulating gain and maintaining the tone. Trends Neurosci 27:262–269.

Seutin V, Engel D (2010) Differences in Na+ conductance density and Na+ channel functional properties between dopamine and GABA neurons of the rat substantia nigra. J Neurophysiol 103:3099–3114.

Shade KTC, Platzer B, Washburn N, Mani V, Bartsch YC, Conroy M, Pagan JD, Bosques C, Mempel TR, Fiebiger E, Anthony RM (2015) A single glycan on IgE is indispensable for initiation of anaphylaxis. J Exp Med 212:457–467.

Shen KZ, Johnson SW (2006) Subthalamic stimulation evokes complex EPSCs in the rat substantia nigra pars reticulata in vitro. J Physiol 573:697–709.

Shepard PD, Bunney BS (1991) Repetitive firing properties of putative dopamine-containing neurons in vitro: regulation by an apamin-sensitive Ca2+-activated K+ conductance. Exp Brain Res 86:141–150.

Sierra H, Cordova M, Chen CSJ, Rajadhyaksha M (2015) Confocal imaging-guided laser ablation of basal cell carcinomas: An ex vivo study. J Invest Dermatol 135:612–615.

Simmons et al. 2020 (2013) Indirect Pathway Control of Firing Rate and Pattern in the Substantia Nigra pars Reticulata. J Chem Inf Model 53:1689–1699.

Simpson EH, Kellendonk C, Kandel E (2010) A Possible Role for the Striatum in the

Pathogenesis of the Cognitive Symptoms of Schizophrenia. Neuron 65:585–596.

Smith Y, Bevan MD, Shink E, Bolam JP (1998) Microcircuitry of the direct and indirect pathways of the basal ganglia. Neuroscience 86:353–387.

Smith Y, Bolam JP (1989) Neurons of the substantia nigra reticulata receive a dense GABA-containing input from the globus pallidus in the rat. Brain Res 493:160–167.

Smith Y, Bolam JP (1991) Convergence of synaptic inputs from the striatum and the globus pallidus onto identified nigrocollicular cells in the rat: A double anterograde labelling study. Neuroscience 44:45–73.

Smith Y, Bolam JP, von Krosigk M (1990a) Topographical and Synaptic Organization of the GABA-Containing Pallidosubthalamic Projection in the Rat. Eur J Neurosci 2:500–511.

Smith Y, Galvan A, Ellender TJ, Doig N, Villalba RM, Huerta-Ocampo I, Wichmann T, Bolam JP (2014) The thalamostriatal system in normal and diseased states. Front Syst Neurosci 8:1–18.

Smith Y, Hazrati L -N, Parent A (1990b) Efferent projections of the subthalamic nucleus in the squirrel monkey as studied by the PHA-L anterograde tracing method. J Comp Neurol 294:306–323.

Smith Y, Parent A (1988) Neurons of the subthalamic nucleus in primates display glutamate but not GABA immunoreactivity. Brain Res 453:353–356.

Smith Y, Séguéla P, Parent A (1987) Distribution of gaba-immunoreactive neurons in the thalamus of the squirrel monkey (Saimiri sciureus). Neuroscience 22:579–591.

Sparta DR, Stamatakis AM, Phillips JL, Hovelsø N, Van Zessen R, Stuber GD (2012) Construction of implantable optical fibers for long-term optogenetic manipulation of neural circuits. Nat Protoc 7:12–23.

Starr PA, Vitek JL BA (1999) Ablative surgery and deep brain stimulation for parkinson's disease. Neurosurgery 43:989–1013.

Stefani A, Lozano AM, Peppe A, Stanzione P, Galati S, Tropepi D, Pierantozzi M, Brusa L, Scarnati E, Mazzone P (2007) Bilateral deep brain stimulation of the pedunculopontine and subthalamic nuclei in severe Parkinson's disease. Brain 130:1596–1607.

Stell BM, Brickley SG, Tang CY, Farrant M, Mody I (2003) Neuroactive steroids reduce neuronal excitability by selectively enhancing tonic inhibition mediated by δ subunit-containing GABAA receptors. Neuroscience 100:14439–14444.

Stephenson-Jones M, Yu K, Ahrens S, Tucciarone JM, Van Huijstee AN, Mejia LA, Penzo MA, Tai LH, Wilbrecht L, Li B (2016) A basal ganglia circuit for evaluating action outcomes. Nature 539:289–293.

Sullivan KL, Ward CL, Hauser RA, Zesiewicz TA (2007) Prevalence and treatment of non-motor symptoms in Parkinson's disease. Park Relat Disord 13:545.

Sulzer D, Zecca L (1999) Intraneuronal dopamine-quinone synthesis: A review.

Neurotox Res 1:181–195.

Tai C-H, Boraud T, Bezard E, Bioulac B, Gross C, Benazzouz A (2003) Electrophysiological and metabolic evidence that high-frequency stimulation of the subthalamic nucleus bridles neuronal activity in the subthalamic nucleus and the substantia nigra reticulata. FASEB J 0892-6638/:1820–1830.

Takakusaki K, Saitoh K, Harada H, Kashiwayanagi M (2004) Role of basal ganglia-brainstem pathways in the control of motor behaviors. Neurosci Res 50:137–151.

Tanibuchi I, Kitano H, Jinnai K (2009) Substantia nigra output to prefrontal cortex via thalamus in monkeys. II. Activity of thalamic relay neurons in delayed conditional go/no-go discrimination task. J Neurophysiol 102:2946–2954.

Taverna S, Canciani B, Pennartz CMA (2007) Membrane properties and synaptic connectivity of fast-spiking interneurons in rat ventral striatum. Brain Res 1152:49–56.

Tepper JM (2010) GABAergic Interneurons of the Striatum. Elsevier Inc.

Tepper JM, Martin LP, Anderson DR (1995) GABA(A) receptor-mediated inhibition of rat substantia nigra dopaminergic neurons by pars reticulata projection neurons. J Neurosci 15:3092–3103.

Tepper M, Lee CR (2007a) Morphological and Physiological Properties of Parvalbumin- and Calretinin-Containing -Aminobutyric Acidergic Neurons in the Substantia Nigra. J Comp Neurol 500:958–972.

Tepper M, Lee CR (2007b) GABAergic control of substantia nigra dopaminergic neurons. Prog Brain Res 160:189–208.

Tiroshi L, Goldberg JA (2019) Population dynamics and entrainment of basal ganglia pacemakers are shaped by their dendritic arbors. PLoS Comput Biol 15:1–29.

Trevitt J, Carlson B, Correa M, Keene A, Morales M, Salamone J (2002) Interactions between dopamine D1 receptors and γ-aminobutyric acid mechanisms in substantia nigra pars reticulata of the rat: Neurochemical and behavioral studies. Psychopharmacology (Berl) 159:229–237.

Tseng KY, Kasanetz F, Kargieman L, Pazo JH, Murer MG, Riquelme LA (2001) Subthalamic nucleus lesions reduce low frequency oscillatory firing of substantia nigra pars reticulata neurons in a rat model of Parkinson's disease. Brain Res 904:93–103.

Tsumori T, Yokota S, Ono K, Yasui Y (2003) Nigrothalamostriatal and nigrothalamocortical pathways via the ventrolateral parafascicular nucleus. Neuroreport 14:81–86.

Veliskova et al. 1998, Kubová H, Friedman LK, Wu R, Sperber EF, Zukin RS, Moshé SL (1998) The expression of GABAA receptor subunits in the substantia nigra is developmentally regulated and region-specific. Ital J Neurol Sci 19:205–210.

Vila M, Périer C, Féger J, Yelnik J, Faucheux B, Ruberg M, Raisman-Vozari R, Agid Y,

Hirsch EC (2000) Evolution of changes in neuronal activity in the subthalamic nucleus of rats with unilateral lesion of the substantia nigra assessed by metabolic and electrophysiological measurements. Eur J Neurosci 12:337–344.

Volkmann J, Sturm V, Weiss P, Kappler J, Voges J, Koulousakis A, Lehrke R, Hefter H, Freund HJ (1998) Bilateral high-frequency stimulation of the internal globus pallidus in advanced Parkinson's disease. Ann Neurol 44:953–961.

von Krosigk M, Smith Y, Bolam JP, Smith AD (1992) Synaptic organization of gabaergic inputs from the striatum and the globus pallidus onto neurons in the substantia nigra and retrorubral field which project to the medullary reticular formation. Neuroscience 50:531–549.

Wallace ML, Saunders A, Huang KW, Philson AC, Goldman M, Macosko EZ, McCarroll SA, Sabatini BL (2017) Genetically Distinct Parallel Pathways in the Entopeduncular Nucleus for Limbic and Sensorimotor Output of the Basal Ganglia. Neuron 94:138-152.e5.

Walters JR, Hu D, Itoga CA, Parr-Brownlie LC, Bergstrom DA (2007) Phase relationships support a role for coordinated activity in the indirect pathway in organizing slow oscillations in basal ganglia output after loss of dopamine. Neuroscience 144:762–776.

Wang Y, Zhang QJ, Liu J, Ali U, Gui ZH, Hui YP, Chen L, Wang T (2010) Changes in firing rate and pattern of GABAergic neurons in subregions of the substantia nigra pars reticulata in rat models of Parkinson's disease. Brain Res 1324:54–63.

Warre R, Thiele S, Talwar S, Kamal M, Johnston TH, Wang S, Lam D, Lo C, Khademullah CS, Perera G, Reyes G, Sun XS, Brotchie JM, Nash JE (2011) Altered function of glutamatergic cortico-striatal synapses causes output pathway abnormalities in a chronic model of parkinsonism. Neurobiol Dis 41:591–604.

Weiser M, Bueno E, Sekirnjak C, Marione ME, Baker H, Hillman D, Chen S, Thornhill W, Ellisman M, Rudy B (1995) The potassium channel subunit KV3.1b is localized to somatic and axonal membranes of specific populations of CNS neurons. J Neurosci 15:4298–4314.

Westin JE, Vercammen L, Strome EM, Konradi C, Cenci MA (2007) Spatiotemporal Pattern of Striatal ERK1/2 Phosphorylation in a Rat Model of L-DOPA-Induced Dyskinesia and the Role of Dopamine D1 Receptors. Biol Psychiatry 62:800–810.

Whissell PD, Lecker I, Wang DS, Yu J, Orser BA (2015) Altered expression of δgABAA receptors in health and disease. Neuropharmacology 88:24–35.

Whissell PD, Rosenzweig S, Lecker I, Wang DS, Wojtowicz JM, Orser BA (2013) γ-aminobutyric acid type A receptors that contain the δ subunit promote memory and neurogenesis in the dentate gyrus. Ann Neurol 74:611–621.

White JH, Wise A, Main MJ, Green A, Fraser NJ, Disney GH, Barnes AA, Emson P, Foord SM, Marshall FH (1998) Heterodimerization is required for the formation of a functional GABA(B) receptor. Nature 396:679–682.

Whitehead RE, Ferrer J V., Javitch JA, Justice JB (2001) Reaction of oxidized dopamine

with endogenous cysteine residues in the human dopamine transporter. J Neurochem 76:1242–1251.

Wichmann T, Bergman H, DeLong MR (1994) The primate subthalamic nucleus. III. Changes in motor behavior and neuronal activity in the internal pallidum induced by subthalamic inactivation in the MPTP model of parkinsonism. J Neurophysiol 72:521–530.

Wichmann T, Bergman H, Starr PA (1999) Comparison of MPTP-induced changes in spontaneous neuronal discharge in the internal pallidal segment and in the substantia nigra pars reticulata in primates. Exp Brain Res 125:397–40:397–409.

Wichmann T, Dostrovsky JO (2011) Pathological basal ganglia activity in movement disorders. Neuroscience 198:232–244.

Wichmann T, Kliem MA (2004) Neuronal Activity in the Primate Substantia Nigra Pars Reticulata during the Performance of Simple and Memory-Guided Elbow Movements. J Neurophysiol 91:815–827.

Wichmann T, Soares J (2006) Neuronal firing before and after burst discharges in the monkey basal ganglia is predictably patterned in the normal state and altered in parkinsonism. J Neurophysiol 95:2120–2133.

Wicker E, Beck VC, Kulick-Soper C, Kulick-Soper C V., Hyder SK, Campos-Rodriguez C, Khan T, N'Gouemo P, Forcelli PA (2019) Descending projections from the substantia nigra pars reticulata differentially control seizures. Neuroscience 116:27084–27094.

Wigmore MA, Lacey MG (2000) A Kv3-like persistent, outwardly rectifying, Cs+-permeable, K+ current in rat subthalamic nucleus neurones. J Physiol 527:493–506.

Willard AM, Isett BR, Whalen TC, Mastro KJ, Ki CS, Mao X, Gittis AH (2019) State transitions in the substantia nigra reticulata predict the onset of motor deficits in models of progressive dopamine depletion in mice. Elife 8:1–27.

Wilson CJ (1993) The generation of natural firing patterns in neostriatal neurons. Prog Brain Res 99:277–297.

Wilson CJ, Weyrick A, Terman D, Hallworth NE, Bevan MD (2004) A Model of Reverse Spike Frequency Adaptation and Repetitive Firing of Subthalamic Nucleus Neurons. J Neurophysiol 91:1963–1980.

Wilson CJ, Young SJ, Groves PM (1977) Statistical properties of neuronal spike trains in the Substantia nigra: Cell types and their interactions. Brain Res 136:243–260.

Wiltgen et al. 2005 (2010) Trace and contextual fear conditioning is enhanced in mice lacking the α4 subunit of the GABAA receptor. Neurobiol Learn Mem 93:383–387.

Windels F, Carcenac C, Poupard A, Savasta M (2005) Pallidal origin of GABA release within the substantia nigra pars reticulata during high-frequency stimulation of the subthalamic nucleus. J Neurosci 25:5079–5086.

Windels F, Kiyatkin EA (2004) GABA, not glutamate, controls the activity of substantia nigra reticulata neurons in awake, unrestrained rats. J Neurosci 24:6751–6754.

Windels F, Kiyatkin EA (2006a) GABAergic mechanisms in regulating the activity state of substantia nigra pars reticulata neurons. Neuroscience 140:1289–1299.

Windels F, Kiyatkin EA (2006b) General anesthesia as a factor affecting impulse activity and neuronal responses to putative neurotransmitters. Brain Res 1086:104–116.

Witjas T, Kaphan E, Azulay JP, Blin O, Ceccaldi M, Pouget J, Poncet M, Ali Chérif A (2002) Nonmotor fluctuations in Parkinson's disease: Frequent and disabling. Neurology 59:408–413.

Wolf E, Seppi K, Katzenschlager R, Hochschorner G, Ransmayr G, Schwingenschuh P, Ott E, Kloiber I, Haubenberger D, Auff E, Poewe W (2010) Long-term antidyskinetic efficacy of amantadine in Parkinson's disease. Mov Disord 25:1357–1363.

Wu Z, Guo Z, Gearing M, Chen G (2014) Tonic inhibition in dentate gyrus impairs long-term potentiation and memory in an Alzhiemer' s disease model. Nat Commun 5:1–12.

Xilouri M, Brekk OR, Stefanis L (2013) α-Synuclein and protein degradation systems: a reciprocal relationship. Mol Neurobiol 47:537–551.

Xilouri M, Vogiatzi T, Vekrellis K, Park D, Stefanis L (2009) Abberant α-synuclein confers toxicity to neurons in part through inhibition of chaperone-mediated autophagy. PLoS One 4:1–15.

Xu-Friedman MA, Regehr WG (2005) Dynamic-clamp analysis of the effects of convergence on spike timing. II. Few synaptic inputs. J Neurophysiol 94:2526–2534.

Yamada H, Aimi Y, Nagatsu I, Taki K, Kudo M, Arai R (2007a) Immunohistochemical detection of l-DOPA-derived dopamine within serotonergic fibers in the striatum and the substantia nigra pars reticulata in Parkinsonian model rats. Neurosci Res 59:1–7.

Yamada J, Furukawa T, Ueno S, Yamamoto S, Fukuda A (2007b) Molecular basis for the GABAA receptor-mediated tonic inhibition in rat somatosensory cortex. Cereb Cortex 17:1782–1787.

Yamaguchi T, Qi J, Wang HL, Zhang S, Morales M (2015) Glutamatergic and dopaminergic neurons in the mouse ventral tegmental area. Eur J Neurosci 41:760–772.

Yamaguchi T, Wang HL, Morales M (2013) Glutamate neurons in the substantia nigra compacta and retrorubral field. Eur J Neurosci 38:3602–3610.

Yanovsky Y, Velte S, Misgeld U (2006) Ca2+ release-dependent hyperpolarizations modulate the firing pattern of juvenile GABA neurons in mouse substantia nigra pars reticulata in vitro. J Physiol 577:879–890.

Yanovsky Y, Zhang W, Misgeld U (2005) Two pathways for the activation of small-conductance potassium channels in neurons of substantia nigra pars reticulata. Neuroscience 136:1027–1036.

Yasumi M, Sato K, Shimada S, Nishimura M, Tohyama M (1997) Regional distribution of GABA transporter 1 (GAT1) mRNA in the rat brain: Comparison with glutamic acid decarboxylase67 (GAD67) mRNA localization. Mol Brain Res 44:205–218.

Yee BK, Hauser J, Dolgov V V., Keist R, Möhler H, Rudolph U, Feldon J (2004) GABAA receptors containing the α5 subunit mediate the trace effect in aversive and appetitive conditioning and extinction of conditioned fear. Eur J Neurosci 20:1928–1936.

Yoshino H, Nakagawa-Hattori Y, Kondo T, Mizuno Y (1992) Mitochondrial complex I and II activities of lymphocytes and platelets in Parkinson's disease. J Neural Transm - Park Dis Dement Sect 4:27–34.

Zappia M, Annesi G, Nicoletti G, Arabia G, Annesi F, Messina D, Pugliese P, Spadafora P, Tarantino P, Carrideo S, Civitelli D, De Marco E V., Cirò-Candiano IC, Gambardella A, Quattrone A (2005) Sex differences in clinical and genetic determinants of levodopa peak-dose dyskinesias in Parkinson disease: An exploratory study. Arch Neurol 62:601–605.

Zhai S, Shen W, Graves SM, Surmeier DJ (2019) Dopaminergic modulation of striatal function and Parkinson's disease. J Neural Transm 0:0.

Zhang Y, Oertner TG (2007) Optical induction of synaptic plasticity using a light-sensitive channel. Nat Methods 4:139–141.

Zhou 2016 (2016) The Substantia Nigra Pars Reticulata. Handb Basal Ganglia Struct Funct 24:293–316.

Zhou and Lee 2011 (2011) Intrinsic and integrative properties of substantia nigra pars reticulata neurons. Neuroscience 198:69–94.

Zhou FM, Wilson CJ, Dani JA (2002) Cholinergic interneuron characteristics and nicotinic properties in the striatum. J Neurobiol 53:590–605.

Zhou FW, Jin Y, Matta SG, Xu M, Zhou FM (2009) An ultra-short dopamine pathway regulates basal ganglia output. J Neurosci 29:10424–10435.

Zhou FW, Matta SG, Zhou FM (2008) Constitutively active TRPC3 channels regulate basal ganglia output neurons. J Neurosci 28:473–482.

Zhou FW, Xu JJ, Zhao Y, LeDoux MS, Zhou FM (2006) Opposite functions of histamine H1 and H2 receptors and H3 receptor in substantia nigra pars reticulata. J Neurophysiol 96:1581–1591.